

12-9-1980

X-Ray Induced Electron Emission

Charles A. Aeby

Follow this and additional works at: https://digitalrepository.unm.edu/cbe_etds



Part of the [Chemical Engineering Commons](#)

Recommended Citation

Aeby, Charles A.. "X-Ray Induced Electron Emission." (1980). https://digitalrepository.unm.edu/cbe_etds/61

This Dissertation is brought to you for free and open access by the Engineering ETDs at UNM Digital Repository. It has been accepted for inclusion in Chemical and Biological Engineering ETDs by an authorized administrator of UNM Digital Repository. For more information, please contact disc@unm.edu.

X-RAY
INDUCED
ELECTRON
EMISSION

AEBY

LD
3783
C34
1980
A47

A14403 290021

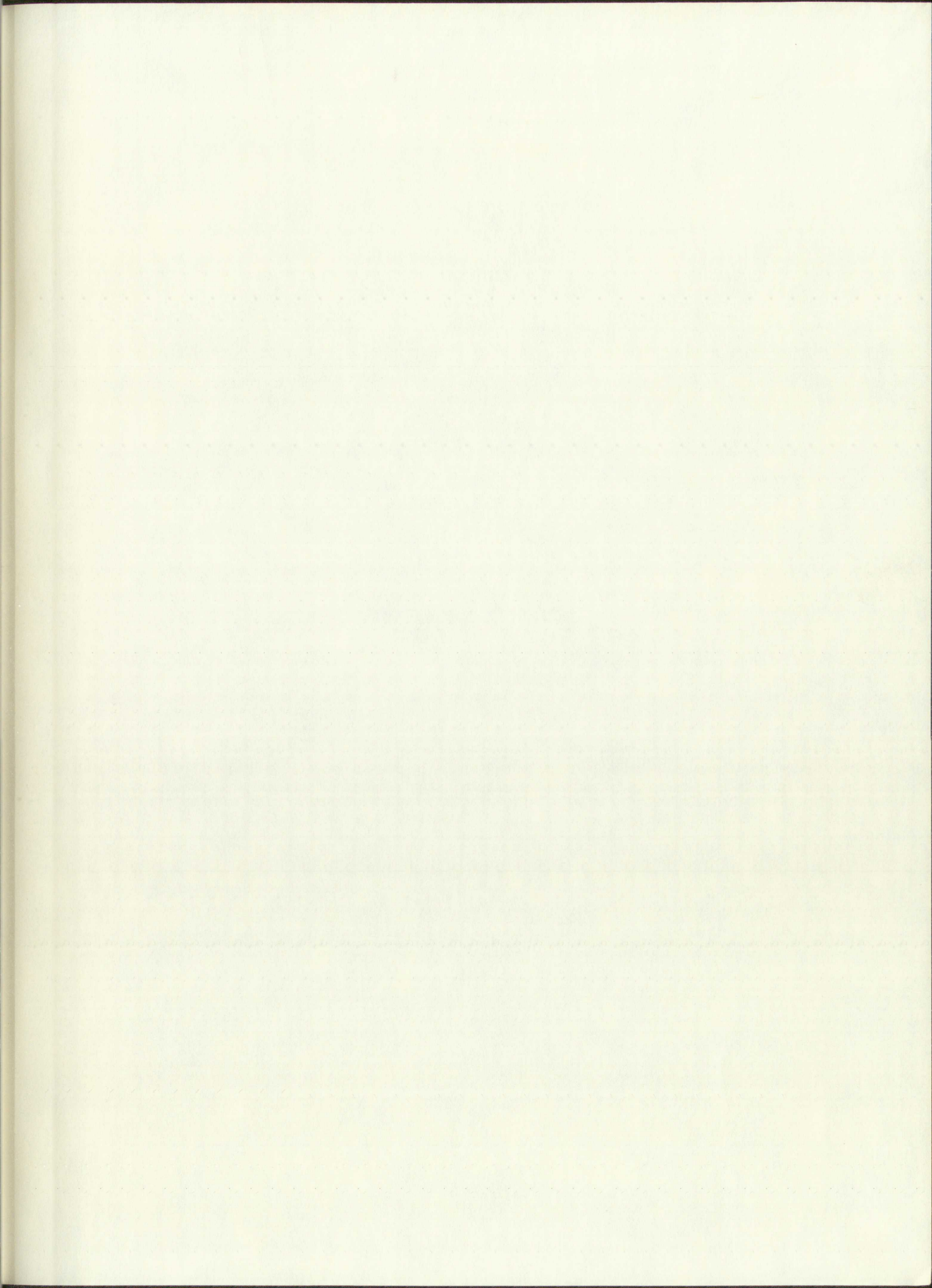
DATE DUE

JAN 29 1982

REC'D UNM FEB 19 '82

DEMCO 38-297





LD
3783
C34
1980
A47

STATIONER
(CORRIGIBLE)
BOND
U.S.A.
REINFORCED
STATIONER



CATON'S
CORRUGABLE
BOND
NPA
GAYLOR
25% COTTON FIBRE

THE UNIVERSITY OF NEW MEXICO
ALBUQUERQUE, NEW MEXICO 87131

POLICY ON USE OF THESES AND DISSERTATIONS

Unpublished theses and dissertations accepted for master's and doctor's degrees and deposited in the University of New Mexico Library are open to the public for inspection and reference work. *They are to be used only with due regard to the rights of the authors.* The work of other authors should always be given full credit. Avoid quoting in amounts, over and beyond scholarly needs, such as might impair or destroy the property rights and financial benefits of another author.

To afford reasonable safeguards to authors, and consistent with the above principles, anyone quoting from theses and dissertations must observe the following conditions:

1. Direct quotations during the first two years after completion may be made only with the written permission of the author.
2. After a lapse of two years, theses and dissertations may be quoted without specific prior permission in works of original scholarship provided appropriate credit is given in the case of each quotation.
3. Quotations that are complete units in themselves (e.g., complete chapters or sections) in whatever form they may be reproduced and quotations of whatever length presented as primary material for their own sake (as in anthologies or books of readings) ALWAYS require consent of the authors.
4. The quoting author is responsible for determining "fair use" of material he uses.

This thesis/dissertation by Charles A. Aeby has been used by the following persons whose signatures attest their acceptance of the above conditions. (A library which borrows this thesis/dissertation for use by its patrons is expected to secure the signature of each user.)

NAME AND ADDRESS

DATE

_____	_____
_____	_____
_____	_____
_____	_____
_____	_____

THE UNIVERSITY OF NEW MEXICO ALBUQUERQUE, NEW MEXICO 87131

POLICY ON USE OF THESIS AND DISSERTATIONS

Unpublished theses and dissertations, prepared for master's and doctoral degrees and deposited in the University of New Mexico Library are open to the public for inspection and reference work. They are to be used only with the regard to the rights of the author. The work of other authors should always be given full credit. Avoid quoting in statements over and beyond scholarly needs such as might impair or destroy the property rights and financial benefits of another author.

To avoid unreasonable safeguards to authors and consistent with the above principles, anyone quoting from theses and dissertations must observe the following conditions:

1. Direct quotations during the first two years after completion may be made only with the written permission of the author.
2. After a lapse of two years, theses and dissertations may be quoted without specific prior permission in works of original scholarship provided appropriate credit is given in the case of each quotation.
3. Quotations that are complete units in themselves (e.g., complete chapters or sections) in whatever form they may be reproduced and quotations of whatever length prepared as primary material for their own sake (as in anthologies or books of readings) ALWAYS require consent of the author.
4. The quoting author is responsible for determining "fair use" of material he uses.

This thesis/dissertation by Charles A. Leiby has been used by the following persons whose signatures attest their acceptance of the above conditions: (A library which borrows this thesis/dissertation for use by its patron is expected to secure the signature of each user.)

NAME AND ADDRESS	DATE
_____	_____
_____	_____
_____	_____
_____	_____
_____	_____

Charles Allen Aeby
Candidate

Chemical and Nuclear Engineering
Department

This dissertation is approved, and it is acceptable in quality and form for publication on microfilm:

Approved by the Dissertation Committee:

Glen A. Whan, Chairperson

Lawrence D. Frey

Harry W. Cooper

Harold D. Southward

Accepted:

Donald T. Benevento
Dean, Graduate School

Dec. 9, 1980
Date

Charles Allen Babb

Chemical and Nuclear Engineering

This dissertation is approved and it is acceptable in quality

and form for publication on microfilm

I approve for the Dissertation Committee

Chairperson

[Signature]
James W. Cooper

[Signature]
Donald E. Johnston

Accepted

[Signature]
James T. Babb

Dean, Graduate School

[Signature]
Date

X-RAY INDUCED ELECTRON EMISSION

BY

CHARLES A. AEBY

B.S., University of New Mexico, 1962

M.S., University of New Mexico, 1964

DISSERTATION

Submitted in Partial Fulfillment of the
Requirements for the Degree of

Doctor of Philosophy in Engineering

The University of New Mexico
Albuquerque, New Mexico

December 1980

(C) Copyright by Charles A. Aeby, 1981



ACKNOWLEDGEMENTS

I wish to thank Dr. Glenn Whan for his patience, guidance and continuing support during the course of this effort. Dr. Frank Guy offered critical encouragement during the formative phases of the experiment and has been of invaluable assistance through discussion of the results and their interpretation. Dr. Gary Scrivner provided helpful suggestions on data processing and Dr. Jerry Sawyer offered assistance during instrument calibration. A special debt of gratitude is owed to my wife Marjorie, and daughters Katherine and Cynthia for their patience, understanding and loving support.

ACKNOWLEDGMENTS

I wish to thank Dr. Glenn Wren for his patience, guidance and continuing support during the course of this effort. Dr. Frank Gay offered critical management during the formative phases of the experiment and has been of invaluable assistance through discussion of the results and their interpretation. Dr. Gary Bortner provided helpful suggestions on data processing and Dr. Betty Hawley offered assistance during instrument calibration. A special debt of gratitude is owed to my wife, Marie, and daughters, Katherine and Cynthia for their patience, understanding and loving support.

X-RAY INDUCED ELECTRON EMISSION

BY

CHARLES A. AEBY

ABSTRACT OF DISSERTATION

Submitted in Partial Fulfillment of the
Requirements for the Degree of
Doctor of Philosophy in Engineering

The University of New Mexico
Albuquerque, New Mexico

December 1980

NON FIBRE
BOND

ABSTRACT OF THE PROCEEDINGS

OF THE
SOCIETY OF THE
SACRED

OF THE

OF THE

X-RAY INDUCED ELECTRON EMISSION

Charles A. Aeby

B.S., Physics, University of New Mexico, 1962

M.S., Physics, University of New Mexico, 1964

Ph.D., Nuclear Engineering, University of
New Mexico, 1980

The development and use of a magnetic spectrograph for the measurement of X-ray induced electron emission is described. Results are presented for metal and dielectric targets ranging in atomic number from $Z=6$ to $Z=82$. Materials studied were lead, tantalum, copper, aluminum, magnesium, solar cell cover glass, silica cloth, thermal control paint, Kevlar, Mylar and conducting and non-conducting epoxy. Direct measurement was made of the quantum yield and energy distribution of electrons emitted at angles of 0° , 30° , 45° and 60° with respect to the surface normal of targets exposed to normal incidence filtered and unfiltered 50kV bremsstrahlung X rays.

Experimental results are compared with previous measurements where possible and with computer code predictions where predictive capability matches the measurement range. The experimental results corroborate

the $\cos\theta$ angular dependence predicted by simple theoretical models, particularly for medium and high Z materials. A trend toward isotropic emission distribution is noted for the lower Z materials. Compared to the measured results, the emission yields predicted by a commonly used analytical model are low by approximately a factor of two for the unfiltered X-ray spectrum. This spectrum has a relatively large low energy component and highlights a deficiency in predictive capability for X-ray energies below ~ 10 keV.

the core regular dependence produced by light
inherent in media, particularly for media and high
energy, a large energy isotropic relation
distinction is noted for the lower a medium.
Compared to the regular medium, the energy relation
produced by a core, a regular medium, and the
approximately a factor of two for the difference in
energy. This spectrum has a relatively large
energy component and light, gives a distinction in
productive capability for light angles below 10 deg.

TABLE OF CONTENTS

	Page
List of Figures	x
List of Tables	xiii
Section I	
Introduction	2
Statement of Problem	2
Sequence of Events Leading to	3
Electron Emission	
Theoretical Model	5
Summary of Existing Information	9
Specific Objective	15
Experimental Approach	17
Section II	
Spectrograph Design	22
Basic Instrument	22
Modifications for Yield, Emission	25
Angle and Energy Determination	
Section III	
Instrument Calibration	39
X-ray Source	39
Detector Characteristics	45
Background Count Rates	50
Magnetic Field Conditions	53
Energy Resolution	55

TABLE OF CONTENTS

Page	
x	List of Figures
xiii	List of Tables
	Section I
1	Introduction
2	Statement of Problem
3	Sequence of Events Leading to
4	Electron Emission
5	Theoretical Model
6	Summary of Existing Information
12	Specific Objective
13	Experimental Approach
	Section II
22	Spectrograph Design
22	Basic Instrument
28	Modifications for Yield, Emission
	Angle and Energy Determination
	Section III
38	Instrument Calibration
39	X-ray Source
45	Detector Characteristics
50	Background Count Rates
53	Magnetic Field Conditions
55	Energy Resolution

Section IV	
Experimental Results	66
Data Reduction Method	66
Reproducibility, Errors and Accuracy	68
Differential and Integrated Reverse	73
Emission Yield	
Section V	
Discussion and Summary	94
Features of Emission Curves	94
Yield Dependence on Atomic Number	100
Comparative Results for Metal Targets,	102
Filtered Spectrum	
Comparative Results for Metal Targets,	109
Unfiltered Spectrum	
Results for Dielectric Targets,	117
Unfiltered Spectrum	
Summary	122
Appendices	
Appendix A Basic Equations	124
Appendix B Raw Data	129
List of Tables	130
(Appendix B)	
References	203

263	References
130	(Appendix B)
129	List of Tables
128	Appendix B Raw Data
124	Appendix A Basic Equations
123	Appendices
117	Summary
117	Unfiltered Spectrum
117	Kesive for Dielectric Targets,
109	Unfiltered Spectrum
109	Comparative Results for Metal Targets,
103	Filtered Spectrum
103	Comparative Results for Metal Targets,
100	Yield Dependence on Atomic Number
94	Features of Emission Curves
94	Discussion and Summary
84	Section V
73	Emission Yield
73	Differential and Integrated Yields
65	Reproducibility, Errors and Accuracy
48	Data Reduction Method
48	Experimental Results
48	Section IV

LIST OF FIGURES

Figure		Page
1	Electron Emission Interactions	4
2	Photoelectric Yield Model Geometry	7
3	Experimental Setup	19
4	Basic Instrument Geometry	24
5	Spectrograph Coordinate System	26
6	Target-Aperture-Detector Geometry	28
7	ρ, θ Acceptance Bands at $0^\circ, 30^\circ, 45^\circ$ and 60° Emission Angles	31
8	Vertical Collimation Geometry	34
9	Spectrograph Configuration	37
10	Absolute Flux Measurement	41
11	X-ray Energy Distribution	42
12	Detector Efficiency Versus Electron Energy	46
13	Magnetic Field Effect Measurement	49
14	Detector Efficiency Versus Magnetic Field	51
15	Target Mount	53
16	Energy Calibration Electron Source	56
17	Target Mount-Detector-Electron Source	58

Page 7

1. [illegible]
2. [illegible]
3. [illegible]
4. [illegible]
5. [illegible]
6. [illegible]
7. [illegible]
8. [illegible]
9. [illegible]
10. [illegible]
11. [illegible]
12. [illegible]
13. [illegible]
14. [illegible]
15. [illegible]
16. [illegible]
17. [illegible]

18	Channel 1 (0°) Energy Resolution	61
19	Channel 2 (30°) Energy Resolution	62
20	Channel 3 (45°) Energy Resolution	63
21	Channel 4 (60°) Energy Resolution	64
22	Differential Yield Versus Energy; Cu with Filter	76
23	Differential Yield Versus Energy; Ta with Filter	77
24	Differential Yield Versus Energy; Mg, Unfiltered	78
25	Differential Yield Versus Energy; Al, Unfiltered	79
26	Differential Yield Versus Energy; Cu, Unfiltered	80
27	Differential Yield Versus Energy; Ta, Unfiltered	81
28	Differential Yield Versus Energy; Pb, Unfiltered	82
29	Differential Yield Versus Energy; Cover Glass, Unfiltered	83
30	Differential Yield Versus Energy; Silica Cloth, Unfiltered	84
31	Differential Yield Versus Energy; Thermal Control Paint, Unfiltered	85
32	Differential Yield Versus Energy; Kevlar, Unfiltered	86

18	Channel 1
19	Channel 2
20	Channel 3
21	Channel 4
22	Differential
23	Co with
24	Differential
25	Co with
26	Differential
27	Co with
28	Differential
29	Co with
30	Differential
31	Co with
32	Differential
33	Co with
34	Differential
35	Co with
36	Differential
37	Co with
38	Differential
39	Co with
40	Differential
41	Co with
42	Differential
43	Co with
44	Differential
45	Co with
46	Differential
47	Co with
48	Differential
49	Co with
50	Differential
51	Co with
52	Differential
53	Co with
54	Differential
55	Co with
56	Differential
57	Co with
58	Differential
59	Co with
60	Differential
61	Co with
62	Differential
63	Co with
64	Differential
65	Co with
66	Differential
67	Co with
68	Differential
69	Co with
70	Differential
71	Co with
72	Differential
73	Co with
74	Differential
75	Co with
76	Differential
77	Co with
78	Differential
79	Co with
80	Differential
81	Co with
82	Differential
83	Co with
84	Differential
85	Co with
86	Differential
87	Co with
88	Differential
89	Co with
90	Differential
91	Co with
92	Differential
93	Co with
94	Differential
95	Co with
96	Differential
97	Co with
98	Differential
99	Co with
100	Differential

33	Differential Yield Versus Energy; Mylar, Unfiltered	87
34	Differential Yield Versus Energy; Non Conducting Epoxy, Unfiltered	88
35	Differential Yield Versus Energy; Conducting Epoxy, Unfiltered	89
36	Energy Integrated Yield Versus θ_k	90
37	Normalized Yield Versus θ_k ; Metal Targets	91
38	Normalized Yield Versus θ_k ; Non Metallic Targets	92
39	Yield Versus Atomic Number	101
40	Experiments and Code Comparisons; Cu, with Filter	103
41	Experiments and Code Comparisons; Ta, with Filter	104
42	Experiment/Code Comparison; Al, Unfiltered	111
43	Experiment/Code Comparison; Cu, Unfiltered	112
44	Experiment/Code Comparison; Ta, Unfiltered	113
45	Experiment/Code Comparison; Pb, Unfiltered	114
46	Measured Yield for Cover Glass, Silica Cloth, Thermal Control Paint	120

32	Experimental results
33	Discussion
34	References
35	Appendix
36	Energy levels
37	Experimental results
38	References
39	Appendix
40	Experimental results
41	References
42	Appendix
43	Experimental results
44	References
45	Appendix
46	Experimental results
47	References
48	Appendix
49	Experimental results
50	References
51	Appendix
52	Experimental results
53	References
54	Appendix
55	Experimental results
56	References
57	Appendix
58	Experimental results
59	References
60	Appendix
61	Experimental results
62	References
63	Appendix
64	Experimental results
65	References
66	Appendix
67	Experimental results
68	References
69	Appendix
70	Experimental results
71	References
72	Appendix
73	Experimental results
74	References
75	Appendix
76	Experimental results
77	References
78	Appendix
79	Experimental results
80	References
81	Appendix
82	Experimental results
83	References
84	Appendix
85	Experimental results
86	References
87	Appendix
88	Experimental results
89	References
90	Appendix
91	Experimental results
92	References
93	Appendix
94	Experimental results
95	References
96	Appendix
97	Experimental results
98	References
99	Appendix
100	Experimental results

	and Kevlar; Unfiltered Spectrum	
47	Measured Yield for Mylar, Non- conducting Epoxy and Conducting Epoxy; Unfiltered Spectrum	121

LIST OF TABLES

Table		Page
1	Code Characteristics	14
2	Primary and Secondary Slit Parameters	29
3	Angular Acceptance Band Parameters	30
4	Background Count Rates	53
5	Summary of Experimental Reproducibility	70
6	Total Reverse Emission Yield Summary, $E_e > 0.1$ keV; Filtered and Unfiltered Spectra	75
7	Comparison of Previous Reverse Emission Yield Results and Code Predictions Normalized to Present Experiment	102
8	Reverse Emission Yield	107

Table

1	Code Comparison	1
2	Primary and Secondary Parameters	2
3	Angular Acceleration Parameters	3
4	Background Count Rates	4
5	Summary of Experimental Reproducibility	5
6	Total Reversal Rate Summary, R ₀ , and Unitless Comparison of Reversal Rates	6
7	Comparison of Reversal Rates with Prediction Yields	7
8	Reversal Rate Prediction Error	8

Comparisons, Filtered
Spectrum

- 9 Experimental Reverse Emission Yield 115
Comparisons with QUICKE 2M Calculations,
Unfiltered Spectrum, for Aluminum,
Copper, Tantalum and Lead

Experiment 1

Experiment 2

Experiment 3

Experiment 4

Experiment 5

SECTION I

SECTION I

INTRODUCTION

Statement of Problem

Satellites and other exoatmospheric systems are subject to various radiation effects due to natural and manmade environments which result in the generation of localized electromagnetic conditions. These conditions can disrupt normal electronic system functions. One effect, known as System Generated Electromagnetic Pulse (SGEMP) results from X-ray interactions with the materials comprising the system. The source term generating the SGEMP environment, given a photon source of known intensity and energy distribution, is the X-ray induced emission of electrons from external and internal surfaces of the system. To accurately calculate the electromagnetic environment, the emitted electrons must be characterized in terms of their yield and energy distribution as a function of emission angle. This characterization is required as a function of emitting material, photon energy, and various angles of photon incidence. An understanding of and a solution to the SGEMP problem must therefore begin with quantitative understanding of the X-ray induced electron emission.

Sequence of Events Leading to Electron Emission

A beam of photons characterized by the number of photons of given energy per unit time per unit area impinges on a target. The properties of the material, i.e., the cross sections for various types of interactions with electromagnetic radiation, and the incident flux determine the reaction rate within the material. The energy of the incident photons and the appropriate cross sections determine the depth at which an interaction takes place and the type of interaction through the relative magnitudes of the cross sections for the interactions possible. The specific interaction then determines the initial conditions for the residual particles. Principal photon-material interactions which produce electrons are (Fig. 1):

- a. Photoelectric interactions with a "bound" electron
- b. Compton interactions with "free" electrons
- c. Pair production interactions with the Coulomb field of a charged particle

Residual photons will have additional interactions determined by their energy and the material properties until they are absorbed or escape. Primary electrons generated by the photon interactions undergo various types of collisions, likewise determined by their energy and the characteristics of the material. Subsequent

Interaction of Electrons with Matter

A beam of electrons is characterized by the number of electrons of given energy, per unit time and unit area, impinging on a target. The properties of the material, i.e., the cross sections for various types of interactions with electromagnetic radiation, and the incident flux determine the reaction rate within the material. The energy of the incident photons and the appropriate cross sections determine the depth at which an interaction takes place and the type of interaction through the relative magnitude of the cross sections for the interaction processes. The specific interaction then determines the initial conditions for the residual particles. Principal photon-matter interactions which produce electrons are (Fig. 1):

- a. Photoelectric interactions with a "bound" electron
- b. Compton interactions with "free" electrons
- c. Pair production interactions with the Coulomb

Field of a charged particle

Residual photons will have additional interactions determined by their energy and the material properties until they are absorbed or escape. Primary electrons generated by the photon interactions undergo various types of collisions, likewise determined by their energy and the characteristics of the material. Subsequent

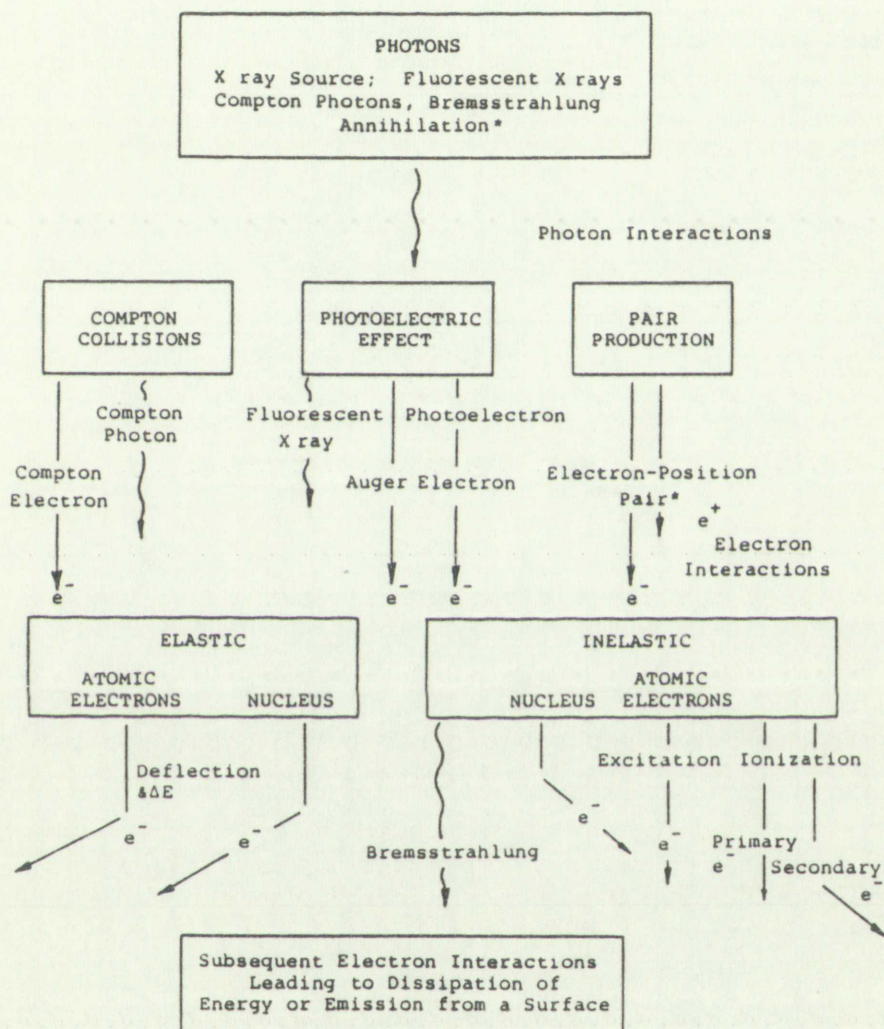


FIGURE 1. Electron Emission Interactions

transport of these electrons to a surface, with intervening deflections and energy losses determine their emission characteristics in terms of the number, energy and angular distribution. The principal electron interactions are elastic and inelastic collisions with target nuclei and atomic electrons. Residual particles from these interactions are generally the initial electron degraded in energy deflected from its original path plus secondary electrons resulting from ionization. bremsstrahlung in turn results from nuclear inelastic electron collisions.

For the X-ray energy range of interest for satellite SGEMP effects, the primary interactions are the photoelectric and Compton effects, subsequent generation of Auger electrons and electron scattering processes.

Theoretical Model

A simple empirical model for X-ray induced electron emission has been proposed [1] which develops the major features of the emission process.¹ It accounts for emission yield contributions from photoelectrons, Auger

¹The experimental results will be compared primarily with QUICKE 2M, a state-of-the-art analytical code currently used for electron emission calculations.

transport of ...
interacting ...
their emission ...
energy and ...
interactions ...
target nuclei ...
from these ...
electron ...
path plus ...
demonstrating ...
electron ...
For the ...
satellite ...
the photo ...
generation ...
processes.

Theoretical Model
A simple ...
emission has ...
features of ...
emission yield ...
The experiment ...
with QUICK ...
currently used

and secondary (knock-on) electrons, defines an expected angular dependence and predicts the electron energy distribution. The model will predict reverse emission of electrons from a vacuum/material interface exposed to an arbitrary fluence of X rays. Four simplifying assumptions are made: (1) the electrons are generated with uniform density in the exposed material with the photoelectron source densities given by $\phi\mu/\cos\alpha$ where ϕ is the X-ray fluence at the surface, μ is the photoelectric linear absorption coefficient and α is the angle of incidence of the X rays with respect to the surface normal; (2) the electrons propagate isotropically from their point of origin; (3) electrons in the material travel their mean forward range, determined by their energy at birth, in straight lines and; (4) the electrons lose energy continuously according to an effective stopping power approximately twice the ordinary stopping power. This assumption is based on the observation in some materials that the mean forward range is approximately one half the mean path length (comparable to the continuous slowing down approximation range); and that dE/dx is relatively material independent for electron energies of a few keV to several hundred keV.

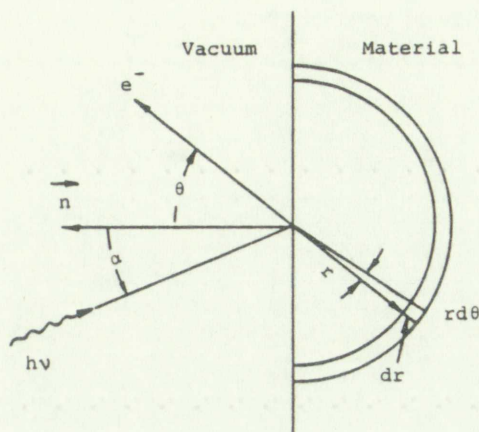


FIGURE 2. Photoelectric Yield Model Geometry

With reference to Fig. 2 the contribution to the yield coming from a primary photoelectron created by an X ray of energy $h\nu$ in a unit volume dv at slant range r and angle θ is

$$\frac{dy}{dv} = \frac{\mu(h\nu) \cos\theta}{\cos\alpha \, 4\pi r^2} \quad (1)$$

In this equation $\mu(h\nu)/\cos\alpha$ is the source density per photon interacting in dv and $\cos\theta/4\pi r^2$ represents the angular distribution of electrons leaving the surface at angle θ from an isotropic source at range r . The unit volume dv can also be written as $r^2 d\Omega dr$; hence the differential yield can be expressed as



FIGURE 1. Photoelectric Effect Geometry

With reference to Fig. 1 the contribution to the yield coming from a primary photoelectron created by an X ray of energy $h\nu$ in a unit volume dv at point P and angle θ is

$$dy = \frac{n(h\nu) \cos \theta}{dv \cos \theta} dv$$

In this equation $n(h\nu) \cos \theta$ is the source density per photon interacting in dv and $\cos \theta$ represents the angular distribution of electrons leaving the surface at angle θ from an isotropic source at range r . The unit volume dv can also be written as $r^2 \sin \theta d\theta d\phi$. The differential yield can be expressed as

$$\frac{dy}{d\Omega dr} = \frac{\mu(h\nu) \cos\theta}{\cos\alpha \ 4\pi} \quad (2)$$

The differential yield per unit energy and unit solid angle is then

$$\frac{dy}{d\Omega dE} = \frac{\mu(h\nu) \cos\theta}{\cos\alpha \ 4\pi} \left(\frac{dE}{dr}\right)^{-1} \quad (3)$$

Integration of equation 3 over angle to obtain the electron energy spectrum gives

$$\frac{dy}{dE} = \frac{\mu(h\nu)}{4\cos\alpha} \left(\frac{dE}{dr}\right)^{-1} \quad (4)$$

The equations were developed for primary photoelectrons. However, the same energy and angle distributions apply to the Auger and secondary electrons. The Auger electrons result from atomic de-excitation after photoelectron ejection and the secondaries arise from collisions of the primary photoelectrons and Auger electrons with atomic electrons. Their contribution to the emission yield is determined by the efficiency with which they are created in the target material and the limits of their energy distribution determined by the energies they obtain at birth. The total yield of emitted electrons from this model is the sum of the individual contributions from photo, Auger and secondary

electrons. The energy distribution is obtained by superposition of the individual distributions.

The major features of X-ray induced electron emission predicted by this model are: (1) the angular distribution of emitted electrons per unit solid angle is proportional to $\cos\theta$; (2) the shape of the energy distribution is independent of angle; (3) since the range of electrons in many materials is proportional to E^2 , the yield distribution, (equation 4), will be proportional to E , that is, a simple triangular distribution; and (4) for angles of X-ray incidence other than $\alpha = 0$, the yield increases as $1/\cos\alpha$. The model does not treat Compton interactions nor low energy secondaries, but does include the primary elements of electron emission resulting from photoelectric interactions.

Summary of Existing Information

The characteristics of electrons emitted from materials exposed to X rays have been the subject of intense investigation since Roentgen's discovery of X rays in the late 1800's. Much of this work has been focused on experiments which yield information on the details of the interactions of the photons with individual atoms to clearly define the cross sections

electrons. The energy distribution is dependent on
superposition of the individual distributions.
The major features of X-ray induced electron
emission predicted by this model are: (1) the energy
distribution of emitted electrons per unit area
is proportional to energy in the range of the energy
distribution is independent of angle; (2) since the
range of electrons in many materials is proportional to
 $E^{1.5}$, the yield distribution, (equation 4), will be
proportional to $E^{1.5}$; that is, a simple triangular dis-
tribution; and (3) for angles of X-ray incidence other
than $\alpha = 0$, the yield increases as $1/\cos \alpha$. The model does
not treat Compton interactions nor low energy
excitations but does include the primary elements of
electron emission resulting from photoelectric
interactions.

Summary of Existing Information

The characteristics of electrons emitted from
materials exposed to X-rays have been the subject of
intense investigation since Röntgen's discovery of X
rays in the late 1890's. Much of this work has been
focused on experiments which yield information on the
details of the interactions of the photons with
individual atoms; this defines the cross sections

for the various interactions taking place. By analyzing the products of the interactions, i.e., the residual particles, the nature of the encounter can be inferred and the fate of the initial particles established. Experiments performed for this purpose were intentionally designed to minimize effects such as multiple scattering of the primary electrons so that the details of the individual interactions would not be masked. It is precisely these effects, however, that determine the characteristics of the electron emission that are investigated in this experiment.

Prior to the early 1970's the bulk of the experimental work had been directed at the measurement of individual features of photon-induced electron emission of importance to specific problems. Independent measurements were made to determine emission yield or energy distribution or angular distributions for given source conditions and target materials. For example the Soviet work in the early-to-mid 1960's [2,3,4,5] concentrated on measurements of total yield, energy and angular dependence of emission from various cathode materials exposed to X rays in ionization chamber and spherical condensers. X rays used in these works were "monochromatic", obtained by selective filtration of continuous bremsstrahlung spectra. (The discrete X-ray energies covered a range of 4-28 keV).

These results, corroborated by later experiments [6], gave relative numbers of primary photoelectrons, Auger electrons and secondary electrons emitted from the materials studied. Later Soviet work [7] gave experimental evidence for the cosine behavior of emission yield and the relative angular independence of the emission spectrum on emission angle.²

The problem of interest to the satellite community required corroboration of the Soviet experimental data, an expansion of the data base to a wider variety of materials and validation of the various computer codes which can be used to predict electron emission. Toward this goal, just prior to design and development of the magnetic spectrograph system employed in this work, Bradford [8] performed a series of measurements on aluminum, copper, tantalum, and molybdenum employing an electrostatic analyzer. The targets were placed in an evacuated chamber and irradiated with a collimated beam of bremsstrahlung X rays from a tungsten anode source operating at 50kV potential. Two different X-ray spectra were employed, determined by the presence or absence of a thick aluminum filter. Electrons were measured in 1 keV energy intervals from approximately 3

²The cathode materials investigated in references 2 through 7 included Al, Cr, Fe, Co, Cu, Ag, Sn, Te, Ta, W, Pb and Bi.

These results, which are presented in Table I, show that the relative intensity of the primary photoelectron peak is independent of the emission angle and the relative angular independence of the emission yield and the relative angular independence of the emission yield.

The emission spectrum on emission angle, θ , is shown in Fig. 2. The problem of interest to the cathode community required consideration of the Soviet experimental data, an expansion of the data base to a wider variety of materials and verification of the various computer codes which can be used to predict electron emission. Toward this goal, just prior to design and development of the magnetic spectrograph system employed in this work, Bradford [8] performed a series of measurements on aluminum, copper, cerium, and molybdenum employing an electrostatic analyzer. The targets were placed in an evacuated chamber and irradiated with a collimated beam of deuterium K rays from a tungsten anode source operating at 50 kV potential. Two different X-ray spectra were employed, determined by the presence or absence of a thick aluminum filter. Electrons were measured in 1 keV energy intervals from approximately 1

The cathode materials investigated in reference 2 through 7 included Al, Cu, Fe, Co, Ni, Ag, Au, Pt, W, Pb and Bi.

keV up to 50 keV. A variable source/target/detector geometry permitted a determination of angular dependence. The initial data (originally in error as a result of a calibration source saturation problem) were revised.³ This work was later augmented by an experimental determination of the dependence of the emission properties on X-ray angle of incidence [9].

In 1974 Dolan [10] published the results of bremsstrahlung X-ray induced electron emission from aluminum, copper, silver and tantalum. Various accelerating voltages and filter combinations were employed to provide X-ray spectrum variations. Two configurations common to Bradford's measurements were used for comparison. The experiment used lithium drifted solid state devices to detect electrons of energy greater than 5 keV. Variable positioning of the detector permitted determination of the emission yield angular dependence. The measurements of Bradford and Dolan have been used as primary sources of experimental data for comparisons with computer code predictions of X-ray induced electron emission.

A number of computer codes have evolved with capabilities of predicting X-ray induced electron

³The revision was documented as a 26 December 1972 addendum to Air Force Cambridge Research Labs Physical Sciences Research Paper 510.

has up to 40 keV. A vacuum source/detector geometry provided a determination of angular dependence. The initial data (originally in error as a result of a calibration source calibration problem) were revised. This work was later augmented by an experimental determination of the dependence of the emission properties on X-ray angle of incidence (5).

In 1974 Dolan (18) published the results of determining X-ray induced electron emission from aluminum, copper, silver and tantalum. Various accelerating voltages and filter combinations were employed to provide X-ray spectral variations. Two configurations common to Bradford's measurements were used for comparison. The experiment used lithium drifted solid state devices to detect electrons of energy greater than 2 keV. Variable positioning of the detector permitted determination of the emission yield angular dependence. The measurements of Bradford and Dolan have been used as primary sources of experimental data for comparisons with computer code predictions of X-ray induced electron emission. A number of computer codes have evolved with capabilities of predicting X-ray induced electron

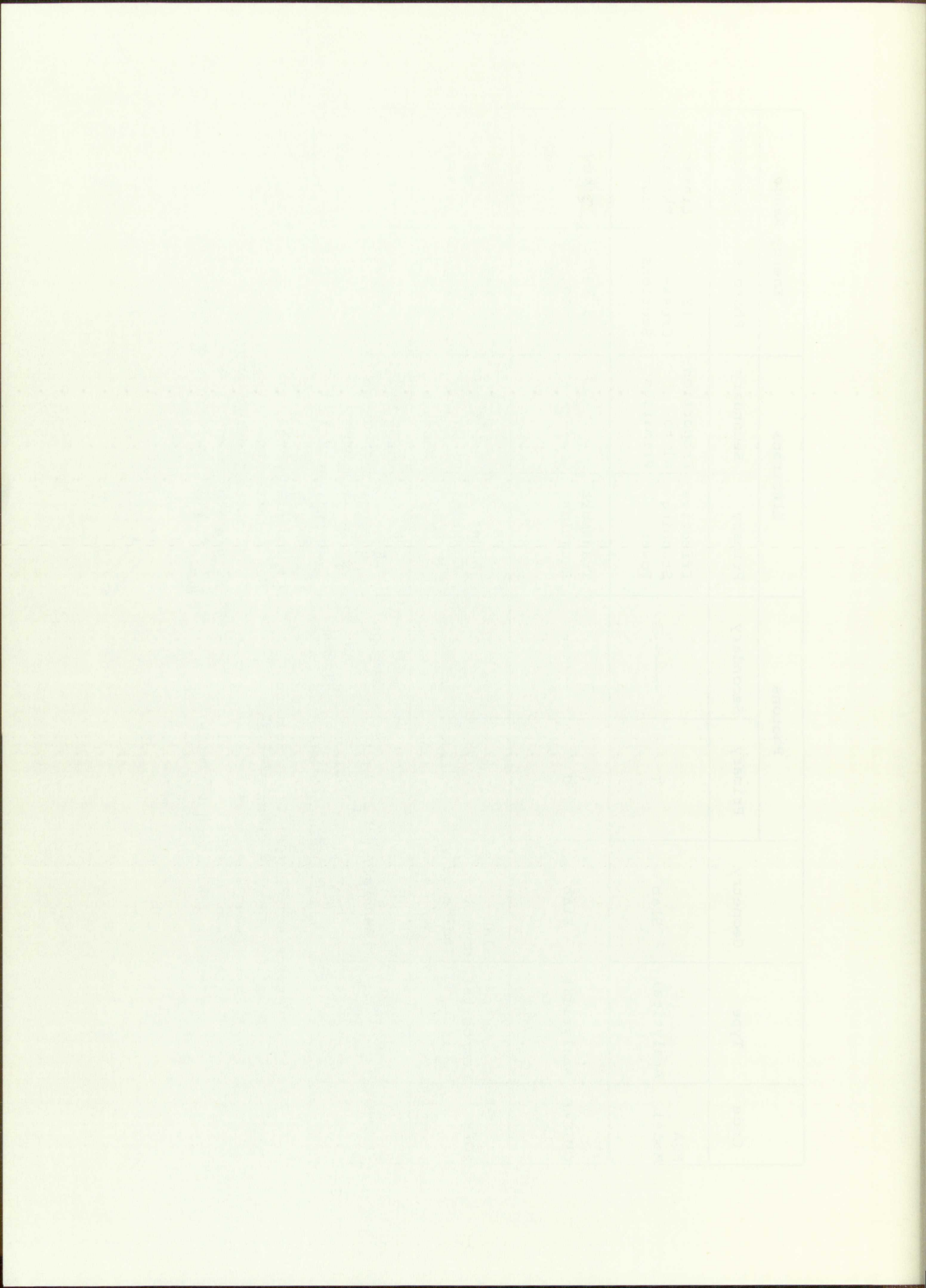
⁵The revision was documented as a 15 December 1972 addendum to the report Cambridge Research Labs Physical Sciences Research Paper 519.

emission. Their genesis has followed one of two primary paths (see Table 1). The more complex detailed codes have been built on the Monte Carlo technique employed by Berger and Seltzer in the ETRAN (electron transport) family of codes [11]. Codes of this type e.g., SANDYL [12] include primary and secondary photon interactions and primary and secondary electron interactions. Primary and secondary electrons are treated with single and multiple scattering techniques in the Monte Carlo codes. On the other hand the analytical codes (e.g., RDA model [1] and QUICKE 2 [13]) use simple exponential attenuation for X-ray interactions and transport, and approximations (effective electron stopping power) or exact solutions to transport equations for electron interactions. The analytical codes ignore secondary photons and electrons and their subsequent interactions. Another code, POEM [14], is a composite employing analytical treatment of photon transport and condensed Monte Carlo treatment of the electrons. Improved versions of this code include secondary photon and electron interactions. A common deficiency of all these codes is their inability to predict the emission characteristics of low energy electrons. Although these codes are "forced" to run at energies as low as 1 keV, their low energy cut-off is typically in the 5-10 keV region. This deficiency is a result of poorly known

Code	Type	Geometry	Photons		Electrons		Energy Range	
			Primary	Secondary	Primary	Secondary	Photons	Electrons
RDA Model	Analytical	Slab	τ	-----	Effective Stopping Power	Proportional to Primaries	PE Cross-Sections	Linear Extrapolation
QUICKE ₂	Analytical	Slab	τ σ κ	-----	Transport Equation	-----	1 keV to 10 MeV	\sim keV to 10 MeV
POEM	Composite	Slab Normal Incidence	τ σ'	F	PE Auger Compton (C/MC)	σ_e σ_{in} Knock-on	\sim keV to \sim MeV	\sim keV to \sim MeV
SANDYL	Monte Carlo	General	τ σ_r σ κ	F Compton K AN Brems	PE Auger Compton Pair (MS/CSD)	σ_e σ_{in} Knock-on Brems SS & MS	\sim keV to \sim MeV	\sim I _k to 15 MeV

τ Photoelectric (PE) Cross Section
 σ , σ' , σ_r Compton Cross Sections
 κ Pair Production Cross Section
F X-ray Fluorescence
I_k K-Shell Ionization Potential
C/MC Condensed Monte Carlo
MS Multiscattering
CSD Continuous Slowing Down
SS Single Scattering
 $\sigma_{e,in}$ Elastic or Inelastic Scattering

Table 1. Code Characteristics



X-ray and electron interaction cross sections at these low energies as well as the complications introduced by the dominance of multi-scattering processes at low energy for the primary and secondary electrons.

Other measurements and comparisons with code predictions have been made on materials and at photon energies outside the range of interest for the satellite applications [15,16,17]. These experiments have often employed MeV photon energies typical of medical diagnostic equipment and have studied the distribution of electrons emitted from bone, lead (source shielding) and lucite to determine tissue dose distributions. In addition Bernstein [18,19] has performed a series of measurements employing pulsed and steady state sources of extremely low energy X rays (<5 keV) to determine emission characteristics of various conducting and nonconducting materials using a plasma radiation source.

Specific Objective

The specific objective of this experimental work is to develop and employ a technique to measure directly the yield, energy distribution and angular distribution of X-ray induced electron emission from various materials. Experimental results will be compared with previous measurements, where they exist, and with

X-ray and electron interaction cross sections at these low energies as well as the experimental limitations by the design of the electron gun and the geometry of the target for the primary and secondary electrons. Other measurements and comparisons with other results have been made on materials and at photon energies outside the range of interest for the satellite applications (1,2,3,4). These experiments have often employed MeV photon energies typical of medical diagnostic equipment and have studied the distribution of electron emission from thin, lead (source shielding) and tissue to determine tissue dose distributions. In addition Bernstein (1,2,3) has performed a series of measurements employing pulsed and steady state sources of extremely low energy X rays (0.2 KeV) to determine emission characteristics of various conducting and nonconducting materials using a plasma radiation source.

Specific Objective

The specific objective of this experimental work is to develop and employ a technique to measure directly the yield, energy distribution and angular distribution of X-ray induced electron emission from various materials. Experimental results will be compared with previous measurements, where they exist, and with

analytical predictions where predictive capability matches the measurement range.

The measurement instrument has been designed and fabricated to make simultaneous determination of electron emission yield and energy distributions at four discrete emission angles, markedly increasing the efficiency of data accumulation relative to other techniques. Its configuration is adaptable to measuring both forward and reverse emission (relative to the direction of incident X rays) over a limited range of X-ray incidence angles. Measurements presented here are limited to reverse emission from normal incidence X rays, a condition of fundamental importance in understanding electron emission characteristics. Extension of the electron energy range over which these measurements are made allows intercomparison with existing data, but more importantly, the determination of yield below a few keV provides an experimental data base previously missing. This experimental information is important for comparison with analytical calculations to determine the validity of the various computer codes which are presently used to predict electron emission as a first step in calculating SGEMP response. Limited predictive capability of available codes at X-ray and electron energies below a few keV contribute to

unacceptably large uncertainties in response calculations.

Data for materials of particular interest to satellite applications have been included in these measurements. The dielectrics studied represent an important, widely used class of materials which have received inadequate attention in previous investigations.

Experimental Approach

The experimental technique is based on magnetic analysis of the energy of the emitted electrons. The analysis is done in a semicircular magnetic spectrograph, configured to define specific emission angles relative to the direction of the incident photon beam and surface normal of the target. Target materials are placed in the beam to obtain the emission characteristics at normal incidence. Emission yields are measured in terms of the number of electrons of energy E at selected emission angles θ_k for specified conditions of target material and orientation relative to the photon beam. Measurements are made using a photon source of known intensity and energy distribution.

The photons are generated by a constant potential industrial radiographic X-ray unit employing a tube rated at 2.5 kW at 100 kV potential. The tube contains a tungsten anode and X rays exit through a beryllium window. X-ray flux and energy spectrum are measured by a NaI scintillation detector in conjunction with a multi-channel analyzer. The materials to be investigated are placed in the evacuated spectrograph body with the collimated X-ray beam entering through a thin Mylar window. Vacuum conditions are maintained by a mechanical roughing pump and a gas absorption pump. The variable magnetic field required for energy analysis of the emitted electrons is established by an electromagnet enclosing the spectrograph body. "Windowless" helical channel electron multipliers (Channeltrons or CEM) are used in the pulse saturation mode as electron counters. The output of these detectors is fed through amplifiers to scalers. (This experimental setup is shown schematically in Fig. 3).

The X-ray source generates a bremsstrahlung spectrum with a maximum energy variable from 25 keV to 100 keV. Instrument calibration permits reliable detection of electrons in the energy range 100 eV to a few hundred keV. Data are obtained by counting for a predetermined period at a given magnetic field strength for a number of field intensities. The electron energy

The photons are generated by a constant potential industrial radiographic X-ray unit employing a tube rated at 1.5 W at 100 kV potential. The tube contains a tungsten anode and X rays exit through a beryllium window. X-ray flux and energy spectrum are measured by a NaI scintillation detector in conjunction with a multi-channel analyzer. The analyzer, to be investigated are placed in the evacuated spectrograph body with the collimated X-ray beam entering through a thin Mylar window. Vacuum conditions are maintained by a mechanical roughing pump and a gas absorption pump. The variable magnetic field required for energy analysis of the emitted electrons is established by an electromagnet enclosing the spectrograph body. "Windowless" helical channel electron multipliers (Channeltrons or CHN) are used in the pulse saturation mode as electron counters. The output of these detectors is fed through amplifiers to scalars. (This experimental setup is shown schematically in Fig. 3).

The X-ray source generates a bremsstrahlung spectrum with a maximum energy variable from 25 keV to 100 keV. Instrument calibration points reliable detection of electrons in the energy range 100 eV to a few hundred keV. Data are obtained by counting for a predetermined period at a given magnetic field strength for a number of field intensities. The electron energy

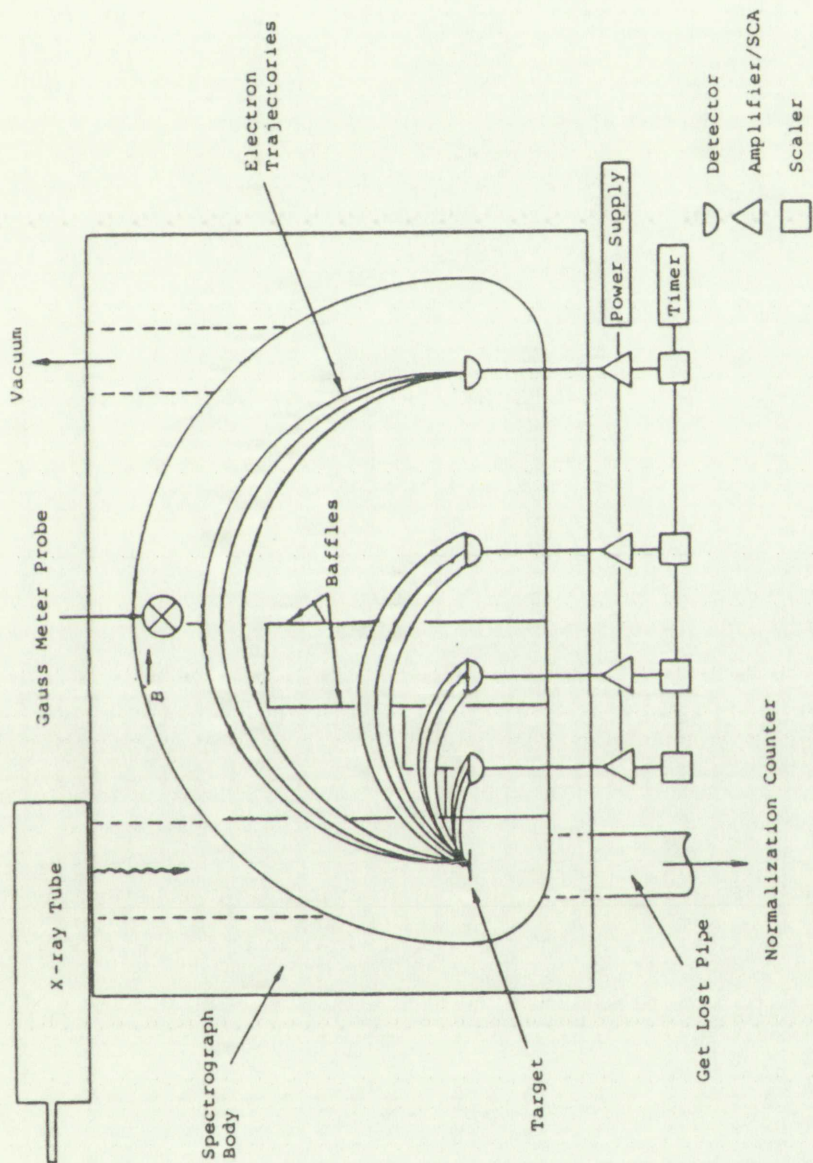
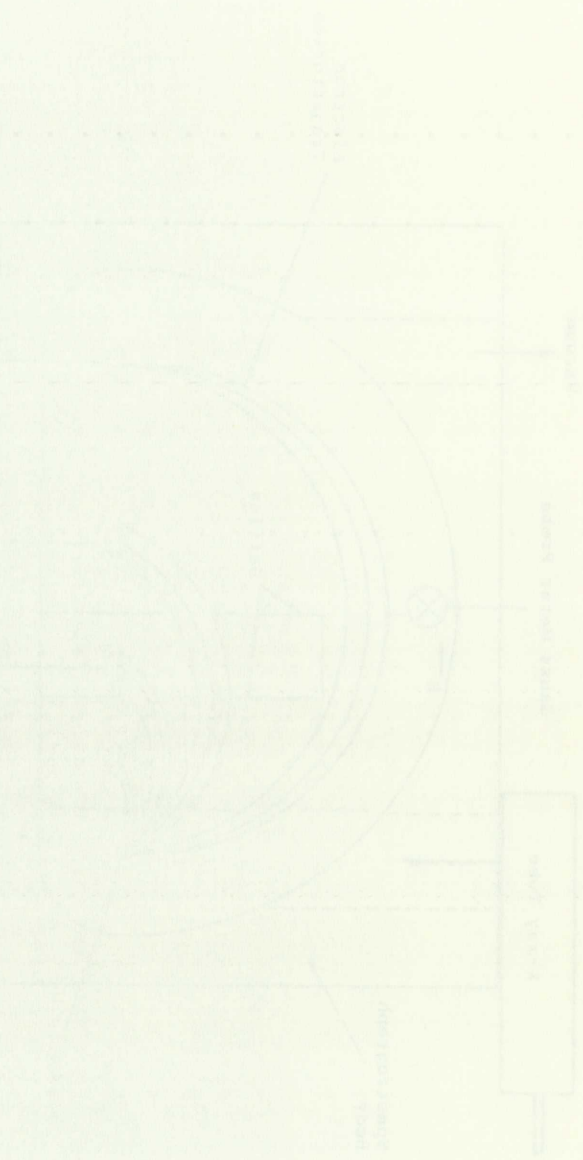


FIGURE 3. Experimental Set-up

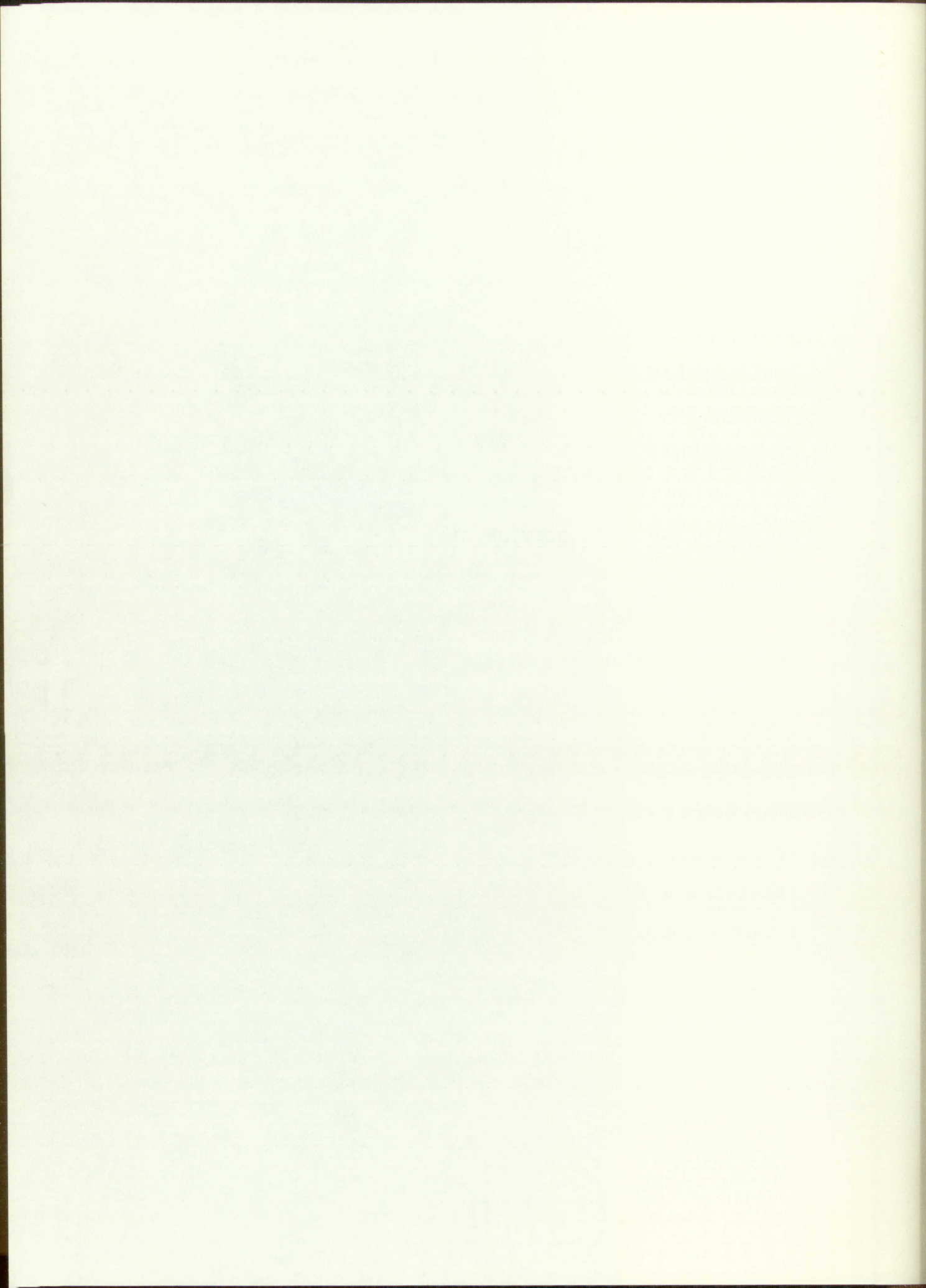


spectrum is constructed in a stepwise fashion. The targets were thick compared to the range of the most energetic electrons created by the X-ray interactions. Investigation of backward emission under these conditions maximizes the effect on the yield due to multiple scattering events. Representative metals investigated for backward emission characteristics were magnesium, aluminum, copper, tantalum and lead. Measurements were also made on the following materials used extensively in satellite construction: Mylar, silica cloth (external thermal blanket), SiO_2 (solar cell cover glass), Kevlar (antenna dishes), conducting and nonconducting epoxies (structural members) and a conducting paint (thermal control surface).

The remainder of the dissertation describing this effort is organized as follows: Section II details the spectrograph design and describes experimental equipment. Section III discusses instrument calibration. Section IV contains the experimental results and Section V concludes with interpretation of results, comparisons with existing data and a summary.

specimen is mounted in a special holder. The
specimen was then exposed to the range of the
energetic electron beam by the X-ray instrument.
Investigation of the electron beam under the
condition of the electron beam on the specimen
surface is necessary. The electron beam is
investigated for backward emission characteristics
magnesium, aluminum, copper, carbon and lead.
Measurements were first made on the following materials
used extensively in nuclear construction: Al, Fe, Cu,
Ni, Pb, Zn, Ag, Au, Pt, W, Mo, Ti, Zr, Nb, Ta, V, Cr,
Mn, Co, Ni, Cu, Zn, Al, Si, P, S, Cl, Br, I, As,
Se, Te, Ge, Sn, Pb, Bi, Po, At, Rn, Fr, Ac, Th,
Pa, U, Np, Pu, Am, Cm, Bk, Cf, Es, Fm, Md, No, Lr,
conducting paint (thermal conductive material).
The remainder of the dissertation describing this
effort is organized as follows: Section II details the
spectrograph design and describes experimental
equipment. Section III discusses instrument
calibration. Section IV contains the experimental
results and Section V concludes with interpretation of
results, comparisons with existing data and a summary.

SECTION II



SPECTROGRAPH DESIGN

Basic Instrument

Basic design parameters and theory of standard semicircular magnetic spectrographs are described by Siegbahn [20]. In its simplest form, such a device consists of a source of energetic charged particles, defining slits which define a beam of particles in the plane of the spectrograph, deflecting magnets producing a field perpendicular to the particle trajectories and a means of detection arranged in such a way that particles in the beam with equal radii of curvature in the magnetic field will be focused on the detectors after traversing a semicircular path. Depending on the application intended, such devices can be made for high-resolution beta spectrometry or other charged particle analysis. Various detectors can be employed (photographic plates, nuclear emulsions, GM tubes, solid state detectors, photo multipliers, Faraday cups, etc.) and several operating configurations (relative locations of source and detector) are possible. The basic advantages of the single focusing semicircular spectrometer are simplicity of design and operation, accuracy of magnetic field control and measurement,

Basic Instrument

Basic Design Features

Sample Preparation Methods

Signal Processing

Consists of a source of radio frequency energy

defining slice with a magnetic field

plane of the slice, and a means of detection

a field perpendicular to the plane of the slice

means of detection and a means of detection

in the beam with a means of detection

magnetic field with a means of detection

traversing a radio frequency field

rotation in the plane of the slice

high-resolution image of the slice

particle analysis of the slice

(photographic plate) of the slice

state detector, photo detector, photo detector

and several optical systems

of source and detector

advantages of the system

spectrometer

accuracy of measurement

adaptability to various detector types and ease of calibration.

The fundamental scalar equation governing the behavior of electrons in the constant magnetic field region of the spectrograph is

$$\frac{mv^2}{\rho} = qvB \quad (5)$$

where m is the relativistic mass of the electron, ρ the radius of curvature of the electron trajectory, q the electronic charge, v the velocity component in the plane of the spectrograph determined by the electron kinetic energy upon emission from the surface of the source and B is the uniform magnetic field perpendicular to the spectrograph plane. Based on Fig. 4, two important quantities describing performance parameters of a semicircular spectrograph with a finite source of width s are as follows:

$$R^\circ = \frac{s}{2\rho} + \frac{\phi^2}{2} \quad (6)$$

$$\Omega = \frac{\phi\psi}{\pi} \quad (7)$$

These quantities are strictly determined by the instrument geometry and can be determined by simple physical measurement. The resolution can be readily

adaptability to various detector types and calibration.

The fundamental scalar equation governing the behavior of electrons in the constant magnetic field region of the spectrograph is

$$\frac{mv^2}{p} = \frac{e\hbar}{2m} \quad (15)$$

where m is the relativistic mass of the electron, p the radius of curvature of the electron trajectory, v the electronic charge, v the velocity component in the plane of the spectrograph determined by the electron kinetic energy upon emission from the surface of the source and B is the uniform magnetic field perpendicular to the spectrograph plane. Based on Fig. 4, two important quantities describing performance parameters of a semicircular spectrograph with a finite source of width a are as follows:

$$R^* = \frac{a}{2p} + \frac{a^2}{2} \quad (16)$$

$$p = \frac{e\hbar}{2m} \quad (17)$$

These quantities are strictly determined by the instrument geometry and can be determined by simple physical measurement. The resolution can be readily

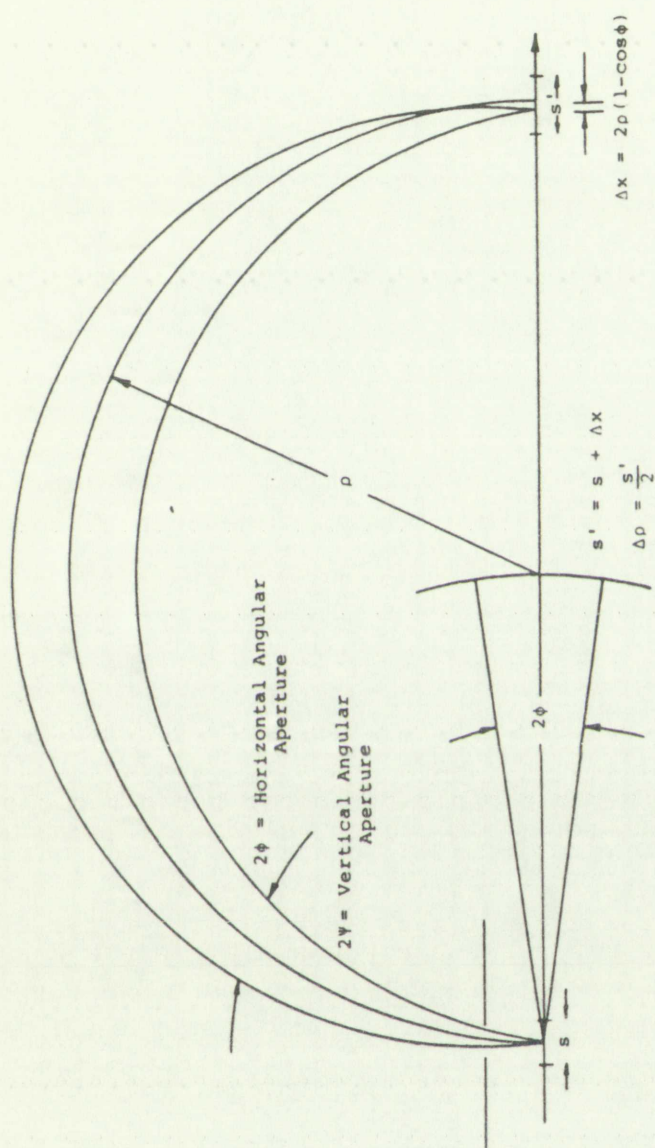


FIGURE 4. Basic Instrument Geometry

confirmed by calibration measurements with appropriate sources. The base resolution R^0 determines the range of acceptable values of ρ (at fixed B) which can be detected by the instrument. The spread in the $B\rho$ values ($\Delta B\rho$) divided by $B\rho_0$ is the momentum resolution of the device. For instruments with fixed geometry in which the magnetic field is a variable, the momentum resolution is a constant. Ω defines the solid angle determined by the height and width of the defining slit. Since the slit openings are normally small compared to the electron path length from the source to the slits, the area defined by the aperture is approximately $4\ell^2\phi\psi$ where ℓ is the path length to the aperture and 2ϕ and 2ψ are the horizontal and vertical angular apertures, respectively. The fraction of the total 4π solid angle is then given by equation 7.

Modifications for Yield, Emission Angle and Energy Determination

The instrument used in these measurements is an adaptation of a semicircular magnetic spectrograph. The coordinate system used to describe the trajectories of the electrons within the spectrograph is shown in Fig. 5. The target is represented by the rectangle in the X,Z plane at the origin of the coordinate system with \vec{n}

controlled by means of a control system.

The input signal is a function of the position of the

object being measured.

The output signal is a function of the position of the

object being measured.

The output signal is a function of the position of the

object being measured.

The output signal is a function of the position of the

object being measured.

The output signal is a function of the position of the

object being measured.

The output signal is a function of the position of the

object being measured.

The output signal is a function of the position of the

object being measured.

The output signal is a function of the position of the

object being measured.

The output signal is a function of the position of the

object being measured.

The output signal is a function of the position of the

object being measured.

The output signal is a function of the position of the

object being measured.

The output signal is a function of the position of the

object being measured.

The output signal is a function of the position of the

object being measured.

The output signal is a function of the position of the

object being measured.

The output signal is a function of the position of the

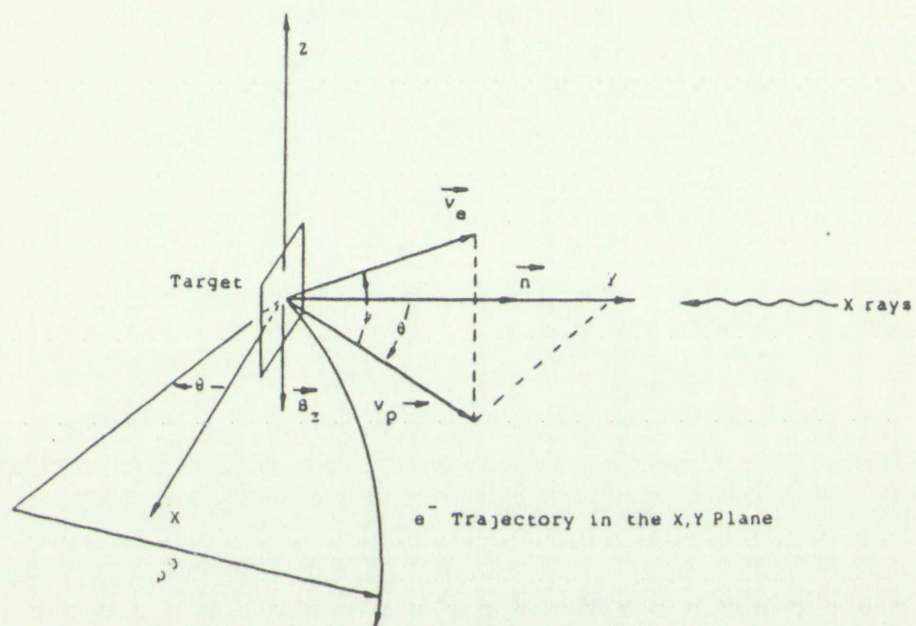


FIGURE 5. Spectrograph Coordinate System



FIGURE 2. Spectrograph Coordinate System

defining the surface normal. Electrons are emitted with a velocity vector \vec{v}_e forming angle ψ with respect to the plane of the spectrograph (X,Y plane) and whose component in the spectrograph plane forms angle θ with respect to \vec{n} . Electron trajectories with radius of curvature ρ_0 are described in the plane of the spectrograph as determined from equation 5 by $|\vec{v}_p|$ and the magnitude of the magnetic field $|\vec{B}_z|$ perpendicular to the plane of the spectrograph.

The fundamental adaptation to the basic design was to define four separate channels viewing different emission angles relative to the target normal. This was done by locating defining slits (primary and secondary) and detectors for each emission angle θ in accordance with Fig. 6. From this figure, it is seen that in terms of emission angle in the plane of the spectrograph, coordinates x_i, y_i (an edge of a defining slit) and a radius of curvature ρ of a trajectory passing through (0,0) and (X,Y),

$$\rho^2 = x_b^2 + y_a^2 \quad (8)$$

$$y_a = Y + \rho \sin \theta \quad (9)$$

$$x_b = \rho \cos \theta - X \quad (10)$$

defining the angle θ between the velocity vector \vec{v} and the normal to the plane of the aperture \vec{n} (Fig. 1). The angle θ is determined by the radius of curvature R of the trajectory passing through the point $P(x, y)$ and the coordinates x, y of the point P relative to the origin $O(0, 0)$ of the coordinate system Ox, Oy (Fig. 1). The angle θ is determined by the radius of curvature R of the trajectory passing through the point $P(x, y)$ and the coordinates x, y of the point P relative to the origin $O(0, 0)$ of the coordinate system Ox, Oy (Fig. 1). The angle θ is determined by the radius of curvature R of the trajectory passing through the point $P(x, y)$ and the coordinates x, y of the point P relative to the origin $O(0, 0)$ of the coordinate system Ox, Oy (Fig. 1).

The fundamental adaptation to the basic design was to define four separate channels viewing different emission angles relative to the target normal. This was done by locating detector units (primary and secondary) and detectors for each emission angle θ in accordance with Fig. 2. From this figure, it is seen that in terms of emission angle to the plane of the aperture, coordinates x, y and edge of a defining slit and a radius of curvature R of a trajectory passing through $O(0, 0)$ and (x, y) .

$$R^2 = x^2 + y^2 \quad (8)$$

$$y = R \sin \theta \quad (9)$$

$$x = R \cos \theta \quad (10)$$

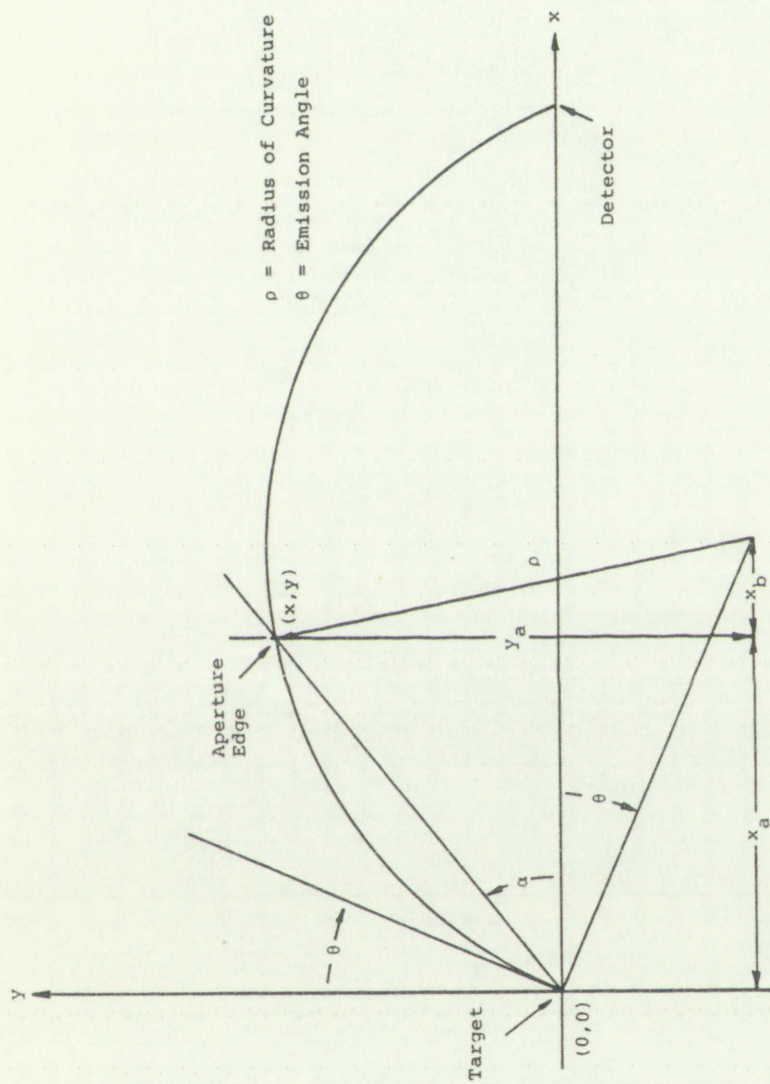


FIGURE 6. Target--Aperture--Detector Geometry

Table 2. Primary and Secondary Slit Parameters

Emission Angle	Type	X ₁ (cm)	Y ₁ (cm)	X ₂ (cm)	Y ₂ (cm)
0°	Primary	10.00	10.26	10.00	9.74
0°	Secondary	19.90	2.57	19.91	2.44
30°	Primary	8.66	5.08	8.66	4.92
30°	Secondary	15.85	2.07	15.72	1.95
45°	Primary	7.07	2.96	7.07	2.90
45°	Secondary	12.16	1.58	12.12	1.51
60°	Primary	5.00	1.35	5.00	1.33
60°	Secondary	7.67	.99	7.66	.96

Wavelength (nm)	Y ₁ (cm)	Y ₂ (cm)	Y ₃ (cm)	Y ₄ (cm)	Y ₅ (cm)
600	1.41	1.41	1.41	1.41	1.41
500	2.00	2.00	2.00	2.00	2.00
400	3.12	3.12	3.12	3.12	3.12
300	4.00	4.00	4.00	4.00	4.00
200	12.00	12.00	12.00	12.00	12.00
100	0.00	0.00	0.00	0.00	0.00
0	15.00	15.00	15.00	15.00	15.00
0	10.00	10.00	10.00	10.00	10.00

Figure 1. Schematic diagram of the experimental setup.

Table 3. Angular Acceptance Band Parameters

Emission Angle	Source Position (cm)	ρ_1 (cm)	ρ_2 (cm)	ρ_3 (cm)	ρ_4 (cm)	$\Delta\theta_{\max}$	$\int_{\rho_1}^{\rho_4} \Delta\theta d\rho$ (cm)
0°	(-1, 0, 0)	9.80	9.86	10.24	10.31	.041	.0177
0°	(0, 0, 0)	9.75	9.80	10.18	10.25	.041	.0175
0°	(1, 0, 0)	9.70	9.74	10.13	10.19	.041	.0178
30°	(-1, 0, 0)	9.85	10.10	10.10	10.37	.0175	.00442
30°	(0, 0, 0)	9.75	10.00	10.00	10.25	.0175	.00463
30°	(1, 0, 0)	9.65	9.9	9.9	10.15	.0175	.00475
45°	(-1, 0, 0)	9.89	10.14	10.14	10.40	.0090	.00229
45°	(0, 0, 0)	9.75	9.99	9.99	10.25	.0090	.00225
45°	(1, 0, 0)	9.61	9.85	9.85	10.10	.0090	.00220
60°	(-1, 0, 0)	9.99	10.23	10.23	10.50	.0034	.000893
60°	(0, 0, 0)	9.75	9.99	9.99	10.25	.0036	.00100
60°	(1, 0, 0)	9.50	9.74	9.74	9.98	.0038	.000936

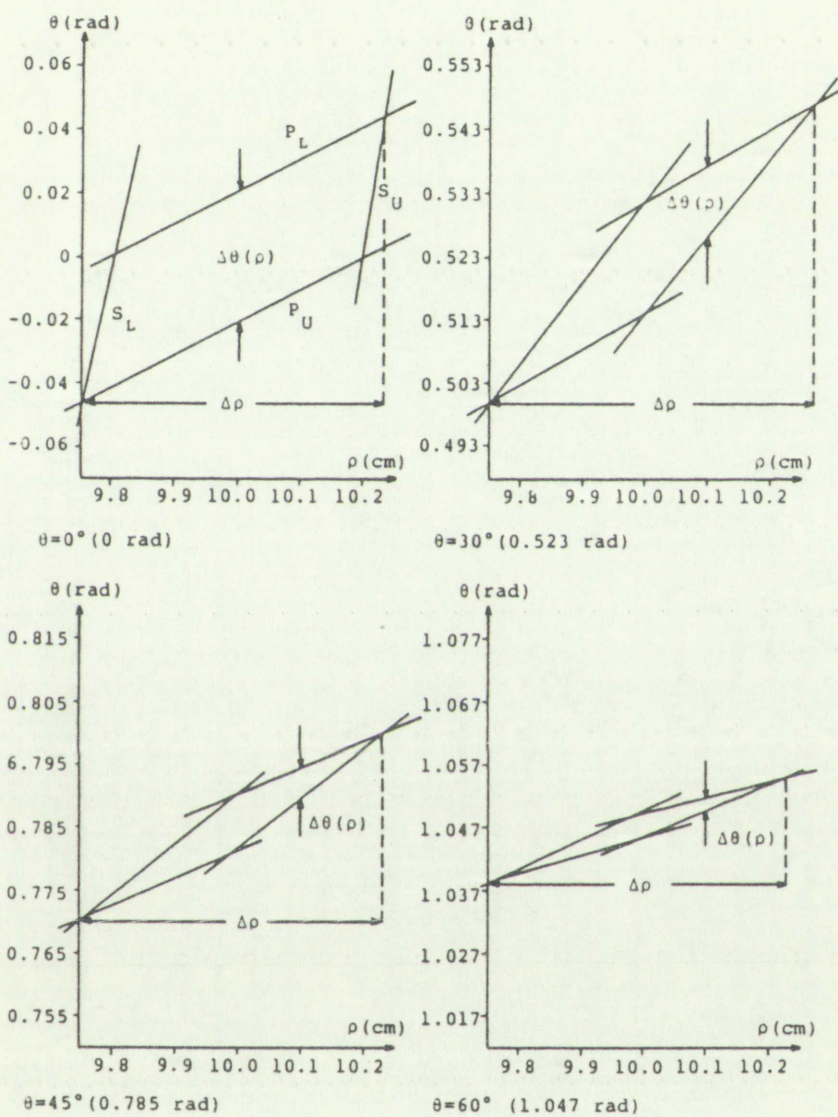


FIGURE 7. ρ, θ Acceptance Bands at $0^\circ, 30^\circ, 45^\circ$, and 60° Emission Angles



FIGURE 1. Acceptance Band at 0°, 10°, 15°, and 60° Emission Angles

and

$$\tan \alpha = \frac{Y}{X} \quad (11)$$

These equations reduce to

$$\cos(\theta + \alpha) = \frac{(X^2 + Y^2)^{\frac{1}{2}}}{2\rho} \quad (12)$$

Angular acceptance bands as a function of ρ and the coordinates of the primary and secondary defining slits can now be calculated from equation 12. Table 2 gives the primary and secondary defining slit parameters, and Table 3 contains the angular acceptance band parameters for source locations corresponding to the finite extent of the target, the value of $\Delta\theta_{\max}$ and the area of the acceptance bands. Fig. 7 shows the predicted acceptance bands for a source located at (0,0). The acceptance bands are obtained from equation 12 by plotting the values of θ as a function of ρ for specific locations of primary and secondary defining slits. The line marked P_U is determined by the upper edge of the primary, P_L is determined by the lower edge of the primary and S_U and S_L by the corresponding edges of the secondaries. Notice the anticipated response curve from a monoenergetic source for such an arrangement would consist of no response for $\rho < \rho_1$, a linear rise in response from ρ_1 to ρ_2 , flat response from ρ_2 to ρ_3 , a

$$(11) \quad \text{and } \frac{1}{2}$$

These equations reduce to

$$(12) \quad \text{and } \frac{1}{2}$$

Angular acceptance bands as a function of θ and the co-ordinates of the primary and secondary defining sites can now be calculated from equation 12. Table 2 gives the primary and secondary defining site parameters, and Table 3 contains the angular acceptance band parameters for source locations corresponding to the limits of extent of the target, the value of θ_{\max} and the area of the acceptance bands. Fig. 7 shows the predicted acceptance bands for a source located at (0,0). The acceptance bands are obtained from equation 12 by plotting the values of θ as a function of ϕ for specific locations of primary and secondary defining sites. The line marked θ_0 is determined by the upper edge of the primary, θ_1 is determined by the lower edge of the primary and θ_2 and θ_3 by the corresponding edges of the secondary. Notice the anticipated response curve from a nonenergetic source for each an arrangement would consist of no response for $\theta < \theta_0$ a linear rise in response from θ_0 to θ_1 , a constant response from θ_1 to θ_2 , a

linear decrease from ρ_3 to ρ_4 and no response for $\rho > \rho_4$. (This predicted behavior will be examined experimentally in Section III). In a manner similar to that described for the simple semicircular spectrograph, the baseline resolution is given by

$$\frac{\Delta\rho}{\rho_0} = \frac{\rho_4 - \rho_1}{\rho_0} \quad (13)$$

For the configuration used, the value of $\Delta\rho/\rho_0$ for each channel for a source located at (0,0) is approximately 0.05.

The use of the secondary defining slits between the primary slits and the detector is necessitated by the mounting arrangement of the detectors and their finite extent. Without the secondary slits serving as a detector aperture, the entire detector area would be available to intercept electrons which had passed through the primary. The detector width (1 cm) relative to the target width (0.2 cm) would significantly degrade the energy resolution since electrons with a larger range of B_ρ values would be accepted. In addition, the secondary apertures prevent off-trajectory electrons from striking the detector mount surrounding the detector opening thus eliminating a source of secondary electrons which would be counted by the detectors. Definition of the vertical extent of the beam is accomplished at the primary aperture. The geometry for

linear detector from $\theta = 0$ and an response for $\theta = \pi$. This predicted behavior will be compared experimentally in Section III. In a manner similar to that described for the single channel spectrograph,

the baseline response is given by

$$B_0 = \frac{1}{2} \left(\frac{1}{\sin \theta} + \frac{1}{\sin \pi} \right) \quad (1)$$

For the configuration used, the value of B_0 for each channel for a source located at $(0,0)$ is approximately 0.65.

The use of the secondary defining slit between the primary slit and the detector is necessitated by the mounting arrangement of the detectors and their finite extent. Without the secondary slit serving as a detector aperture, the entire detector area would be available to intercept electrons which had passed through the primary. The detector width (1 cm) relative to the target width (0.5 cm) would significantly degrade the energy resolution since electrons with a larger range of B_0 values would be accepted. In addition, the secondary apertures prevent off-trajectory electrons from striking the detector mount surrounding the detector opening thus eliminating a source of secondary electrons which would be counted by the detectors. Definition of the vertical extent of the beam is accomplished at the primary aperture. The geometry for

vertical collimation as a function of the source height h_s , height of the primary aperture h_p (placed midway along the electron path length from target to detector) and detector height h_d is shown in Fig. 8. The detector height is selected in such a way that any electron leaving the source and passing through h_p is intercepted by the detector. It is seen that the source height is given by

$$h_s = h_d - 2h_p \quad (14)$$

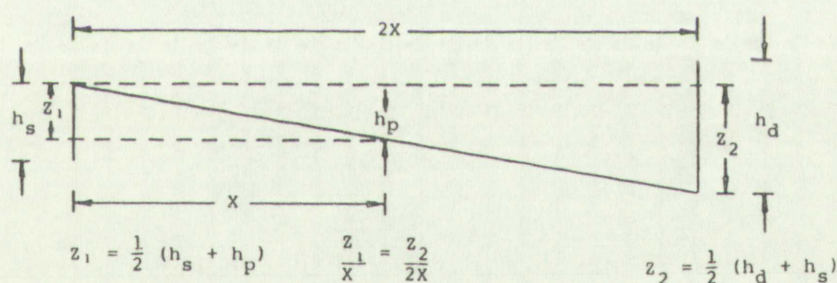


FIGURE 8. Vertical Collimation Geometry

The detector response r as a function of source height and primary aperture height is proportional to their product. That is

vertical collision and a function of the source height h_s . Height of the primary aperture h_p is fixed along the electron path length from source to detector and detector height h_d is shown in fig. 2. The detector height is selected in such a way that any electron leaving the source and passing through h_p is intercepted by the detector. It is seen that the source height is given by

$$h_s = h_d - h_p \quad (11)$$

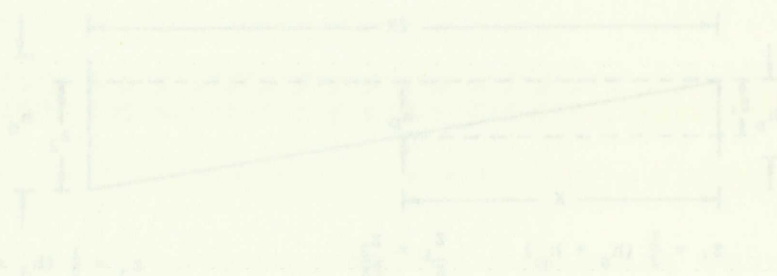


FIGURE 2. Vertical Collision Geometry

The detector response r as a function of source height and primary aperture height is proportional to their product. That is

$$r \propto h_s h_p \quad (15)$$

To maximize the response, equation 14 is substituted in equation 15, the result differentiated with respect to h_p and set equal to zero. From this it is found that

$$h_s = \frac{h_d}{2} \quad (16)$$

and

$$h_p = \frac{h_d}{4} \quad (17)$$

The final internal configuration of the spectrograph included two other sets of isolation barriers in addition to the primary and secondary apertures. The functions of these barriers were to (1) minimize virtual sources of electrons "seen" by the primary aperture resulting from scattered X rays within the spectrograph; (2) suppress the number of "noise" electrons emitted from the target or scattered within the target region from reaching the primary aperture and (3) isolate the individual channels from one another. The first two functions were performed by a baffle isolating the target region from the primary apertures. This baffle consisted of a lead sheet (covered on the target and aperture sides by low-Z material) with openings provided

To maximize the response, equation (1) is substituted in equation (2), the result being differentiated with respect to θ and set equal to zero. From this it is found that

$$\frac{d\theta}{d\theta} = \frac{d\theta}{d\theta} \quad (10)$$

and

$$\frac{d\theta}{d\theta} = \frac{d\theta}{d\theta} \quad (11)$$

The final internal configuration of the spectrograph included two other sets of isolation barriers in addition to the primary and secondary apertures. The functions of these barriers were to (1) minimize virtual sources of electrons "seen" by the primary aperture resulting from scattered X rays within the spectrograph; (2) suppress the number of "noise" electrons emitted from the target or scattered within the target region from reaching the primary aperture and (3) isolate the individual channels from one another. The first two functions were performed by a baffles isolating the target region from the primary aperture. This baffle consisted of a lead sheet (mounted on the target and aperture sides by ion-2 material) with openings provided

such that beam definition by the primaries was not compromised. Isolation between channels was provided by thin aluminum barriers placed between the primary apertures and the detectors which separated a detector region from its neighbors. The resulting "trajectory tubes" are open to electrons at the primary aperture, enclose the secondary aperture between the primary and the detector and terminate in the detector itself. The arrangement of target, barriers, apertures and detectors within the spectrograph are shown in Fig. 9.

such light beam defined by the prism was not
compensated. Isolation between channels was provided by
thin aluminum barriers placed between the primary
apertures and the detectors which separated a detector
region from its neighbors. The resulting detector
tubes are open to electrons at the primary aperture,
enclose the secondary aperture between the primary and
the detector and terminate in the detector itself. The
arrangement of target, barrier, apertures and detectors
within the spectrograph are shown in Fig. 5.

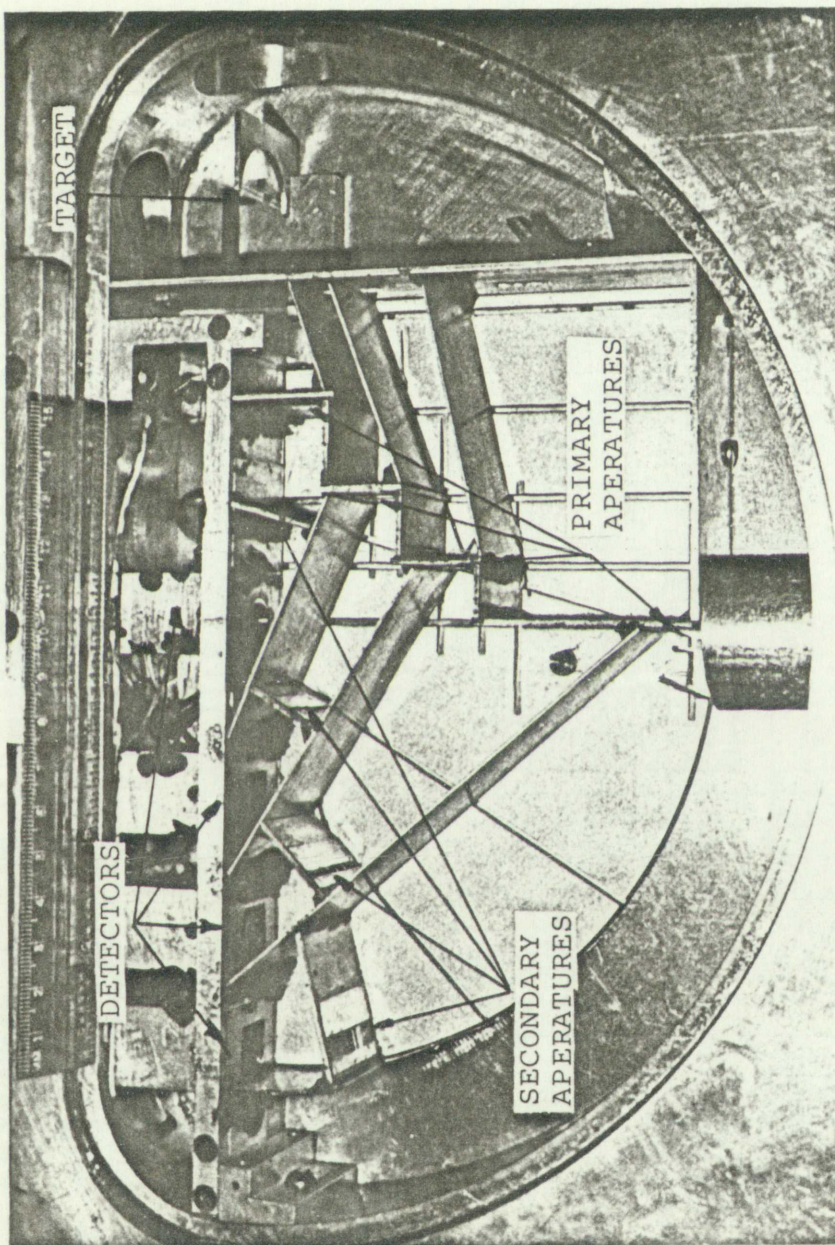


FIGURE 9. Spectrograph Configuration

FIGURE 3. Spectral energy distribution



SECTION III

SECTION III

INSTRUMENT CALIBRATION

X-ray Source Characteristics

Any attempt to measure the yield of photon induced electron emission in an absolute sense (i.e., electrons emitted per incident photon) requires certain knowledge of the photon source. Ideally, intense monoenergetic X rays of known intensity should be used. Practical limitations imposed by X-ray source strength and electron emission efficiencies dictate the use of sources with X rays distributed in energy. With this constraint the minimum information required about the X-ray source is the total number of photons incident on the target. Information regarding the spectral distribution is of value for intercomparison of experimental data and comparison with calculations from computer codes which will accommodate photon energy distributions. Qualitative and semi-quantitative evaluation of the relative importance of photon energy in emission efficiency also requires knowledge of the X-ray energy spectrum.

For the purpose of initial experimental determination of the beam intensity, energy distribution and spatial distribution, the X-ray source was set up as follows: The X-ray tube was placed in the position it

X-ray Source Characterization

Any attempt to measure the yield of photon induced electron emission is an absolute measurement. The electron emitted per incident photon requires a knowledge of the photon source. Ideally, the photon source is a source of known intensity which is used. Practical limitations imposed by X-ray sources, however, and electron emission efficiencies hinder the use of sources with X rays distributed in energy. With this constraint the minimum information required about the X-ray source is the total number of photons incident on the target. Information regarding the spectral distribution is of value for intercomparison of experimental data and comparison with calculations. Computer codes which will accommodate photon energy distributions. Qualitative and semi-quantitative evaluation of the relative importance of photon energy in emission efficiency also requires knowledge of the X-ray energy spectrum.

For the purpose of initial experimental determination of the beam intensity, energy distribution and spectral distribution, the X-ray source was set up as follows: The X-ray tube was placed in the position of

occupies during backward emission measurements with a lead collimator used to define the beam. Because of the detection method used and the intensity of the source, the detector was placed a significant distance from the source and the detector area severely restricted. (See Fig. 10). Detector output was routed through a preamp to a linear amplifier. Direct output from the amplifier was sent to a 400 channel analyzer and the multichannel analyzer coupled to an X-Y plotter. In parallel with the direct output, a signal was routed to a single channel analyzer and from the SCA to a scaler. To further reduce the beam intensity the X-ray generator was operated at 1 ma current. These restrictions permitted measurements to be made of the source output at 25, 50 and 100 kV potential at counting rates below saturation level of the electronics.

Energy calibration points for the X-ray pulse height distributions were obtained using isotopes of cesium and americium. Cs^{137} and Am^{241} give usable reference energies of 32 and 8 keV (Cs^{137} ; $\text{BaK}\alpha/\text{BaK}\beta$ and iodine $\text{K}\alpha$ escape) and 60, 31.5 and 18 keV (Am^{241} ; γ_1/γ_2 , iodine $\text{K}\alpha$ escape and $\text{NpL}\beta$ X rays). The single channel analyzer (SCA) "window" was established by a precision pulser and was set to cover the energy range resulting from a given X-ray tube potential. Resolution of the scintillation detector as a function of energy was

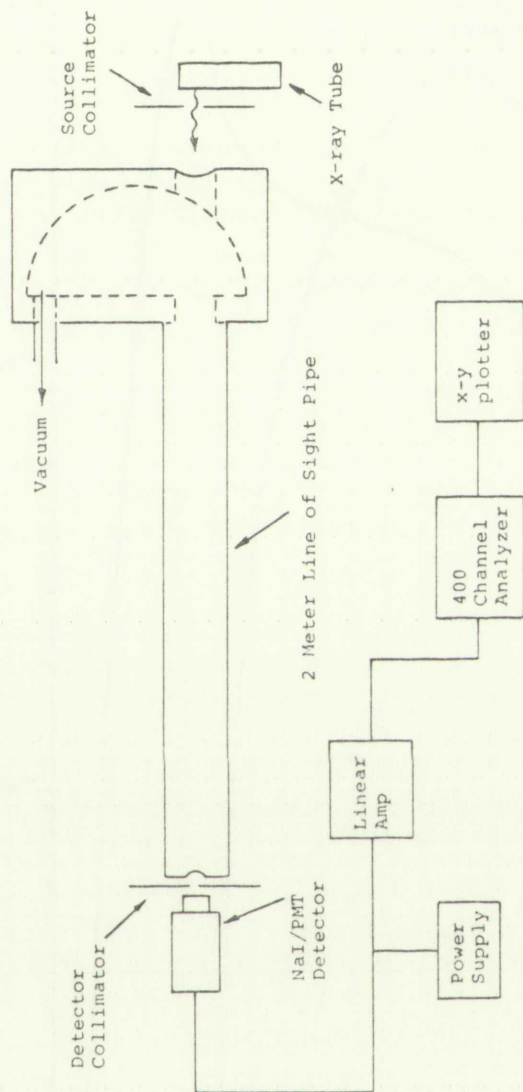


FIGURE 10. Absolute Flux Measurement

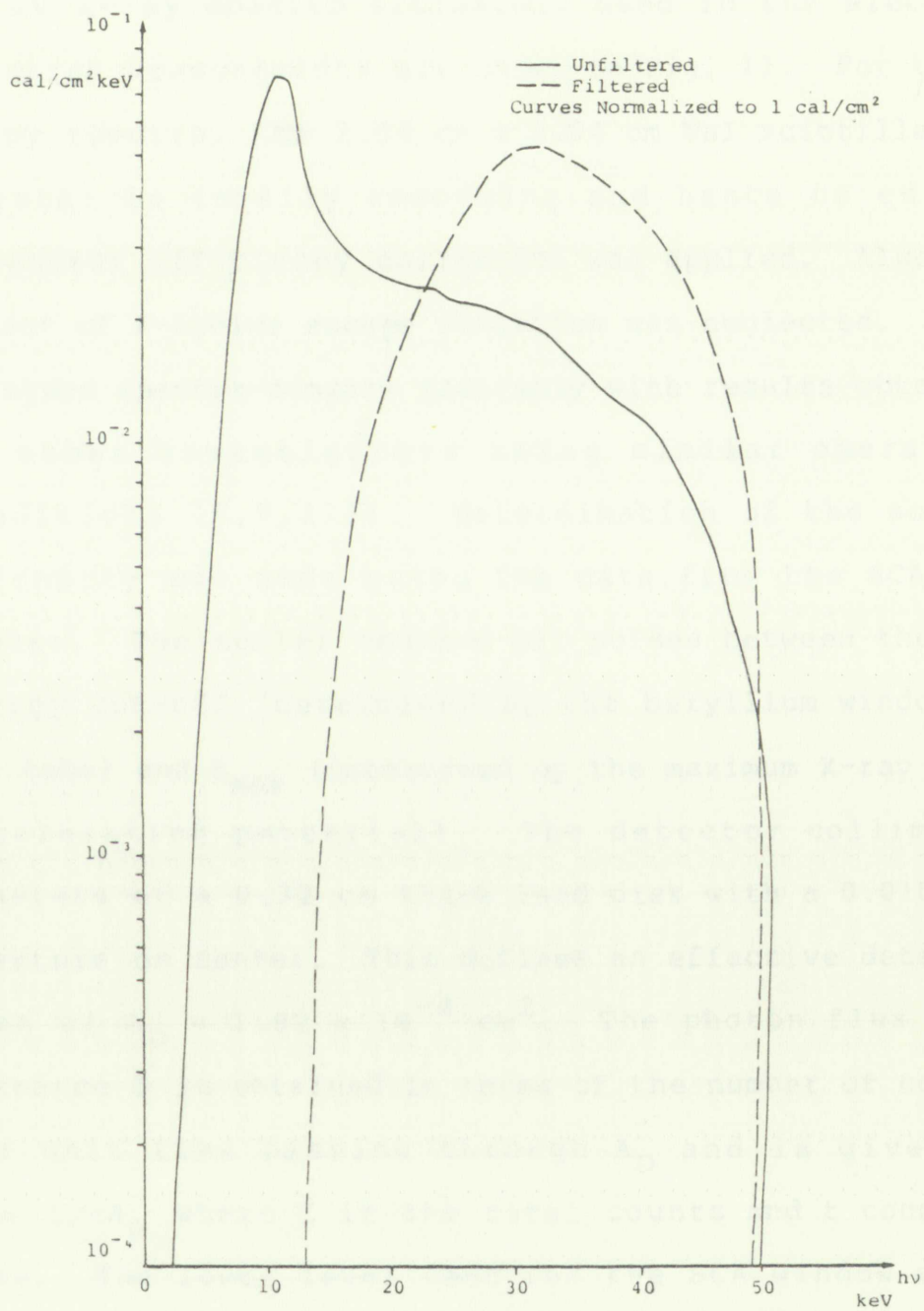


FIGURE 11. X-Ray Energy Distribution.



FIGURE 11. X-Ray Energy Distribution

determined using the isotopes above and information provided by the manufacturer. The filtered and unfiltered 50 kV X-ray spectra ultimately used in the electron emission measurements are shown in Fig. 11. For these X-ray spectra, the 2.54 cm x 2.54 cm NaI scintillation crystal is totally absorbing and hence no energy dependent efficiency correction was applied. Also the effect of K-iodine escape radiation was neglected. (The measured spectra compare favorably with results obtained by other investigators using similar operating conditions [8,9,21]). Determination of the source intensity was made using the data from the SCA and scaler. The scaler counted all pulses between the low energy cut-off (determined by the beryllium window in the tube) and E_{max} (determined by the maximum X-ray tube accelerating potential). The detector collimator consists of a 0.32 cm thick lead disk with a 0.0152 cm aperture on center. This defines an effective detector area of $A_D = 1.82 \times 10^{-4} \text{ cm}^2$. The photon flux at a distance D is obtained in terms of the number of counts per unit time passing through A_D and is given by $\phi_D = C/tA_D$ where C is the total counts and t counting time. The lower level used for the SCA window was 3 keV. The upper level was arbitrarily set above the maximum energy anticipated for each accelerating potential (46, 82 and 122 keV) for 25, 50 and 100 kV potentials re-

determined by the ratio of the two quantities

which is the same as the ratio of the two quantities

to be determined by the ratio of the two quantities

which is the same as the ratio of the two quantities

to be determined by the ratio of the two quantities

which is the same as the ratio of the two quantities

to be determined by the ratio of the two quantities

which is the same as the ratio of the two quantities

to be determined by the ratio of the two quantities

which is the same as the ratio of the two quantities

to be determined by the ratio of the two quantities

which is the same as the ratio of the two quantities

to be determined by the ratio of the two quantities

which is the same as the ratio of the two quantities

to be determined by the ratio of the two quantities

which is the same as the ratio of the two quantities

to be determined by the ratio of the two quantities

which is the same as the ratio of the two quantities

to be determined by the ratio of the two quantities

which is the same as the ratio of the two quantities

to be determined by the ratio of the two quantities

which is the same as the ratio of the two quantities

to be determined by the ratio of the two quantities

which is the same as the ratio of the two quantities

to be determined by the ratio of the two quantities

which is the same as the ratio of the two quantities

to be determined by the ratio of the two quantities

spectively. The photon fluxes determined in this manner with 1 ma tube current were:

<u>Tube Potential (kV)</u>	<u>$\phi_D \left(\frac{\text{photons}}{\text{cm}^2 \text{ sec}} \right)$</u>
25	7.44×10^6
50	19.38×10^6
100	54.06×10^6

The source intensity at the target position in the spectrometer (25.4 cm) was too high to measure directly with the scintillation detector. However, measurements can be made closer than $D = 198.9$ cm at 25 kV potential and 1 ma current. Using the source detector collimator and identical settings on the SCA from the previous 25 kV run, the X-ray flux was again determined, this time at $D = 50$ cm. Since the source dimensions are small compared to the source/detector separation and the detector views the entire radiating area of the source, a $1/D^2$ behavior is anticipated. The expected X-ray flux under these conditions would be 1.18×10^8 photons/cm² sec. Measured values (averaged) yielded an X-ray flux of 1.18×10^8 photons/cm² sec. This $1/D^2$ behavior is also valid at the target location (i.e., 25.4 cm source/target separation compared to a projected X-ray source spot size of 7mm x 7mm) and hence the photon flux at the target can be calculated from measurements made

respectively. The photon fluxes determined in this experiment with a 10 cm diameter were:

(continued)

1.44 x 10 ⁸	10
1.23 x 10 ⁸	50
1.06 x 10 ⁸	100

The source intensity at the target position in the spectrometer (15.4 cm) was too high to measure directly with the scintillation detector. However, measurements can be made directly at 15.4 cm at 25 kV potential and 1 mA current. When the source detector collimator and identical window on the SCA from the previous 25 kV run, the X-ray flux was again determined. This time at D = 50 cm. Since the source dimensions are small compared to the source detector separation and the detector views the entire radiating area of the source, a I/D^2 behavior is anticipated. The expected X-ray flux under these conditions would be 1.18×10^8 photons/cm² sec. Measured values (averaged) yielded an X-ray flux of 1.18×10^8 photons/cm² sec. This I/D^2 behavior is also valid at the target position (15.4 cm) and the source detector separation compared to a projected X-ray source that size at 15.4 cm and hence the photon flux at the target can be calculated from measurements made

with the scintillation detector used as a normalization counter.

Detector Characteristics

The quantum efficiency as a function of electron energy for channeltron detectors is a function of several variables associated not only with their specific design but also of the experimental configuration in which they are used. Ideally, detectors should be measured individually to determine the energy sensitivity function in their intended mounting configuration. This involves an elaborate calibration arrangement requiring an accurately controlled electron source for the absolute measurement of detector efficiency which was not available for these experiments. Other investigators have measured the quantum efficiency of several types of channeltrons and data from these investigations compare favorably with manufacturers specifications. Information supplied by the manufacturer of the detectors used in this spectrograph (Fig. 12) has been used to obtain the following expression for detector quantum efficiency.

$$\epsilon_E = \exp \left[4.5954 - (2.79306 \times 10^{-2}) \ln E - 7.7847 \times 10^{-3} E - \frac{1.15498 \times 10^{-2}}{E} \right] \quad (18)$$

with the solid-state detector used as a normalizing factor.

Detector Characteristics

The quantum efficiency as a function of photon energy for channeltron detectors is a function of several variables associated not only with their specific design but also of the experimental configuration in which they are used. Ideally, detectors should be measured individually to determine the energy sensitivity function in their intended manner. This involves an elaborate calibration arrangement requiring an accurately controlled electron source for the absolute measurement of detector efficiency which was not available for these experiments. Other investigators have measured the quantum efficiency of several types of channeltrons and data from these investigations compare favorably with manufacturer's specifications. Information supplied by the manufacturer of the detectors used in this spectrograph (Fig. 1) has been used to obtain the following expression for detector quantum efficiency:

$$\eta = 0.004 \times 10^{-10} \times E^{-1.5} \times 10^{-10} \times 10^{-10}$$

(1)

$$1.15 \times 10^{-10}$$

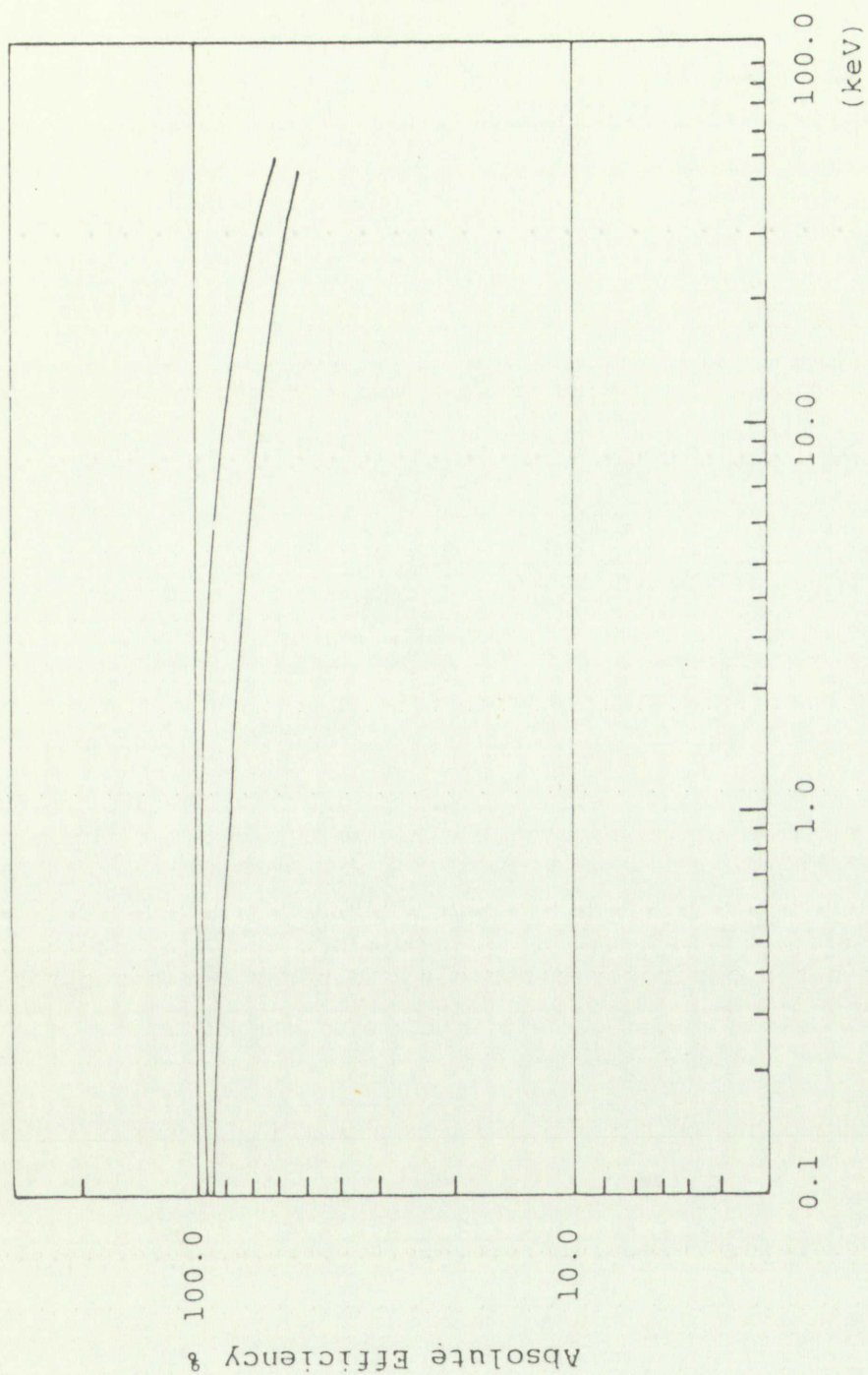
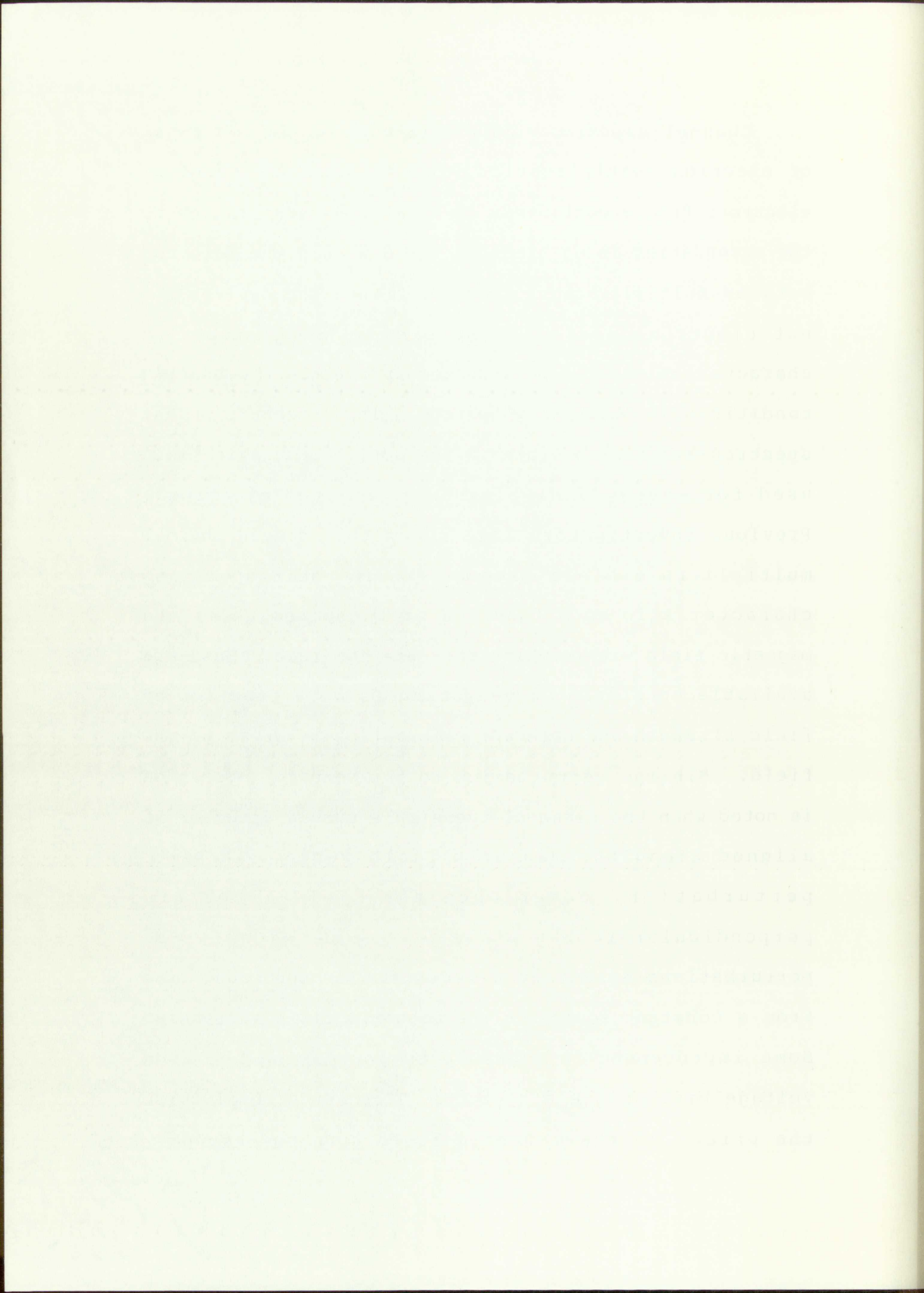


FIGURE 12. Detector Efficiency versus Electron Energy

Channel electron multipliers work on the principal of electron multiplication via emission of secondary electrons from a continuous "dynode" and acceleration of the secondaries in an electric field within the detector between multiplication "stages". Since the devices are not electromagnetically shielded, their operating characteristics will be affected by the electromagnetic conditions in which they operate. The detectors in the spectrograph must operate in the applied magnetic field used for energy analysis of the emitted electrons. Previous investigators have shown that curved channel multipliers exhibit alterations in their operating characteristic as a function of the strength of the magnetic field within which they are immersed. Data are available on simple curved channels as a function of field strength and detector orientation relative to the field. Minimum perturbation to the detector operation is noted when the plane of the simple curved detector is aligned along the magnetic field vector. Maximum perturbations occur when the field lines are perpendicular to the plane of the detector. The perturbations appear as a reduction in the count rate from a constant source as the magnetic field increases. Some improvement is possible by increasing the high voltage bias on the detectors. This tends to diminish the effect of the magnetic field turning secondary



electrons into the wall of the channel before they have acquired sufficient energy to create additional secondaries. Proper orientation of the detectors and increasing bias to the maximum level recommended by the device manufacturers yields a flat response up to ~ 150 gauss for a simple curved channel.

The same characteristics were investigated for helical detectors used in this electron emission spectrograph. If the helix has a very shallow pitch and is oriented such that the axis of the helix is perpendicular to the magnetic field, behavior similar to that obtained with the curved channel with the plane of the curve parallel to the field should be expected.

The X-ray generator was used to provide a constant source of particles uninfluenced by the magnetic field. This gives a controllable source of excitation which can be turned on and off for source and dark count and dark count only comparisons as a function of field strength. Source strength and exposure geometry were such that beam filtration and a limiting aperture were employed to obtain a reasonable count rate (i.e., $< 10^3$ cps.). Use of a 0.08 cm aluminum filter and a 0.015 cm diameter source aperture provided a constant count rate of ~ 350 cps at $B = 0$ gauss. Background (dark current) count rate at $B = 0$ gauss was < 4 cps. A diagram of the measurement geometry is shown in Fig. 13. Results of

electrons into the wall of the detector. The detector was
scattered sufficient energy to produce a secondary
electron. These electrons were then scattered by the
retarding bias to the screen and were recorded by the
device simultaneously with a time delay of 150
nanoseconds for a single curved channel.

The same characteristics were investigated for
helical detectors used in this electron spectroscopy.
If the helix has a very shallow pitch and
is oriented such that the axis of the helix is
perpendicular to the magnetic field, the results
that obtained with the curved channel with the plane of
the curve parallel to the field should be expected.

The X-ray generator was used to provide a constant
source of particles unimpeded by the magnetic field.
This gives a continuous source of excitation which can
be turned on and off for source and dark count and dark
count only comparisons as a function of field strength.
Source strength and exposure geometry were such that
beam filtration and a limiting aperture were employed to
obtain a reasonable count rate (1.0×10^5 cps). Use
of a 0.08 cm aluminum filter and a 0.015 cm diameter
source aperture provided a constant count rate of 350
cps at $B = 0$ gauss. Background (dark current) count
rate at $B = 0$ gauss was 4 cps. A diagram of the
measurement geometry is shown in Fig. 12. Results of

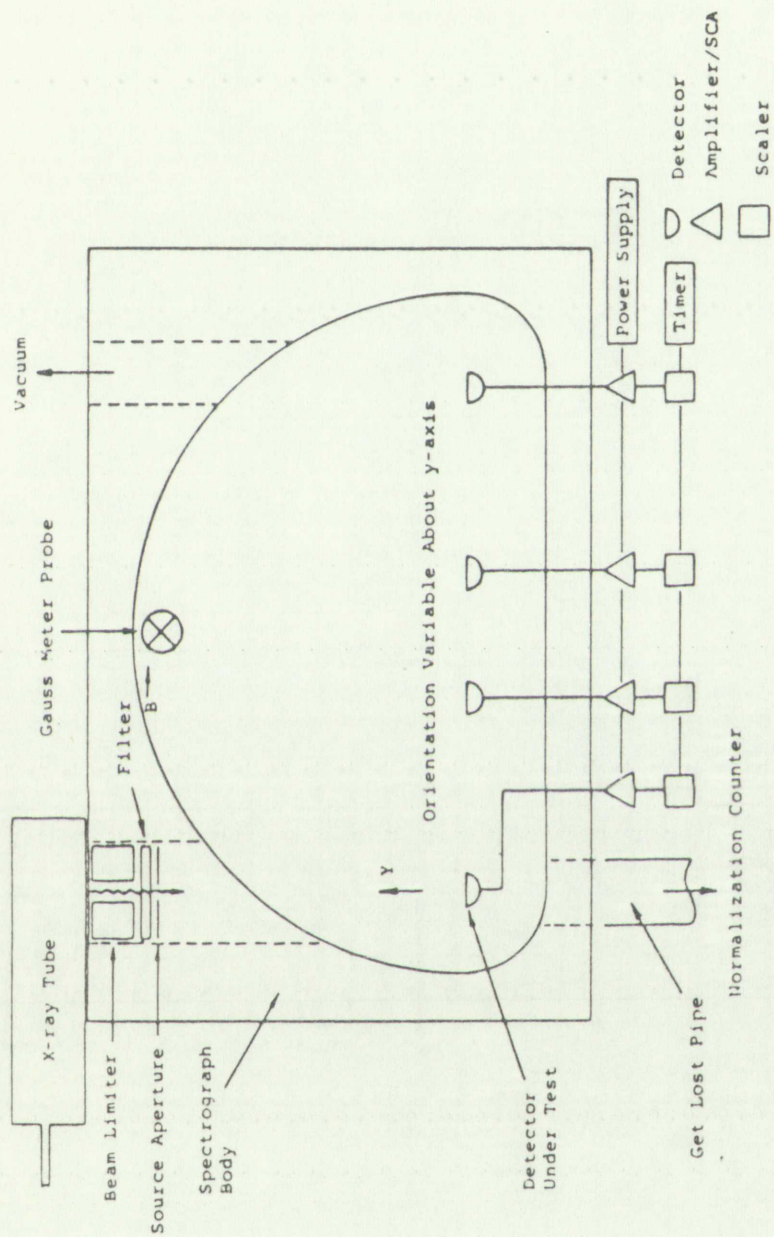


FIGURE 13. Magnetic Field Effect Measurement

the measurements made at 3.5 and 4.0 kV detector bias are shown in Fig. 14. The 4.0 kV operating condition was used for the magnetic field correction in electron emission measurements. Subsequent calculations used the following magnetic field correction to the detector response,

$$\epsilon_M = 1 - aB^3 \quad (19)$$

where ϵ_M is the efficiency as a function of magnetic field strength B and the constant $a = 0.13 \times 10^{-6}$. (The maximum correction required was $\sim 3\%$ at $B = 60$ gauss).

Background Count Rates

Since the experiment is designed to measure electrons emitted at extremely low count rates into small solid angles, the detectors must exhibit an inherently low "dark count". In addition, since the X rays enter the spectrograph to interact with the target and must subsequently traverse the instrument to exit, the potential exists for many secondary sources of electrons which would constitute background in the signal to be measured. In particular, the target mount must present an extremely small interaction cross section for the X rays. This was accomplished by

The experiments made at 1.5 and 2.5 eV are shown in Fig. 11. The 2.5 eV experiment was used for the magnetic field correction. Subsequent measurements at 1.5 eV showed the following magnetic field correction factor:

$$\mu = 1 - 2\alpha$$

where μ is the efficiency as a function of magnetic field strength H and the constant $\alpha = 0.15 \times 10^{-6}$. The maximum correction required was 2.5% at $H = 10$ Gauss.

Backscattered Count Rates

Since the experiment is designed to measure electrons emitted at extremely low count rates and small solid angles, the detectors must exhibit an inherently low "dark count", in addition, since the X-rays enter the spectrometer to interact with the target and must subsequently traverse the instrument to exit, the potential exists for many spurious counts at electrons which would constitute background signal to be measured. In particular, the target must not present an extremely small cross section for the X-rays. This was accomplished by

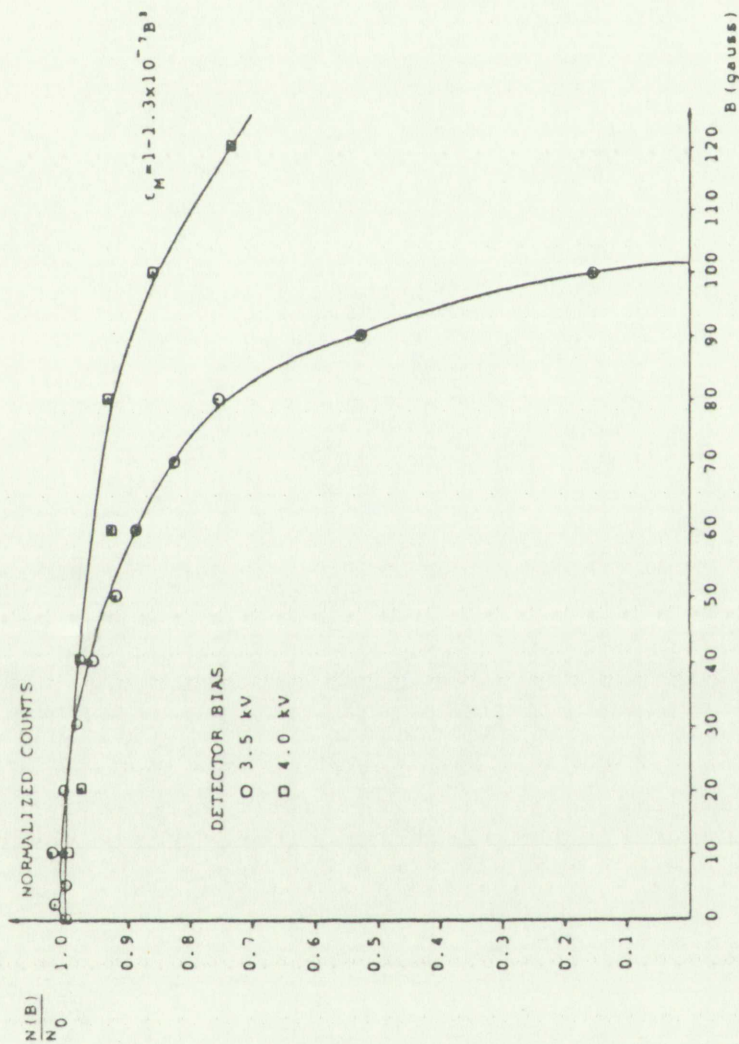


FIGURE 14. Detector Efficiency vs. Magnetic Field

FIGURE 10. DEFORMATION CHARACTERISTICS OF POLYETHYLENE LITHIUM



designing the mount in such a way that the only material in the target plane other than the target was small segments of 0.0025 cm diameter aluminum wire (Fig. 15). The background from the target holder alone, which was subtracted from the target emission, was obtained by direct measurement of emission in each channel reduced by the fraction of the counts which comes from those portions of the wires which would normally be covered by the target.

Measurements of the dark count C_D in the detectors operating at 4 kV potential with no intentional source of electrons in the spectrograph (i.e., X-ray source and ionization gauge off) established a baseline of $C_D < 1$ cpm. Specifically, determinations were made under the conditions shown in Table 4. For data runs the background was established under condition 3. Corrections for background including dark counts were made for all targets. The degree of background suppression from secondary sources within the spectrograph (the target volume is a virtual sea of scattered X rays and electrons) is evidenced by the lack of cross-talk among the channels and the absence of off-peak signal when using the electron source for energy resolution measurements as will be shown in the following section.

Designing the ...
in the larger ...
segments of 0.05 ...
The background ...
subtracted from ...
direct measurement ...
by the fraction ...
portions of the ...
the larger.

Measurements ...
operating at 4 kV ...
of electrons in ...
ionization gauge ...
cm. Specifically ...
conditions ...
background ...
Corrections for ...
made for all ...
suppression ...
spectrograph ...
scattered X rays ...
of cross-talk ...
off-peak signal ...
energy resolution ...
following section

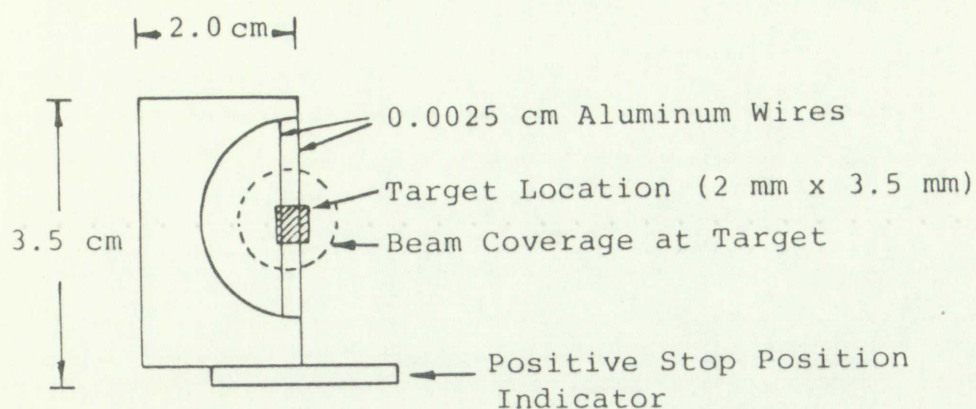


FIGURE 15. Target Mount

TABLE 4

Background Count Rates

	<u>Count Rate</u>
1. Holder removed	< 1 cpm all channels
Source <u>off</u> ion gauge <u>on</u>	
2. Holder in place	< 1 cpm all channels
Source <u>off</u> ion gauge <u>on</u>	
3. Holder in place	< 4 cpm all channels
Source <u>on</u> ion gauge <u>on</u>	

Magnetic Field Conditions

The magnetic field conditions within the spectrograph are coupled with the spherical aberrations of the electron optics to determine the instrument



FIGURE 15. Target mount

TABLE 1

Background Count Rates

Count Rate

1. Holder removed	1 cpm all channels
Source off ion gauge on	
2. Holder in place	1 cpm all channels
Source off ion gauge on	
3. Holder in place	1 cpm all channels
Source on ion gauge on	

Magnetic Field Conditions

The magnetic field conditions within the spectrometer are varied with the spherical aberration of the electron optics to determine the instrument

resolution. Ideally, the magnetic field should be constant and uniform throughout the working volume and in the absence of intentional space focusing should exhibit negligible gradients perpendicular to the plane of the spectrograph. Direct measurements within the active volume were made to determine the field distribution. Two Hall effect gaussmeters were cross-calibrated with reference magnets to establish correct settings for the internal calibration mode of the instruments used for subsequent measurements. One unit was used with its probe in a fixed reference position to monitor any drift in the field established within the active volume while the probe from the second unit was mounted to permit measurements along the paths of 10 cm radius defined by specific emission angles. Measurements were made at 5° intervals along the arcs with field strength settings at the control probe locations of 0, 5 and 95 gauss. Deviations in the fields were ≤ 0.02 gauss, ≤ 0.07 gauss and $\leq .25$ gauss respectively indicating approximately $\pm 1.5\%$ uniformity. Measurements of the spectrograph resolution discussed in the next section include the effects of magnetic field uniformity.

transmission. In this case the magnetic field should be constant and uniform throughout the working volume and in the absence of external space focusing agents exhibit negligible gradients perpendicular to the plane of the spectrograph. Direct measurements within the active volume were made to determine the field distribution. Two Hall effect transducers were cross-calibrated with reference magnets to establish correct readings for the internal calibration ends of the instruments used for subsequent measurements. One unit was used with the probe in a fixed reference position to monitor any drift in the field established within the active volume while the probe from the record unit was moved to permit measurements along the paths of 15 cm radius defined by specific excitation angles. Measurements were made at 5° intervals along the axis with field strength readings at the control probe locations of 0, 2 and 5 gauss. Deviations in the fields were ± 0.02 gauss, ± 0.07 gauss and ± 0.12 gauss respectively indicating approximately 1.2% uniformity. Measurements of the spectrograph resolution discussed in the next section include the effects of magnetic field uniformity.

Energy Resolution

Measurement of the energy resolution of the spectrograph was used to verify the operation of the instrument and as a cross-check on the mathematical formalism used to determine emission yield from measured quantities. From the discussions in Section II it is noted that for a spectrograph operating with a fixed radius of curvature and uniform magnetic field strength, the momentum resolution $\Delta B\rho/B\rho_0$ is a constant determined by geometry. In the range of magnetic field strengths of interest to this experiment the energy resolution $\Delta E/E \approx 2\Delta B\rho/B\rho_0$.

Experimentally, the resolution was determined by measurement of electrons emitted by a thermionic source. The energy was established by accelerating electrons in a fixed geometry through an electric field accurately controlled by a regulated high voltage power supply. A thermionic source was chosen in preference to a conversion electron isotope source due to the larger currents available from the electron gun and its adaptability to the spectrograph geometry. This choice was made with some sacrifice in source stability. A schematic and block diagram of the electron source and its control circuit are shown in Fig. 16. The electron source consisted of a thin walled machined brass cylinder 1.25 cm high and 0.83 cm diameter. Insulated

Measurement of the energy resolution of the spectrometer was made to verify the operation of the spectrometer and as a check on the mathematical treatment used to determine electron yield from various quantities. From the discussion in Section II it is noted that for a spectrograph operating with a fixed radius of curvature and uniform magnetic field strength, the momentum resolution $\Delta p/p$ is a constant determined by geometry. In the range of magnetic field strengths of interest to this experiment, the energy resolution $\Delta E/E$ is given by

Experimentally, the resolution was determined by measurement of electrons emitted by a thermionic source. The energy was established by accelerating electrons in a fixed geometry through an electric field accurately controlled by a regulated high voltage power supply. A thermionic source was chosen in preference to a conversion electron isotope source due to the larger currents available from the electron gun and its adaptability to the spectrograph geometry. This choice was made with some sacrifice in source stability. A schematic and block diagram of the electron source and its control circuit are shown in Fig. 16. The electron source consisted of a thin-walled machined brass cylinder 1.5 cm high and 0.63 cm diameter. Insulated

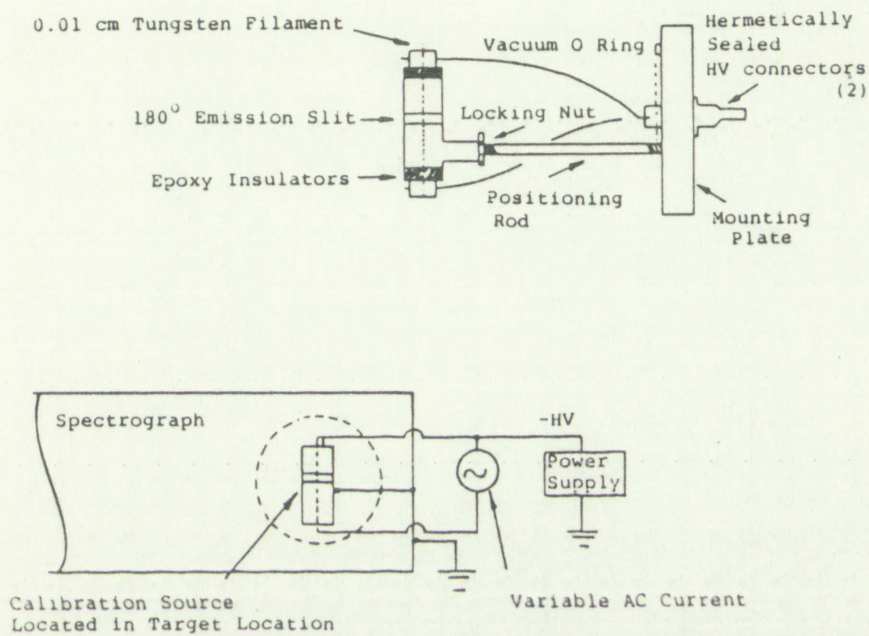


FIGURE 16. Energy Calibration Electron Source



FIGURE 16. Energy Calibration Electron Source

end caps of machined epoxy were center drilled and used to position a 0.01 cm diameter tungsten filament along the axis of the cylinder. Small brass connector assemblies on each end provided mechanical support and electrical contact for the AC current supply to the tungsten filament.¹ The accelerating voltage was applied to the filament as a negative DC bias. The brass cylinder was clamped at the spectrograph (ground) potential. The electrons were emitted in a 180° pattern in the plane of the spectrograph through a 0.076 cm wide half circumferential slot in the middle of the brass cylinder. Currents on the order of 1 ampere were sufficient to generate on the order of 10^4 counts/min (peak) in the detectors. (Figure 17 shows a photograph of the target mount, a detector and the electron source).

The energy of the electrons was established by setting the accelerating potential via the regulated power supply. With the spectrograph at vacuum ($\sim 10^{-5}$ torr) the AC supply current was turned on, the location of the peak count rate was then established by

¹ It should be noted that the initial electron gun configuration employed a DC current source which was ultimately rejected due to the introduction of a magnetic field component in the electron source region which seriously perturbed the electron trajectories; the AC current source eliminated the problem.

and caps of machined epoxy were cemented to the ends of the
to position a 0.51 cm diameter tungsten filament at the
the axis of the cylinder. The filament was supported by
insulators on each end provided mechanical support and
electrical contact for the AC current supply to the
tungsten filament. The accelerating voltage was ap-
plied to the filament as a negative bias. The glass
cylinder was clamped at the spectrograph (photo-
potential). The electrons were emitted in a 180° pattern
in the plane of the spectrograph through a 0.03 cm wide
hole at one end of the cylinder. The hole in the other
cylinder. Currents on the order of 1 ampere were
sufficient to generate on the order of 10^{14} electrons
(peak) in the detector. (Figure 17 shows a photograph
of the target mount, a detector and the electron
source).
The energy of the electrons was controlled by
setting the accelerating potential via the regulated
power supply. With the spectrograph at vacuum (10⁻⁶
torr) the AC supply current was turned on, the location
of the peak count rate was then established by

It should be noted that the initial electron gun
configuration employed a DC current source which was
ultimately rejected due to the introduction of a
magnetic field component in the electron source region
which seriously perturbed the electron spectroscopy.
The AC current source eliminated the problem.

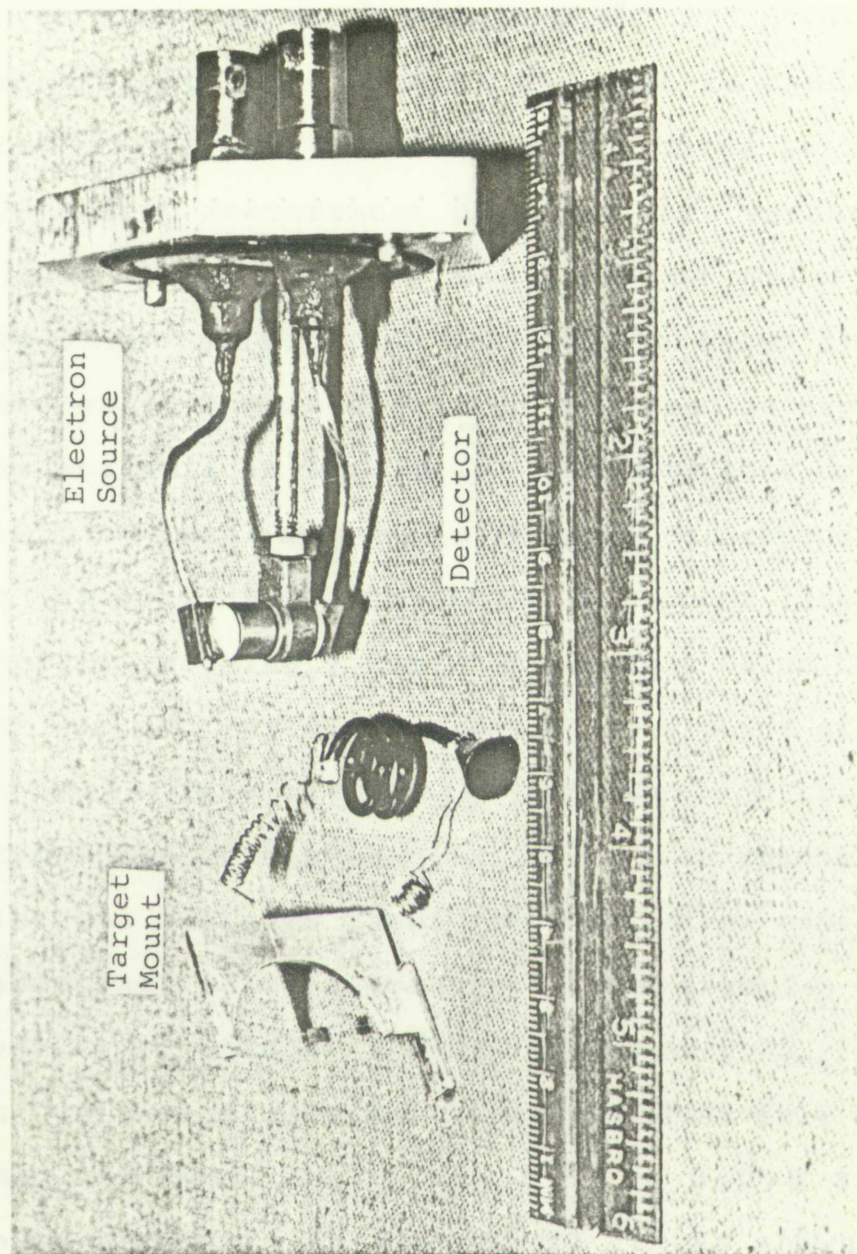


FIGURE 17. Target Mount--Detector,
Electron Source

FIGURE 11. Laser beam - detection



sweeping the magnet field settings through the anticipated region of peak response, and then sequential measurements were made at the peak to confirm source stability. With the electron source stabilized, a systematic measurement of count rate versus magnetic field strength was made in the four channels simultaneously. From the results shown in Figs. 18 through 21 the spectrograph performed as expected from the analysis in Section II. The detectors do not "see" electrons until a magnetic rigidity corresponding to $B\rho_1$ is reached. Past that point the count rate increases rapidly reaching a somewhat constant value between $B\rho_2$ and $B\rho_3$ and rapidly decreasing to a point at $B\rho_4$ where the detectors are again at background count rates. Inspection of the results in a given channel at three electron energies shows the resolution expressed as a percentage to be a constant. For example, using the results of channel 1 measurements at 0.25, 1 and 3 keV the values of $(\Delta B\rho/B\rho_0)$ determined at full width half maximum amplitude are 0.037, 0.038 and 0.039 respectively. In Section II it was shown that the geometry of the spectrograph yields a value of $(\Delta B\rho/B\rho_0) \approx 0.05$ for baseline resolution. Hence, the following has been demonstrated:

measuring the magnetic field surface through the
 anticipated region of good response, and then sequential
 measurements were made at 100 gauss to obtain a series
 of 100 measurements. With the above procedure, a
 systematic measurement of count rate versus magnetic
 field strength was made in the four channels
 simultaneously. From the results shown in Figs. 10
 through 14 the spectrograph performed as expected from
 the analysis in Section II. The detectors do not "see"
 electrons until a magnetic rigidity corresponding to 800
 is reached. After that point the count rate increases
 rapidly reaching a somewhat constant value between 800
 and 900 and rapidly decreasing to a point at 900 where
 the detectors are again at background count rates.
 Inspection of the results in a given channel at three
 electron energies shows the resolution expressed as a
 percentage to be a constant. For example, using the
 results of channel 1 measurements at 0.25, 1 and 3 kev
 the values of $(\Delta E/E)$ determined at full width half
 maximum amplitude are 0.037, 0.038 and 0.039
 respectively. In Section II it was shown that the
 geometry of the spectrograph yields a value of
 $(\Delta E/E) = 0.04$ for baseline resolution. Hence, the

following has been demonstrated:

1. Experimental measurements using a line source confirm the anticipated resolution based on the spectrograph geometry.

2. Calculations of the instrument sensitivity as a function of line source position in the target plane shows the resolution to be constant over the target width of 0.2 cm (Table 3).

The final experimental results presented in the next section include the effects of finite source width in determining differential electron yields.

Experimental measurements using a line source
confirm the anticipated resolution based on the

aperture geometry.

Resolution of the instrument essentially as a
function of line source position in the focal
plane shows the resolution to be constant over

the target width of 0.1 cm (Table 1).

The final experimental results presented in the next
section include the effects of finite source width in
determining differential electron yields.

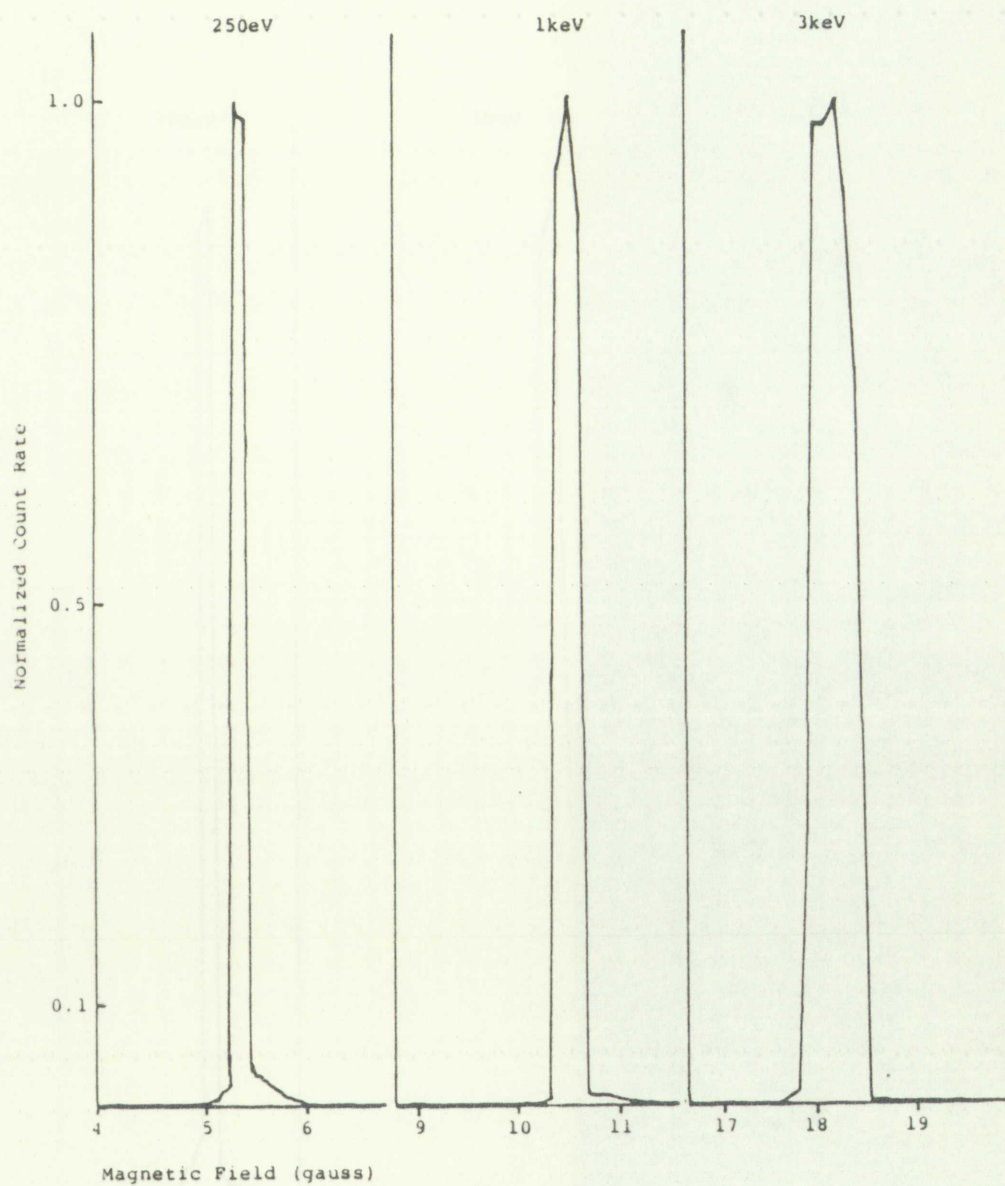


FIGURE 18. Channel 1 (0°) Resolution



FIGURE 18. Channel 1 (10°) Resolution

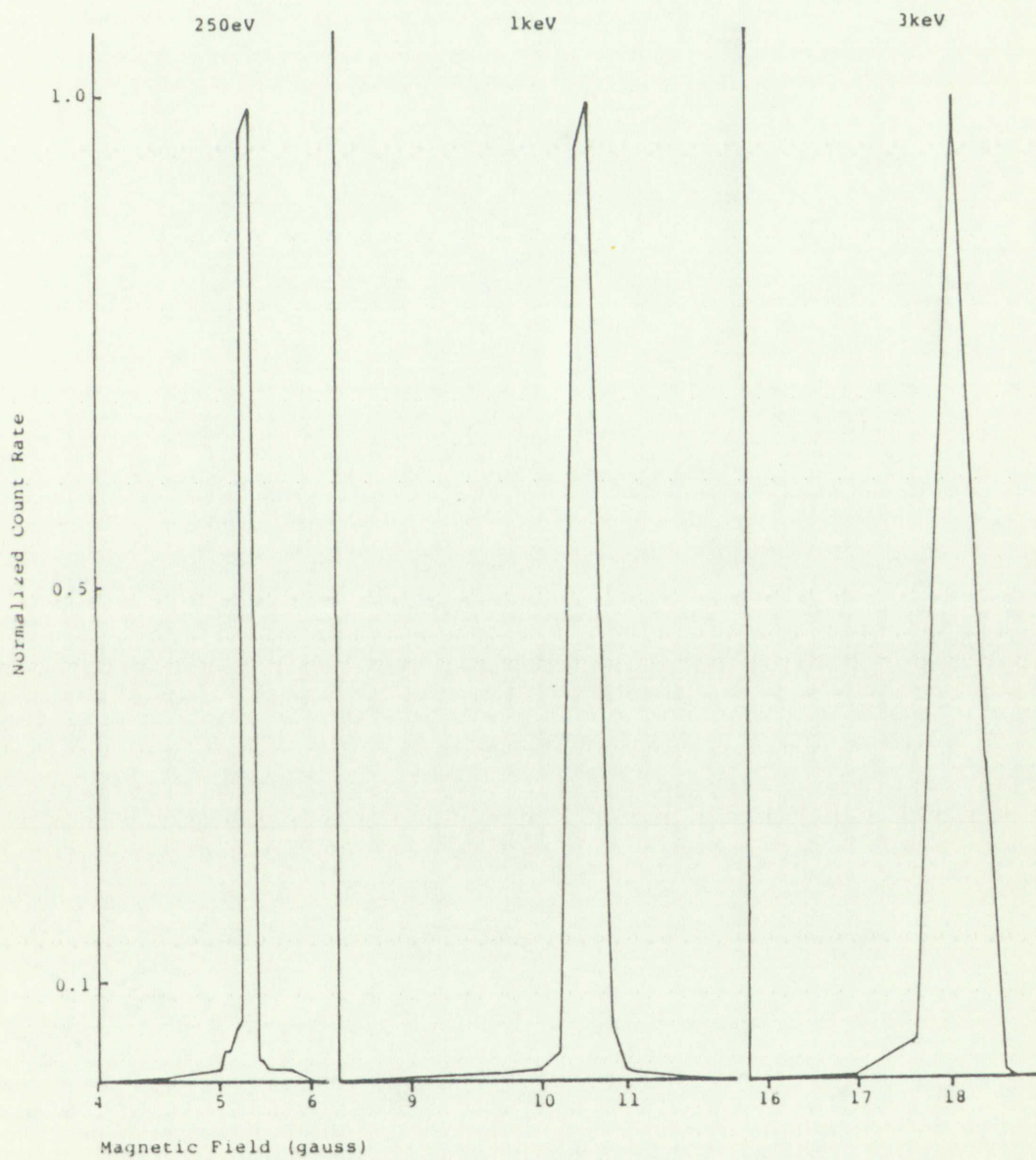


FIGURE 19. Channel 2 (30°) Resolution

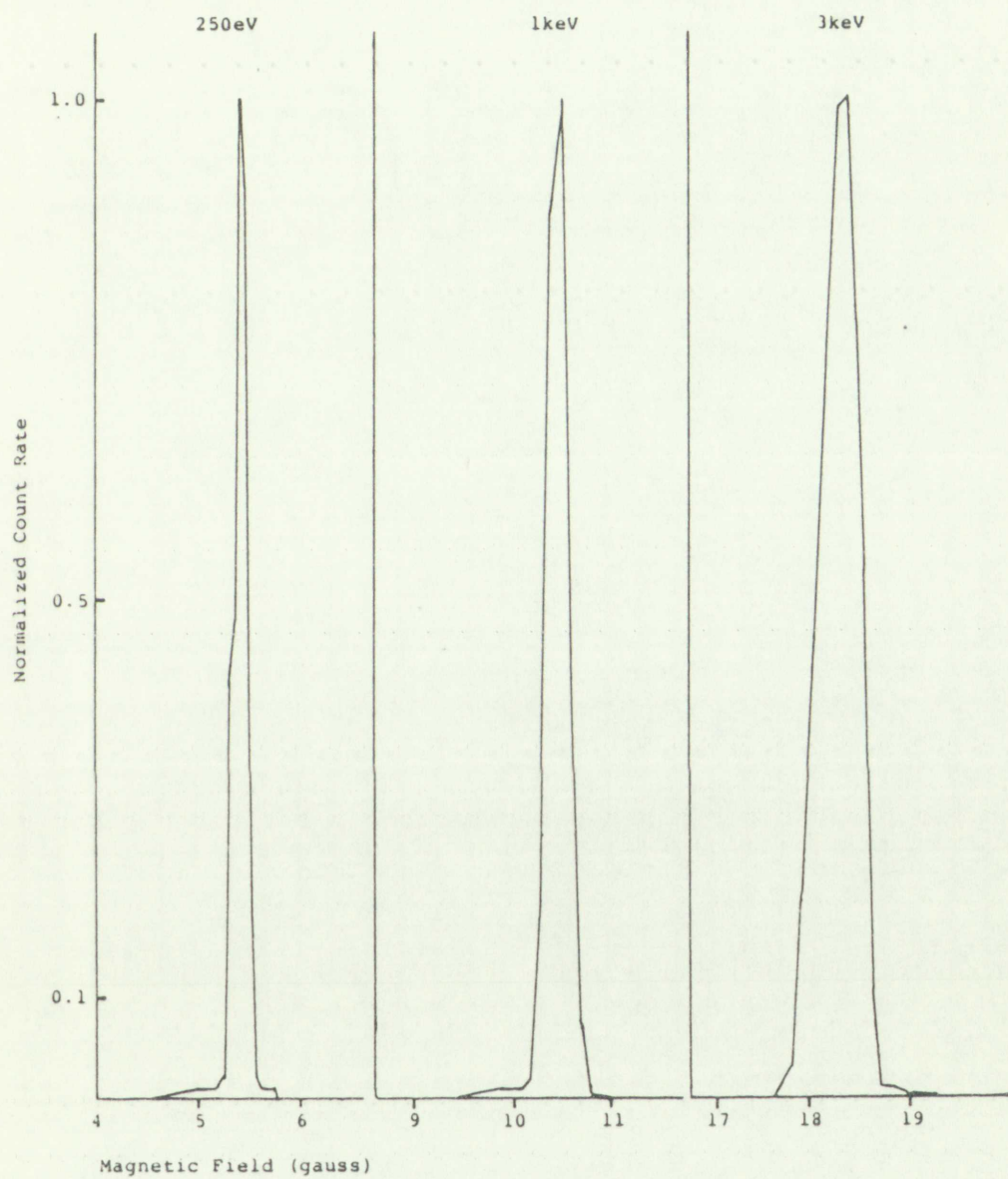


FIGURE 20. Channel 3 (45°) Resolution



FIGURE 10. Channel 1 (42) Reaction

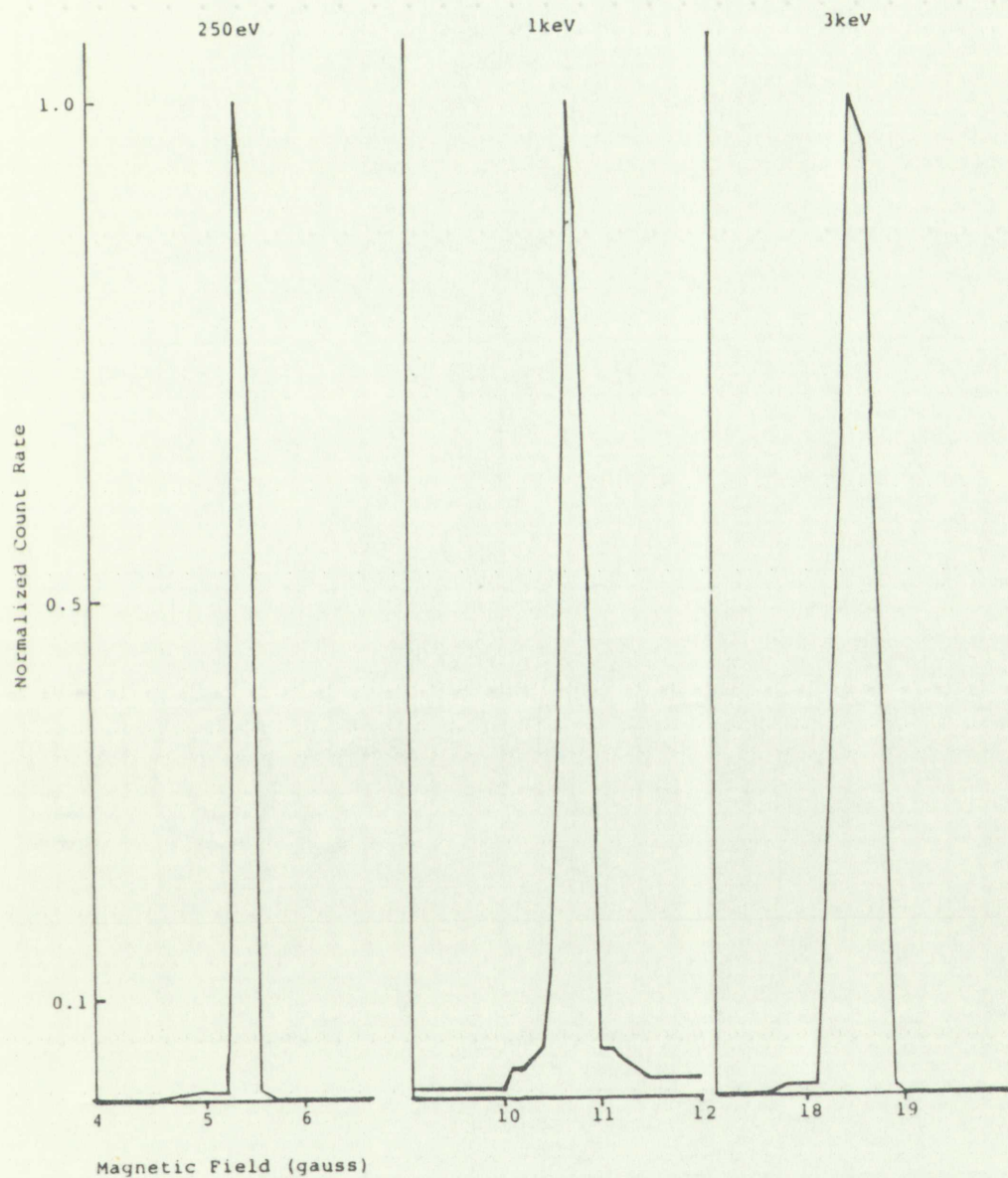


FIGURE 21. Channel 4 (60°) Resolution



FIGURE 21. Channel A (60°) Resolution

SECTION IV

SECTION IV

EXPERIMENTAL RESULTS

Data Reduction Method

Data accumulated for determination of the electron emission from various targets consisted of the number of electrons counted in each detector over a measured time interval as a function of magnetic field strength. During this interval the fluence of X rays incident on the target was also measured with the normalization counter. The X-ray spectrum was determined from the scintillation/PMT detector and the vacuum condition inside the spectrograph was also noted. Counting intervals were determined on the basis of count statistics, emission efficiency and peak count rate to background ratios and were varied depending on target material examined. Counting intervals ranged from approximately 5 minutes per datum point (high Z targets near distribution peaks) to as long as 30 minutes for the low Z targets. Processing of the raw data (counts versus magnetic field strength) into differential emission yield (electrons/ photon keV sr) involved the use of the following equation.

(20)

$$\epsilon_E \epsilon_M G(\alpha, \theta_k) = \frac{N_k}{N_x} \frac{A_x}{A_t} \left(\frac{\ell_t}{\ell_x} \right)^2 \frac{S_k/2}{h_p} \frac{1}{A_k} \left[\frac{\rho_0}{m_0 c^2} \frac{\alpha + 1}{\alpha(\alpha + 2)} \right]$$

(Development of this equation is included in Appendix A and raw data from 12 materials are included in Appendix B). $G(\alpha, \theta_k)$ is the differential yield of electrons of energy E emitted at angle θ_k from the target. N_k and N_x are the measured electron counts in each detector and X-ray counts in the normalization counter respectively, A_x and A_t are the areas of the normalization counter detector collimator and emission target, while ℓ_x and ℓ_t represent the source-to-detector and source-to-target distances. S_k is the path length from the target to the k^{th} detector and h_p is the height of the primary aperture. A_k is the integrated ρ dependent angular acceptance band $\Delta\theta_k$ defined by the primary slit width and ρ_0 defines the design radius of curvature for the spectrograph. The quantity in brackets is the relativistic conversion factor from momentum to energy in terms of $\alpha = E/m_0 c^2$. ϵ_E and ϵ_M are the energy and magnetic field efficiency factors respectively for the detectors. (See equations 18 and 19). Note that for the electron energies of interest $\alpha \ll 1$ and equation 20 reduces to the non-relativistic approximation.

$$G(E, \theta_k) \approx \frac{N_k}{N_x} \frac{A_x}{A_t} \left(\frac{\ell_t}{\ell_x} \right)^2 \frac{S_k/2}{h_p} \frac{\rho_0}{2E_0} \frac{1}{A_k} \frac{1}{\epsilon_E \epsilon_M} \quad (21)$$

(Development of a model for the calculation of the
 and the data for the calculation of the
 Fig. 1 shows the calculation of the
 energy of the incident electron
 are the measured effect of the
 K-ray counts in the detector
 A_1 and A_2 are the angles of the
 detector: collimator and
 represent the source
 distance. S_1 is the
 detector and the source
 aperture. A_1 is the
 acceptance band of the
 and A_2 defines the
 spectrograph. The
 is the conversion factor
 of $n = E/m_0 c^2$
 field efficiency factor
 (See equations 18 and 19)
 energies of interest
 The non-relativistic

$$G_{1,0,1} = \frac{A_1}{A_2} \cdot \frac{N_1}{N_2}$$

This can be compared to a geometrical approximation (which assumes the angular acceptance bands are independent of ρ) given by

$$G(E, \theta_k) \approx \frac{N_k}{N_x} \frac{A_x}{A_t} \left(\frac{\ell_t}{\ell_x} \right)^2 \frac{S_k/2}{h_p} \frac{S_k/2}{W_k} \frac{1}{\Delta E} \frac{1}{\epsilon_E \epsilon_M} \quad (22)$$

In equation 21

$$A_k \approx \Delta\theta = \frac{W_k}{S_k/2} \quad (23)$$

where W_k is the width of the primary aperture located halfway between the target and detector along the electron trajectory and ΔE is the measured energy resolution of the spectrograph.

Reproducibility, Errors and Accuracy

Examination of the reproducibility of the differential emission measurements was made with the following sets of measurements. Data from Mylar, aluminum, copper and lead were used to determine the reproducibility of the ratio of the number of electron counts in each channel to the number of X-ray counts in the normalization counter at a specific magnetic field strength. The magnetic field strength chosen was that corresponding to the peak count rate in Channel 1. The

This can be compared to a geometrical approximation which assumes the angular acceptance bands are independent of λ given by

$$\sin \theta_{\lambda} = \frac{N}{\lambda} \left(\frac{1}{2} \frac{1}{N} \frac{1}{\lambda} \frac{1}{\lambda} \frac{1}{\lambda} \right)$$

In equation (2) N is the width of the primary spectrum focused

$$N = \frac{W}{2\lambda} \quad (2)$$

where N is the width of the primary spectrum focused halfway between the target and detector along the electron trajectory and ΔE is the measured energy resolution of the spectrometer.

Reproducibility, Error and Accuracy

Examination of the reproducibility of the differential emission measurements was made with the following sets of measurements. Data from Mylar, aluminum, copper and lead were used to determine the reproducibility of the ratio of the number of electron counts in each channel to the number of X-ray counts in the normalized counter at a specific magnetic field strength. The magnetic field strength chosen was that corresponding to the peak count rate in Channel 1. The

reproducibility is stated in terms of the average of the ratio N_k/N_x for n measurements with a standard deviation obtained using "inefficient" statistics for sample sizes $n \leq 10$ (aluminum, copper and lead) and "efficient" statistics for Mylar $n = 12$. For example, for the Mylar target twelve separate measurements were made of the electron counts in each channel as a function of the number of X rays detected in the normalization counter at a magnetic field strength of 25.5 gauss. For each measurement, the ratio of electron counts to X-ray counts was computed and the results averaged for each channel. The standard deviation was obtained using the expression

$$\sigma^2 \approx \frac{1}{n-1} \sum \left[\left(\frac{N_k}{N_x} \right) - \left(\frac{\overline{N_k}}{\overline{N_x}} \right) \right]^2 \quad (24)$$

Similar calculations were done for aluminum, copper and lead using an approximation for the standard deviation given by [24]

$$\sigma \approx \frac{\text{range}}{\sqrt{n}} = \frac{\left(\frac{N_k}{N_x} \right)_{\max} - \left(\frac{N_k}{N_x} \right)_{\min}}{\sqrt{n}} \quad (25)$$

A summary of the results is given in Table 5 where the reproducibility of the X-ray counts is included as well as that of the electron to X-ray ratio. The X-ray source reproducibility is within 4% and a reasonable

reproducibility is stated in terms of the average of the ratio \bar{N}_K/N_X for measurements with a standard deviation obtained using "weighted" statistics for unequal sizes $n = 10$ (aluminum, copper and lead) and "efficient" statistics for $N_X = 12$. For example, for the X-ray larger twelve separate measurements were made of the electron counts in each channel as a function of the number of X-rays detected in the normalization channel at a magnetic field strength of 35.5 gauss. For each measurement, the ratio of electron counts to X-ray counts was computed and the results averaged for each channel. The standard deviation was obtained using the

expression

$$\sigma^2 = \frac{1}{n-1} \sum \left[\left(\frac{N_K}{N_X} \right) - \left(\frac{\bar{N}_K}{\bar{N}_X} \right)^2 \right] \quad (24)$$

Similar calculations were done for aluminum, copper and lead using an approximation for the standard deviation

given by (24)

$$\sigma = \frac{\text{range}}{\sqrt{n}} = \frac{\left(\frac{N_K}{N_X} \right)_{\text{MAX}} - \left(\frac{N_K}{N_X} \right)_{\text{MIN}}}{\sqrt{n}} \quad (25)$$

A summary of the results is given in Table 2 where the reproducibility of the X-ray counts is included as well as that of the electron to X-ray ratio. The X-ray source reproducibility is within 4% and a reasonable

TABLE 5. Summary of Experimental Reproducibility

Material	B (gauss)	n	$10^{-4} N_x$	$10^7 \frac{N_1}{N_x}$	$10^7 \frac{N_2}{N_x}$	$10^7 \frac{N_3}{N_x}$	$10^7 \frac{N_4}{N_x}$
Mylar	25.5	12	39903 ± 1380	25.17 ± 2.02	8.73 ± 0.67	7.54 ± 0.49	3.79 ± 0.40
Al	24.3	4	5929 ± 67	196.05 ± 5.07	50.79 ± 5.50	28.89 ± 2.09	10.16 ± 0.77
Cu	25.1	6	1715 ± 24	1166.45 ± 16.24	261.22 ± 19.47	155.69 ± 5.60	42.76 ± 3.17
Pb	25.1	6	1145 ± 27	1747.14 ± 40.80	451.98 ± 22.45	288.64 ± 11.87	87.85 ± 9.72

Классификация предприятий по размеру - 2 этап

№	Наименование предприятия	Численность персонала	Объем производства, млн руб.	Объем реализации, млн руб.	Среднегодовая прибыль, млн руб.
1	ООО "А"	10	100	100	10
2	ООО "Б"	20	200	200	20
3	ООО "В"	30	300	300	30
4	ООО "Г"	40	400	400	40
5	ООО "Д"	50	500	500	50
6	ООО "Е"	60	600	600	60
7	ООО "Ж"	70	700	700	70
8	ООО "З"	80	800	800	80
9	ООО "И"	90	900	900	90
10	ООО "К"	100	1000	1000	100

estimate of the reproducibility of the ratio of electron counts to X-ray counts is $\pm 12\%$.

Random errors influencing the precision of the experiment, once a series of measurements has begun, are associated primarily with establishing and maintaining the X-ray source parameters, setting timer/scalers and regulating the magnetic field strength. With the exception of the X-ray source, these devices employ digital set-points and readouts; their precision is determined by the instrument capability and the accuracy of its calibration. The digital gaussmeter used in conjunction with calibration magnets has a precision of $\pm 2\%$. Errors in timing are not relevant since the emission measurements are made as a function of X-ray fluence rather than flux. Variations in the output of the X-ray source were accounted for by use of the normalization counter. Readout of the X-ray and electron counts were obtained on electromechanical scalars minimizing random errors associated with estimates of scale readings. Based on the reproducibility data, the precision of the measurement technique as used is estimated to be $\pm 15\%$.

Statistical errors, as they apply to this experiment (the events recorded are not strictly random in the same sense as nuclear disintegrations) are treated by assuming a measurement of X-ray or electron

counts can be expressed as $N \pm \sqrt{N}$. The electron count includes background (dark count plus electrons from sources other than the target). Hence $N_k = (N_k' - N_{bkg})$ where N_k' is the measured count, N_{bkg} is the background and $\sigma_k = \sqrt{N_k' + N_{bkg}}$. The quantity N_k/N_x is then expressed as

$$\frac{N_k}{N_x} = \frac{N_k' - N_{bkg}}{N_x} \pm \sigma_{kx} \quad (26)$$

where

$$\sigma_{kx} = \frac{N_k' - N_{bkg}}{N_x} \sqrt{\frac{1}{N_k' + N_{bkg}} + \frac{1}{N_x}} \quad (27)$$

Further, for all cases studied $N_x \gg N_k' + N_{bkg}$ and equation 27 can be approximated by

$$\frac{N_k}{N_x} \approx \frac{N_k' - N_{bkg}}{N_x} \left(1 \pm \frac{1}{\sqrt{N_k' + N_{bkg}}} \right) \quad (28)$$

The expression for the energy integrated differential yield is obtained by adding the individual differential yields for each emission angle. The propagated statistical error is given by $\sigma = (\sigma_1^2 + \sigma_2^2 + \dots + \sigma_n^2)^{1/2}$. The data in Appendix B includes these statistical errors.

The dominant source of uncertainty contributing to the accuracy of the results is the lack of exact data on

count can be expressed as $N = N_0 + N_1 + N_2 + \dots$. The electron count
includes background N_0 and counts from electrons from
sources other than the source. Hence $N = N_0 + N_1 + N_2 + \dots$
where N_1 is the source count, N_2 is the background
and N_0, N_1, N_2, \dots are the quantities N_i is then
expressed as

$$(26) \quad N = N_0 + N_1 + N_2 + \dots$$

where

$$(27) \quad \frac{1}{N} = \frac{1}{N_0 + N_1 + N_2 + \dots} + \frac{1}{N_1 + N_2 + \dots} + \frac{1}{N_2 + \dots}$$

Further, for all cases studied $N_0 \gg N_1 + N_2 + \dots$ and
equation 27 can be approximated by

$$(28) \quad \left(\frac{1}{N} \right) = \frac{1}{N_0 + N_1 + N_2 + \dots} + \frac{1}{N_1 + N_2 + \dots} + \frac{1}{N_2 + \dots}$$

The expression for the energy integrated differential
yield is obtained by adding the individual differential
yields for each emission angle. The propagated
statistical error is given by
 $\sigma = (\sigma_1^2 + \sigma_2^2 + \dots + \sigma_n^2)^{1/2}$. The data in Appendix B

includes these statistical errors.
The dominant source of uncertainty contributing to
the accuracy of the results is the lack of exact data on

the energy dependence of the detector response. Referring to Fig. 12, the manufacturers data show a range of values for detection efficiency as a function of energy. Other investigators [25] have made measurements of detector efficiency on various types of channel electron multipliers and reported similar variations. Over the energy range employed in these measurements the variation in the detector efficiency is no larger than approximately $\pm 15\%$. Other systematic errors associated with the geometry of the spectrograph (target, aperture and detector positions, target area, aperture dimensions etc.) are of smaller values. The combined estimated accuracy and measured precision of the measurements is $\pm 30\%$ obtained by assuming the systematic and random errors are additive.

Differential and Integrated Reverse Emission Yield

Using the experimental data from Appendix B and the appropriate spectrograph parameters in equation 20 the differential electron yields for the various materials are plotted in Figs. 22 through 35.¹ Figure 36 shows

¹The curves for steeper emission angles with the filtered spectrum and those for lower Z targets with the unfiltered spectrum exhibit the effects of poorer signal-to-noise ratios. This effect is seen as the less smooth behavior of the differential curves relative to the high Z targets.

the energy dependence of the detector response. Referring to Fig. 13, the manufacturer's data show a range of values for detector efficiency as a function of energy. Other investigators (15) have made measurements of detector efficiency on various types of channel electron multipliers and reported similar variations. Over the energy range employed in these measurements the variation in the detector efficiency is no larger than approximately 15%. Other systematic errors associated with the geometry of the spectrograph (slit, aperture and detector position, target area, aperture dimensions etc.) are of smaller values. The combined estimated accuracy and measured precision of the measurements is $\pm 3\%$ obtained by assuming the systematic and random errors are additive.

Differential and Integrated Reverse Emission Yield

Using the experimental data from Appendix B and the appropriate spectrograph parameters in equation 20 the differential electron yields for the various materials are plotted in Figs. 12 through 15. Figure 16 shows

The curves for average emission angles with the filtered spectra and those for lower λ targets with the unfiltered spectra exhibit the effects of poorer signal-to-noise ratios. This effect is seen as the less smooth behavior of the differential curves relative to the high λ targets.

$G(\theta_k)$, the differential yield integrated over energy, as a function of emission angle for each material, where

$$G(\theta_k) = \int_{\alpha} G(\alpha, \theta_k) d\alpha \quad (29)$$

Included in this figure are the error bars associated with the combined experimental accuracy and precision ($\pm 30\%$) as well as yield curves proportional to $\cos^2\theta$, $\cos\theta$ and isotropic angular distributions. Figures 37 and 38 show the energy integrated emission of 30° , 45° and 60° normalized to 0° emission compared with $\cos\theta$ and $\cos^2\theta$ emission distributions. The typical error bars shown in these figures include only the random error ($\pm 15\%$) of the total experimental accuracy. (The systematic error cancels out of the normalized quantities). The fractional error is defined $\sqrt{2}$ (0.15), assuming the random error is the same for both quantities in the quotient $G(\theta_k)/G(\theta_1)$.

In order to compute the total yield of reverse emitted electrons, the energy integrated yield $G(\theta_k)$ is integrated over the solid angle with the appropriate angular dependence. Using $\cos\theta$ behavior based on data in Figs. 36 and 37,

$$Y = \frac{G(\theta_k)}{\cos\theta_k} \int_0^{2\pi} \int_0^{\pi/2} \cos\theta \sin\theta d\theta d\phi \quad (30)$$

the differential yield integrated over angles as a function of emission angle for each material, where

$$Y(\theta) = \frac{1}{4\pi} \int_{-90^\circ}^{+90^\circ} \int_{-90^\circ}^{+90^\circ} Y(\theta, \phi) d\phi d\theta$$

included in this figure are the error bars associated with the combined experimental accuracy and precision (1.3%) as well as yield curves proportional to $\cos^2\theta$, \cos and isotropic angular distributions. Figures 37 and 38 show the energy integrated emission of 30° , 45° and 60° normalized to 0° emission compared with \cos^2 and \cos emission distributions. The typical error bars shown in these figures include only the random error (1.3%) of the total experimental accuracy. (The systematic error cancels out of the normalized quantities). The fractional error is defined $\sqrt{0.12}$, assuming the random error is the same for both quantities in the quotient $G(\theta)/G(0^\circ)$.

In order to compute the total yield of reverse emitted electrons, the energy integrated yield $G(\theta)$ is integrated over the solid angle with the appropriate angular dependence. Using \cos^2 behavior based on data

in Figs. 36 and 37,

$$G(\theta) = \int_{-90^\circ}^{+90^\circ} \int_{-90^\circ}^{+90^\circ} Y(\theta, \phi) d\phi d\theta$$

$$G(0^\circ) = \int_{-90^\circ}^{+90^\circ} \int_{-90^\circ}^{+90^\circ} Y(0^\circ, \phi) d\phi d\theta$$

$$Y(\theta, \phi) = \frac{d^2N}{d\theta d\phi dE}$$

or

$$Y = \frac{\pi G(\theta_k)}{\cos\theta_k} \quad (31)$$

Using the experimentally measured data for 0° emission and employing equation 22, the total yield for each material was calculated. This information is summarized in Table 6.

Table 6. Total Reverse Emission Yield Summary,
 $E_e > 0.1$ keV; Filtered and Unfiltered Spectra

Target Material	$G_1 \times 10^3$ $\left(\frac{\text{electrons}}{\gamma \text{ sr}}\right)$	$Y \times 10^3$ $\left(\frac{\text{electrons}}{\gamma}\right)$	$Y \times 10^7$ $\left(\frac{\text{coul}}{\text{cal}}\right)$
Pb	7.96	25.02	66.82
Ta (Filtered)	1.17	3.68	4.92
Ta	7.08	22.24	59.43
Cu (Filtered)	0.58	1.82	2.43
Cu	2.19	6.87	18.38
Al	0.78	2.45	6.55
Mg	0.56	1.76	4.70
Cover Glass	0.55	1.73	4.62
Silica Cloth	0.34	1.07	2.85
Thermal Control Paint	0.17	0.53	1.43
Kevlar	0.11	0.35	0.92
Mylar	0.10	0.31	0.84
Non Conducting Epoxy	0.07	0.22	0.58
Conducting Epoxy	0.06	0.19	0.50

1971

0.01

Using the experimentally measured data for 0° emission and applying equation (2), the total yield for each material was calculated. This information is summarized in Table 2.

Table 2. Total Average Emission Yield Summary.
0.01 MeV, Filtered and Unfiltered Spectra

Target Material	$0^\circ \times 10^3$ (electrons) (cal)	$Y \times 10^3$ (electrons) (cal)	$Y \times 10^3$ (cal)
Pb	7.85	25.02	60.62
Ta (Filtered)	1.17	3.58	4.92
Ta	7.90	22.24	59.41
Cu (Filtered)	0.58	1.82	2.42
Cu	2.19	6.87	18.18
Al	0.18	2.42	6.22
Mo	0.86	1.76	4.70
Cover Glass	0.52	1.72	4.62
Silica Glass	0.34	1.07	2.82
Thermal Control Paint	0.12	0.22	1.42
Kevlar	0.12	0.22	0.92
Mylar	0.10	0.21	0.82
Non Conducting Epoxy	0.67	0.22	0.88
Conducting Epoxy	0.56	0.19	0.50

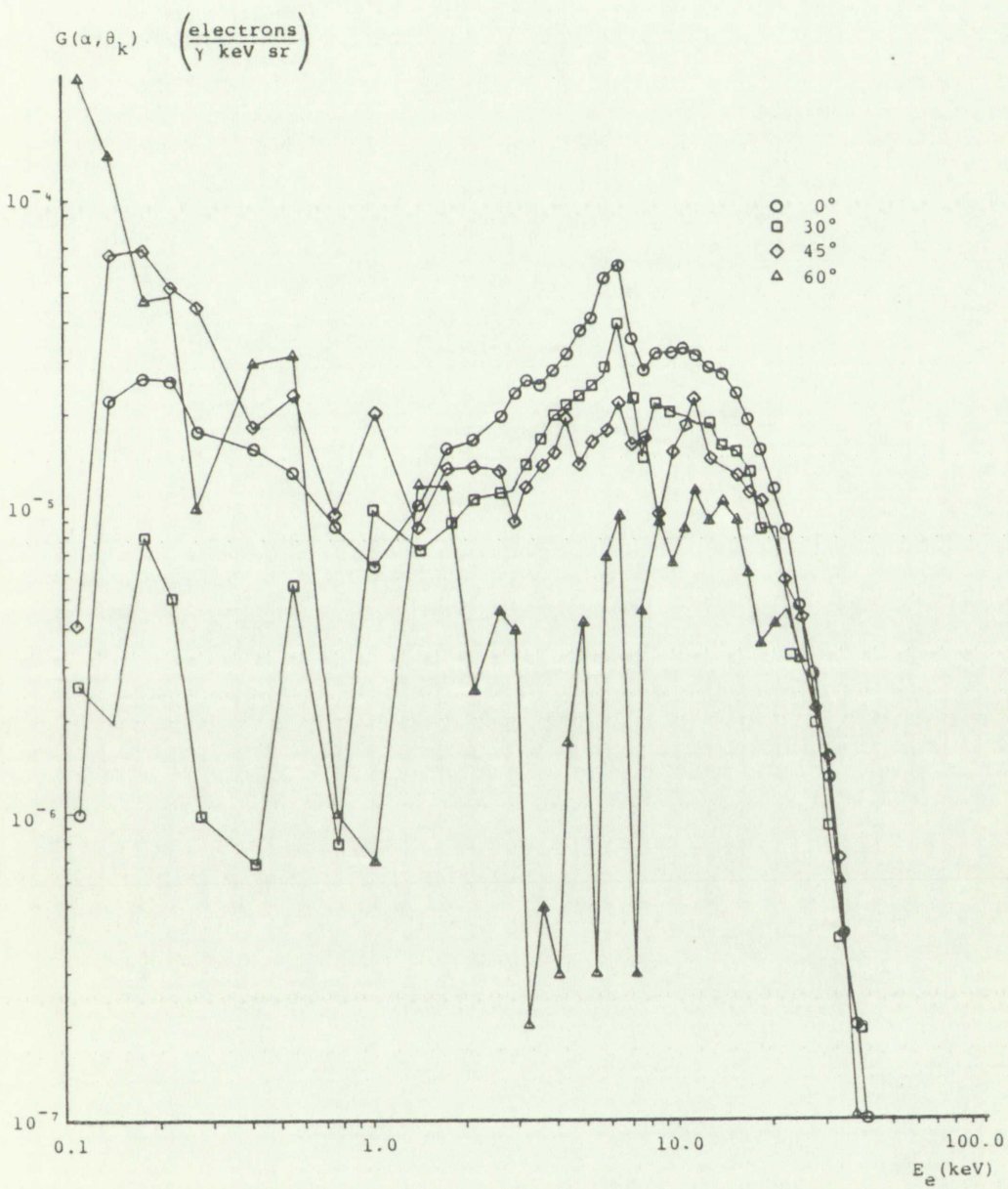


FIGURE 22. Differential Yield vs. Energy;
Cu with Filter



FIGURE 10. Differential yield vs. Energy
 Cu with filter

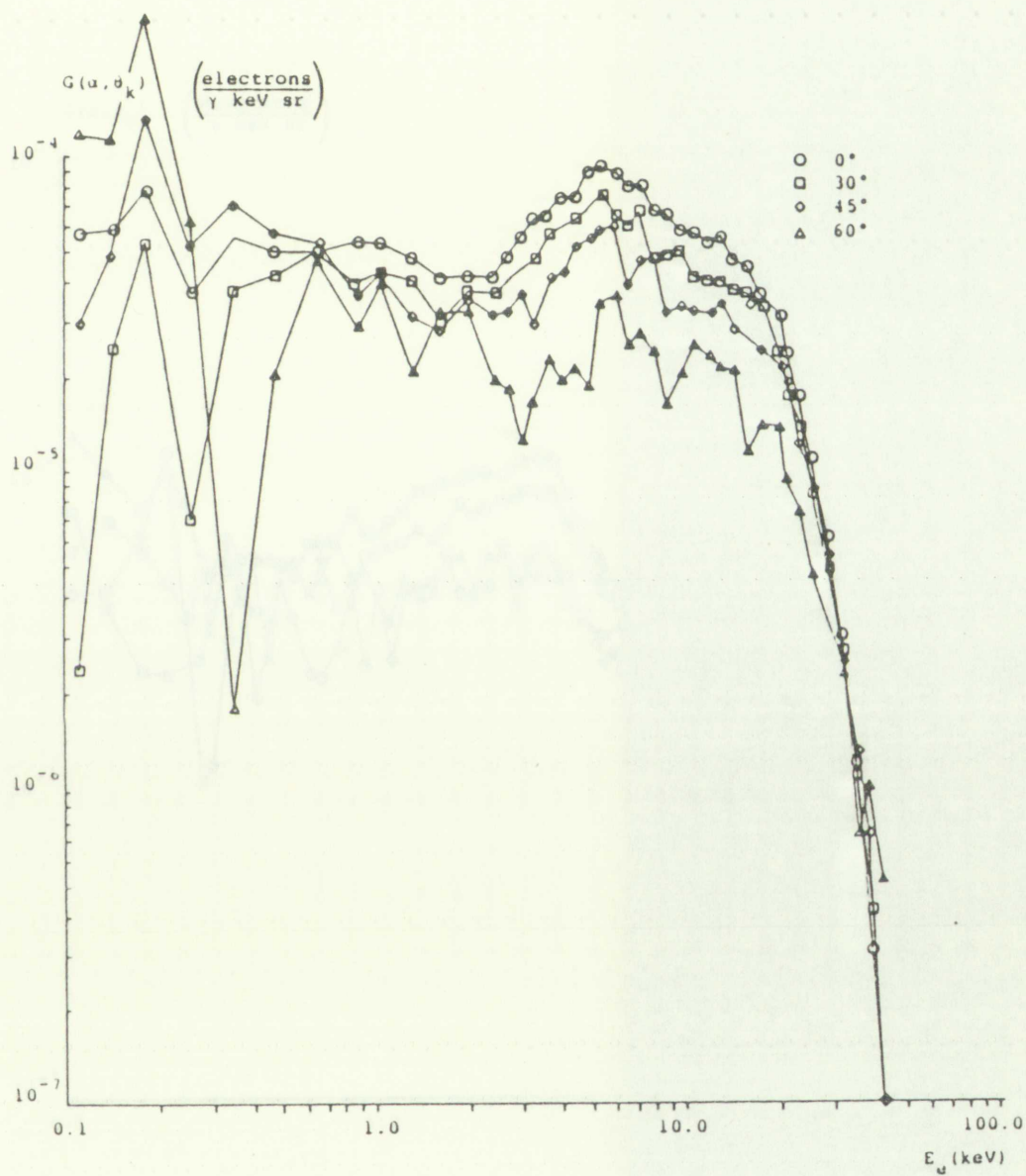


FIGURE 23. Differential Yield vs. Energy;
Ta with Filter



FIGURE 23. Differential Yield vs. Energy
 The Weib Filter

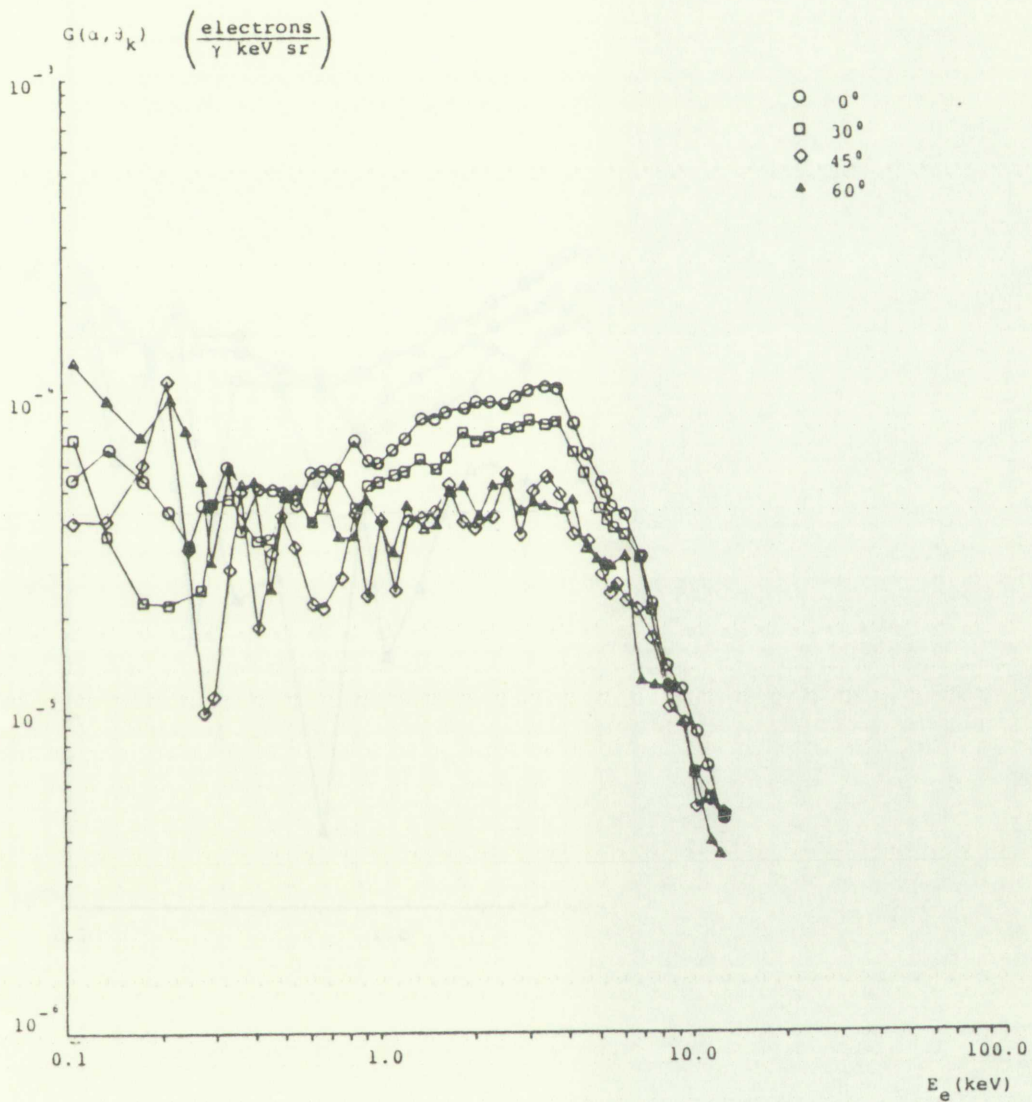


FIGURE 24. Differential Yield Versus Energy;
Mg, Unfiltered

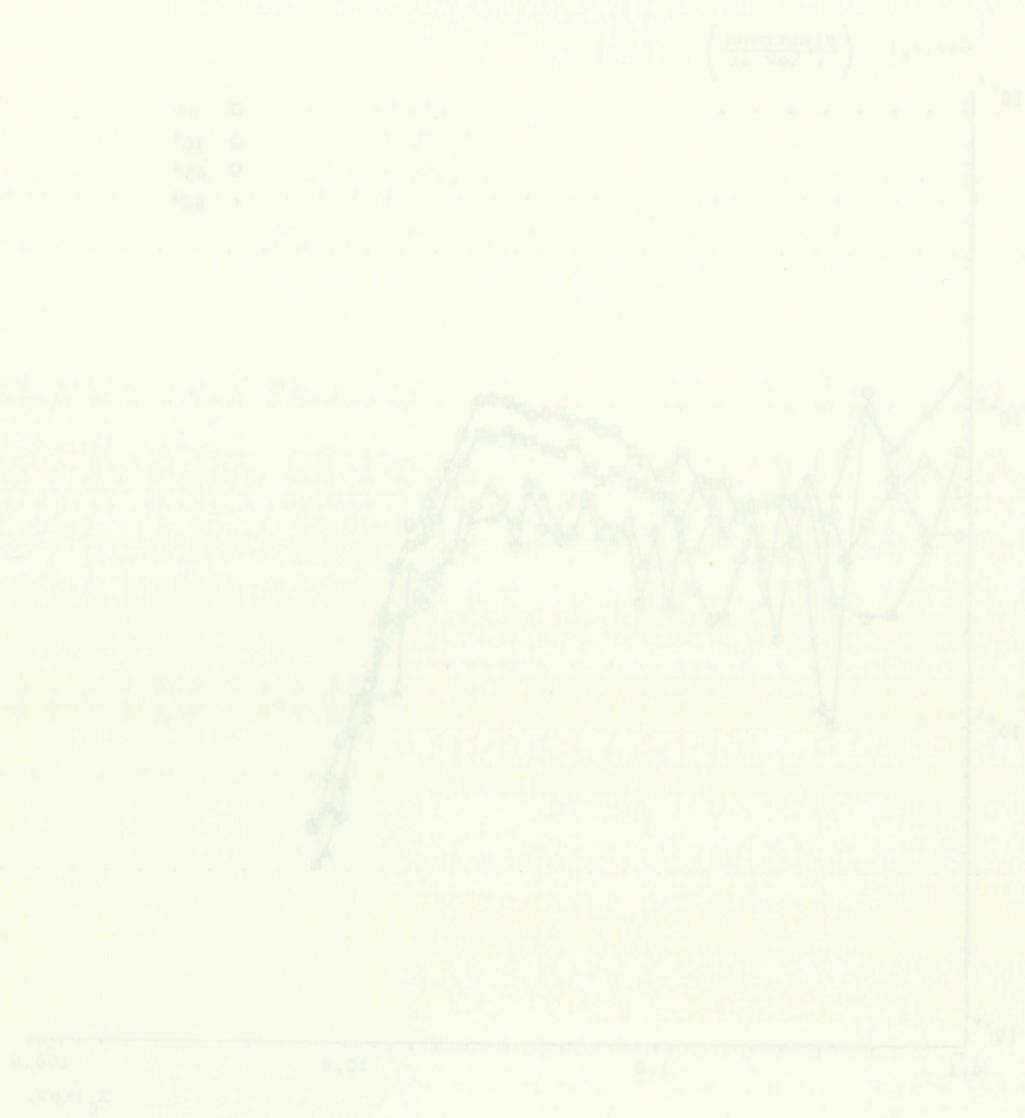


FIGURE 2A. Differential Yield versus Energy
No. Unfiltered

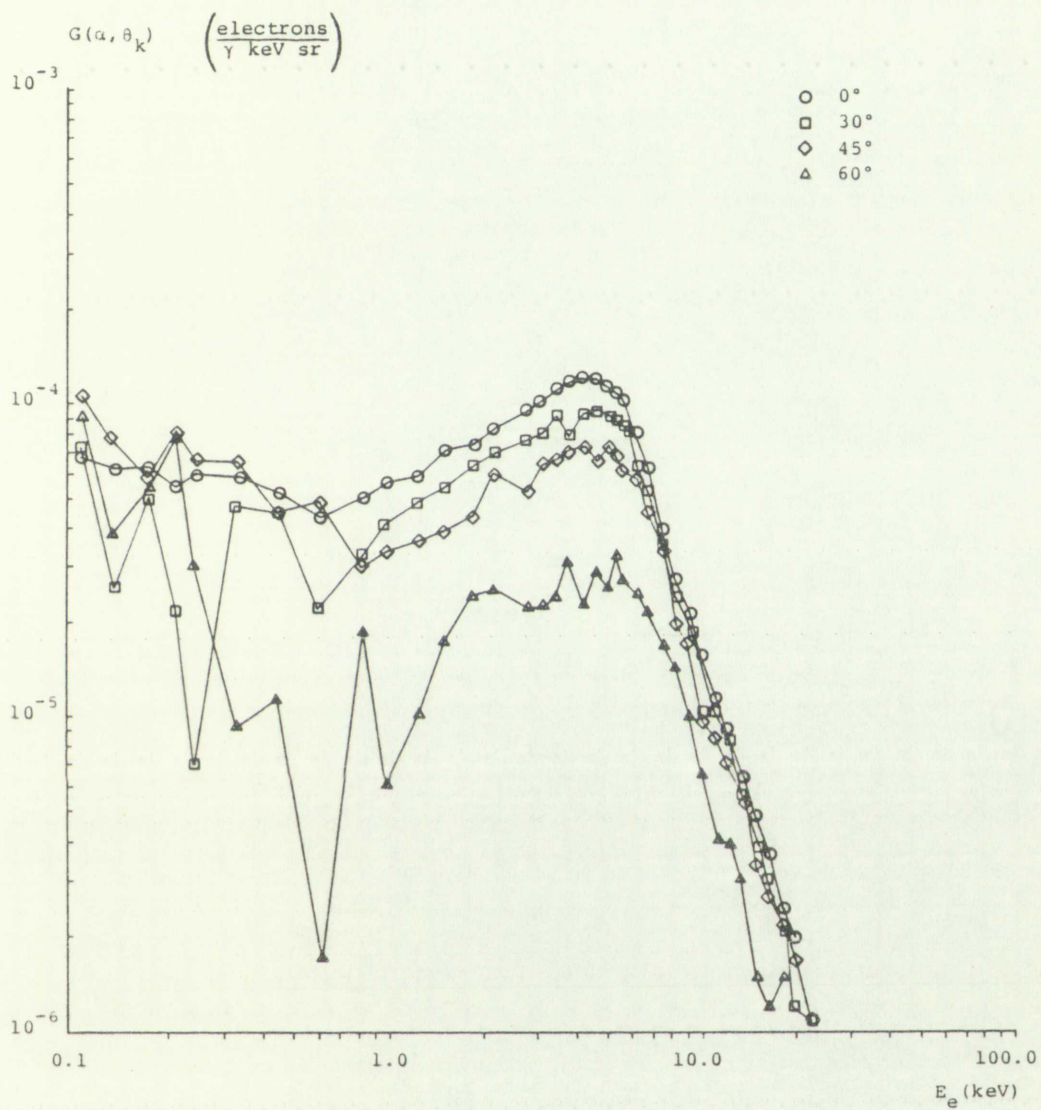


FIGURE 25. Differential Yield vs. Energy;
Al, Unfiltered

(continued)



FIGURE 2. Difference
A1, Unit

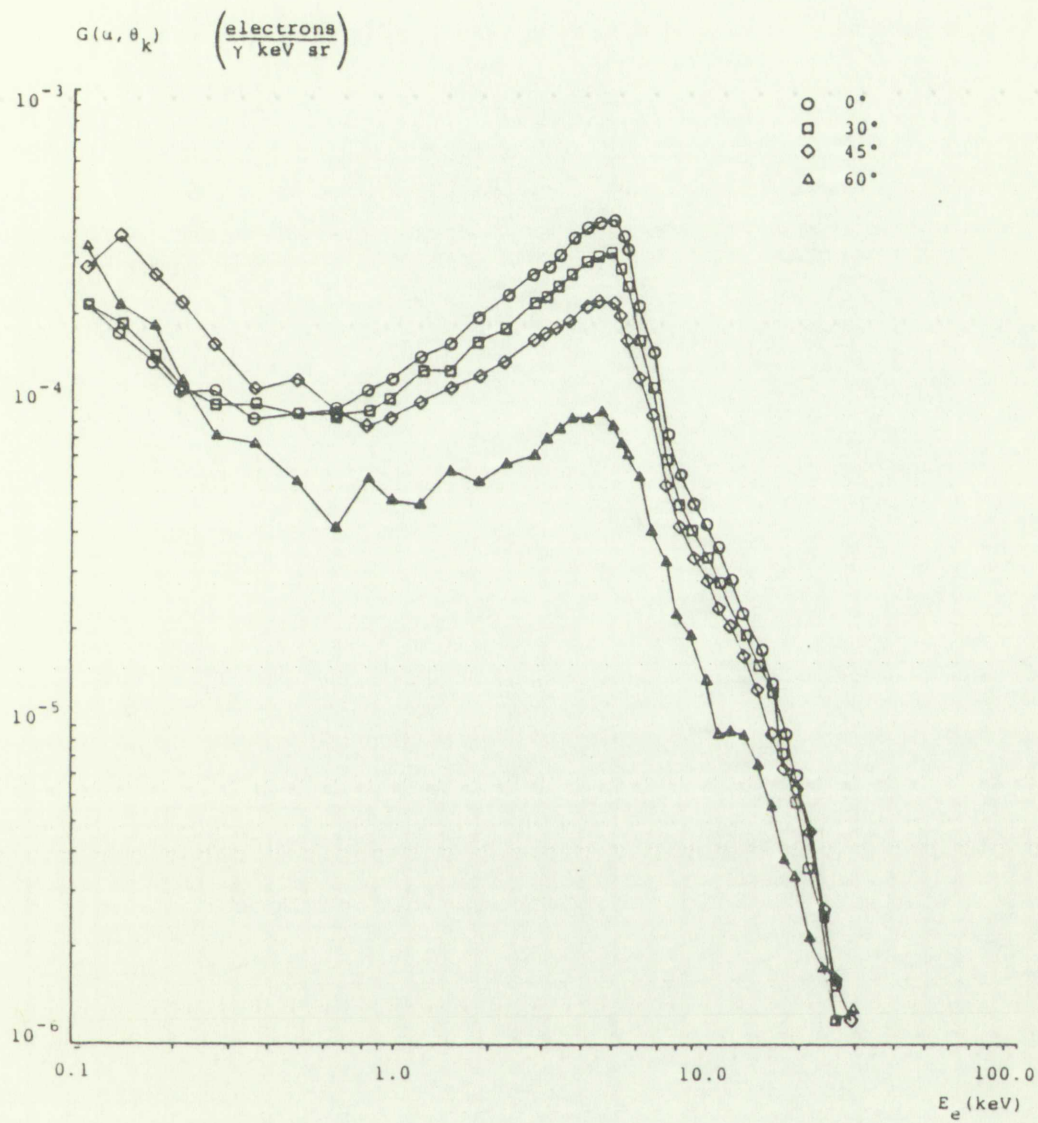


FIGURE 26. Differential Yield vs. Energy;
Cu, Unfiltered



FIGURE 36. Differential Yield vs. Energy
Cu, unfiltered

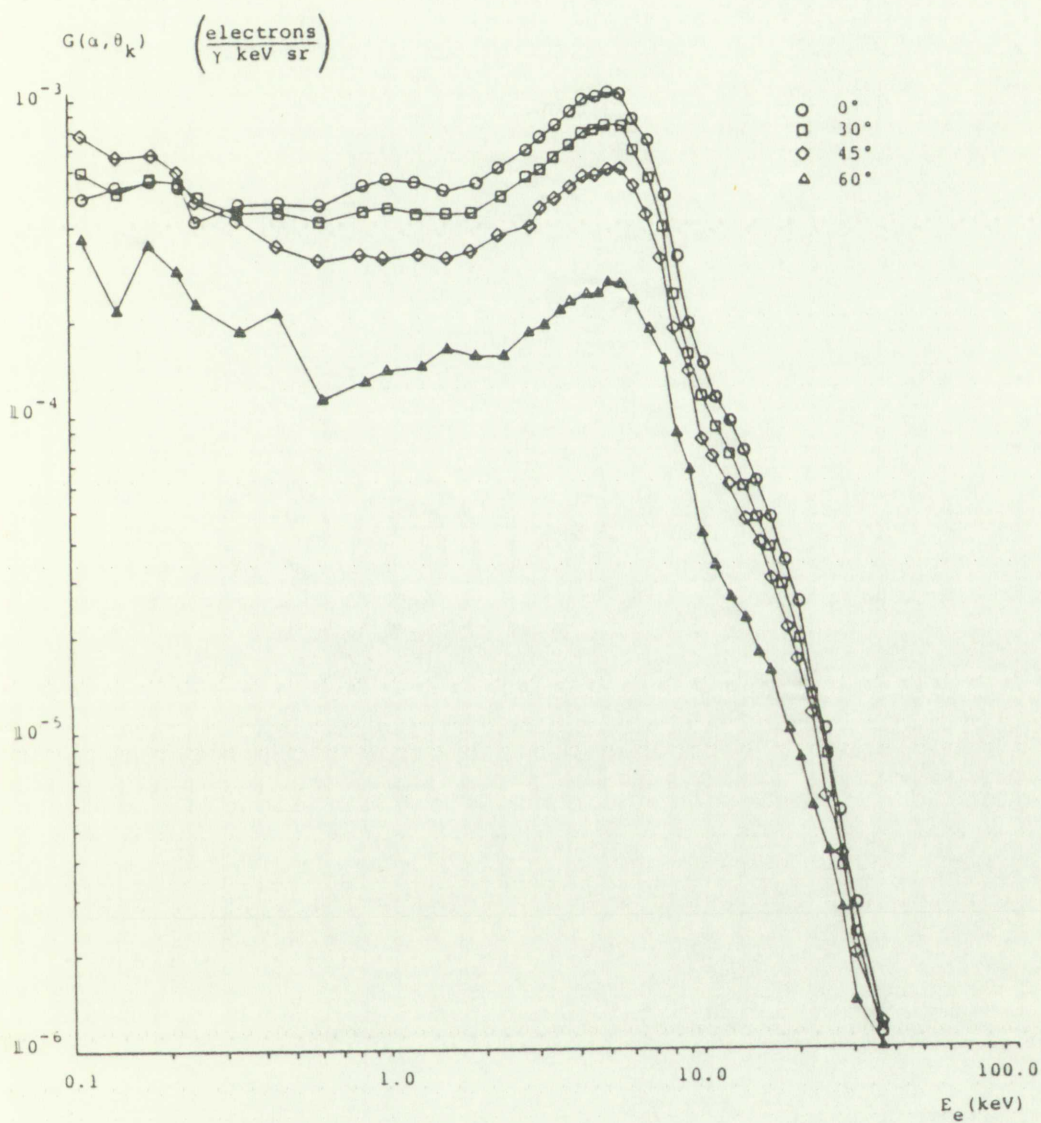


FIGURE 27. Differential Yield vs. Energy;
Ta, Unfiltered

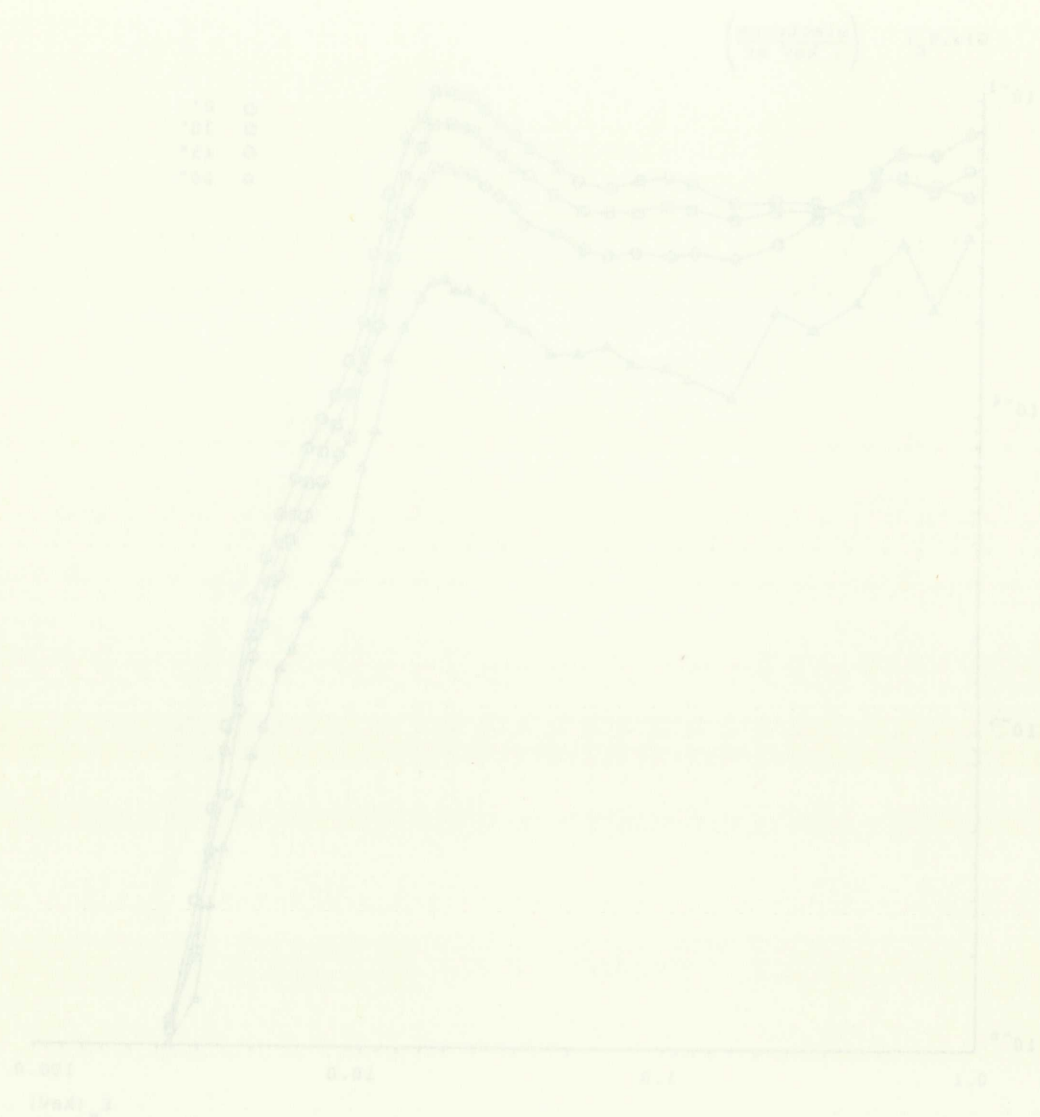


FIGURE 27. Differential Yield vs. Energy.
T₀ = 0°C.

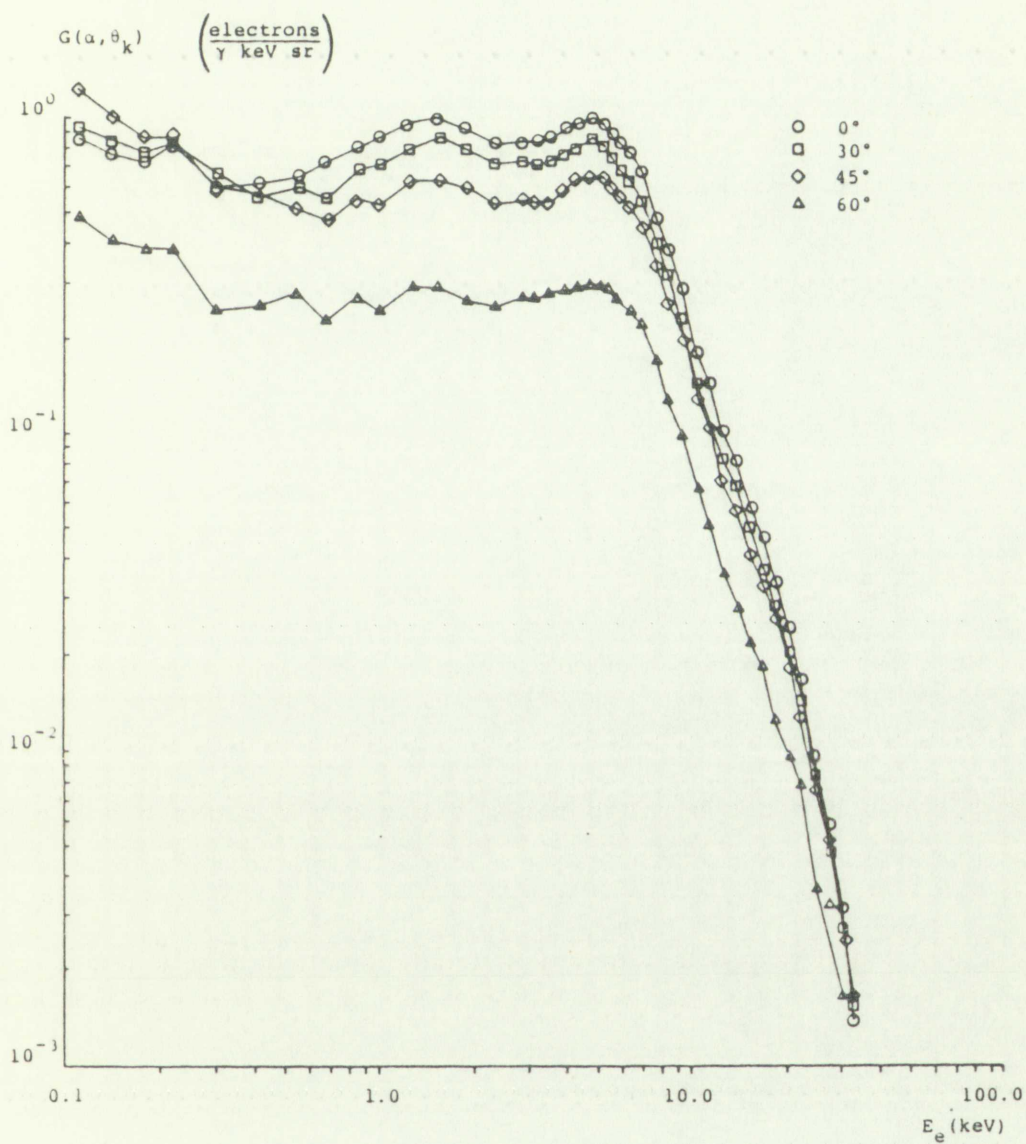


FIGURE 28. Differential Yield vs. Energy;
Pb, Unfiltered



FIGURE 10

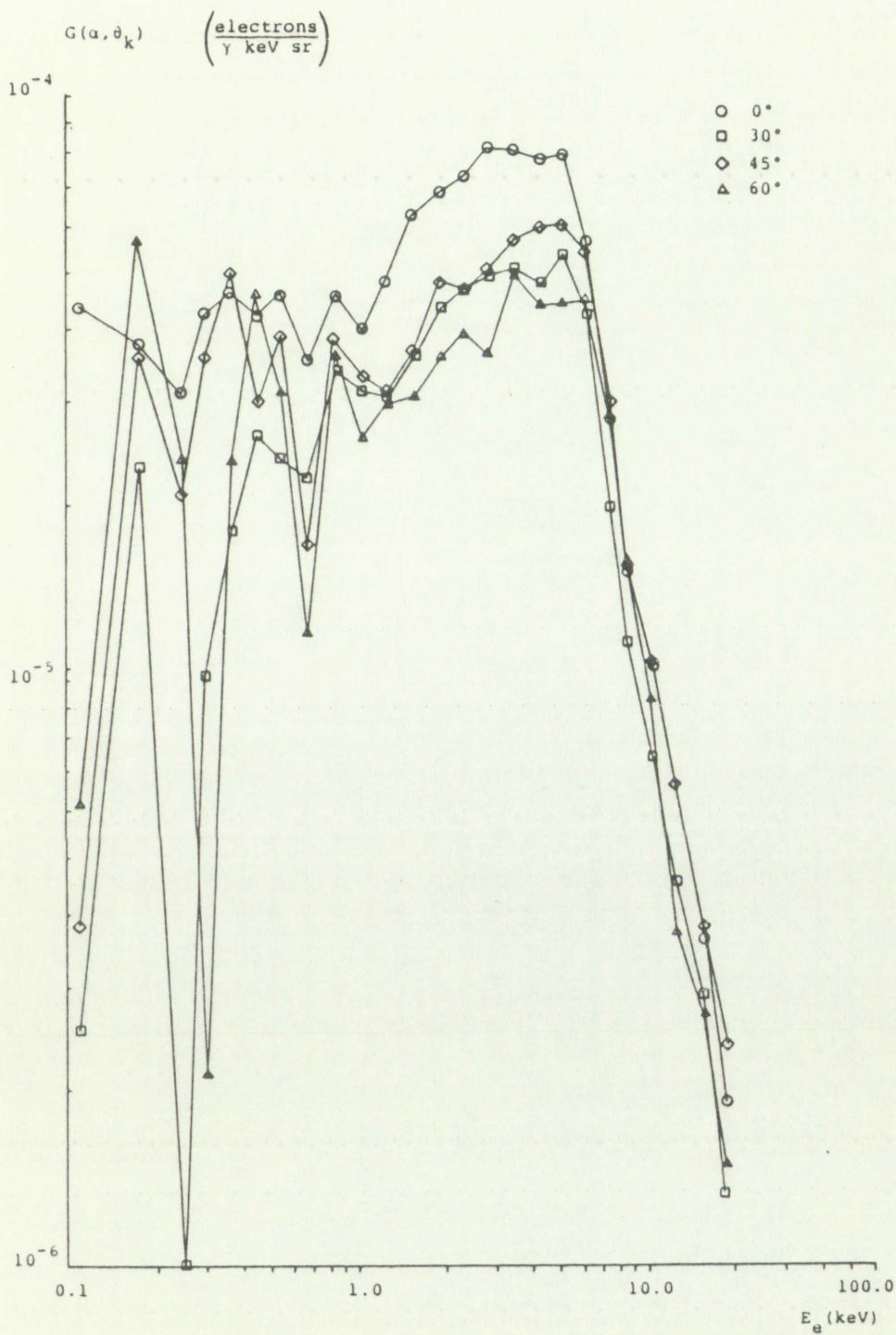


FIGURE 29. Differential Yield vs. Energy;
Cover Glass, Unfiltered



FIGURE 1. Relationship of Yield vs. Energy.
Yield (Y) vs. Energy (E)

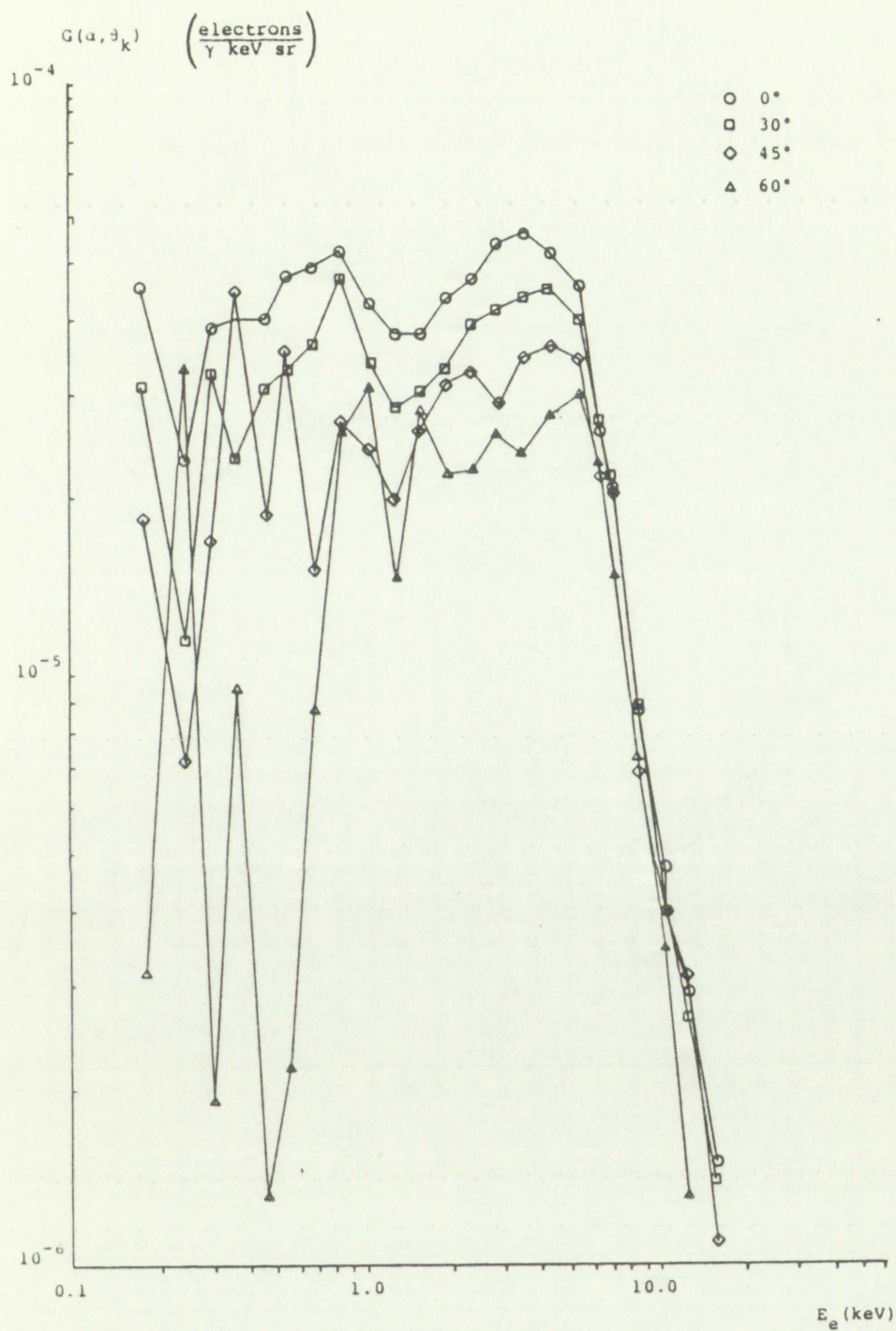


FIGURE 30. Differential Yield vs. Energy;
Silica Cloth, Unfiltered



FIGURE 10. Yield of different species as a function of electron energy. The yield is defined as the number of molecules of a given species produced per unit energy of the incident electron beam.

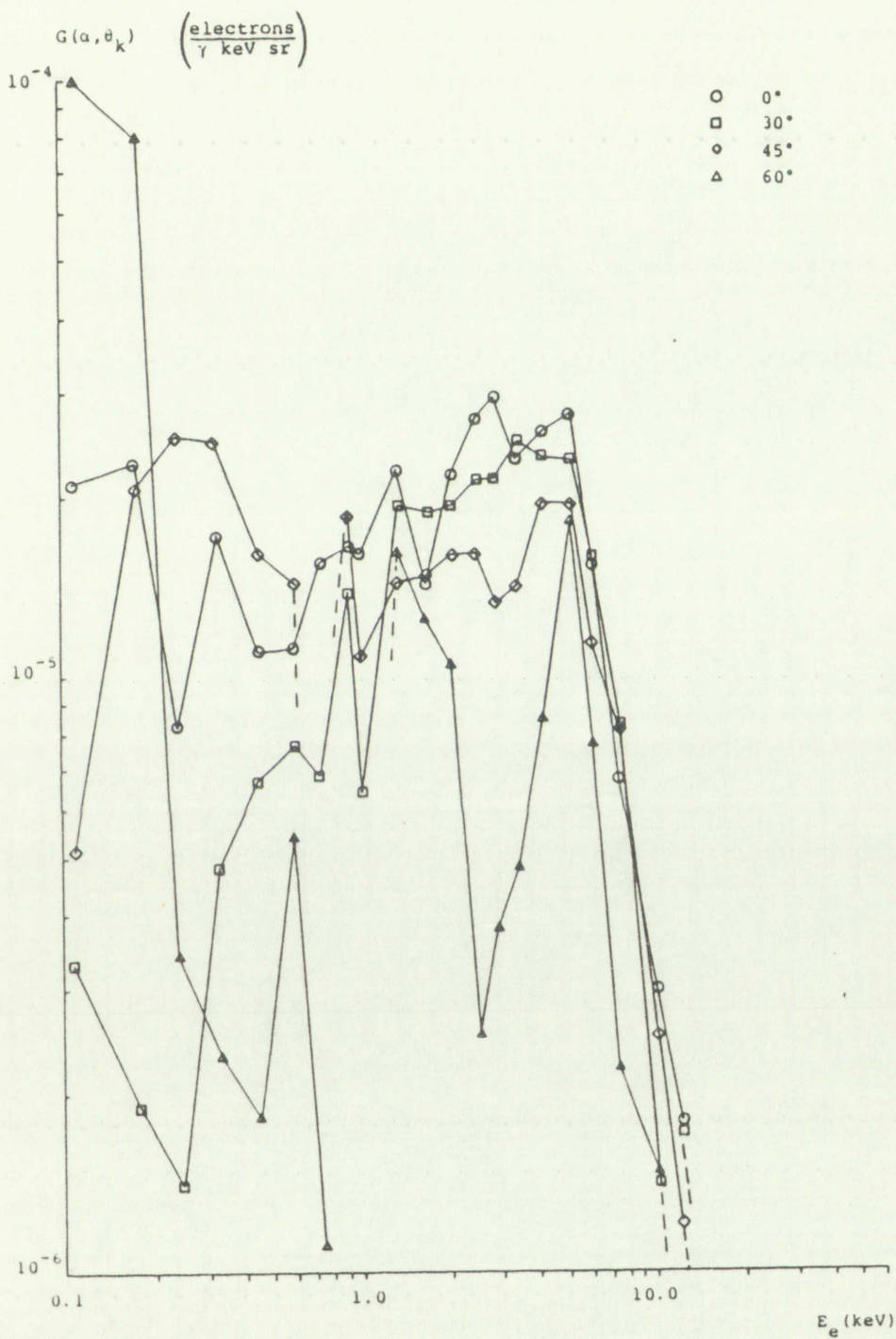


FIGURE 31. Differential Yield vs. Energy;
Thermal Control Paint, Unfiltered



FIGURE 11. Differential Yield vs. Energy,
Thermal Control Paint, Unlabeled

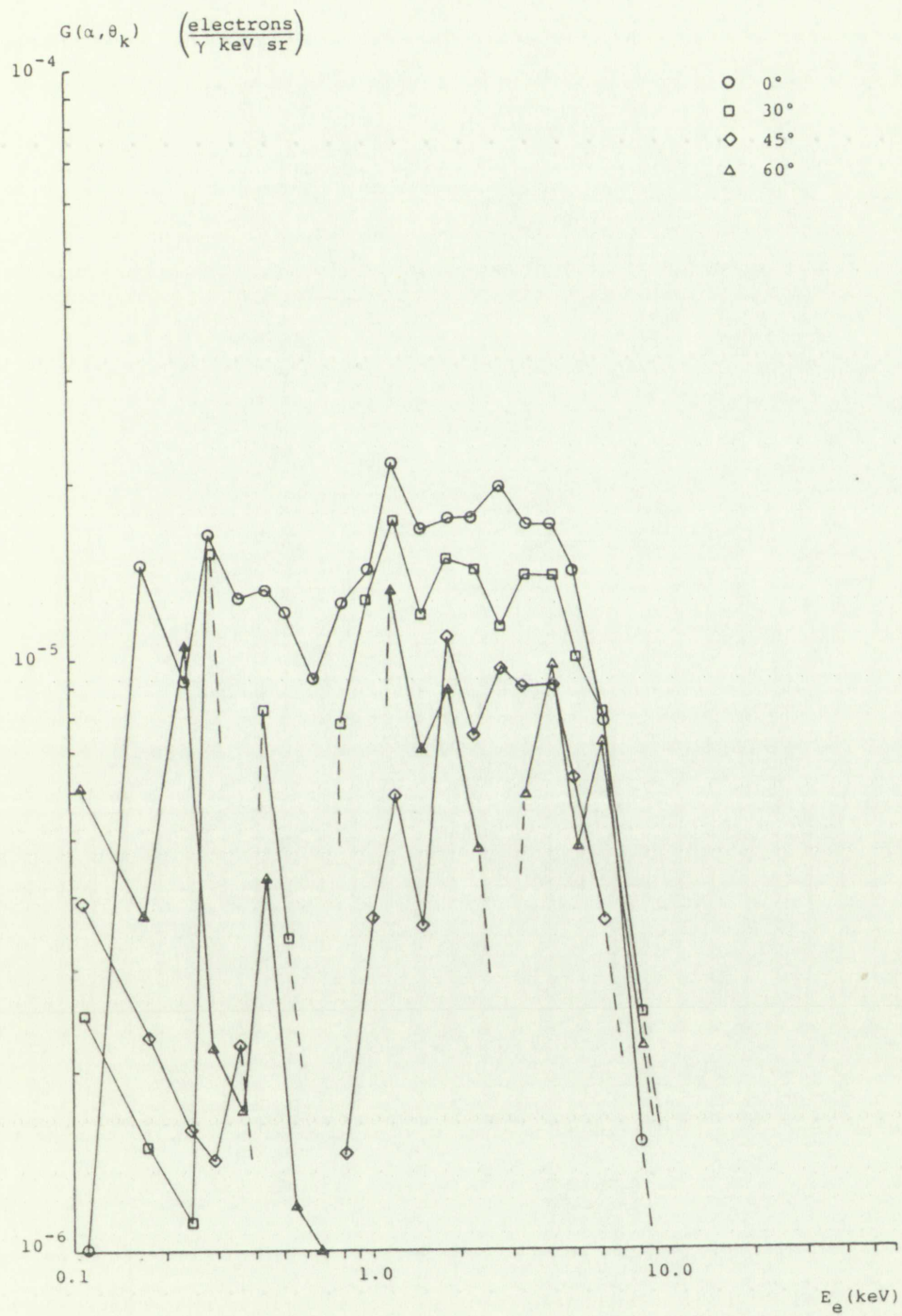


FIGURE 32. Differential Yield vs. Energy;
Kevlar, Unfiltered



FIGURE 15. Differential Yield vs. Energy
Neutron-Induced Reactions



FIGURE 33. Differential Yield vs. Energy;
Mylar, Unfiltered



FIGURE 11. Difference between the two series.

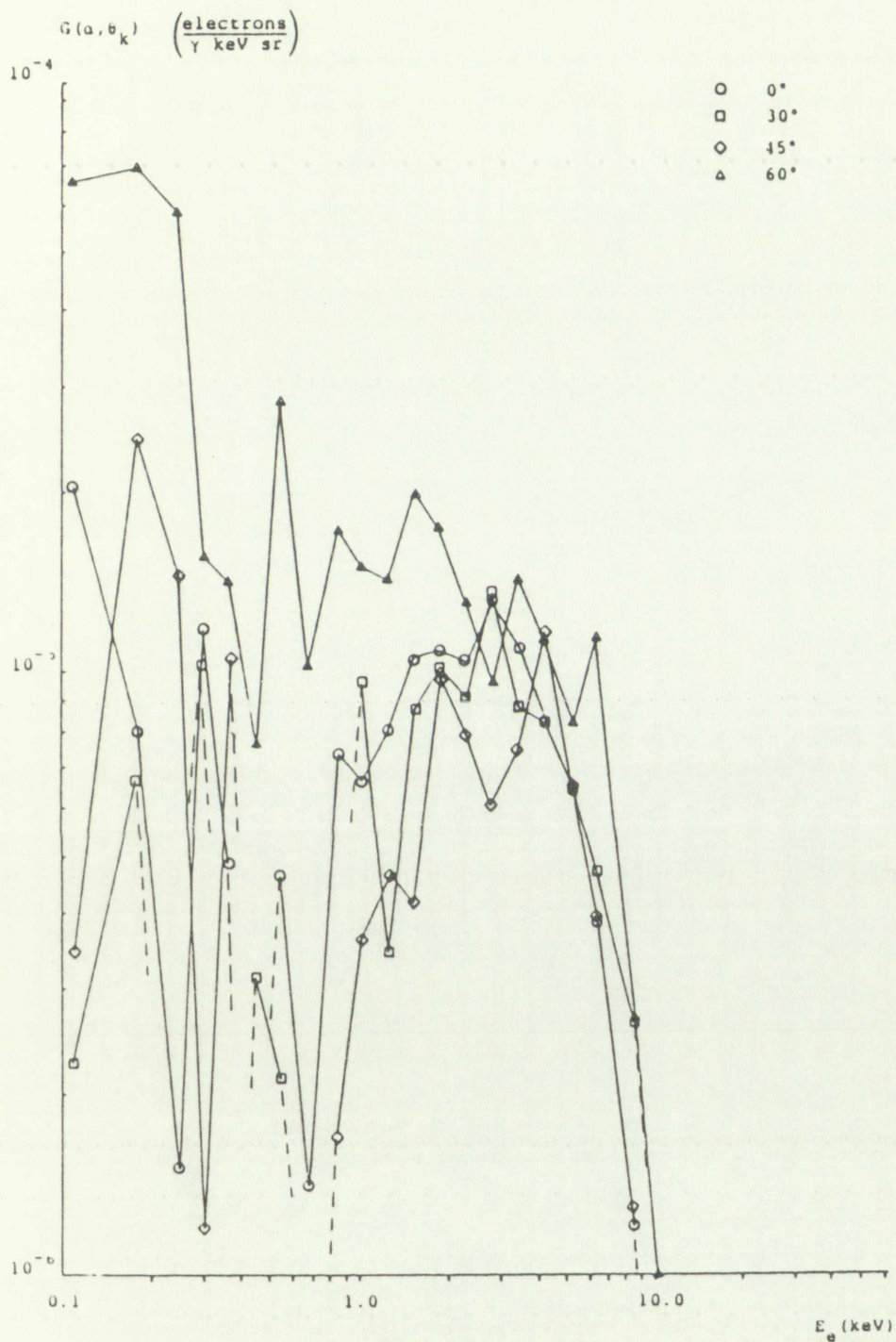


FIGURE 34. Differential Yield vs. Energy;
Non-conducting Epoxy, Unfiltered



FIGURE 1. Potential Field vs. Energy
Unilaminar Epoxy, Unilaminar

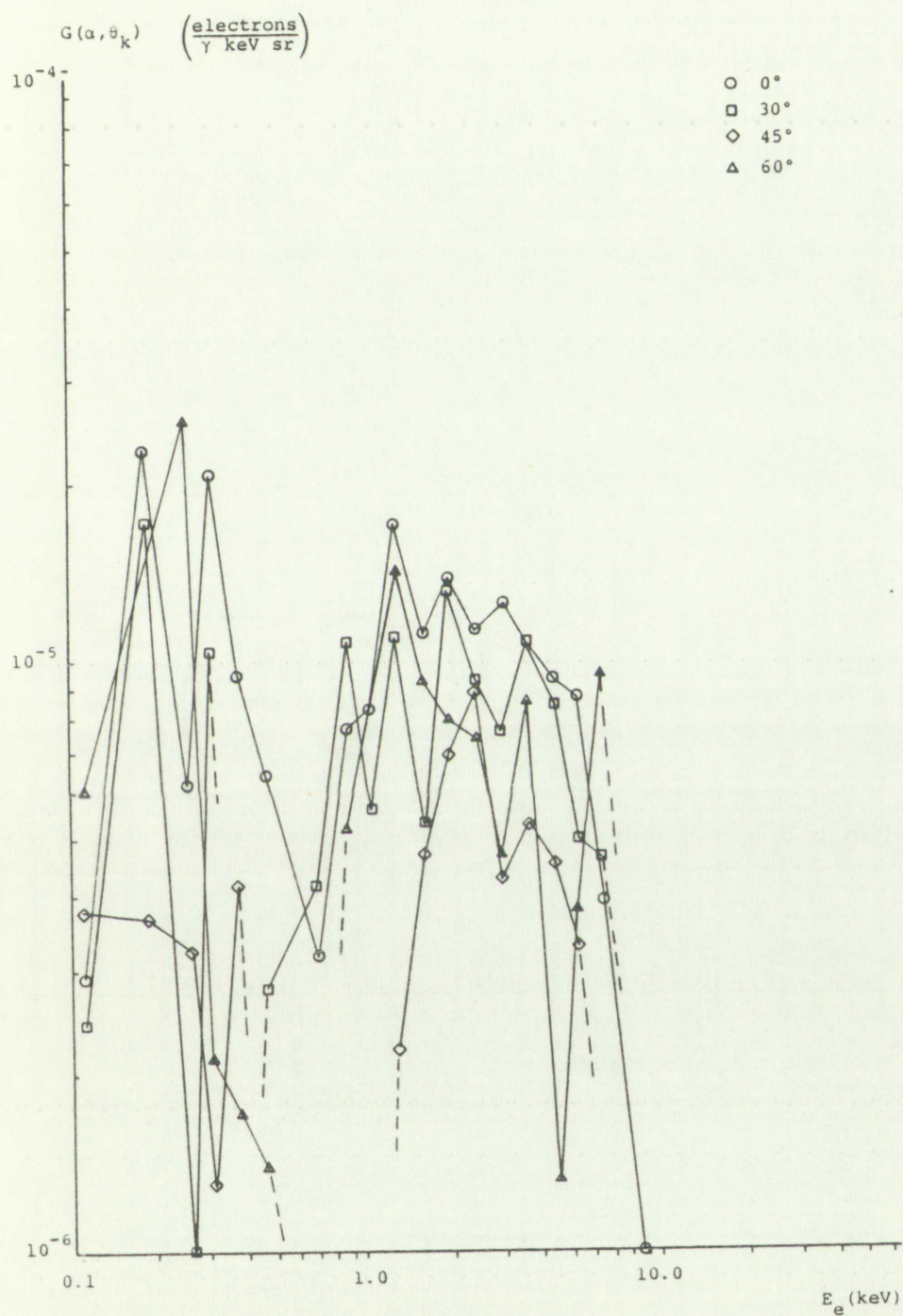


FIGURE 35. Differential Yield vs. Energy;
Conducting Epoxy, Filtered



FIGURE 12. Differential Yield vs. Energy for
Conducting Epoxy, Filtered

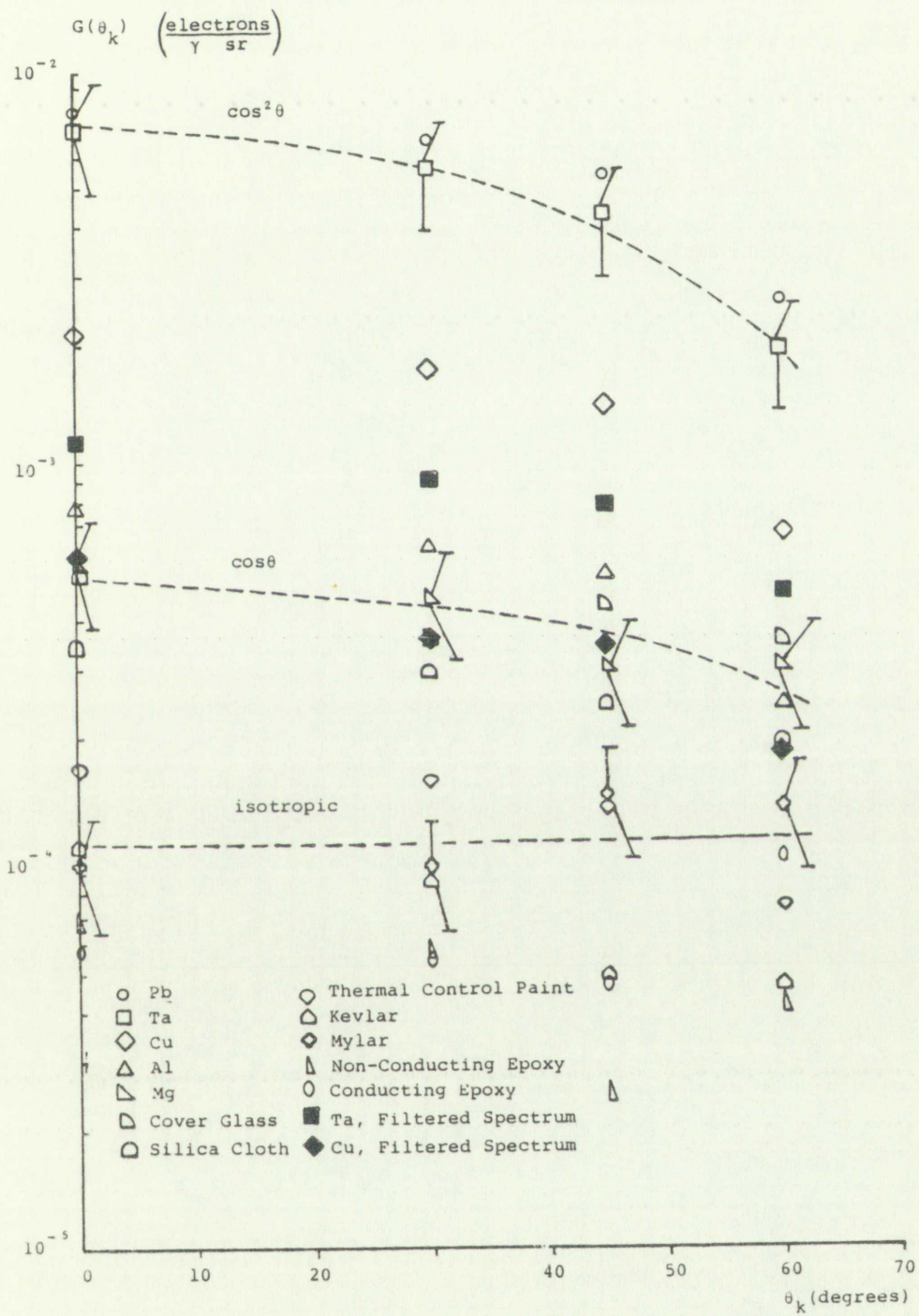


FIGURE 36. Energy Integrated Yield



FIGURE 10. Energy Integrated Yield

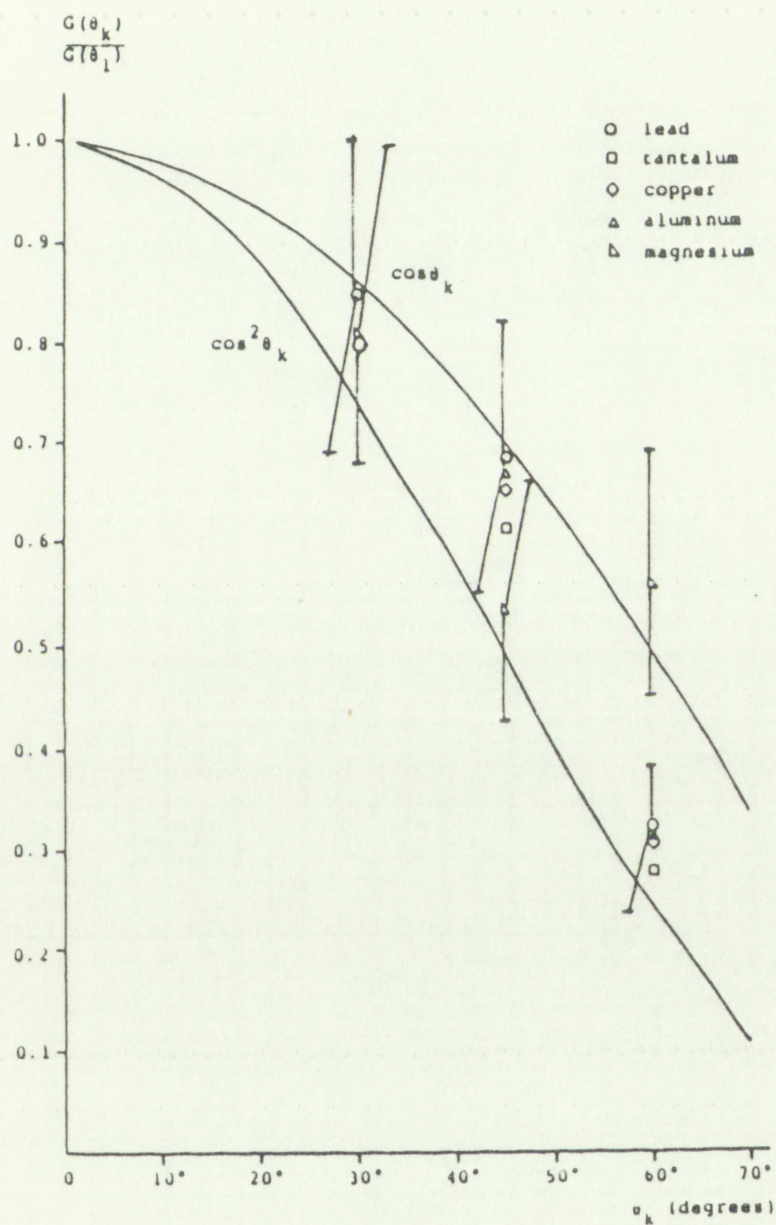


FIGURE 37. Normalized Yield vs. θ_k ; Metal Targets

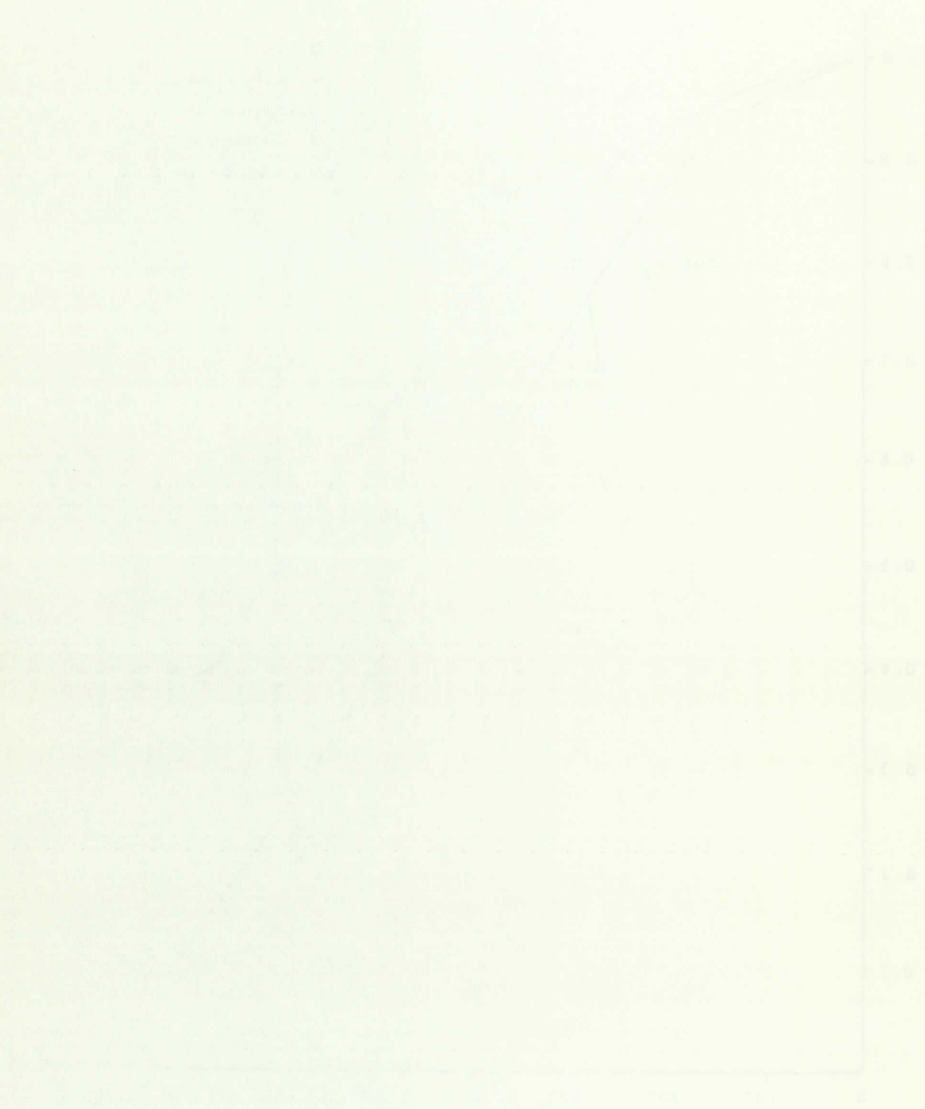


Figure 1. The effect of the concentration of the reactants on the rate of the reaction.

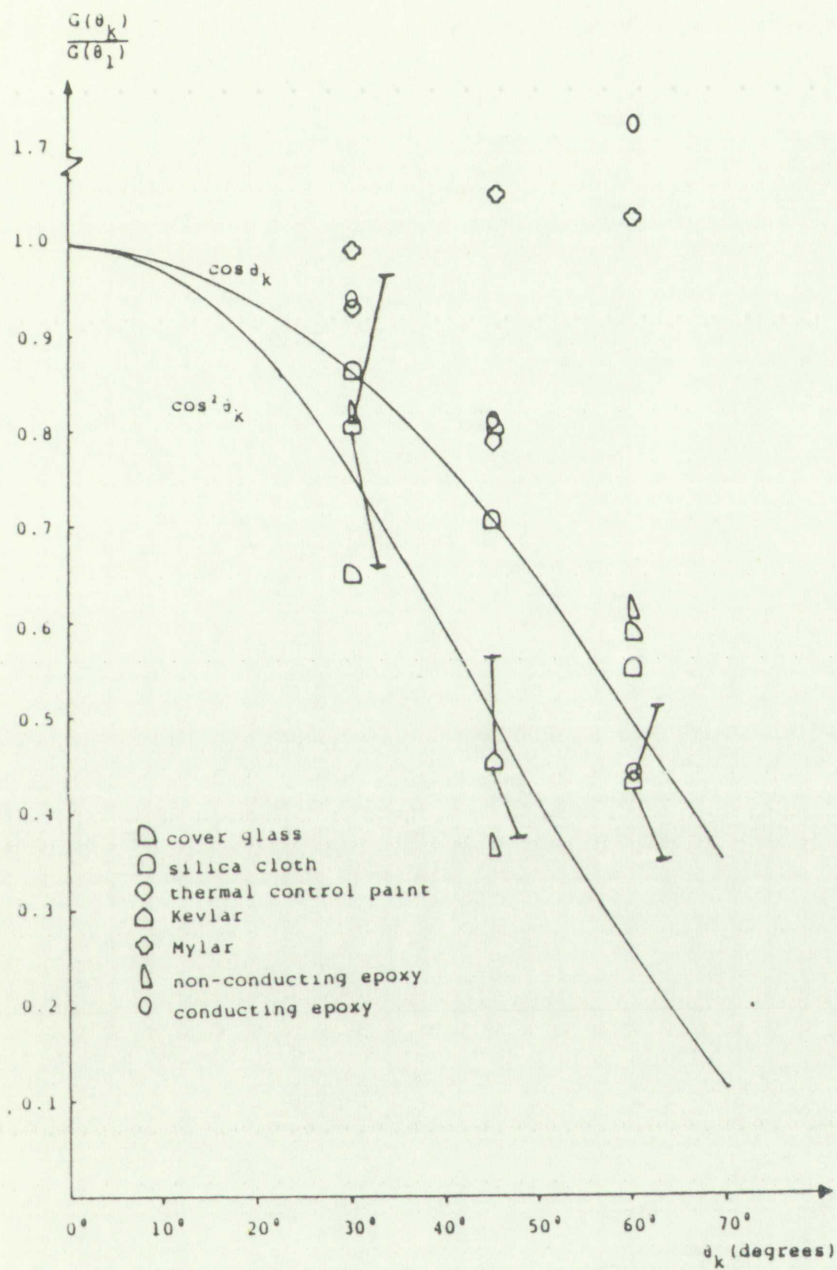


FIGURE 38. Normalized Yield Versus θ ; Non Metallic Targets



FIGURE 1. Relationship between \log_{10} of the response and the concentration of the stimulus.

SECTION V

V. 8017382

DISCUSSION AND SUMMARY

Features of Emission Curves

The dependence of electron emission characteristics on the incident X-ray spectrum can be seen by comparing the differential yields of copper and tantalum measured with filtered and unfiltered 50 kV bremsstrahlung spectra. Comparing the results for copper, Fig. 22 with Fig. 26, it is seen that for the filtered spectrum (broad peak in X-ray energy at ~ 30 keV, Fig. 11) there is a correspondingly broad buildup in the electron energy distribution between 8 and 25 keV. This corresponds to the generation of primary photoelectrons of energy $E_e = h\nu - BE_k$ from K-shell interactions. The unfiltered spectrum has a much larger fraction of its fluence below 20 keV and consequently gives a significantly larger electron yield due to K-shell or L-shell photoelectron interactions from X rays below this energy. Both curves show a more rapid increase in yield just below the K-edge (8.9 keV) in X-ray absorption coefficient as the energy of the X rays falls below the K-shell binding energy and L-shell interactions begin to dominate the photoelectric process. In particular, Fig. 26 shows a peak in emission occurring at approximately 5 keV which correlates with the increase in L-shell photo-

Features of Emission Curves

The dependence of electron emission characteristics on the incident X-ray spectrum can be seen by comparing the differential yields of copper and tantalum measured with filtered and unfiltered 50 kV x-ray emitting spectra. Comparing the results for copper, Fig. 12 with Fig. 10, it is seen that for the filtered spectrum (broad peak in X-ray energy at 30 keV, Fig. 11) there is a correspondingly broad buildup in the electron energy distribution between 8 and 32 keV. This corresponds to the generation of primary photoelectrons of energy $E_e = h\nu - E_K$ from K-shell interactions. The unfiltered spectrum has a much larger fraction of its fluence below 30 keV and consequently gives a significantly larger electron yield due to K-shell or L-shell photoelectron interactions from X rays below this energy. Both curves show a more rapid increase in yield just below the K-edge (8.9 keV) in X-ray absorption coefficient as the energy of the X rays falls below the K-shell binding energy and L-shell interactions begin to dominate the photoelectric process. In particular, Fig. 12 shows a peak in emission occurring at approximately 5 keV which correlates with the increase in L-shell photo-

electron generation and KLL Auger electrons ($E_e = BE_K - 2BE_L \approx 7$ keV). Electrons created by K-shell fluorescence X rays and subsequent L-shell photoelectrons will also contribute to this portion of the emission spectrum. Both curves exhibit a decrease in yield between 5 keV and 1 keV, the filtered spectrum falling noticeably faster, as the relative number of X rays in the incident spectrum decreases. The buildup in yield below 1 keV is most likely attributable to lower order Auger electrons and to low energy secondary electrons generated near the target surface from ionization caused by the more energetic photoelectrons and Auger electrons.

A similar comparison can be made for the tantalum data (Fig. 23 and Fig. 27). The electron emission spectrum with filter shows a relatively larger contribution from the 20 to 40 keV X rays than does the unfiltered X-ray electron emission spectrum. The distribution in Fig. 23 shows evidence of a broad peak around 15 keV which corresponds to K-shell photoelectrons ($E_e \leq h\nu - BE_K$ keV) from the peak of the X-ray distribution. The L-edge in tantalum also occurs at 15 keV, and an increasing steepness in the yield occurs from about 12 keV to a peak at approximately 5-6 keV. This increase with the unfiltered spectrum results from increasing L-shell photoelectron generation ($E_e \leq$

electron generation and subsequent emission is - 20%
100% - 70% (Electron emission from a K-shell is 100%
since X rays and subsequent electron emission are 100% efficient)
also contributes to the generation of the electron
emission. Both electron emission and electron emission
from 2 keV and 1 keV. The filtered spectrum shows
noticeably faster, as the electron emission is a fast
the incident spectrum decreases. The output in terms
below 1 keV is most likely attributable to lower energy
Auger electrons and to low energy secondary electrons
generated near the target surface from electron emission
by the more energetic photoelectrons and Auger
electrons.
A similar comparison can be made for the emission
data (Fig. 1) and Fig. 2). The electron emission
spectrum with filter shows a relatively low
contribution from the 20 to 50 keV X rays than does the
unfiltered X-ray electron emission spectrum. The
distribution in Fig. 2) shows evidence of a small peak
around 15 keV which corresponds to K-shell photo-
electrons ($E_p = 20 - 25 \text{ keV}$) from the peak of the
X-ray distribution. The L-edge in tantalum also occurs
at 15 keV, and an increasing steepness in the peak
occurs from about 15 keV to a peak at approximately 20
keV. This increase with the unfiltered spectrum results
from increasing L-shell photoelectron generation in

$h\nu_{pk} - BE_L \approx 6 \text{ keV}$), and competing LMM Auger electrons ($E_e \leq BE_L - 2BE_M \approx 7 \text{ keV}$). A decrease in yield, similar to that observed in copper, occurs between the peak and 1-2 keV (the filtered spectrum decreasing more rapidly), and an increase from lower order Augers, fluorescent X rays and low energy secondaries below this energy.

The increase in yield with decreasing X-ray energy is noted by the difference in ordinate scales for filtered and unfiltered data for copper and tantalum, and a similar comparison for these materials for the energy integrated yield as a function of emission angle shown in Fig. 36 (the subscript F indicates the filtered X-ray spectrum). For the same X-ray fluence in terms of cal/cm^2 , the low energy spectrum gives factors of 6 and 4 greater electron yields for tantalum and copper respectively.

Examination of Figs. 24 and 25 for magnesium and aluminum, respectively, shows basically similar features for the unfiltered spectrum. The K-edge absorption in both materials is well below the low energy cutoff of the X-ray spectrum, hence no noticeable discontinuities appear in the electron energy distributions. Both show contribution to their low energy electron emission spectra from K-shell Auger electrons ($E_e = 1.3$ and 1.15 keV for Al and Mg, respectively). Figure 28 shows data for lead with an unfiltered spectrum. The K-edge in

lead occurs at 88 keV, well beyond the high energy limit of the X-ray spectrum. The L-edge absorption occurs at approximately 16 keV, and a slight increase in the rate of change of yield with decreasing energy can be noted below this energy. M-shell absorption edges occur from 3 to 4 keV and a peak in the emission yield appears at ~ 5 keV corresponding to M-shell photoelectrons ($E_e \leq h\nu_{pk} - BE_M \approx 5$ keV) generated from the peak of the X-ray energy spectrum. Electrons of energy $E_e \leq BE_L - 2BE_M \approx 7.8$ keV will also be generated by L-shell X-ray fluorescence and the subsequent M-shell photoelectrons. The peak in the yield distribution around 1.5 keV correlates with fluorescence transitions between M- and N-shell electrons after M-shell photoelectron interactions; for example $E_e \leq BE_M - 2BE_N \approx 2.1$ keV. Low energy secondary electrons are seen to increase below 0.4 keV.

Comparing the electron emission at specific emission angles for a given material, it is generally observed that there is not a significant variation in energy distribution as a function of angle. Examination of Figs. 24 through 28 for magnesium, aluminum, copper, tantalum and lead show that the differences in emission spectra which do exist are primarily in the low energy region ($E_e \leq 1$ keV) where emission tends to be more nearly isotropic. A similar behavior is exhibited by

lead occurs at 85 keV, well beyond the high energy limit of the X-ray spectrum. The L-edge absorption occurs at approximately 15 keV, and a slight increase in the rate of change of yield with decreasing energy can be noted below this energy. M-shell absorption edges occur from 1 to 4 keV and a peak in the emission yield appears at 1.5 keV corresponding to M-shell photoelectrons ($E_p = 2.5 E_M = 38.5$ keV) generated from the peak of the X-ray energy spectrum. Emissions of energy $E_p \leq 38.5$ keV $\approx 2.5 E_M$ will also be generated by L-shell X-ray fluorescence and the subsequent M-shell photoelectrons. The peak in the yield distribution around 1.5 keV correlates with fluorescence transitions between M- and N-shell electrons. After M-shell photoelectron transitions for example $E_p \leq 38.5$ keV $\approx 2.5 E_M$, low energy secondary electrons are seen to increase below 0.4 keV.

Comparing the electron emission at specific emission angles for a given material, it is generally observed that there is not a significant variation in energy distribution as a function of angle. Examination of Figs. 14 through 18 for magnesium, aluminum, copper, tantalum and lead show that the differences in emission spectra which do exist are primarily in the low energy region ($E_p \leq 1$ keV) where emission tends to be more nearly isotropic. A similar behavior is exhibited by

the dielectric targets (Figs. 29 through 35), although the measurement conditions (poorer signal-to-noise ratios) tend to mask the similarity of the electron emission spectra at different emission angles for each material.

Contribution to the total electron emission yield from electrons of energy $0.1 \leq E_e \leq 1.0$ keV for the filtered and unfiltered X-ray spectra for all materials examined was $<10\%$. As a result, the electrons generated by photoelectric, Auger and X-ray fluorescence interactions will dominate the number of electrons emitted from a surface exposed to X rays. The energy distribution, angular distribution and quantum yield of these electrons will basically determine the nature of the source term for SGEMP response calculations. Low energy secondaries $E_e \leq 0.1$ keV will always be present due to ionizing events very near the surface from escaping primaries. Their contribution to the SGEMP response will be minimal due to their relatively small numbers and the presence of a space charge barrier which will limit their travel from the surface.

As noted previously in Fig. 36 the energy integrated electron emission yield varies as $\cos^2 \theta$ for high Z materials; $\cos \theta$ from medium Z to low Z targets; and exhibits a nearly isotropic distribution for the lowest atomic number materials investigated. From this

figure and the data shown in Figs. 37 and 38, the energy integrated electron emission yield can be approximated by a $\cos \theta$ dependence. (This approximation will over estimate the spatially integrated yield for high Z metals by 33% and under estimate the yield from lowest Z materials by a factor of 2). The $\cos \theta$ dependence is in agreement with simple models which assume isotropic generation of photoelectrons within an electron range of the material/vacuum interface and more complex mathematical models which predict electron emission and include angle dependent X-ray and electron interaction cross sections. The $\cos^2 \theta$ curves shown in these figures represent the relative angular distribution of backscattered electrons for normal incidence of high energy electrons on thick foils. Under these conditions, electrons created by penetrating primary electrons undergo a large number of scattering and energy loss collisions before being backscattered from the surface of the foil [26]. The $\cos^2 \theta$ behavior corresponds to the diffusion limit and is analogous to the condition where penetrating X rays create electrons at sufficient depth within a material that escaping electrons undergo multiple scattering interactions before being reverse emitted from the surface.

Yield Dependence on Atomic Number

Figure 39 illustrates the dependence of integrated reverse emission yield on the atomic number of the target material. Experimental data includes dielectrics as well as elements for the unfiltered X-ray spectrum, copper and tantalum results with predictions for the filtered X-ray spectrum and predicted yield for aluminum, copper, tantalum and lead with the unfiltered spectrum. The atomic number of the dielectrics is represented with some uncertainty since the exact composition of the samples was unknown. The solar cell cover glass and silica cloth are basically SiO_2 compounds (effective $Z \approx 11$); the thermal control paint, Kevlar, Mylar and epoxy samples are basically carbon base compounds with estimated effective atomic numbers ranging from 5 to 7.

The yield curve for the unfiltered spectrum shows a $Z^{3.3}$ dependence from $Z = 6$ to $Z = 13$. From $Z = 13$ to $Z = 73$ the yield varies approximately as $Z^{1.3}$ and from $Z = 73$ to $Z = 82$ approximately as Z . This behavior (and its departure from the Z dependence of the photoelectric cross section) is a result of the spectrum of X rays generating the emission and the contribution to the yield from multiple interactions. The curve based on QUICKE 2M results is similar in shape to the experimental data. The slope of the yield curve from Z

Figure 2 illustrates the dependence of integrated
 reverse bremsstrahlung yield on the atomic number of the
 target material. Experimental data included 511 keV
 as well as a spectrum for the unfiltered X-ray spectrum.
 copper and tantalum spectra with predictions for the
 filtered X-ray spectrum and predicted yield for
 aluminum, copper, tantalum and lead with the unfiltered
 spectrum. The atomic number of the diatomic is
 represented with some uncertainty since the exact
 composition of the samples was unknown. The solar cell
 cover glass and silica cloth are basically SiO_2
 compounds (effective $Z = 11$); the thermal control panel,
 Kevlar, Mylar and epoxy samples are basically carbon
 base compounds with estimated effective atomic numbers
 ranging from $Z = 5$ to $Z = 10$.
 The yield curve for the unfiltered spectrum shows a
 $Z^{-1.2}$ dependence from $Z = 5$ to $Z = 13$. From $Z = 13$ to $Z = 20$
 the yield varies approximately as $Z^{-1.2}$ and from $Z = 20$
 to $Z = 30$ approximately as Z^{-1} . This behavior and its
 departure from the Z dependence of the photoelectric
 cross section is a result of the spectrum of X rays
 generating the emission and the contribution to the
 yield from multiple interactions. The curve based on
 QUICK 25 results is similar in shape to the
 experimental data. The slope of the yield curve from $Z = 5$

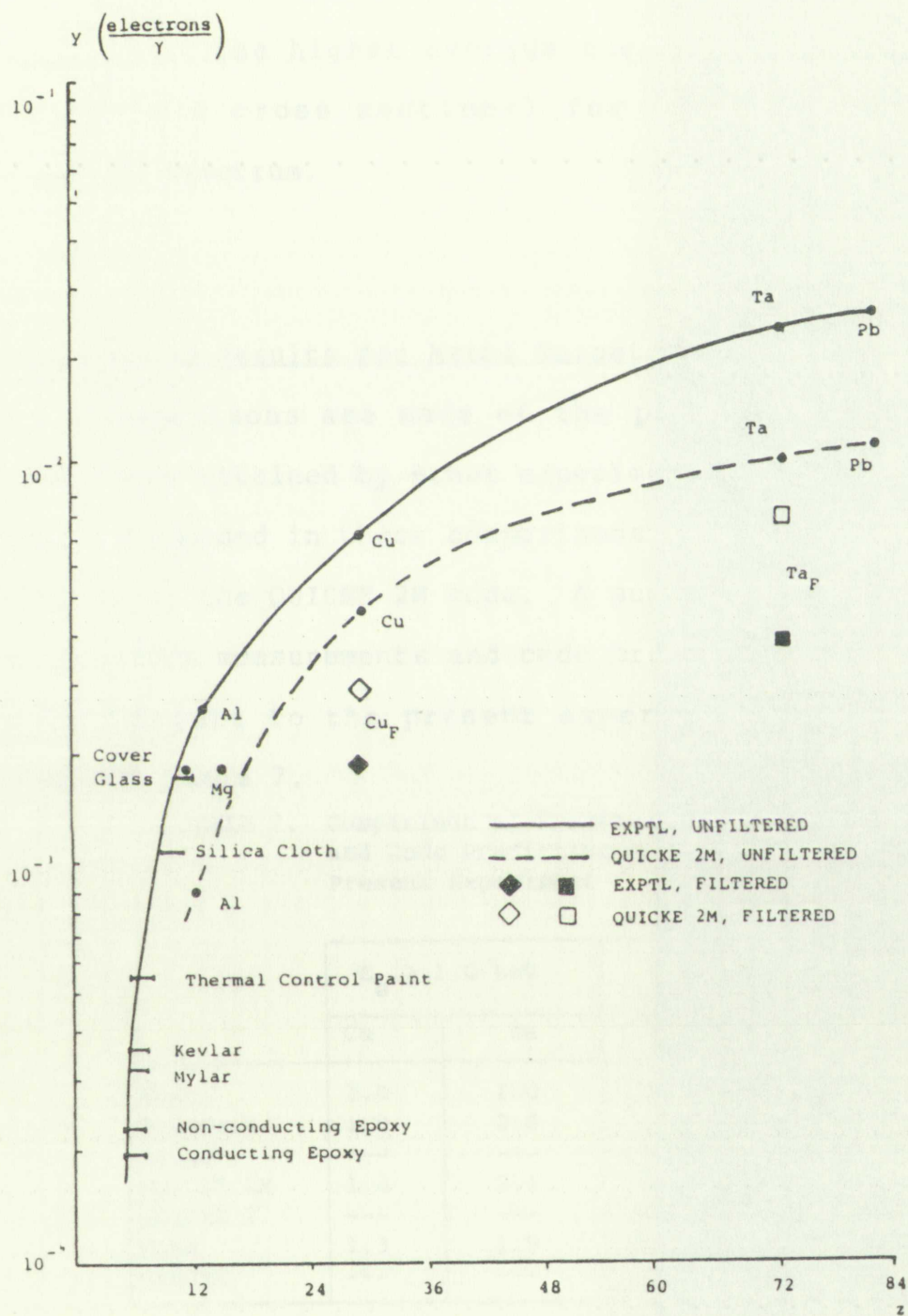


FIGURE 39. Yield Versus Atomic Number

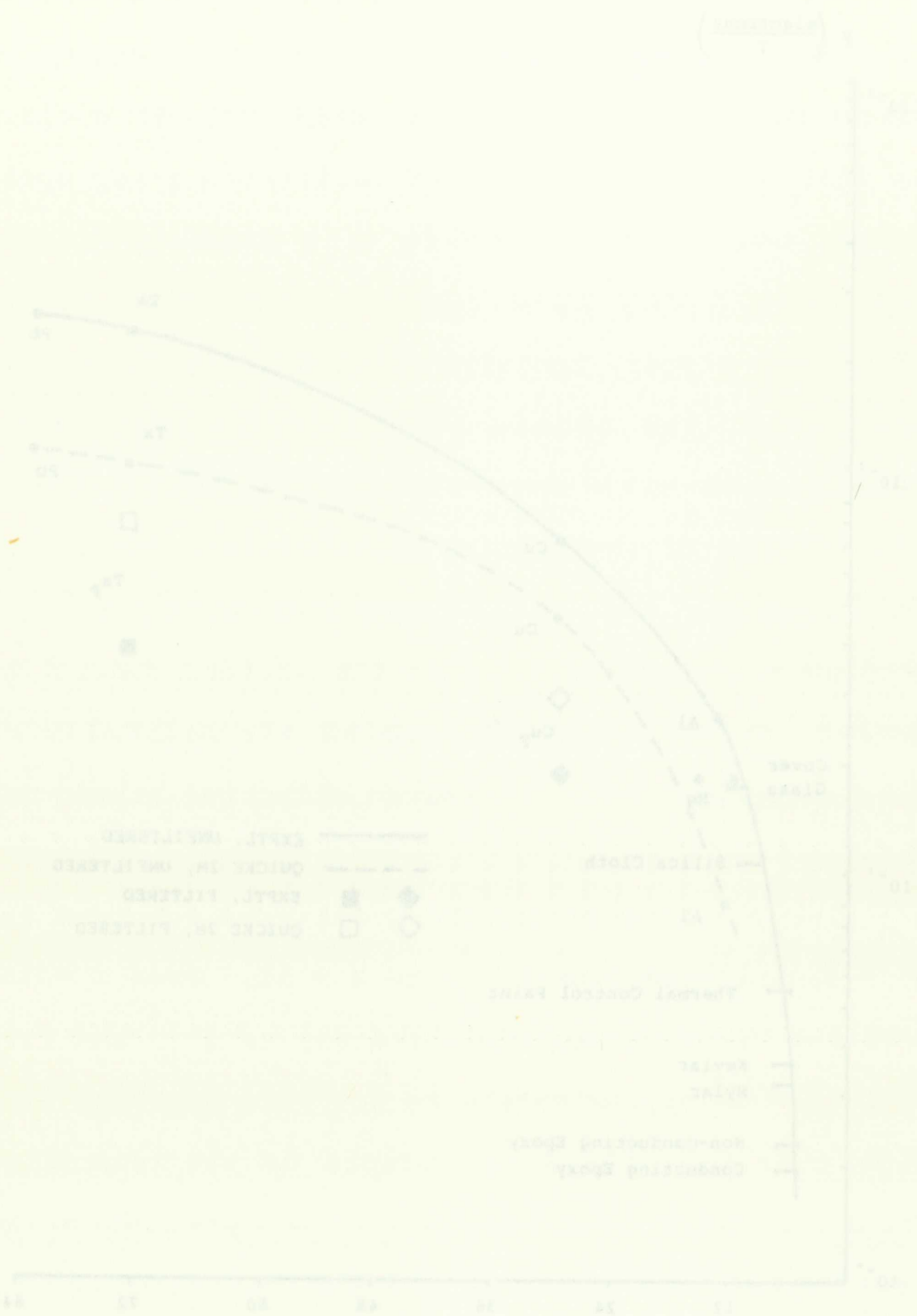


FIGURE 10. Yield versus Acromis Number

= 29 to $Z = 73$ for the filtered spectrum ($Z^{0.8}$) is lower than for the unfiltered spectrum as would be anticipated because of the higher average energy (and lower photoelectric cross sections) for the X rays in the filtered spectrum.

Comparative Results for Metal Targets, Filtered Spectrum

Comparisons are made of the present measurements with those obtained by other experimenters (Figs. 40 and 41). Included in these comparisons are the predictions made using the QUICKE 2M code. A summary of comparisons of previous measurements and code predictions normalized with respect to the present experimental results is given in Table 7.

TABLE 7. Comparison of Previous Yield Results and Code Prediction Normalized to Present Experiment

	$E_e > 1.0 \text{ keV}$		$E_e > 5.0 \text{ keV}$	
	Cu	Ta	Cu	Ta
Exptl	1.0	1.0	1.0	1.0
Bradford	1.9	2.6	---	---
Dolan	---	---	1.5	2.0
QUICKE 2M	1.4	2.1	1.7	2.3
QUICKE 2	---	---	1.6	2.0
POEM	1.3	1.9	---	---
SANDYL	---	---	1.4	1.6

than for the unfiltered spectrum as would be anticipated because of the higher average energy (and lower the bremsstrahlung cross section) for the X rays in the filtered spectrum.

Comparative Results for Metal Targets, Filtered Spectrum

Comparisons are made of the present measurements with those obtained by other experimenters (Figs. 4b and 4c). Included in these comparisons are the predictions made using the QUICK 2M code. A summary of comparisons of previous measurements and code predictions normalized with respect to the present experimental results is

given in Table 7.

TABLE 7
Comparison of Previous Yield Results
and Code Prediction Normalized to
Present Experiment

	$E_0 > 1.0 \text{ keV}$		$E_0 > 2.0 \text{ keV}$	
	Cu	Ta	Cu	Ta
Exptl	1.0	1.0	1.0	1.0
Bradford	1.2	2.6	---	---
Collins	---	---	1.5	2.0
QUICK 2M	1.4	2.1	1.7	2.3
QUICK 2	---	---	1.6	2.0
POW	1.2	1.8	---	---
SAHOY	---	---	1.4	1.8

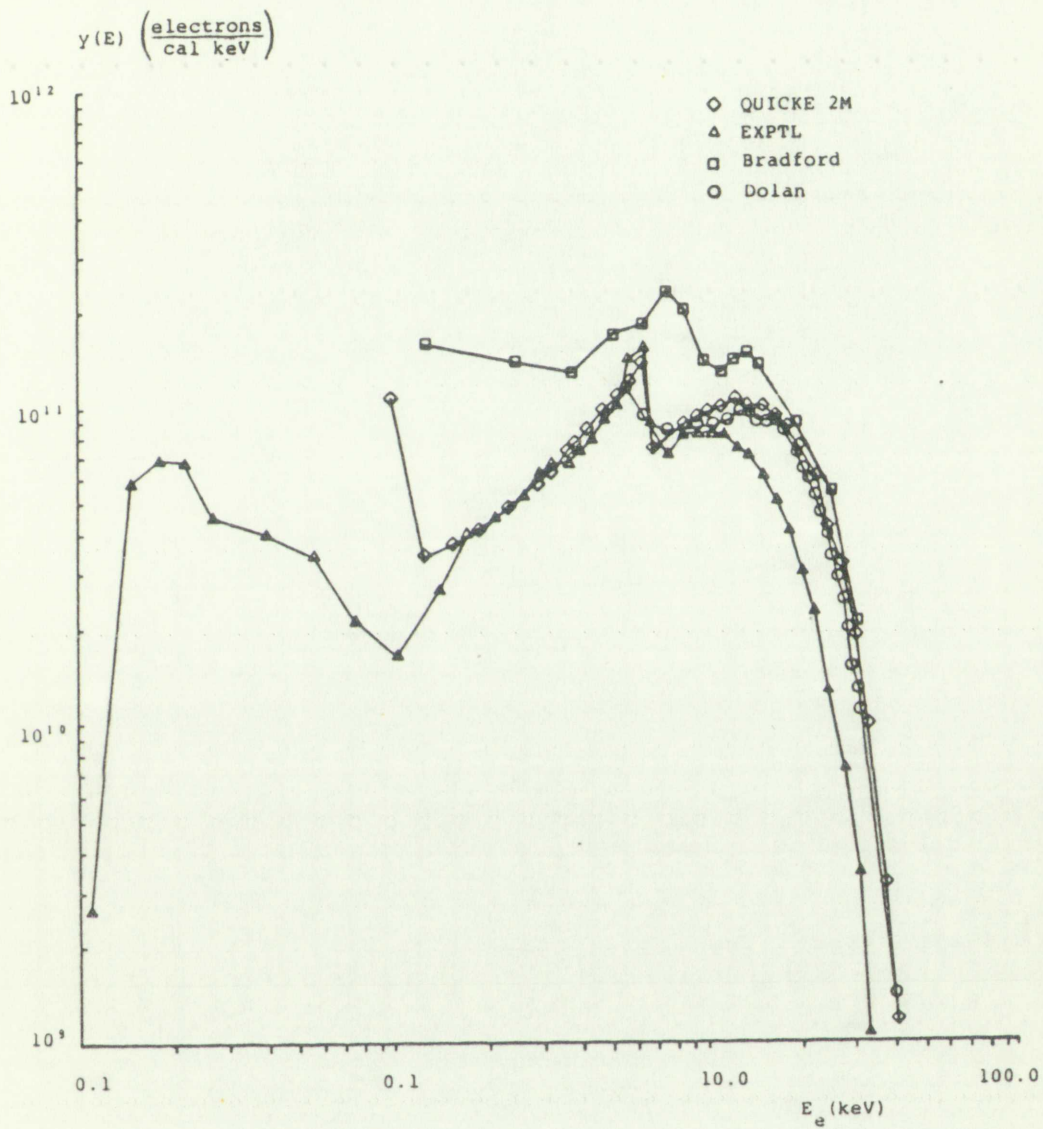


FIGURE 40. Experiment and Code Comparisons;
Cu, Filtered Spectrum



FIGURE 40. Experiment and theoretical curves for the transmission of light through a medium with a random distribution of scattering centers.

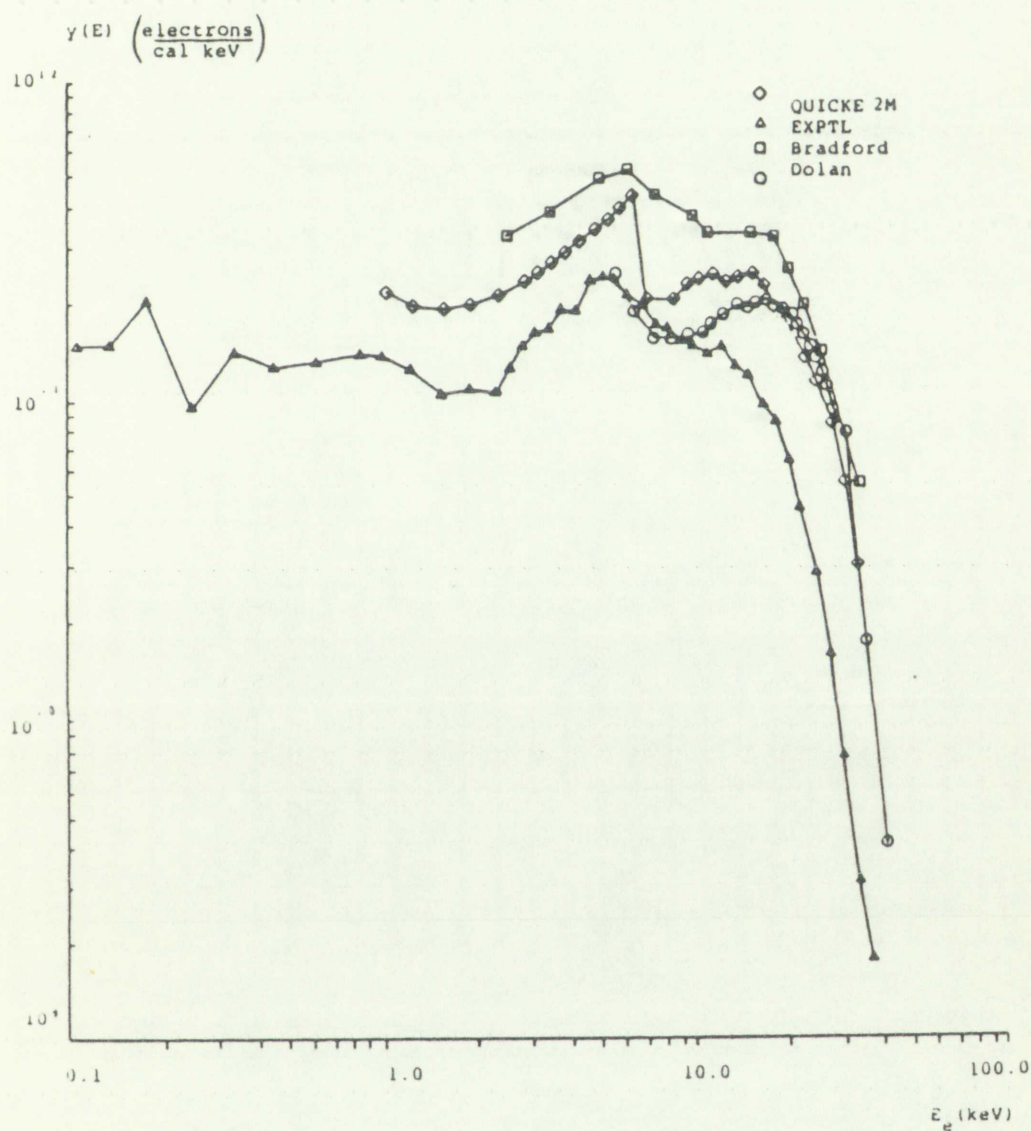


FIGURE 41 . Experiment and Code Comparison;
Ta Filtered Spectrum



FIGURE 11. Experimental and Theoretical
7-Fluorinated Spectrum

Examination of Fig. 40 shows general agreement among the three sets of experimental results for copper with similar X-ray spectra. Relative to the present measurements, the peak yield from Bradford's data is 50% larger and shifted approximately 1 keV higher in energy. Dolan's data at 5 keV shows a yield 23% lower. From Table 7, the integrated reverse emission yields from Bradford's and Dolan's data are approximately a factor 2 and 1.5 higher than the present measurements over comparable energy intervals. The major contribution to these yield differences occurs at electron energies above 6 keV (Bradford) and 12 keV (Dolan). Comparison of the present measurements with the QUICKE 2M calculations shows excellent agreement from approximately 1.5 keV to 10 keV. The code predicts a sharp increase near the 1.1 keV L-edge which is not observed as distinctly in the measured distribution. QUICKE 2M predicts an integrated yield 42% greater than observed with the major contribution being at electron energies greater than 10 keV. Bradford's results for integrated yield are approximately 40% larger than predictions, with QUICKE 2M and POEM within 4% agreement. At electron energies above 5.0 keV Dolan's measurements are within 4% of predictions, with agreement among QUICKE 2M, QUICKE 2 and SANDYL codes better than 1%.

Examination of the above general agreement among the three sets of experimental results for copper with similar energy spectra. Relative to the present measurements, the data from Bradford's data is 50% larger and shifted approximately 1 keV higher in energy. Dolan's data at 5 keV shows a yield 33% lower. From Table 7, the integrated reverse emission yields from Bradford's and Dolan's data are approximately a factor 2 and 1.5 higher than the present measurements over comparable energy intervals. The major contribution to these yield differences occurs at electron energies above 6 keV (Bradford) and 12 keV (Dolan). Comparison of the present measurements with the QUICK 2M calculations shows excellent agreement from approximately 1.5 keV to 10 keV. The code predicts a sharp increase near the 1.1 keV L-edge which is not observed as distinctly in the measured distribution. QUICK 2M predicts an integrated yield 43% greater than observed with the major contribution being at electron energies greater than 10 keV. Bradford's results for integrated yield are approximately 40% larger than predictions, with QUICK 2M and BOEM within 4% agreement. At electron energies above 5.0 keV Dolan's measurements are within 4% of predictions, with agreement among QUICK 2M, QUICK 3 and SANDL codes better than 1%.

Comparison of experimental results for tantalum are shown in Fig. 41. Again the general shapes of the yield distributions are similar with their peaks occurring within 1 keV. Bradford's results are consistently high; the peak yield is a factor of two larger than Dolan's results and the present measurements. For electron energies greater than 1 keV, Bradford's integrated yield exceeds the present measurements by a factor of 2.6. For electron energies above 5.0 keV Dolan's results for integrated yield are a factor of two larger. Comparison of QUICKE 2M predictions with the present experimental results show reasonable agreement but stronger definition of absorption edge features and consistently higher yields. The code predicts an integrated yield a factor of 2.1 larger than measured. For energies above 1.0 keV Bradford's integrated yield is 30% higher than predictions, with QUICKE 2M and POEM within 6% agreement. Above 5.0 keV, Dolan's results agree with the average of the QUICKE 2M, QUICKE 2, and SANDYL predictions, with the codes agreeing within 15%.

A summary of comparisons of previous measurements (with quoted experimental errors) and code predictions with the present experimental results is given in Table 8. The three sets of experimental data (EXPTL, BRADFORD, and DOLAN) include experimental errors of $\pm 30\%$, $\pm 20\%$ and $\pm 15\%$ respectively. The present

Comparison of experimental results for various energies is shown in Fig. 4. Again the general shape of the yield distribution is similar with their peaks occurring within 1 keV. Bradford's results are consistently higher than the peak yield in a factor of two larger than Dolan's results and the present measurements. For electron energies greater than 1 keV, Bradford's integrated yield exceeds the present measurements by a factor of 2.6. For electron energies above 5.0 keV Dolan's results for integrated yield are a factor of two larger. Comparison of QUICK 2M predictions with the present experimental results show reasonable agreement but stronger definition of absorption edge features and consistently higher yields. The code predicts an integrated yield a factor of 2.1 larger than measured. For energies above 1.0 keV Bradford's integrated yield is 30% higher than predictions, with QUICK 2M and POEM within 5% agreement. Above 5.0 keV, Dolan's results agree with the average of the QUICK 2M, QUICK 3, and BANGS predictions, with the codes agreeing within 15%.

A summary of comparisons of previous measurements (with quoted experimental errors) and code predictions with the present experimental results is given in Table 8. The three sets of experimental data (EXPT, BRADFORD, and DOLAN) include experimental errors of $\pm 10\%$, $\pm 10\%$ and $\pm 15\%$ respectively. The present

TABLE 8. Reverse Emission Yield^a
Comparisons, Filtered Spectrum

	$E_e > 0.1 \text{ keV}$		$E_e > 1.0 \text{ keV}$		$E_e > 5.0 \text{ keV}$	
	Cu	Ta	Cu	Ta	Cu	Ta
EXPTL ($\pm 30\%$)	1.9 ± 0.6	3.7 ± 1.1	1.8 ± 0.5	3.5 ± 1.1	1.5 ± 0.5	2.7 ± 0.8
QUICKE 2M	---	---	2.7	7.4	2.5	6.1
BRADFORD ($\pm 20\%$)	---	---	3.6 ± 0.7	9.0 ± 1.8	2.9 ± 0.6	7.2 ± 1.4
POEM	---	---	2.5	6.6	---	---
DOLAN ($\pm 15\%$)	---	---	---	---	2.2 ± 0.3	5.3 ± 0.8
QUICKE 2	---	---	---	---	2.4	5.4
SANDYL	---	---	---	---	2.1	4.2

^a units are $\left(\frac{\text{electrons}}{10^3 \gamma} \right)$

TABLE 2
SILICATE POLYMERIZATION KINETICS
AVERAGE INITIAL CONCENTRATIONS

	Yield 0.3 < \bar{M}_n < 0.5		Yield 0.5 < \bar{M}_n < 1.0		Yield 1.0 < \bar{M}_n < 2.0		
	\bar{M}_n	\bar{M}_w	\bar{M}_n	\bar{M}_w	\bar{M}_n	\bar{M}_w	
STARCH (100%)	0.000	0.000	1.000	1.000	1.000	1.000	(100%) STARCH
GLUCOSE 50	0.0	0.0	0.0	0.0	0.0	0.0	(50%) GLUCOSE
GLUCOSE 25	0.000	0.000	0.000	0.000	0.000	0.000	(25%) GLUCOSE
GLUCOSE 12.5	0.000	0.000	0.000	0.000	0.000	0.000	(12.5%) GLUCOSE
GLUCOSE 6.25	0.000	0.000	0.000	0.000	0.000	0.000	(6.25%) GLUCOSE
GLUCOSE 3.125	0.000	0.000	0.000	0.000	0.000	0.000	(3.125%) GLUCOSE
GLUCOSE 1.5625	0.000	0.000	0.000	0.000	0.000	0.000	(1.5625%) GLUCOSE
GLUCOSE 0.78125	0.000	0.000	0.000	0.000	0.000	0.000	(0.78125%) GLUCOSE
GLUCOSE 0.390625	0.000	0.000	0.000	0.000	0.000	0.000	(0.390625%) GLUCOSE
GLUCOSE 0.1953125	0.000	0.000	0.000	0.000	0.000	0.000	(0.1953125%) GLUCOSE
GLUCOSE 0.09765625	0.000	0.000	0.000	0.000	0.000	0.000	(0.09765625%) GLUCOSE
GLUCOSE 0.048828125	0.000	0.000	0.000	0.000	0.000	0.000	(0.048828125%) GLUCOSE
GLUCOSE 0.0244140625	0.000	0.000	0.000	0.000	0.000	0.000	(0.0244140625%) GLUCOSE
GLUCOSE 0.01220703125	0.000	0.000	0.000	0.000	0.000	0.000	(0.01220703125%) GLUCOSE
GLUCOSE 0.006103515625	0.000	0.000	0.000	0.000	0.000	0.000	(0.006103515625%) GLUCOSE
GLUCOSE 0.0030517578125	0.000	0.000	0.000	0.000	0.000	0.000	(0.0030517578125%) GLUCOSE
GLUCOSE 0.00152587890625	0.000	0.000	0.000	0.000	0.000	0.000	(0.00152587890625%) GLUCOSE
GLUCOSE 0.000762939453125	0.000	0.000	0.000	0.000	0.000	0.000	(0.000762939453125%) GLUCOSE
GLUCOSE 0.0003814697265625	0.000	0.000	0.000	0.000	0.000	0.000	(0.0003814697265625%) GLUCOSE
GLUCOSE 0.00019073486328125	0.000	0.000	0.000	0.000	0.000	0.000	(0.00019073486328125%) GLUCOSE
GLUCOSE 0.000095367431640625	0.000	0.000	0.000	0.000	0.000	0.000	(0.000095367431640625%) GLUCOSE
GLUCOSE 0.0000476837158203125	0.000	0.000	0.000	0.000	0.000	0.000	(0.0000476837158203125%) GLUCOSE
GLUCOSE 0.00002384185791015625	0.000	0.000	0.000	0.000	0.000	0.000	(0.00002384185791015625%) GLUCOSE
GLUCOSE 0.000011920928955078125	0.000	0.000	0.000	0.000	0.000	0.000	(0.000011920928955078125%) GLUCOSE
GLUCOSE 0.0000059604644775390625	0.000	0.000	0.000	0.000	0.000	0.000	(0.0000059604644775390625%) GLUCOSE
GLUCOSE 0.00000298023223876953125	0.000	0.000	0.000	0.000	0.000	0.000	(0.00000298023223876953125%) GLUCOSE
GLUCOSE 0.000001490116119384765625	0.000	0.000	0.000	0.000	0.000	0.000	(0.000001490116119384765625%) GLUCOSE
GLUCOSE 0.0000007450580596923828125	0.000	0.000	0.000	0.000	0.000	0.000	(0.0000007450580596923828125%) GLUCOSE
GLUCOSE 0.00000037252902984619140625	0.000	0.000	0.000	0.000	0.000	0.000	(0.00000037252902984619140625%) GLUCOSE
GLUCOSE 0.000000186264514923095703125	0.000	0.000	0.000	0.000	0.000	0.000	(0.000000186264514923095703125%) GLUCOSE
GLUCOSE 0.0000000931322574615478515625	0.000	0.000	0.000	0.000	0.000	0.000	(0.0000000931322574615478515625%) GLUCOSE
GLUCOSE 0.00000004656612873077392578125	0.000	0.000	0.000	0.000	0.000	0.000	(0.00000004656612873077392578125%) GLUCOSE
GLUCOSE 0.000000023283064365386962890625	0.000	0.000	0.000	0.000	0.000	0.000	(0.000000023283064365386962890625%) GLUCOSE
GLUCOSE 0.0000000116415321826934814453125	0.000	0.000	0.000	0.000	0.000	0.000	(0.0000000116415321826934814453125%) GLUCOSE
GLUCOSE 0.00000000582076609134674072265625	0.000	0.000	0.000	0.000	0.000	0.000	(0.00000000582076609134674072265625%) GLUCOSE
GLUCOSE 0.000000002910383045673370361328125	0.000	0.000	0.000	0.000	0.000	0.000	(0.000000002910383045673370361328125%) GLUCOSE
GLUCOSE 0.0000000014551915228366851806640625	0.000	0.000	0.000	0.000	0.000	0.000	(0.0000000014551915228366851806640625%) GLUCOSE
GLUCOSE 0.00000000072759576141834259033203125	0.000	0.000	0.000	0.000	0.000	0.000	(0.00000000072759576141834259033203125%) GLUCOSE
GLUCOSE 0.000000000363797880709171295166015625	0.000	0.000	0.000	0.000	0.000	0.000	(0.000000000363797880709171295166015625%) GLUCOSE
GLUCOSE 0.0000000001818989403545856475830078125	0.000	0.000	0.000	0.000	0.000	0.000	(0.0000000001818989403545856475830078125%) GLUCOSE
GLUCOSE 0.00000000009094947017729282379150390625	0.000	0.000	0.000	0.000	0.000	0.000	(0.00000000009094947017729282379150390625%) GLUCOSE
GLUCOSE 0.000000000045474735088646411895751953125	0.000	0.000	0.000	0.000	0.000	0.000	(0.000000000045474735088646411895751953125%) GLUCOSE
GLUCOSE 0.0000000000227373675443232059478759765625	0.000	0.000	0.000	0.000	0.000	0.000	(0.0000000000227373675443232059478759765625%) GLUCOSE
GLUCOSE 0.00000000001136868377216160297393798828125	0.000	0.000	0.000	0.000	0.000	0.000	(0.00000000001136868377216160297393798828125%) GLUCOSE
GLUCOSE 0.000000000005684341886080801486968994140625	0.000	0.000	0.000	0.000	0.000	0.000	(0.000000000005684341886080801486968994140625%) GLUCOSE
GLUCOSE 0.000000000002842170943040400743484497072265625	0.000	0.000	0.000	0.000	0.000	0.000	(0.000000000002842170943040400743484497072265625%) GLUCOSE
GLUCOSE 0.0000000000014210854715202003717422485361328125	0.000	0.000	0.000	0.000	0.000	0.000	(0.0000000000014210854715202003717422485361328125%) GLUCOSE
GLUCOSE 0.00000000000071054273576010018587112426806640625	0.000	0.000	0.000	0.000	0.000	0.000	(0.00000000000071054273576010018587112426806640625%) GLUCOSE
GLUCOSE 0.000000000000355271367880050092935562134033203125	0.000	0.000	0.000	0.000	0.000	0.000	(0.000000000000355271367880050092935562134033203125%) GLUCOSE
GLUCOSE 0.0000000000001776356839400250464677810670166015625	0.000	0.000	0.000	0.000	0.000	0.000	(0.0000000000001776356839400250464677810670166015625%) GLUCOSE
GLUCOSE 0.00000000000008881784197001252323389053350830078125	0.000	0.000	0.000	0.000	0.000	0.000	(0.00000000000008881784197001252323389053350830078125%) GLUCOSE
GLUCOSE 0.000000000000044408920985006261616945266754150390625	0.000	0.000	0.000	0.000	0.000	0.000	(0.000000000000044408920985006261616945266754150390625%) GLUCOSE
GLUCOSE 0.0000000000000222044604925031308084726333770751953125	0.000	0.000	0.000	0.000	0.000	0.000	(0.0000000000000222044604925031308084726333770751953125%) GLUCOSE
GLUCOSE 0.00000000000001110223024625156540423631668853759765625	0.000	0.000	0.000	0.000	0.000	0.000	(0.00000000000001110223024625156540423631668853759765625%) GLUCOSE
GLUCOSE 0.0000000000000055511151231257827021181583344268798828125	0.000	0.000	0.000	0.000	0.000	0.000	(0.0000000000000055511151231257827021181583344268798828125%) GLUCOSE
GLUCOSE 0.00000000000000277555756156289135105907916721343969140625	0.000	0.000	0.000	0.000	0.000	0.000	(0.00000000000000277555756156289135105907916721343969140625%) GLUCOSE
GLUCOSE 0.000000000000001387778780781445675529539583606719845703125	0.000	0.000	0.000	0.000	0.000	0.000	(0.000000000000001387778780781445675529539583606719845703125%) GLUCOSE
GLUCOSE 0.0000000000000006938893903907228377647697918033599228515625	0.000	0.000	0.000	0.000	0.000	0.000	(0.0000000000000006938893903907228377647697918033599228515625%) GLUCOSE
GLUCOSE 0.00000000000000034694469519536141888238489590167996142578125	0.000	0.000	0.000	0.000	0.000	0.000	(0.00000000000000034694469519536141888238489590167996142578125%) GLUCOSE
GLUCOSE 0.000000000000000173472347597680709441192447950839980712890625	0.000	0.000	0.000	0.000	0.000	0.000	(0.000000000000000173472347597680709441192447950839980712890625%) GLUCOSE
GLUCOSE 0.0000000000000000867361737988403547205962239754199903564453125	0.000	0.000	0.000	0.000	0.000	0.000	(0.0000000000000000867361737988403547205962239754199903564453125%) GLUCOSE
GLUCOSE 0.00000000000000004336808689942017736029811198770999517822265625	0.000	0.000	0.000	0.000	0.000	0.000	(0.00000000000000004336808689942017736029811198770999517822265625%) GLUCOSE
GLUCOSE 0.000000000000000021684043449710088680149055993854997589111328125	0.000	0.000	0.000	0.000	0.000	0.000	(0.000000000000000021684043449710088680149055993854997589111328125%) GLUCOSE
GLUCOSE 0.0000000000000000108420217248550443400745279969274987945556640625	0.000	0.000	0.000	0.000	0.000	0.000	(0.0000000000000000108420217248550443400745279969274987945556640625%) GLUCOSE
GLUCOSE 0.00000000000000000542101086242752217003726399846374939727783203125	0.000	0.000	0.000	0.000	0.000	0.000	(0.00000000000000000542101086242752217003726399846374939727783203125%) GLUCOSE
GLUCOSE 0.000000000000000002710505431213761085018631999231874698638916015625	0.000	0.000	0.000	0.000	0.000	0.000	(0.000000000000000002710505431213761085018631999231874698638916015625%) GLUCOSE
GLUCOSE 0.000000000000000001355252715606880542500930999615937349319458078125	0.000	0.000	0.000	0.000	0.000	0.000	(0.000000000000000001355252715606880542500930999615937349319458078125%) GLUCOSE
GLUCOSE 0.0000000000000000006776263578034402712500465499807968746597290390625	0.000	0.000	0.000	0.000	0.000	0.000	(0.0000000000000000006776263578034402712500465499807968746597290390625%) GLUCOSE
GLUCOSE 0.00000000000000000033881317890172013562500232749990393732986451953125	0.000	0.000	0.000	0.000	0.000	0.000	(0.00000000000000000033881317890172013562500232749990393732986451953125%) GLUCOSE
GLUCOSE 0.000000000000000000169406589450860067812500116374999519664932259765625	0.000	0.000	0.000	0.000	0.000	0.000	(0.000000000000000000169406589450860067812500116374999519664932259765625%) GLUCOSE
GLUCOSE 0.000000000000000000084703294725430033906250005818749997592466112890625	0.000	0.000	0.000	0.000	0.000	0.000	(0.000000000000000000084703294725430033906250005818749997592466112890625%) GLUCOSE
GLUCOSE 0.0000000000000000000423516473627150169531250002909374999879623064453125	0.000	0.000	0.000	0.000	0.000	0.000	(0.0000000000000000000423516473627150169531250002909374999879623064453125%) GLUCOSE
GLUCOSE 0.00000000000000000002117582368135750847656250001454687499939811522265625	0.000	0.000	0.000	0.000	0.000	0.000	(0.00000000000000000002117582368135750847656250001454687499939811522265625%) GLUCOSE
GLUCOSE 0.000000000000000000010587911840678754238281250000727343749969905761328125	0.000	0.000	0.000	0.000	0.000	0.000	(0.000000000000000000010587911840678754238281250000727343749969905761328125%) GLUCOSE
GLUCOSE 0.0000000000000000000052939559203393771191406250000363671874984953806640625	0.000	0.000	0.000	0.000	0.000	0.000	(0.0000000000000000000052939559203393771191406250000363671874984953806640625%) GLUCOSE
GLUCOSE 0.0000000000							

experimental results for copper ($E_e > 1.0$ keV) agree with Bradford's results within 26%. Predictions made with POEM are in closer agreement (9%) than those made with QUICKE 2M (17%). For $E_e > 5.0$ keV Dolan's results and the present measurements agree within experimental error. SANDYL predicts results within 5%, QUICKE 2M within 25%. Bradford's results agree within 15%.

For the tantalum target ($E_e > 1.0$ keV) Bradford's results are 57% higher than the present measurements. The POEM predictions are 43% high with QUICKE 2M predictions 60% high. For electrons above 5 keV, Dolan's results are 29% above the present measurements and Bradford's results are 66% higher. The SANDYL predictions exceed the present measurements by 20%. QUICKE 2M predictions are high by 74%.

In general, for the filtered spectrum, agreement among the experimental results is better for electron energies above 5.0 keV. Better agreement between the present experimental results and code predictions are obtained with the more complex codes (POEM or SANDYL) than with QUICKE 2M. With the exception of Bradford's results, the codes tend to over predict the measured quantities with QUICKE 2M consistently above SANDYL or POEM.

experimental results for copper ($E_{\beta} = 1.9$ keV) agree with Bradford's results within 15%. Predictions made with POEM are in closer agreement (5%) than those made with QUICK 2M (11%). For $E_{\beta} = 2.0$ keV Dolan's results and the present measurements agree within experimental error. SANDYL predicts results within 5%, QUICK 2M within 25%. Bradford's results agree within 15%.

For the cathode target ($E_{\beta} = 1.0$ keV) Bradford's results are 27% higher than the present measurements. The POEM predictions are 43% high with QUICK 2M predictions 60% high. For electrons above 2 keV, Dolan's results are 79% above the present measurements and Bradford's results are 88% higher. The SANDYL predictions exceed the present measurements by 10%. QUICK 2M predictions are high by 74%.

In general, for the filtered spectrum, agreement among the experimental results is better for electron energies above 2.0 keV. Better agreement between the present experimental results and code predictions are obtained with the more complex codes (POEM or SANDYL) than with QUICK 2M. With the exception of Bradford's results, the codes tend to over predict the measured quantities with QUICK 2M consistently above SANDYL or POEM.

Comparative Results for Metal Targets, Unfiltered Spectrum

Comparisons are made between the measured results and predictions using QUICKE 2M for aluminum, copper, tantalum and lead with the unfiltered X-ray spectrum. Based on the acknowledged omissions in the physical model used in this code (discussed later in this section) only fair agreement with experimental results should be anticipated. The unfiltered spectrum will emphasize interactions in an energy region where the deficiencies are most important. Figures 42 through 45 show the energy dependent reverse emission yield integrated over 2π steradians using $\cos\theta$ angular dependence. Table 9 compares experimental and calculated energy integrated yield at θ_1 for energies $E_e > 0.1$ keV, 1.0 keV and 5.0 keV. The experimental quantum yield determined by $\cos\theta$ and $\cos^2\theta$ angular dependence is also compared with calculated results. Unlike the results for the filtered spectrum, experimental results with the unfiltered X rays are consistently larger than the predicted results. For electron energies greater than 1.0 keV the ratios of measured differential yield at θ_1 to the predicted yield are 2.9, 1.4, 2.4 and 2.4 for aluminum, copper, tantalum and lead respectively. For electron energies greater than 5.0 keV the ratios are 2.5, 1.1, 2.8 and 2.6. With

Comparisons are made between the calculated results and predicted values using QDCX for aluminum, copper, and lead and lead with the calculated results. Based on the acknowledged corrections to the physical model used in this code (discussed later in this section) only fair agreement with experimental results should be anticipated. The unfiltered spectrum will emphasize interactions in an energy region where the deficiencies are most important. Figures 1 through 4 show the energy dependent reverse emission yield integrated over 2° steradians using cos angular dependence. Table 2 compares experimental and calculated energy integrated yield at 0° for energies > 0.1 keV, 1.0 keV and 2.0 keV. The experimental quantum yield determined by cos θ and cos² angular dependence is also compared with calculated results. Unlike the results for the filtered spectrum, experimental results with the unfiltered X-rays are consistently larger than the predicted results. For electron energies greater than 1.0 keV the ratios of measured differential yield at 0° to the predicted yield are 2.0, 1.4, 2.4 and 2.4 for aluminum, copper, tantalum and lead respectively. For electron energies greater than 2.0 keV the ratios are 2.2, 1.4, 2.8 and 2.8.

the possible exception of copper the agreement is outside the estimated $\pm 30\%$ experimental accuracy.

As noted in Section I, QUICKE 2M treats electron creation from Compton, photoelectric and Auger processes ignoring secondary photon interactions (Compton scattered photons, X-ray fluorescence) and the generation of energetic secondary electrons (knock-ons) caused by the primary photo, Compton and Auger electrons. For the X-ray energies used, the error introduced by ignoring Compton scattered photons and the subsequent generation of electrons is negligible. In aluminum for example, the Compton cross section at 10 keV is only 1% of the photoelectric cross section and is even smaller for higher Z materials. X-ray fluorescence in aluminum is less than 2% of the Auger yield and is also of negligible importance. Fluorescence in copper, tantalum and lead can account for some increase in yield with the ratio of X-ray fluorescence to Auger interactions being 0.7, 0.3 and 0.7 for copper (K-shell), tantalum (L-shell) and lead (L-shell) respectively. The correction would not be applied to the total yield but only as a partial contribution to the Auger yield since the resulting electron created by photoelectric absorption of the fluorescent X ray may or may not be emitted.

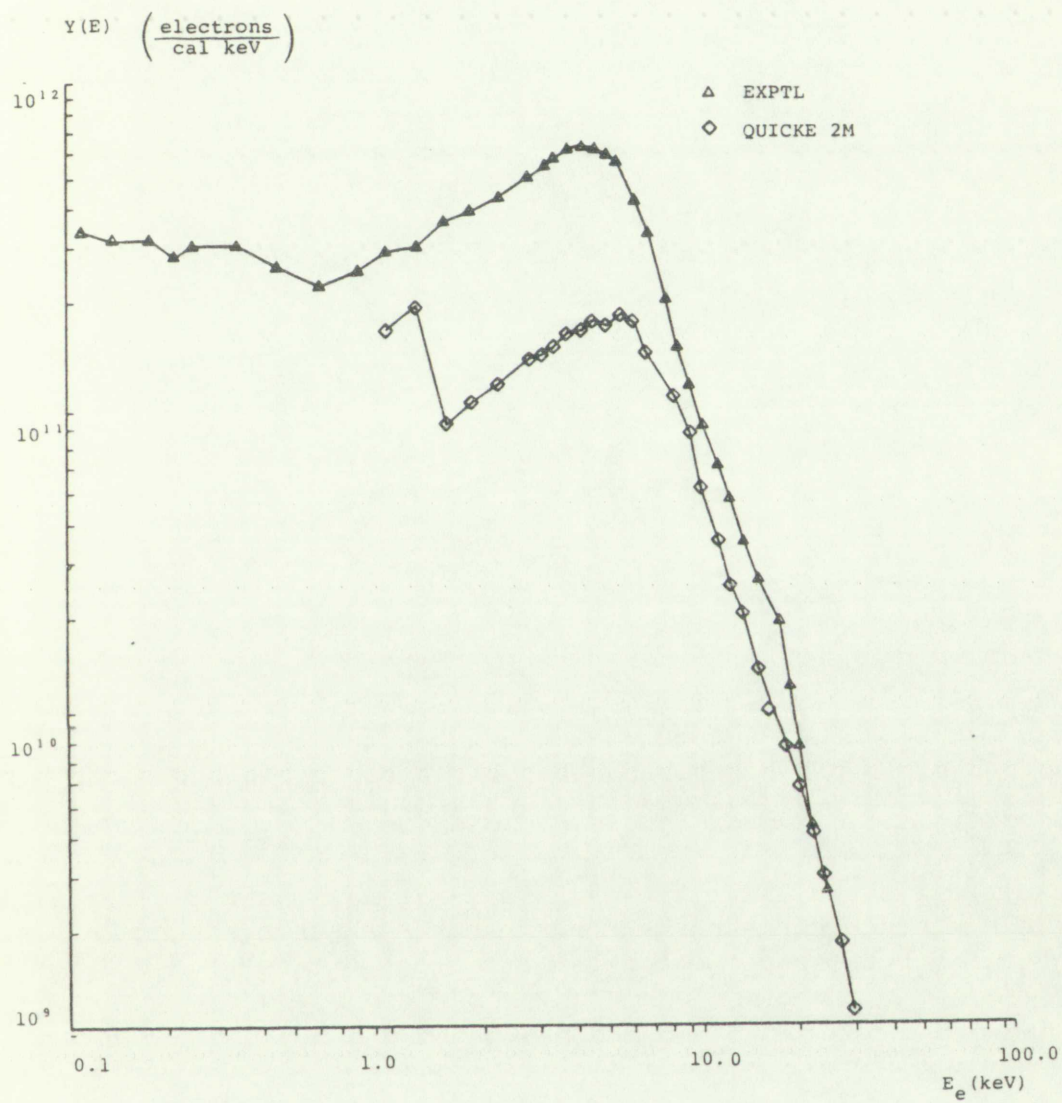


FIGURE 42. Experiment/Code Comparison;
Al, Unfiltered



FIGURE 11. Experiment/Code Comparison:
A, Unfiltered

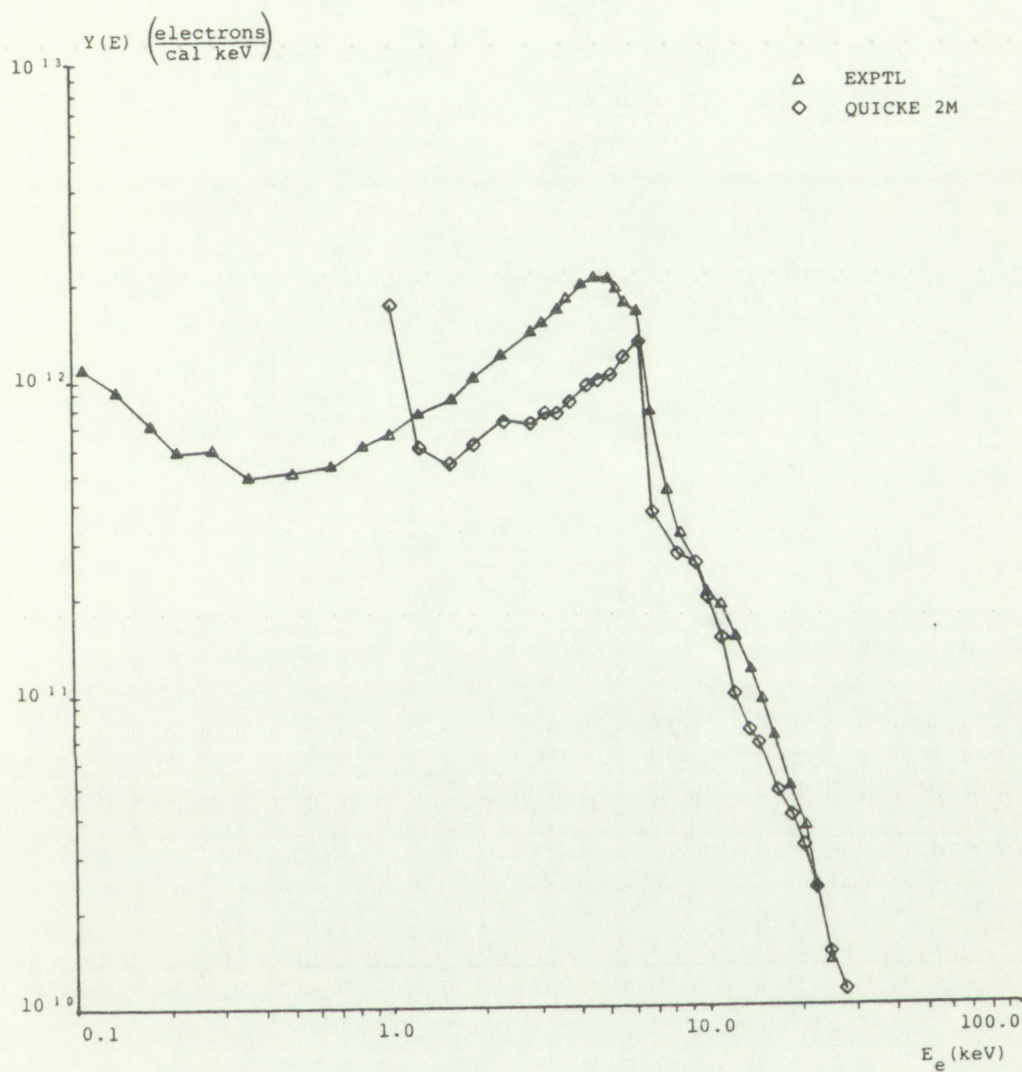


FIGURE 43. Experiment Code Comparison;
Cu, Unfiltered



FIGURE 4). Experiment Code Comparison
Cu, Unirradiated

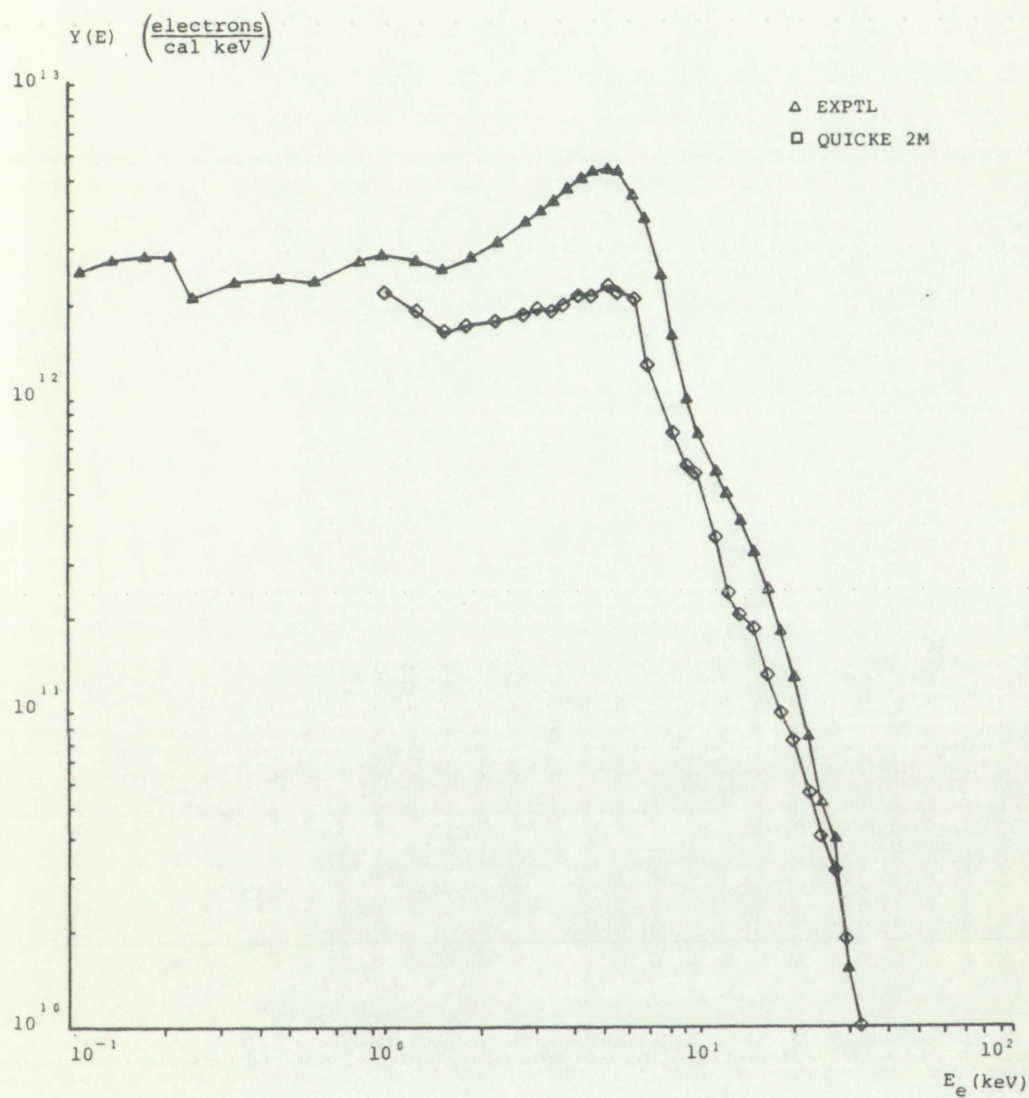


FIGURE 44. Experiment/Code Comparison;
Ta, Unfiltered



FIGURE 11. Experiment Code Comparison
TA, Unfiltered

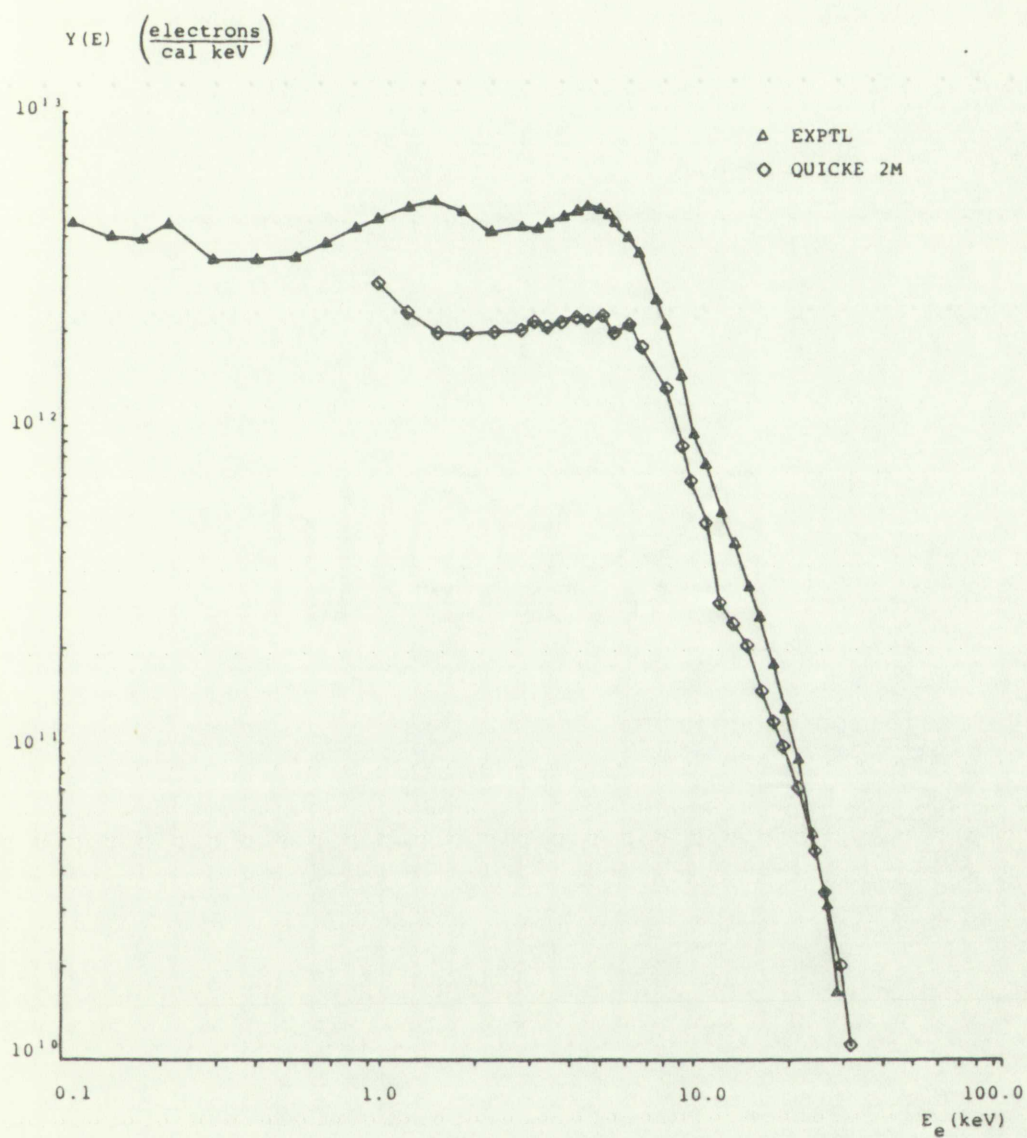


FIGURE 45. Experiment/Code Comparison;
Pb, Unfiltered



FIGURE 4. Experimental/Code Comparison
 Pd, Unfiltered

TABLE 9. Experimental Reverse Emission Yield Comparisons with QUICKE 2M Calculations, Unfiltered Spectrum, for Aluminum, Copper, Tantalum and Lead

	$G_1 \times 10^3 \left(\frac{\text{electrons}}{\gamma \text{ sr}} \right)$				$Y \times 10^3 \left(\frac{\text{electrons}}{\gamma} \right)$				$Y \times 10^7 \left(\frac{\text{coul}}{\text{cal}} \right)$			
	>0.1 keV		>1.0 keV		>5.0 keV		>1.0 keV		>1.0 keV		>1.0 keV	
Ee	EXPTL	EXPTL	CALC	EXPTL	CALC	$\cos^2 \theta$	$\cos \theta$	CALC	$\cos^2 \theta$	$\cos \theta$	CALC	
MTL												
Al	0.78	0.73	0.25	0.33	0.13	1.53	2.30	0.88	4.10	6.15	2.34	
Cu	2.19	2.08	1.46	0.94	0.82	4.37	6.55	4.40	11.67	17.50	11.76	
Ta	7.08	6.63	2.81	3.50	1.27	13.88	20.82	10.26	37.08	55.62	27.42	
Pb	7.96	7.30	3.01	3.55	1.34	15.29	22.93	11.82	40.85	61.28	31.58	

32	1.26	1.30	3.01	1.22	1.74	12.58	8.123	11.53	40.52	1.10
33	1.08	1.53	3.01	1.20	1.51	13.28	30.25	30.50	13.08	1.07
34	3.73	3.03	1.48	0.84	0.95	1.33	8.23	8.90	11.61	1.1
37	0.18	0.12	0.32	0.77	0.13	1.23	5.30	2.88	4.10	0.72
38	EXPLC	EXPLP	CHTC	EXPLC	CHTC	EXPLP	EXPLC	CHTC	EXPLP	CHTC
	>0.13 KPa	>1.0 KPa	>2.0 KPa	>2.0 KPa	>2.0 KPa	>2.0 KPa	>2.0 KPa	>2.0 KPa	>2.0 KPa	>2.0 KPa
$0.1 \times 10^3 \left(\frac{1}{\text{STRESSOR}} \right)$										$1 \times 10^3 \left(\frac{1}{\text{STRESSOR}} \right)$
$1 \times 10^3 \left(\frac{1}{\text{STRESSOR}} \right)$										$1 \times 10^3 \left(\frac{1}{\text{STRESSOR}} \right)$

32-37 - EXPLC/EXPLP/CHTC/EXPLC/CHTC/EXPLP/EXPLC/CHTC/EXPLP/CHTC/EXPLP/CHTC
 38 - EXPLC/EXPLP/CHTC/EXPLC/CHTC/EXPLP/EXPLC/CHTC/EXPLP/CHTC/EXPLP/CHTC

Perhaps of more significance (but difficult to quantify) is the contribution to the yield coming from knock-on secondary electrons; particularly those created near the emitting surface. These secondaries would be created as a result of the multiple scattering and energy loss collisions of the primary electrons and would in turn become a source for additional knock-on interactions. Since subsequent collisions of these secondary, tertiary, etc. electrons result in energy loss, their contribution can be important only if they are created very near the emission surface. This condition is most nearly satisfied by the last interaction of an electron before it escapes the surface. The yield of secondary electrons from surfaces bombarded by energetic electrons can be a few tens of percent ($\approx 30\%$) of the incident primaries for normal incidence bombardment and is significantly enhanced (factor of 2 to 3) for grazing incidence conditions. The emission of electrons from a surface exposed to X rays can be thought of as analogous to the enhanced condition since the last interactions of escaping electrons will occur near the surface. Certainly not all the knock-on electrons created in this fashion would escape. But assuming they are generated isotropically, approximately half could contribute to the yield. These electrons would all be of lower energy than the

perhaps of more significance (and difficulty) is the contribution to the total electron knock-on secondary electron yield which is created near the emitting surface. These secondary electrons are generated as a result of the collision of the primary electron and energy loss collisions of the primary electron and would in turn become a source for additional knock-on interactions. Since subsequent collisions of these secondary, tertiary, etc. electrons result in energy loss, their contribution can be important only if they are created very near the emitting surface. This condition is most easily satisfied by the interaction of an electron before it escapes the surface. The yield of secondary electrons from surfaces bombarded by energetic electrons can be a few tens of percent (1-10%) of the incident primary electron normal incidence bombardment and is significantly enhanced (factor of 2 to 3) for grazing incidence conditions. The emission of electrons from a surface exposed to x-rays can be thought of as analogous to the enhanced condition since the last interactions of incoming electrons will occur near the surface. Certainly not all the knock-on electrons created in this fashion would escape. But assuming they are generated isotropically, approximately half could contribute to the yield. These electrons would all be of lower energy than the

primaries that created them and contribute to enhanced yield at energies of the primaries less the knock-on electron binding energy and subsequent energy losses prior to emission from the surface. This argument, if valid, could account for at most a 30 to 45% increase in yield. Such a correction applied to the QUICKE 2M predictions brings them to within 10 to 40% agreement with the lower limit of the experimental values. The validity of this approach has limited merit, however; the same argument applied to the filtered spectrum results would produce a correction in the wrong direction since the code over predicts results for that case.

Aside from the lack of the code's consideration of interactions previously discussed, the most plausible explanation for the divergence of measured and predicted results is the acknowledged deficiencies in the treatment of X-ray and electron interactions below ~ 10 keV; a situation common to all the codes discussed in Section I.

Results for Dielectric Targets, Unfiltered Spectrum

Differential reverse emission yields from the dielectric samples were shown in Figs. 29 through 35. These materials are all basically low Z compounds ($Z_{\text{eff}} <$

properties that are...
yield at...
electric...
prior to...
which could...
yield. Such...
predictions...
with the...
validity of...
the same...
results would...
direction since...
case.

Aside from...
interactions...
explanation for...
results is...
treatment of...
key; a...
Section 1.

Results for...
Differential...
dielectric...
These materials...

11) and as a result their quantum efficiencies are quite low. Consequently, to obtain usable count rates, only the unfiltered X-ray spectrum was used. The impact of the low emission efficiency is seen in the less smooth behavior of the differential emission curves relative to the higher Z targets, and results from a poorer signal-to-noise ratio in the detectors. That is, with a fixed lower limit on background counts the data from low Z targets will have larger relative uncertainties from background subtraction. As stated earlier, the exact composition of the dielectric samples (with the exception of Mylar) was unknown. The silica cloth, Kevlar and solar cell cover glass are basically SiO_2 compounds. The silica cloth is a woven fabric (which unduly complicated mounting the sample) and is treated with an unknown surface coating. Kevlar is similar to fiberglass, bonded with an epoxy resin which is most likely a carbon based compound. The solar cell cover glass contains about 2% (by weight) cerium doping. The thermal control paint, Mylar and the epoxy samples are carbon compounds. No information was available on the paint sample and the epoxy materials were from company proprietary samples. The composition assumed for Mylar was $\text{C}_{10}\text{H}_8\text{O}_4$. With the uncertainties in composition of the dielectric samples, calculations of the reverse emission yields were not made although the codes

the low emission efficiency is seen in the low amount of the differential emission current relative to the higher 3 response, and results from a poorer signal-to-noise ratio in the detector. That is, with a fixed lower limit on background counts the data from low 3 response will have larger relative uncertainty from background subtraction. As stated earlier, the exact composition of the dielectric samples with the exception of Mylar was unknown. The silver chloride Kevlar and solar cell cover glasses are basically silver compounds. The silver chloride is a known fabric which undergoes complicated mounting the samples and is treated with an unknown surface coating. Kevlar is similar to fiberglass, bonded with an epoxy resin which is most likely a carbon based compound. The solar cell cover glass contains about 1% by weight carbon doping. The thermal control paint, Mylar and the epoxy samples are carbon compounds. No information was available on the paint sample and the epoxy materials were from company proprietary samples. The composition assumed for Mylar was $C_{10}H_8O_4$. With the uncertainties in composition of the dielectric samples, calculations of the reverse emission yields were not made although the codes

generally have this capability if the constituent elements and their relative proportions are known.

The angular dependence of the yield for these low Z materials (Fig. 38) is less accurately represented by a $\cos\theta$ dependence and a trend toward an isotropic distribution can be noted from the data. This effect was reported by Dolan [10] and is tentatively explained on the basis of the low Z materials being less efficient in multiple scattering of electrons. Less than complete multiple scattering would imply the emitted electrons would retain some portion of the angular distribution from the photoelectric interaction. This distribution is peaked at right angles to the electric vector of the incident radiation. That is, parallel to the emitting surface in the case of normal X-ray incidence. Reliable interpretation of the angular distribution is hindered by the poorer signal-to-noise ratio achieved with the low Z materials. In some cases the background counts were comparable to the measured emission, particularly in the higher emission angles channels. The effect of reduced signal-to-noise is seen in the differential yield curves in Section IV.

Figures 46 and 47 show the reverse emission yield energy distributions integrated over angle with $\cos\theta$ dependence. As in the case of the metals discussed earlier, features attributable to the photoelectric and

generally have this capability if the conditions elements and their relative positions are known.

The angular dependence of the yield for these low energy materials (Fig. 3b) is less accurately represented by a cosine dependence and a broad spread in isotropic distribution can be noted from the data. This effect was reported by Dainton (19) and is tentatively explained on the basis of the low energy materials being less efficient in multiple scattering of electrons. Less than complete multiple scattering would imply the emitted electrons would retain some portion of the angular distribution from the photoelectric interaction. This distribution is peaked at right angles to the electric vector of the incident radiation. That is, parallel to the emitting surface in the case of normal X-ray incidence. Reflection interpretation of the angular distribution is hindered by the poorer signal-to-noise ratio achieved with the low energy materials. In some cases the background counts were comparable to the measured emission, particularly in the higher emission angles channels. The effect of reduced signal-to-noise is seen in the differential yield curves in Section IV.

Figures 4a and 4b show the reverse emission yield energy distributions integrated over angle with cosine dependence. As in the case of the metals discussed earlier, features attributable to the photoelectric and

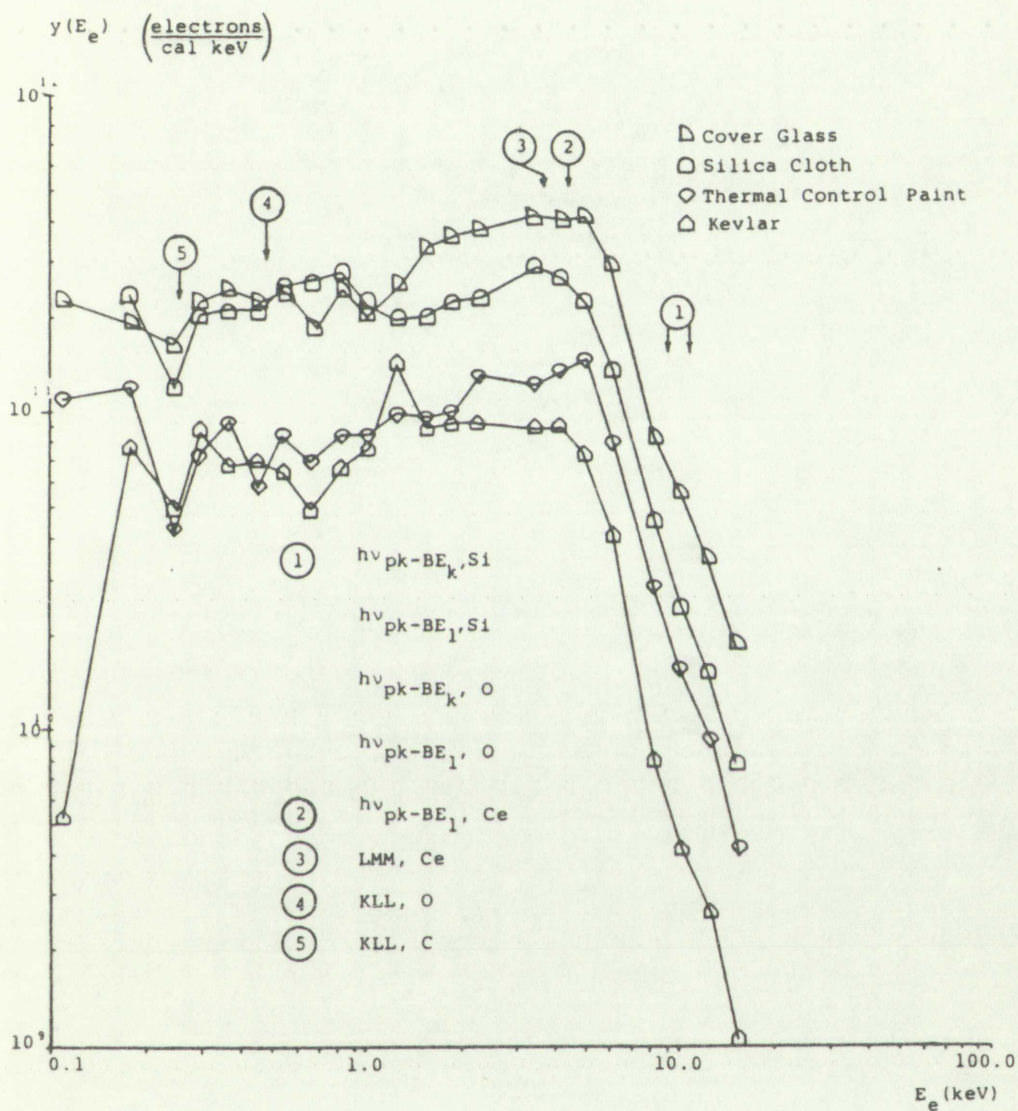


FIGURE 46. Measured Yield for Cover Glass, Silica Cloth, Thermal Control Paint and Kevlar; Unfiltered Spectrum



FIGURE 46. Measured Yield for Cover Crops: Slices Clock, Thermal, Control, Rain, and Kevlar; Unfilled Squares.

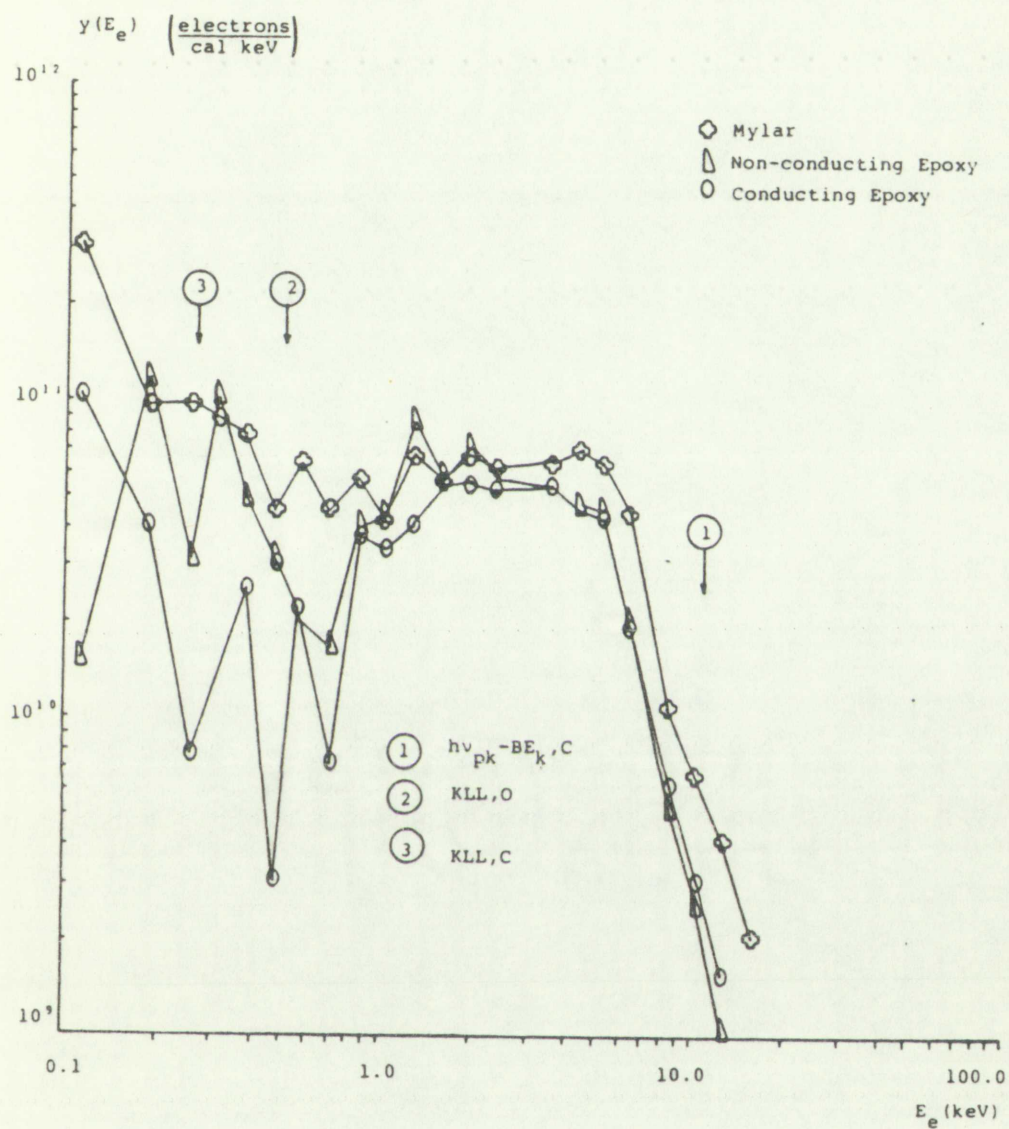


FIGURE 47. Measured Yield for Mylar, Non-conducting Epoxy and Conducting Epoxy; Unfiltered Spectrum



FIGURE 47. Measured Yield for Vylar, Non-Conducting Epoxy and Conducting Epoxy; Unfilled Spectrum

Auger processes in the known major constituents of the sample are readily apparent.

Summary

The specific objectives of this effort have been met. An experimental technique has been developed and successfully used in the measurement of X-ray induced electron emission from a variety of materials including a group of significance to satellite applications. A data base has been established which extends measured emission characteristics to an order of magnitude lower energies than previously available. Direct measurement of the angular dependence of differential yield distributions has been made. Total yields based on these measurements have been compared with previous measurements and basic computational models. Departure from the assumed $\cos\theta$ dependence for low Z materials was noted. The quantum yield of electrons of energy between 0.1 and 1.0 keV has been shown to be less than 10% of the total yield for all materials investigated with the X-ray spectra used in this experiment. Agreement with data from previous measurements and code predictions using a filtered X-ray spectrum is generally good with exceptions noted. Comparison of the experimental results obtained using the unfiltered X-ray spectrum

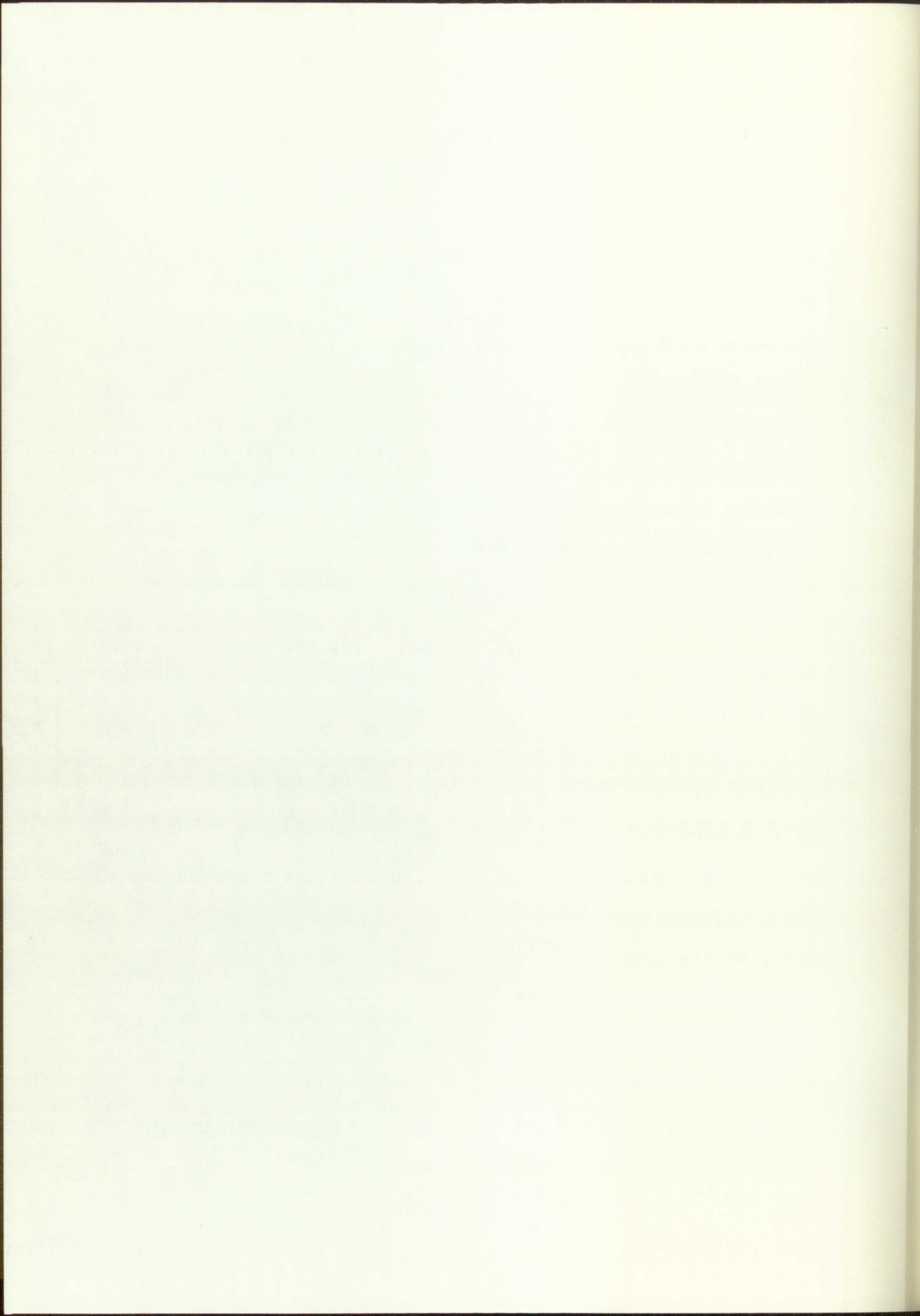
with calculations from QUICKE 2M highlight a deficiency in the code's ability to predict emission yield at X-ray energies below 10 keV. The predictions ranged from factors of 2.6 to 1.5 below measured yields. Only a portion of this is attributable to not including secondary (knock-on) electrons in the computational model. The data base established will prove useful for comparison of other computational methods and further development of improved models of the X-ray induced electron emission process.

The experimental apparatus and measurement technique represent a powerful tool for direct measurement of emission parameters. The present configuration can easily be used to measure the yield of low energy (<100 eV) "true" secondary electrons. The spectrograph is readily adaptable to measurement of forward as well as reverse electron emission and with more extensive modifications could be employed with an X-ray tube operating in a common vacuum environment. This eliminates the need for a "window" between the X-ray source and target, thereby significantly enhancing the flux of low energy X rays. Improvements in the accuracy require detailed measurement of the energy response of the detectors--an effort not undertaken for the current experiment.

with calculations from QUANTUM 3D highlight a deficiency in the code's ability to predict emission yields at X-ray energies below 10 keV. The predictions ranged from factors of 1.5 to 1.5 below assumed yields. Only a portion of this is attributable to not including secondary knock-on electrons in the computational model. The data base established will prove useful for comparison of other computational methods and further development of improved models of the X-ray induced electron emission process.

The experimental apparatus and measurement techniques represent a powerful tool for direct measurement of emission parameters. The present configuration can easily be used to measure the yield of low energy (100 eV) "first" secondary electrons. The spectrograph is readily adaptable to measurement of forward as well as reverse electron emission and with more extensive modifications could be employed with an X-ray tube operating in a common vacuum environment. This eliminates the need for a "window" between the X-ray source and target, thereby significantly enhancing the flux of low energy X-rays. Improvements in the accuracy require detailed measurement of the energy response of the detector--an effort not undertaken for the current experiment.

APPENDIX A



APPENDIX A

DIFFERENTIAL EMISSION YIELD EQUATION

Consider a differential target element of area $dxdz$ located at position $(0,0,0)$ in the spectrograph and uniformly illuminated by normal incidence X rays of flux ϕ . $\phi dxdz$ is the number of X rays which strike the differential element. The differential electron yield $G(E, \vec{\Omega})$ is the number of electrons per unit area per unit flux emitted into the solid angle $d\vec{\Omega}$ in the energy interval dE . If $\Omega(x, E)$ is the solid angle viewed by the k^{th} detector the number of electrons $N(E)$ of energy E in dE reaching the detector from the target element is given by

$$dN_k(E) = \phi dxdz \int_{\Omega} G(E, \vec{\Omega}) d\vec{\Omega} dE \quad (A1)$$

With reasonable restriction on the energy and angular resolution of the spectrograph (i.e., the measurement technique selects energy and angle increments which are small relative to the functional variation in energy and emission angle), $G(E, \vec{\Omega})$ is approximately constant and equal to $G(E, \theta_k)$. Therefore, equation A1 reduces to

$$dN_k(E) = \phi dxdz G(E, \theta_k) \Omega_k(x, E) dE \quad (A2)$$

DIFFERENTIAL EMISSION YIELD SPECTROSCOPY

Consider a differential surface element of area dA located at position (θ, ϕ) in the spectrograph and uniformly illuminated by normal incidence X rays of flux Φ . Φ is the number of X rays which strike the differential element. The differential electron yield $G(E, \theta)$ is the number of electrons per unit area per unit flux emitted into the solid angle $d\Omega$ in the energy interval dE . If $G(E, \theta)$ is the solid angle viewed by the $K\alpha$ detector the number of electrons $N(E)$ of energy E in dE reaching the detector from the target element is given by

$$N(E) = \Phi dA \int_{\Omega} G(E, \theta) d\Omega \quad (A1)$$

With reasonable restriction on the energy and angular resolution of the spectrograph (i.e., the measurement technique selects energy and angle increments which are small relative to the functional variation in energy and emission angle), $G(E, \theta)$ is approximately constant and equal to $G(E, \theta_0)$. Therefore, equation A1 reduces to

$$N(E) = \Phi dA G(E, \theta_0) \int_{\Omega} d\Omega \quad (A2)$$

The solid angle for the k^{th} detector is defined by the area of the primary aperture positioned at $S_k/2$ along the electron path from the target to the detector. From Section II the height of the primary is h_p and the angular width is $\Delta\theta(x, \rho)$. From Table 3 (Section II), $\Delta\theta$ is relatively insensitive to x over the target dimensions and $\Omega_k(x, E)$ can be expressed as

$$\Omega_k(\rho) = \frac{h_p \Delta\theta(\rho)}{S_k/2} \quad (\text{A3})$$

To express equation A1 as a function of ρ a change of variable is required. From the following equations

$$E = mc^2 - m_0c^2 \quad (\text{A4})$$

$$p = mv = eB\rho \quad (\text{A5})$$

$$m = \frac{m_0}{\left(1 - \left(\frac{v}{c}\right)^2\right)^{1/2}} \quad (\text{A6})$$

The energy of the emitted electron can be written as

$$E = [(m_0c^2)^2 + (ec)^2 (B\rho)^2]^{1/2} - m_0c^2 \quad (\text{A7})$$

The change in variable becomes

$$\frac{dE}{d\rho} = eBc\beta \quad (\text{A8})$$

Where $\beta = v/c$ and equation A1 then reduces to

$$dN_k(\rho) = \phi dx dz G(E, \theta_k) \Omega_k(\rho) eBc\beta d\rho \quad (\text{A9})$$

The solid angle for the γ emission is defined by the area of the primary aperture projected on a sphere of radius R .

The electron path from the source to the detector is denoted by R . The height of the primary aperture is h and the aperture width is $2a$. From eq. (1) it follows that the relative fluorescence is a function of R over the range

dimensions and γ (λ, Z) can be expressed as

$$F(R) = \frac{h A(R)}{4\pi R^2} \quad (2)$$

To express equation (2) as a function of a single variable is required. From the following equations

$$R = \sqrt{h^2 + a^2} \quad (3)$$

$$p = \frac{a}{R} \quad (4)$$

$$R = \frac{h}{\sqrt{1 - p^2}} \quad (5)$$

The energy of the emitted electron can be written as

$$E = [m_0 c^2]^2 + [h p]^2 \quad (6)$$

The change in variable becomes

$$\frac{dR}{dp} = \frac{h p}{1 - p^2} \quad (7)$$

Where $p = v/c$ and equation (2) then reduces to

$$F(p) = \frac{h A(p)}{4\pi h^2} \quad (8)$$

Substituting for $\Omega_k(\rho)$ and integrating over the target of width w_s and height h_s , equation A9 becomes

$$dN_k(\rho) = \phi w_s h_s G(E, \theta_k) \frac{h_p \Delta\theta_k(\rho)}{S_k/2} \quad (A10)$$

To integrate over ρ the following quantity is defined

$$A_k = \int_{\rho} \Delta\theta_k(\rho) d\rho \quad (A11)$$

and used in equation A10 to give

$$N_k = \phi w_s h_s G(E, \theta_k) \frac{h_p}{S_k/2} A_k eBc\beta \quad (A12)$$

A further simplification of this equation is obtained by expressing $eBc\beta$ in terms of the dimensionless quantity $\alpha = \frac{E}{m_0 c^2}$. From equations A4 and A6 it follows that

$$eBc\beta = \frac{m_0 c^2}{\rho} \frac{\alpha(\alpha + 2)}{\alpha + 1} \quad (A13)$$

Hence,

$$N_k = \phi w_s h_s G(\alpha, \theta_k) \frac{h_p}{S_k/2} A_k \frac{m_0 c^2}{\rho_0} \frac{\alpha(\alpha + 2)}{\alpha + 1} \quad (A14)$$

Solving for $G(\alpha, \theta_k)$ yields

$$G(\alpha, \theta_k) = \frac{N_k}{\phi} \frac{S_k/2}{h_s w_s h_p} \frac{1}{A_k} \frac{\rho_0}{m_0 c^2} \frac{\alpha + 1}{\alpha(\alpha + 2)} \quad (A15)$$

Substituting for α the value of α obtained from equation (1) and using the value of α obtained from equation (2) in equation (3) we obtain

$$\ln \left(\frac{1}{1 - \alpha} \right) = \frac{1}{\alpha} \ln \left(\frac{1}{1 - \alpha} \right) \quad (4)$$

to integrate over α from 0 to α and to obtain

$$\ln \left(\frac{1}{1 - \alpha} \right) = \frac{1}{\alpha} \ln \left(\frac{1}{1 - \alpha} \right) \quad (5)$$

and used in equation (1) to give

$$N = \frac{1}{\alpha} \ln \left(\frac{1}{1 - \alpha} \right) \quad (6)$$

A further simplification of equation (6) is obtained by expanding the logarithm in a power series

$$\ln \left(\frac{1}{1 - \alpha} \right) = \alpha + \frac{\alpha^2}{2} + \frac{\alpha^3}{3} + \dots \quad (7)$$

dimensionless quantities α and N are defined as

$$\alpha = \frac{1}{N} \ln \left(\frac{1}{1 - \alpha} \right) \quad (8)$$

As it follows that

$$\alpha = \frac{1}{N} \ln \left(\frac{1}{1 - \alpha} \right) \quad (9)$$

$$N = \frac{1}{\alpha} \ln \left(\frac{1}{1 - \alpha} \right) \quad (10)$$

Hence,

$$N = \frac{1}{\alpha} \ln \left(\frac{1}{1 - \alpha} \right) \quad (11)$$

$$G(\alpha, N) = \frac{1}{N} \ln \left(\frac{1}{1 - \alpha} \right) \quad (12)$$

$$G(\alpha, N) = \frac{1}{N} \ln \left(\frac{1}{1 - \alpha} \right) \quad (13)$$

The equivalence with equation 20, Section IV, (independent of the detector efficiency corrections) can be seen by noting that

$$\phi = \frac{N_x}{A_x} \left(\frac{\ell_x}{\ell_t} \right)^2 \quad (A16)$$

and

$$A_t = h_s w_s \quad (A17)$$

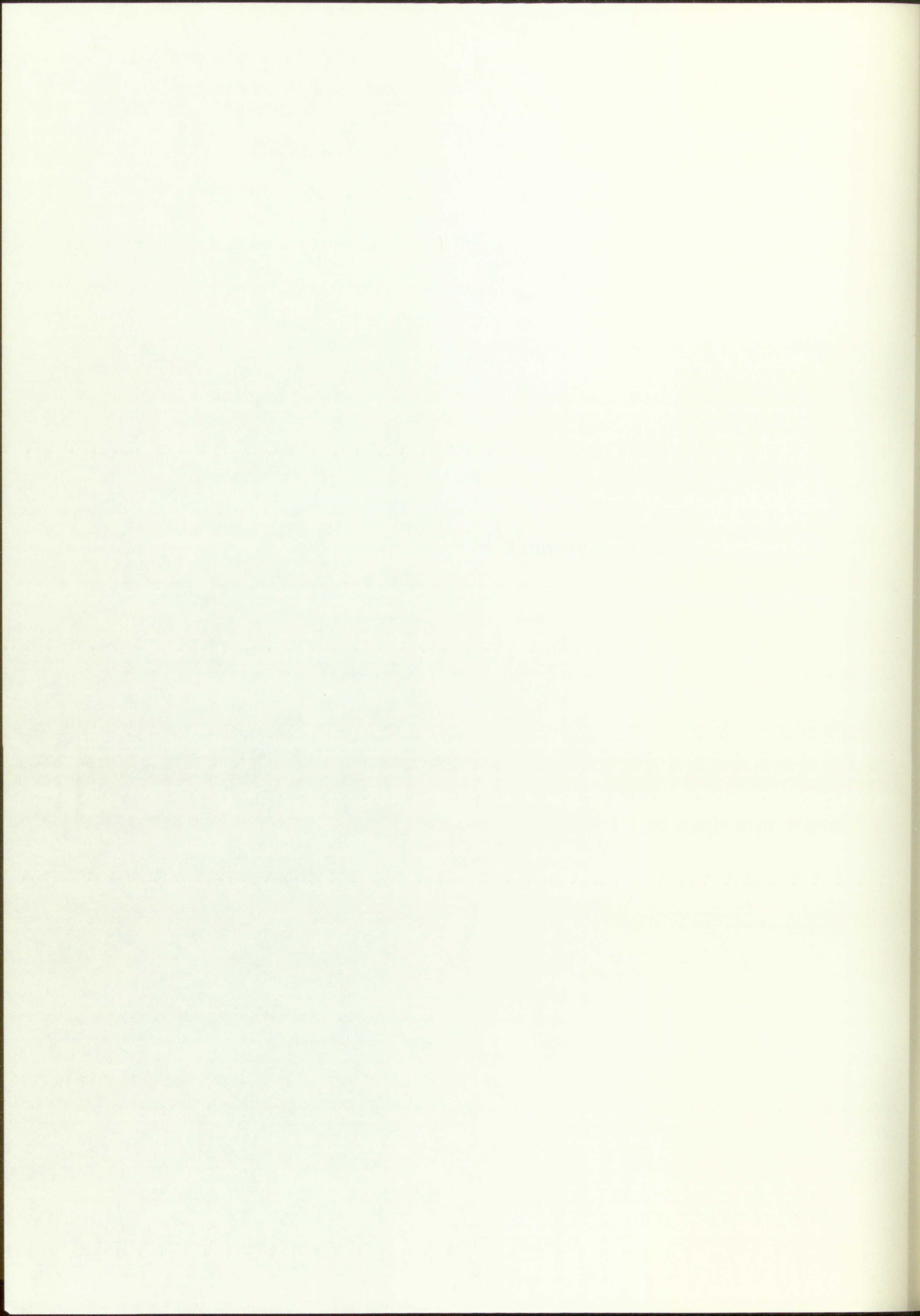
The equivalence with equation 10, Section IV, independent of the detector efficiency correction) can be seen by noting that

$$\left(\frac{N}{A} \right) = \left(\frac{N}{A} \right)_{\text{obs}} \left(\frac{A}{A_{\text{eff}}} \right)$$

(A10)

(A11)

APPENDIX B



APPENDIX B

EXPERIMENTAL DATA

This appendix contains 14 sets of experimental electron emission data from 12 materials. For each set, three tables of data are included. (a) Corrected background in each channel as a function of magnetic field strength, (b) electron counts in each channel (with "error") as a function of magnetic field strength and X rays incident on target and (c) differential electron yield (electrons/photons keV sr) as a function of electron energy. Detector efficiency and energy integrated differential yield are also included.

LIST OF TABLES

a = Corrected Background

b = Electron Counts with Error, X-ray Counts

c = Differential Yield, Detector Efficiency, Energy
Integrated Yield

TABLE	PAGE
B1 Copper, Filtered Spectrum	
B1 (a)	134
B1 (b)	135
B1 (c)	137

TABLE	PAGE
B2 Tantalum, Filtered Spectrum	
B2 (a)	139
B2 (b)	140
B2 (c)	142
B3 Magnesium, Unfiltered Spectrum	
B3 (a)	144
B3 (b)	145
B3 (c)	147
B4 Aluminum, Unfiltered Spectrum	
B4 (a)	149
B4 (b)	150
B4 (c)	152
B5 Copper, Unfiltered Spectrum	
B5 (a)	154
B5 (b)	155
B5 (c)	157
B6 Tantalum, Unfiltered Spectrum	
B6 (a)	159
B6 (b)	160
B6 (c)	162
B7 Lead, Unfiltered Spectrum	
B7 (a)	164
B7 (b)	165
B7 (c)	167

TABLE 1. Unfiltered Spectrum

135	13 (a)
140	13 (b)
145	13 (c)

TABLE 2. Unfiltered Spectrum

145	14 (a)
148	14 (b)
151	14 (c)

TABLE 3. Unfiltered Spectrum

149	15 (a)
150	15 (b)
152	15 (c)

TABLE 4. Unfiltered Spectrum

154	16 (a)
155	16 (b)
157	16 (c)

TABLE 5. Unfiltered Spectrum

158	17 (a)
159	17 (b)
162	17 (c)

TABLE 6. Unfiltered Spectrum

164	18 (a)
165	18 (b)
167	18 (c)

TABLE	PAGE
B8 Cover Glass, Unfiltered Spectrum	
B8 (a)	169
B8 (b)	170
B8 (c)	172
B9 Silica Cloth, Unfiltered Spectrum	
B9 (a)	174
B9 (b)	175
B9 (c)	177
B10 Thermal Control Paint, Unfiltered Spectrum	
B10 (a)	179
B10 (b)	180
B10 (c)	182
B11 Kevlar, Unfiltered Spectrum	
B11 (a)	184
B11 (b)	185
B11 (c)	187
B12 Mylar, Unfiltered Spectrum	
B12 (a)	189
B12 (b)	190
B12 (c)	192
B13 Nonconducting Epoxy, Unfiltered Spectrum	
B13 (a)	194
B13 (b)	195
B13 (c)	197

88 Cover Glass, Unfiltered Spectrum

88 (a)	174
88 (b)	175
88 (c)	176

89 Filter Glass, Unfiltered Spectrum

89 (a)	174
89 (b)	175
89 (c)	176

90 Thermal Control Panel, Unfiltered Spectrum

90 (a)	175
90 (b)	176
90 (c)	177

91 Kevlar, Unfiltered Spectrum

91 (a)	184
91 (b)	185
91 (c)	186

92 Nylon, Unfiltered Spectrum

92 (a)	189
92 (b)	190
92 (c)	191

93 Nonconducting Epoxy, Unfiltered Spectrum

93 (a)	194
93 (b)	195
93 (c)	196

TABLE

PAGE

B14 Conducting Epoxy, Unfiltered Spectrum

B14 (a)

199

B14 (b)

200

B14 (c)

201

2041

214 (a) 214 (b) 214 (c)

214 (a)

214 (b)

214 (c)

TABLE B 1(a)
Copper, Filtered Spectrum
Corrected Background

<u>B, GAUSS</u>	<u>BKG1</u>	<u>BKG2</u>	<u>BKG3</u>	<u>BKG4</u>
3.0	29.	0.	9.	22.
3.5	11.	7.	3.	13.
4.0	15.	0.	13.	12.
4.5	13.	14.	11.	11.
5.0	15.	15.	11.	11.
5.5	14.	13.	12.	14.
6.8	17.	16.	10.	13.
7.9	16.	14.	10.	14.
9.3	22.	16.	14.	9.
10.8	25.	13.	12.	7.
12.6	91.	58.	49.	39.
14.0	71.	39.	29.	26.
15.5	72.	30.	22.	26.
17.2	62.	28.	24.	25.
18.1	50.	25.	25.	23.
19.0	54.	21.	20.	16.
20.0	58.	18.	18.	15.
21.1	56.	19.	15.	10.
22.1	52.	16.	14.	16.
23.2	44.	16.	13.	13.
24.3	40.	16.	13.	11.
25.5	30.	11.	12.	8.
26.8	24.	9.	11.	5.
28.1	28.	11.	14.	9.
29.6	28.	12.	10.	11.
31.0	15.	7.	10.	8.
32.6	11.	5.	8.	5.
34.2	7.	6.	4.	4.
35.9	7.	4.	4.	4.
37.7	5.	3.	4.	4.
39.6	5.	4.	4.	4.
41.6	4.	3.	4.	5.
43.7	4.	3.	4.	5.
45.8	4.	3.	3.	5.
48.2	5.	4.	4.	6.
50.5	6.	5.	6.	7.
53.1	7.	9.	8.	8.
55.7	7.	15.	10.	7.
58.5	14.	21.	18.	19.
61.4	12.	9.	12.	19.
64.5	8.	12.	10.	16.
67.7	5.	7.	11.	15.

TABLE 2 (Cont.)
 Depth, Tilted Spectra
 in Tilted Position

Depth	Wavelength	Wavelength	Wavelength	Wavelength
10.0	48.0	48.0	48.0	48.0
11.0	48.0	48.0	48.0	48.0
12.0	48.0	48.0	48.0	48.0
13.0	48.0	48.0	48.0	48.0
14.0	48.0	48.0	48.0	48.0
15.0	48.0	48.0	48.0	48.0
16.0	48.0	48.0	48.0	48.0
17.0	48.0	48.0	48.0	48.0
18.0	48.0	48.0	48.0	48.0
19.0	48.0	48.0	48.0	48.0
20.0	48.0	48.0	48.0	48.0
21.0	48.0	48.0	48.0	48.0
22.0	48.0	48.0	48.0	48.0
23.0	48.0	48.0	48.0	48.0
24.0	48.0	48.0	48.0	48.0
25.0	48.0	48.0	48.0	48.0
26.0	48.0	48.0	48.0	48.0
27.0	48.0	48.0	48.0	48.0
28.0	48.0	48.0	48.0	48.0
29.0	48.0	48.0	48.0	48.0
30.0	48.0	48.0	48.0	48.0
31.0	48.0	48.0	48.0	48.0
32.0	48.0	48.0	48.0	48.0
33.0	48.0	48.0	48.0	48.0
34.0	48.0	48.0	48.0	48.0
35.0	48.0	48.0	48.0	48.0
36.0	48.0	48.0	48.0	48.0
37.0	48.0	48.0	48.0	48.0
38.0	48.0	48.0	48.0	48.0
39.0	48.0	48.0	48.0	48.0
40.0	48.0	48.0	48.0	48.0
41.0	48.0	48.0	48.0	48.0
42.0	48.0	48.0	48.0	48.0
43.0	48.0	48.0	48.0	48.0
44.0	48.0	48.0	48.0	48.0
45.0	48.0	48.0	48.0	48.0
46.0	48.0	48.0	48.0	48.0
47.0	48.0	48.0	48.0	48.0
48.0	48.0	48.0	48.0	48.0
49.0	48.0	48.0	48.0	48.0
50.0	48.0	48.0	48.0	48.0
51.0	48.0	48.0	48.0	48.0
52.0	48.0	48.0	48.0	48.0
53.0	48.0	48.0	48.0	48.0
54.0	48.0	48.0	48.0	48.0
55.0	48.0	48.0	48.0	48.0
56.0	48.0	48.0	48.0	48.0
57.0	48.0	48.0	48.0	48.0
58.0	48.0	48.0	48.0	48.0
59.0	48.0	48.0	48.0	48.0
60.0	48.0	48.0	48.0	48.0
61.0	48.0	48.0	48.0	48.0
62.0	48.0	48.0	48.0	48.0
63.0	48.0	48.0	48.0	48.0
64.0	48.0	48.0	48.0	48.0
65.0	48.0	48.0	48.0	48.0
66.0	48.0	48.0	48.0	48.0
67.0	48.0	48.0	48.0	48.0
68.0	48.0	48.0	48.0	48.0
69.0	48.0	48.0	48.0	48.0
70.0	48.0	48.0	48.0	48.0
71.0	48.0	48.0	48.0	48.0
72.0	48.0	48.0	48.0	48.0
73.0	48.0	48.0	48.0	48.0
74.0	48.0	48.0	48.0	48.0
75.0	48.0	48.0	48.0	48.0
76.0	48.0	48.0	48.0	48.0
77.0	48.0	48.0	48.0	48.0
78.0	48.0	48.0	48.0	48.0
79.0	48.0	48.0	48.0	48.0
80.0	48.0	48.0	48.0	48.0
81.0	48.0	48.0	48.0	48.0
82.0	48.0	48.0	48.0	48.0
83.0	48.0	48.0	48.0	48.0
84.0	48.0	48.0	48.0	48.0
85.0	48.0	48.0	48.0	48.0
86.0	48.0	48.0	48.0	48.0
87.0	48.0	48.0	48.0	48.0
88.0	48.0	48.0	48.0	48.0
89.0	48.0	48.0	48.0	48.0
90.0	48.0	48.0	48.0	48.0
91.0	48.0	48.0	48.0	48.0
92.0	48.0	48.0	48.0	48.0
93.0	48.0	48.0	48.0	48.0
94.0	48.0	48.0	48.0	48.0
95.0	48.0	48.0	48.0	48.0
96.0	48.0	48.0	48.0	48.0
97.0	48.0	48.0	48.0	48.0
98.0	48.0	48.0	48.0	48.0
99.0	48.0	48.0	48.0	48.0
100.0	48.0	48.0	48.0	48.0

TABLE B 1(b)
Copper, Filtered Spectrum
Electron Counts with Error, X-Ray Counts

B, GAUSS	N1, COUNTS	ERROR	N2, COUNTS	ERROR	N3, COUNTS	ERROR	N4, COUNTS	ERROR	NX, X10000
3.0	2.	6.	1.	1.	1.	3.	5.	5.	24782.
3.5	1.	3.	1.	3.	1.	2.	35.	7.	24543.
4.0	28.	7.	1.	1.	21.	6.	28.	6.	24126.
4.5	42.	7.	5.	4.	28.	6.	12.	5.	24083.
5.0	51.	8.	4.	4.	26.	6.	16.	5.	24090.
5.5	43.	8.	1.	4.	28.	6.	4.	4.	24529.
6.8	60.	9.	1.	4.	18.	5.	18.	6.	25014.
7.9	65.	9.	11.	5.	30.	6.	25.	6.	24059.
9.3	55.	9.	2.	4.	16.	5.	1.	3.	22778.
10.8	53.	9.	32.	7.	44.	7.	1.	3.	21884.
12.6	445.	23.	126.	14.	98.	12.	85.	11.	86053.
14.0	557.	25.	121.	13.	124.	12.	68.	10.	57551.
15.5	568.	25.	142.	13.	121.	12.	14.	6.	45159.
17.2	635.	26.	143.	13.	112.	12.	24.	7.	35280.
18.1	709.	28.	135.	13.	71.	10.	19.	6.	29511.
19.0	692.	27.	145.	13.	81.	10.	1.	4.	23874.
20.0	636.	26.	170.	14.	87.	10.	2.	4.	20439.
21.1	650.	27.	184.	14.	90.	10.	1.	3.	17179.
22.1	669.	27.	185.	14.	110.	11.	6.	5.	14690.
23.2	724.	28.	176.	14.	71.	9.	13.	5.	12124.
24.3	748.	28.	183.	14.	78.	10.	1.	3.	10441.
25.5	813.	29.	164.	13.	66.	9.	16.	5.	7620.
26.8	848.	30.	222.	15.	81.	10.	21.	5.	6598.
28.1	807.	29.	205.	15.	96.	10.	1.	3.	10036.
29.6	810.	29.	170.	13.	128.	12.	21.	6.	11383.
31.0	902.	30.	246.	16.	70.	9.	42.	7.	10442.
32.6	928.	31.	234.	15.	115.	11.	31.	6.	9719.
34.2	953.	31.	229.	15.	141.	12.	41.	7.	8988.
35.9	952.	31.	224.	15.	181.	14.	56.	8.	8597.

TABLE B 1(b) continued

B, GAUSS	N1, COUNTS	ERROR	N2, COUNTS	ERROR	N3, COUNTS	ERROR	N4, COUNTS	ERROR	NX, X10000
37.7	967.	31.	251.	16.	129.	12.	50.	7.	8734.
39.6	967.	31.	223.	15.	149.	12.	59.	8.	8432.
41.6	975.	31.	250.	16.	138.	12.	61.	8.	9118.
43.7	974.	31.	259.	16.	145.	12.	49.	7.	10154.
45.8	973.	31.	206.	14.	164.	13.	35.	6.	11564.
48.1	967.	31.	284.	17.	172.	13.	56.	8.	14497.
50.5	963.	31.	249.	16.	169.	13.	83.	9.	18140.
53.1	955.	31.	246.	16.	227.	15.	101.	10.	29695.
55.7	954.	31.	249.	16.	190.	14.	122.	11.	46104.
58.5	907.	30.	253.	17.	267.	17.	170.	14.	87807.
61.4	214.	15.	82.	10.	100.	11.	48.	8.	64178.
64.5	92.	10.	37.	7.	1.	3.	11.	5.	63462.
67.7	50.	7.	1.	3.	1.	3.	39.	7.	65917.

TABLE B 1(c)
Copper, Filtered Spectrum
Differential Yield, Detector Efficiency, Energy Integrated Yield

E, KEV	G1,/1000	E1,/1000	G2,/1000	E2,/1000	G3,/1000	E3,/1000	G4,/1000	E4,/1000	ED
.08	.0029	.0005	.0037	.0037	.0056	.0018	.0450	.0087	.9181
.11	.0010	.0003	.0026	.0009	.0041	.0020	.2269	.0327	.9460
.14	.0224	.0034	.0020	.0020	.0653	.0112	.1389	.0220	.9626
.18	.0263	.0035	.0079	.0018	.0682	.0109	.0466	.0097	.9726
.22	.0257	.0032	.0051	.0012	.0510	.0084	.0501	.0096	.9785
.27	.0175	.0023	.0010	.0003	.0444	.0070	.0101	.0024	.9819
.41	.0157	.0018	.0007	.0002	.0183	.0035	.0292	.0052	.9839
.55	.0131	.0015	.0056	.0011	.0235	.0037	.0313	.0050	.9818
.76	.0085	.0010	.0008	.0002	.0096	.0018	.0010	.0003	.9769
1.03	.0064	.0007	.0097	.0014	.0205	.0027	.0007	.0003	.9705
1.40	.0101	.0004	.0072	.0005	.0086	.0007	.0119	.0011	.9622
1.72	.0154	.0006	.0085	.0007	.0133	.0011	.0116	.0012	.9555
2.11	.0164	.0006	.0104	.0008	.0136	.0011	.0023	.0004	.9483
2.60	.0193	.0007	.0110	.0008	.0132	.0011	.0045	.0006	.9400
2.88	.0233	.0008	.0113	.0009	.0091	.0009	.0039	.0006	.9356
3.18	.0257	.0009	.0136	.0011	.0117	.0012	.0002	.0001	.9312
3.52	.0250	.0010	.0169	.0012	.0133	.0013	.0005	.0001	.9262
3.92	.0275	.0010	.0197	.0014	.0148	.0014	.0003	.0001	.9207
4.30	.0304	.0011	.0213	.0015	.0194	.0017	.0017	.0004	.9157
4.74	.0364	.0013	.0224	.0016	.0139	.0015	.0041	.0008	.9101
5.20	.0400	.0014	.0248	.0018	.0162	.0017	.0003	.0001	.9045
5.72	.0546	.0019	.0279	.0021	.0172	.0020	.0067	.0014	.8983
6.32	.0600	.0020	.0397	.0026	.0223	.0023	.0092	.0018	.8915
6.95	.0344	.0012	.0221	.0015	.0159	.0015	.0003	.0001	.8846
7.71	.0277	.0010	.0147	.0011	.0170	.0015	.0045	.0008	.8766
8.46	.0310	.0010	.0214	.0013	.0094	.0010	.0090	.0013	.8689
9.35	.0313	.0010	.0200	.0013	.0151	.0014	.0065	.0011	.8600
10.29	.0320	.0010	.0194	.0013	.0184	.0015	.0085	.0013	.8510
11.34	.0307	.0010	.0183	.0012	.0227	.0017	.0112	.0014	.8412
12.51	.0282	.0009	.0185	.0012	.0146	.0013	.0090	.0012	.8306

TABLE B 1(c) continued

<u>E,KEV</u>	<u>G1,/1000</u>	<u>E1,/1000</u>	<u>G2,/1000</u>	<u>E2,/1000</u>	<u>G3,/1000</u>	<u>E3,/1000</u>	<u>G4,/1000</u>	<u>E4,/1000</u>	<u>ED</u>
13.80	.0269	.0009	.0157	.0010	.0161	.0013	.0102	.0013	.8192
15.23	.0231	.0007	.0150	.0009	.0127	.0011	.0090	.0011	.8069
16.81	.0191	.0006	.0129	.0008	.0111	.0009	.0060	.0008	.7937
18.46	.0155	.0005	.0083	.0006	.0102	.0008	.0035	.0005	.7803
20.36	.0114	.0004	.0085	.0005	.0079	.0006	.0041	.0005	.7652
22.44	.0084	.0003	.0055	.0003	.0058	.0004	.0045	.0005	.7491
24.81	.0047	.0002	.0031	.0002	.0044	.0003	.0031	.0003	.7314
27.30	.0028	.0001	.0019	.0001	.0022	.0002	.0023	.0002	.7133
30.12	.0013	.0000	.0009	.0001	.0015	.0001	.0015	.0001	.6934
33.18	.0004	.0000	.0004	.0000	.0007	.0001	.0006	.0001	.6724
36.61	.0002	.0000	.0002	.0000	.0000	.0000	.0001	.0000	.6497
40.33	.0001	.0000	.0000	.0000	.0000	.0000	.0004	.0001	.6259

<u>TOTAL G1</u>	<u>ERROR</u>	<u>TOTAL G2</u>	<u>ERROR</u>	<u>TOTAL G3</u>	<u>ERROR</u>	<u>TOTAL G4</u>	<u>ERROR</u>
.5834	.0086	.3625	.0082	.3443	.0213	.1837	.0436

TIME	CT	WIND	JOINT	WIND	JOINT	WIND	JOINT	WIND	JOINT	WIND	JOINT	WIND	JOINT	WIND	JOINT	WIND	JOINT	WIND	JOINT
TIME	CT	WIND	JOINT	WIND	JOINT	WIND	JOINT	WIND	JOINT	WIND	JOINT	WIND	JOINT	WIND	JOINT	WIND	JOINT	WIND	JOINT
10:00	0000	0000	0000	0000	0000	0000	0000	0000	0000	0000	0000	0000	0000	0000	0000	0000	0000	0000	0000
10:05	0000	0000	0000	0000	0000	0000	0000	0000	0000	0000	0000	0000	0000	0000	0000	0000	0000	0000	0000
10:10	0000	0000	0000	0000	0000	0000	0000	0000	0000	0000	0000	0000	0000	0000	0000	0000	0000	0000	0000
10:15	0000	0000	0000	0000	0000	0000	0000	0000	0000	0000	0000	0000	0000	0000	0000	0000	0000	0000	0000
10:20	0000	0000	0000	0000	0000	0000	0000	0000	0000	0000	0000	0000	0000	0000	0000	0000	0000	0000	0000
10:25	0000	0000	0000	0000	0000	0000	0000	0000	0000	0000	0000	0000	0000	0000	0000	0000	0000	0000	0000
10:30	0000	0000	0000	0000	0000	0000	0000	0000	0000	0000	0000	0000	0000	0000	0000	0000	0000	0000	0000
10:35	0000	0000	0000	0000	0000	0000	0000	0000	0000	0000	0000	0000	0000	0000	0000	0000	0000	0000	0000
10:40	0000	0000	0000	0000	0000	0000	0000	0000	0000	0000	0000	0000	0000	0000	0000	0000	0000	0000	0000
10:45	0000	0000	0000	0000	0000	0000	0000	0000	0000	0000	0000	0000	0000	0000	0000	0000	0000	0000	0000
10:50	0000	0000	0000	0000	0000	0000	0000	0000	0000	0000	0000	0000	0000	0000	0000	0000	0000	0000	0000
10:55	0000	0000	0000	0000	0000	0000	0000	0000	0000	0000	0000	0000	0000	0000	0000	0000	0000	0000	0000
11:00	0000	0000	0000	0000	0000	0000	0000	0000	0000	0000	0000	0000	0000	0000	0000	0000	0000	0000	0000

TABLE 2 (c) continued

TABLE B 2(a)
Tantalum, Filtered Spectrum
Corrected Background

<u>B,GAUSS</u>	<u>BKG1</u>	<u>BKG2</u>	<u>BKG3</u>	<u>BKG4</u>
3.0	37.	6.	32.	27.
3.5	20.	14.	17.	15.
4.0	17.	17.	14.	13.
4.5	15.	16.	13.	13.
5.3	21.	19.	13.	14.
6.2	14.	17.	13.	14.
7.2	24.	16.	12.	15.
8.4	23.	20.	16.	18.
9.8	45.	30.	24.	24.
10.8	44.	23.	21.	23.
12.0	37.	21.	21.	19.
13.3	39.	27.	19.	14.
14.7	39.	17.	13.	14.
16.3	42.	17.	12.	15.
17.2	34.	15.	13.	14.
18.1	26.	13.	13.	12.
19.0	28.	11.	11.	10.
20.0	31.	10.	10.	8.
21.0	26.	10.	6.	7.
22.1	28.	9.	8.	9.
23.2	22.	8.	7.	7.
24.3	21.	8.	7.	6.
25.5	20.	8.	8.	6.
26.8	20.	8.	9.	4.
28.1	15.	5.	7.	7.
29.6	14.	6.	5.	6.
31.0	8.	3.	6.	4.
32.6	6.	3.	5.	3.
34.2	4.	3.	3.	3.
35.9	5.	2.	2.	3.
37.7	3.	2.	2.	2.
39.6	3.	2.	2.	2.
41.6	2.	1.	2.	3.
43.7	2.	2.	2.	3.
45.8	2.	2.	2.	3.
48.1	3.	2.	2.	3.
50.5	3.	3.	3.	3.
53.1	3.	4.	4.	4.
55.7	3.	8.	5.	3.
58.5	7.	10.	9.	9.
61.4	16.	13.	16.	26.
64.5	6.	9.	10.	13.
67.7	3.	10.	10.	10.

TABLE B 2 (b)
Tantalum, Filtered Spectrum
Electron Counts with Error, X-Ray Counts

B, GAUSS	N1, COUNTS	ERROR	N2, COUNTS	ERROR	N3, COUNTS	ERROR	N4, COUNTS	ERROR	NX, X10000
3.0	11.	7.	1.	3.	4.	6.	1.	5.	27934.
3.5	60.	9.	1.	4.	8.	5.	20.	6.	27885.
4.0	79.	10.	13.	5.	17.	6.	25.	6.	26872.
4.5	145.	13.	39.	7.	63.	9.	64.	9.	28963.
5.3	93.	11.	7.	5.	34.	7.	25.	6.	28491.
6.2	194.	14.	53.	8.	65.	9.	1.	4.	28653.
7.2	236.	16.	79.	10.	70.	9.	15.	5.	28576.
8.4	335.	19.	132.	12.	92.	10.	49.	8.	29134.
9.8	754.	28.	220.	16.	133.	13.	65.	9.	46395.
10.8	754.	28.	246.	16.	158.	13.	91.	11.	38521.
12.0	789.	29.	266.	17.	132.	12.	54.	9.	36564.
13.3	796.	29.	238.	16.	144.	13.	100.	11.	35175.
14.7	791.	29.	279.	17.	176.	14.	102.	11.	28541.
16.3	778.	29.	274.	17.	152.	13.	58.	9.	23222.
17.2	824.	29.	278.	17.	144.	13.	51.	8.	19186.
18.1	859.	30.	305.	18.	145.	13.	30.	6.	15499.
19.0	849.	30.	249.	16.	103.	11.	36.	7.	12460.
20.0	836.	29.	292.	17.	139.	12.	49.	8.	11002.
21.0	854.	30.	275.	17.	130.	12.	37.	7.	8965.
22.1	839.	29.	285.	17.	150.	13.	40.	7.	7958.
23.2	871.	30.	258.	16.	133.	12.	29.	6.	6167.
24.3	878.	30.	277.	17.	141.	12.	53.	8.	5498.
25.5	8881.	30.	254.	16.	152.	13.	57.	8.	5274.
26.8	896.	30.	269.	17.	113.	11.	45.	7.	5441.
28.1	917.	31.	303.	18.	137.	12.	51.	8.	5159.
29.6	924.	31.	254.	16.	173.	13.	53.	8.	5634.
31.0	958.	31.	285.	17.	122.	11.	38.	6.	5558.
32.6	965.	31.	329.	18.	145.	12.	54.	8.	5625.
34.2	977.	31.	280.	17.	144.	12.	71.	9.	5410.

TABLE B 2 (b) continued

B, GAUSS	N1, COUNTS	ERROR	N2, COUNTS	ERROR	N3, COUNTS	ERROR	N4, COUNTS	ERROR	NX, X10000
35.9	975.	31.	292.	17.	152.	12.	68.	8.	5302.
37.7	985.	31.	284.	17.	159.	13.	61.	8.	4699.
39.6	983.	31.	316.	18.	154.	12.	70.	8.	5048.
41.6	989.	31.	323.	18.	192.	14.	41.	7.	5018.
43.7	988.	31.	351.	19.	166.	13.	60.	8.	5551.
45.8	988.	31.	300.	17.	188.	14.	70.	9.	6071.
48.1	986.	31.	288.	17.	203.	14.	60.	8.	7272.
50.5	984.	31.	306.	18.	178.	13.	66.	8.	9229.
53.1	982.	31.	308.	18.	204.	14.	68.	8.	13941.
55.7	981.	31.	309.	18.	225.	15.	126.	11.	23022.
58.5	960.	31.	323.	18.	205.	15.	123.	11.	42278.
61.4	907.	12.	327.	18.	238.	16.	87.	11.	88565.
64.5	149.	6.	71.	9.	73.	9.	70.	9.	49328.
67.7	31.		5.	4.	11.	5.	35.	7.	46182.

TABLE B 2(c)
Tantalum, Filtered Spectrum
Differential Yield, Detector Efficiency, Energy Integrated Yield

E, KEV	G1,/1000	E1,/1000	G2,/1000	E2,/1000	G3,/1000	E3,/1000	G4,/1000	E4,/1000	ED
.08	.0142	.0020	.0033	.0012	.0200	.0033	.0080	.0015	.9181
.11	.0552	.0062	.0023	.0006	.0286	.0057	.1141	.0193	.9460
.14	.0567	.0058	.0236	.0043	.0475	.0085	.1114	.0181	.9626
.18	.0755	.0060	.0514	.0069	.1276	.0146	.2069	.0236	.9726
.25	.0352	.0033	.0067	.0013	.0501	.0073	.0587	.0094	.9808
.34	.0532	.0037	.0368	.0044	.0693	.0078	.0017	.0004	.9838
.46	.0481	.0030	.0408	.0042	.0555	.0061	.0190	.0035	.9834
.62	.0494	.0026	.0493	.0040	.0528	.0051	.0449	.0055	.9802
.85	.0156	.0018	.0381	.0024	.0354	.0028	.0276	.0029	.9749
1.03	.0514	.0018	.0424	.0026	.0419	.0031	.0385	.0036	.9705
1.27	.0462	.0016	.0394	.0023	.0300	.0024	.0196	.0023	.9650
1.56	.0397	.0014	.0300	.0018	.0279	.0022	.0309	.0029	.9589
1.90	.0401	.0014	.0358	.0021	.0347	.0025	.0321	.0030	.9522
2.34	.0397	.0014	.0354	.0021	.0302	.0024	.0184	.0022	.9444
2.60	.0460	.0016	.0393	.0023	.0313	.0025	.0177	.0022	.9400
2.88	.0539	.0018	.0484	.0027	.0354	.0028	.0117	.0018	.9356
3.18	.0604	.0020	.0448	.0028	.0285	.0027	.0159	.0023	.9312
3.52	.0611	.0021	.0540	.0031	.0395	.0032	.0222	.0029	.9262
3.88	.0699	.0024	.0570	.0034	.0414	.0035	.0188	.0028	.9212
4.30	.0703	.0024	.0604	.0035	.0489	.0039	.0208	.0030	.9157
4.74	.0860	.0029	.0645	.0040	.0511	.0043	.0178	.0030	.9101
5.20	.0893	.0030	.0713	.0042	.0558	.0046	.0334	.0044	.9045
5.72	.0854	.0028	.0623	.0039	.0573	.0045	.0343	.0043	.8983
6.32	.0769	.0025	.0584	.0035	.0377	.0034	.0240	.0034	.8915
6.95	.0761	.0025	.0636	.0036	.0442	.0037	.0263	.0034	.8846
7.71	.0639	.0021	.0445	.0028	.0465	.0035	.0227	.0030	.8766
8.46	.0618	.0020	.0465	.0027	.0306	.0027	.0152	.0023	.8689
9.35	.0563	.0018	.0485	.0027	.0329	.0027	.0195	.0026	.8600
10.29	.0544	.0017	.0395	.0023	.0312	.0026	.0245	.0029	.8510

TABLE B 2(c) continued

E, KEV	G1,/1000	E1,/1000	G2,/1000	E2,/1000	G3,/1000	E3,/1000	G4,/1000	E4,/1000	ED
11.34	.0509	.0016	.0386	.0023	.0309	.0025	.0220	.0026	.8412
12.51	.0534	.0017	.0390	.0023	.0335	.0026	.0205	.0026	.8306
13.80	.0456	.0015	.0371	.0021	.0278	.0022	.0202	.0024	.8192
15.23	.0425	.0014	.0352	.0020	.0321	.0023	.0109	.0016	.8069
16.81	.0354	.0011	.0319	.0017	.0232	.0018	.0134	.0017	.7937
18.46	.0301	.0010	.0231	.0013	.0222	.0016	.0132	.0015	.7803
20.36	.0232	.0007	.0171	.0010	.0186	.0013	.0088	.0011	.7652
22.44	.0169	.0005	.0133	.0008	.0119	.0009	.0070	.0008	.7491
24.81	.0104	.0003	.0082	.0005	.0084	.0006	.0045	.0005	.7314
27.30	.0059	.0002	.0047	.0003	.0052	.0003	.0047	.0004	.7133
30.12	.0029	.0001	.0025	.0001	.0024	.0002	.0023	.0002	.6934
33.18	.0012	.0000	.0011	.0001	.0013	.0001	.0007	.0001	.6724
36.61	.0003	.0000	.0004	.0000	.0007	.0001	.0010	.0001	.6497
40.33	.0001	.0000	.0000	.0000	.0001	.0000	.0005	.0001	.6259

TOTAL G1	ERROR	TOTAL G2	ERROR	TOTAL G3	ERROR	TOTAL G4	ERROR
1.1671	.0160.	.9223	.0183	.7826	.0276	.4772	.0400

TABLE 1. FRACTIONAL ABUNDANCE OF SELECTED ISOTOPES IN THE SOLAR WIND

ISOTOPE	12C/13C	14C/13C	15N/14N	16O/17O	18O/17O	19F/18F	20Ne/19Ne	21Ne/20Ne	22Ne/20Ne	23Ne/20Ne	24Mg/23Mg	25Mg/24Mg	26Mg/24Mg	27Al/26Al	28Si/27Si	29Si/28Si	30Si/28Si	31P/30P	32S/31S	33S/32S	34S/32S	36S/34S	37Cl/36Cl	38Cl/36Cl	39K/39K	40K/39K	41Ca/40Ca	42Ca/40Ca	43Ca/40Ca	44Ca/40Ca	46Ca/40Ca	48Ca/40Ca	49Ti/48Ti	50Ti/48Ti	51V/50V	52V/50V	54Cr/52Cr	56Cr/52Cr	57Cr/52Cr	58Cr/52Cr	60Cr/52Cr	63Cu/63Cu	65Cu/63Cu	66Zn/64Zn	67Zn/64Zn	68Zn/64Zn	70Zn/64Zn	72Zn/64Zn	74Zn/64Zn	76Zn/64Zn	78Zn/64Zn	80Zn/64Zn	81Zn/64Zn	82Zn/64Zn	84Zn/64Zn	86Zn/64Zn	88Zn/64Zn	90Zn/64Zn	92Zn/64Zn	94Zn/64Zn	96Zn/64Zn	98Zn/64Zn	100Zn/64Zn	102Zn/64Zn	104Zn/64Zn	106Zn/64Zn	108Zn/64Zn	110Zn/64Zn	112Zn/64Zn	114Zn/64Zn	116Zn/64Zn	118Zn/64Zn	120Zn/64Zn	122Zn/64Zn	124Zn/64Zn	126Zn/64Zn	128Zn/64Zn	130Zn/64Zn	132Zn/64Zn	134Zn/64Zn	136Zn/64Zn	138Zn/64Zn	140Zn/64Zn	142Zn/64Zn	144Zn/64Zn	146Zn/64Zn	148Zn/64Zn	150Zn/64Zn	152Zn/64Zn	154Zn/64Zn	156Zn/64Zn	158Zn/64Zn	160Zn/64Zn	162Zn/64Zn	164Zn/64Zn	166Zn/64Zn	168Zn/64Zn	170Zn/64Zn	172Zn/64Zn	174Zn/64Zn	176Zn/64Zn	178Zn/64Zn	180Zn/64Zn	182Zn/64Zn	184Zn/64Zn	186Zn/64Zn	188Zn/64Zn	190Zn/64Zn	192Zn/64Zn	194Zn/64Zn	196Zn/64Zn	198Zn/64Zn	200Zn/64Zn	202Zn/64Zn	204Zn/64Zn	206Zn/64Zn	208Zn/64Zn	210Zn/64Zn	212Zn/64Zn	214Zn/64Zn	216Zn/64Zn	218Zn/64Zn	220Zn/64Zn	222Zn/64Zn	224Zn/64Zn	226Zn/64Zn	228Zn/64Zn	230Zn/64Zn	232Zn/64Zn	234Zn/64Zn	236Zn/64Zn	238Zn/64Zn	240Zn/64Zn	242Zn/64Zn	244Zn/64Zn	246Zn/64Zn	248Zn/64Zn	250Zn/64Zn	252Zn/64Zn	254Zn/64Zn	256Zn/64Zn	258Zn/64Zn	260Zn/64Zn	262Zn/64Zn	264Zn/64Zn	266Zn/64Zn	268Zn/64Zn	270Zn/64Zn	272Zn/64Zn	274Zn/64Zn	276Zn/64Zn	278Zn/64Zn	280Zn/64Zn	282Zn/64Zn	284Zn/64Zn	286Zn/64Zn	288Zn/64Zn	290Zn/64Zn	292Zn/64Zn	294Zn/64Zn	296Zn/64Zn	298Zn/64Zn	300Zn/64Zn	302Zn/64Zn	304Zn/64Zn	306Zn/64Zn	308Zn/64Zn	310Zn/64Zn	312Zn/64Zn	314Zn/64Zn	316Zn/64Zn	318Zn/64Zn	320Zn/64Zn	322Zn/64Zn	324Zn/64Zn	326Zn/64Zn	328Zn/64Zn	330Zn/64Zn	332Zn/64Zn	334Zn/64Zn	336Zn/64Zn	338Zn/64Zn	340Zn/64Zn	342Zn/64Zn	344Zn/64Zn	346Zn/64Zn	348Zn/64Zn	350Zn/64Zn	352Zn/64Zn	354Zn/64Zn	356Zn/64Zn	358Zn/64Zn	360Zn/64Zn	362Zn/64Zn	364Zn/64Zn	366Zn/64Zn	368Zn/64Zn	370Zn/64Zn	372Zn/64Zn	374Zn/64Zn	376Zn/64Zn	378Zn/64Zn	380Zn/64Zn	382Zn/64Zn	384Zn/64Zn	386Zn/64Zn	388Zn/64Zn	390Zn/64Zn	392Zn/64Zn	394Zn/64Zn	396Zn/64Zn	398Zn/64Zn	400Zn/64Zn	402Zn/64Zn	404Zn/64Zn	406Zn/64Zn	408Zn/64Zn	410Zn/64Zn	412Zn/64Zn	414Zn/64Zn	416Zn/64Zn	418Zn/64Zn	420Zn/64Zn	422Zn/64Zn	424Zn/64Zn	426Zn/64Zn	428Zn/64Zn	430Zn/64Zn	432Zn/64Zn	434Zn/64Zn	436Zn/64Zn	438Zn/64Zn	440Zn/64Zn	442Zn/64Zn	444Zn/64Zn	446Zn/64Zn	448Zn/64Zn	450Zn/64Zn	452Zn/64Zn	454Zn/64Zn	456Zn/64Zn	458Zn/64Zn	460Zn/64Zn	462Zn/64Zn	464Zn/64Zn	466Zn/64Zn	468Zn/64Zn	470Zn/64Zn	472Zn/64Zn	474Zn/64Zn	476Zn/64Zn	478Zn/64Zn	480Zn/64Zn	482Zn/64Zn	484Zn/64Zn	486Zn/64Zn	488Zn/64Zn	490Zn/64Zn	492Zn/64Zn	494Zn/64Zn	496Zn/64Zn	498Zn/64Zn	500Zn/64Zn	502Zn/64Zn	504Zn/64Zn	506Zn/64Zn	508Zn/64Zn	510Zn/64Zn	512Zn/64Zn	514Zn/64Zn	516Zn/64Zn	518Zn/64Zn	520Zn/64Zn	522Zn/64Zn	524Zn/64Zn	526Zn/64Zn	528Zn/64Zn	530Zn/64Zn	532Zn/64Zn	534Zn/64Zn	536Zn/64Zn	538Zn/64Zn	540Zn/64Zn	542Zn/64Zn	544Zn/64Zn	546Zn/64Zn	548Zn/64Zn	550Zn/64Zn	552Zn/64Zn	554Zn/64Zn	556Zn/64Zn	558Zn/64Zn	560Zn/64Zn	562Zn/64Zn	564Zn/64Zn	566Zn/64Zn	568Zn/64Zn	570Zn/64Zn	572Zn/64Zn	574Zn/64Zn	576Zn/64Zn	578Zn/64Zn	580Zn/64Zn	582Zn/64Zn	584Zn/64Zn	586Zn/64Zn	588Zn/64Zn	590Zn/64Zn	592Zn/64Zn	594Zn/64Zn	596Zn/64Zn	598Zn/64Zn	600Zn/64Zn	602Zn/64Zn	604Zn/64Zn	606Zn/64Zn	608Zn/64Zn	610Zn/64Zn	612Zn/64Zn	614Zn/64Zn	616Zn/64Zn	618Zn/64Zn	620Zn/64Zn	622Zn/64Zn	624Zn/64Zn	626Zn/64Zn	628Zn/64Zn	630Zn/64Zn	632Zn/64Zn	634Zn/64Zn	636Zn/64Zn	638Zn/64Zn	640Zn/64Zn	642Zn/64Zn	644Zn/64Zn	646Zn/64Zn	648Zn/64Zn	650Zn/64Zn	652Zn/64Zn	654Zn/64Zn	656Zn/64Zn	658Zn/64Zn	660Zn/64Zn	662Zn/64Zn	664Zn/64Zn	666Zn/64Zn	668Zn/64Zn	670Zn/64Zn	672Zn/64Zn	674Zn/64Zn	676Zn/64Zn	678Zn/64Zn	680Zn/64Zn	682Zn/64Zn	684Zn/64Zn	686Zn/64Zn	688Zn/64Zn	690Zn/64Zn	692Zn/64Zn	694Zn/64Zn	696Zn/64Zn	698Zn/64Zn	700Zn/64Zn	702Zn/64Zn	704Zn/64Zn	706Zn/64Zn	708Zn/64Zn	710Zn/64Zn	712Zn/64Zn	714Zn/64Zn	716Zn/64Zn	718Zn/64Zn	720Zn/64Zn	722Zn/64Zn	724Zn/64Zn	726Zn/64Zn	728Zn/64Zn	730Zn/64Zn	732Zn/64Zn	734Zn/64Zn	736Zn/64Zn	738Zn/64Zn	740Zn/64Zn	742Zn/64Zn	744Zn/64Zn	746Zn/64Zn	748Zn/64Zn	750Zn/64Zn	752Zn/64Zn	754Zn/64Zn	756Zn/64Zn	758Zn/64Zn	760Zn/64Zn	762Zn/64Zn	764Zn/64Zn	766Zn/64Zn	768Zn/64Zn	770Zn/64Zn	772Zn/64Zn	774Zn/64Zn	776Zn/64Zn	778Zn/64Zn	780Zn/64Zn	782Zn/64Zn	784Zn/64Zn	786Zn/64Zn	788Zn/64Zn	790Zn/64Zn	792Zn/64Zn	794Zn/64Zn	796Zn/64Zn	798Zn/64Zn	800Zn/64Zn	802Zn/64Zn	804Zn/64Zn	806Zn/64Zn	808Zn/64Zn	810Zn/64Zn	812Zn/64Zn	814Zn/64Zn	816Zn/64Zn	818Zn/64Zn	820Zn/64Zn	822Zn/64Zn	824Zn/64Zn	826Zn/64Zn	828Zn/64Zn	830Zn/64Zn	832Zn/64Zn	834Zn/64Zn	836Zn/64Zn	838Zn/64Zn	840Zn/64Zn	842Zn/64Zn	844Zn/64Zn	846Zn/64Zn	848Zn/64Zn	850Zn/64Zn	852Zn/64Zn	854Zn/64Zn	856Zn/64Zn	858Zn/64Zn	860Zn/64Zn	862Zn/64Zn	864Zn/64Zn	866Zn/64Zn	868Zn/64Zn	870Zn/64Zn	872Zn/64Zn	874Zn/64Zn	876Zn/64Zn	878Zn/64Zn	880Zn/64Zn	882Zn/64Zn	884Zn/64Zn	886Zn/64Zn	888Zn/64Zn	890Zn/64Zn	892Zn/64Zn	894Zn/64Zn	896Zn/64Zn	898Zn/64Zn	900Zn/64Zn	902Zn/64Zn	904Zn/64Zn	906Zn/64Zn	908Zn/64Zn	910Zn/64Zn	912Zn/64Zn	914Zn/64Zn	916Zn/64Zn	918Zn/64Zn	920Zn/64Zn	922Zn/64Zn	924Zn/64Zn	926Zn/64Zn	928Zn/64Zn	930Zn/64Zn	932Zn/64Zn	934Zn/64Zn	936Zn/64Zn	938Zn/64Zn	940Zn/64Zn	942Zn/64Zn	944Zn/64Zn	946Zn/64Zn	948Zn/64Zn	950Zn/64Zn	952Zn/64Zn	954Zn/64Zn	956Zn/64Zn	958Zn/64Zn	960Zn/64Zn	962Zn/64Zn	964Zn/64Zn	966Zn/64Zn	968Zn/64Zn	970Zn/64Zn	972Zn/64Zn	974Zn/64Zn	976Zn/64Zn	978Zn/64Zn	980Zn/64Zn	982Zn/64Zn	984Zn/64Zn	986Zn/64Zn	988Zn/64Zn	990Zn/64Zn	992Zn/64Zn	994Zn/64Zn	996Zn/64Zn	998Zn/64Zn	1000Zn/64Zn
---------	---------	---------	---------	---------	---------	---------	-----------	-----------	-----------	-----------	-----------	-----------	-----------	-----------	-----------	-----------	-----------	---------	---------	---------	---------	---------	-----------	-----------	---------	---------	-----------	-----------	-----------	-----------	-----------	-----------	-----------	-----------	---------	---------	-----------	-----------	-----------	-----------	-----------	-----------	-----------	-----------	-----------	-----------	-----------	-----------	-----------	-----------	-----------	-----------	-----------	-----------	-----------	-----------	-----------	-----------	-----------	-----------	-----------	-----------	------------	------------	------------	------------	------------	------------	------------	------------	------------	------------	------------	------------	------------	------------	------------	------------	------------	------------	------------	------------	------------	------------	------------	------------	------------	------------	------------	------------	------------	------------	------------	------------	------------	------------	------------	------------	------------	------------	------------	------------	------------	------------	------------	------------	------------	------------	------------	------------	------------	------------	------------	------------	------------	------------	------------	------------	------------	------------	------------	------------	------------	------------	------------	------------	------------	------------	------------	------------	------------	------------	------------	------------	------------	------------	------------	------------	------------	------------	------------	------------	------------	------------	------------	------------	------------	------------	------------	------------	------------	------------	------------	------------	------------	------------	------------	------------	------------	------------	------------	------------	------------	------------	------------	------------	------------	------------	------------	------------	------------	------------	------------	------------	------------	------------	------------	------------	------------	------------	------------	------------	------------	------------	------------	------------	------------	------------	------------	------------	------------	------------	------------	------------	------------	------------	------------	------------	------------	------------	------------	------------	------------	------------	------------	------------	------------	------------	------------	------------	------------	------------	------------	------------	------------	------------	------------	------------	------------	------------	------------	------------	------------	------------	------------	------------	------------	------------	------------	------------	------------	------------	------------	------------	------------	------------	------------	------------	------------	------------	------------	------------	------------	------------	------------	------------	------------	------------	------------	------------	------------	------------	------------	------------	------------	------------	------------	------------	------------	------------	------------	------------	------------	------------	------------	------------	------------	------------	------------	------------	------------	------------	------------	------------	------------	------------	------------	------------	------------	------------	------------	------------	------------	------------	------------	------------	------------	------------	------------	------------	------------	------------	------------	------------	------------	------------	------------	------------	------------	------------	------------	------------	------------	------------	------------	------------	------------	------------	------------	------------	------------	------------	------------	------------	------------	------------	------------	------------	------------	------------	------------	------------	------------	------------	------------	------------	------------	------------	------------	------------	------------	------------	------------	------------	------------	------------	------------	------------	------------	------------	------------	------------	------------	------------	------------	------------	------------	------------	------------	------------	------------	------------	------------	------------	------------	------------	------------	------------	------------	------------	------------	------------	------------	------------	------------	------------	------------	------------	------------	------------	------------	------------	------------	------------	------------	------------	------------	------------	------------	------------	------------	------------	------------	------------	------------	------------	------------	------------	------------	------------	------------	------------	------------	------------	------------	------------	------------	------------	------------	------------	------------	------------	------------	------------	------------	------------	------------	------------	------------	------------	------------	------------	------------	------------	------------	------------	------------	------------	------------	------------	------------	------------	------------	------------	------------	------------	------------	------------	------------	------------	------------	------------	------------	------------	------------	------------	------------	------------	------------	------------	------------	------------	------------	------------	------------	------------	------------	------------	------------	------------	------------	------------	------------	------------	------------	------------	------------	------------	------------	------------	------------	------------	------------	------------	------------	------------	------------	------------	------------	------------	------------	------------	------------	------------	------------	------------	------------	------------	------------	------------	------------	------------	------------	------------	------------	------------	------------	------------	------------	------------	------------	------------	------------	------------	------------	------------	------------	------------	------------	------------	------------	------------	------------	------------	------------	------------	------------	------------	------------	------------	------------	------------	-------------

Source: R. S. (1971) COSMOCHEMISTRY

TABLE B 3(a)
Magnesium, Unfiltered Spectrum
Corrected Background

<u>B, GAUSS</u>	<u>BKG1</u>	<u>BKG2</u>	<u>BKG3</u>	<u>BKG4</u>
3.5	10.	10.	9.	8.
4.0	9.	9.	8.	7.
4.5	8.	8.	7.	7.
5.0	10.	9.	7.	7.
5.3	11.	10.	7.	7.
5.6	9.	9.	7.	8.
5.8	6.	7.	8.	10.
6.2	7.	9.	7.	9.
6.5	8.	11.	6.	8.
6.8	10.	10.	6.	8.
7.2	12.	8.	6.	8.
7.6	11.	9.	6.	8.
7.9	10.	9.	6.	9.
8.4	11.	9.	8.	9.
8.8	14.	11.	10.	9.
9.3	14.	10.	9.	9.
9.8	14.	9.	8.	8.
10.3	16.	9.	8.	8.
10.8	16.	8.	8.	8.
11.4	16.	9.	8.	8.
12.0	15.	9.	9.	8.
12.6	15.	10.	8.	7.
13.3	16.	11.	8.	6.
14.0	18.	10.	7.	7.
14.7	20.	8.	7.	7.
15.5	23.	10.	7.	8.
16.3	27.	11.	8.	9.
17.2	26.	12.	10.	10.
18.1	24.	12.	12.	11.
19.0	33.	13.	12.	11.
20.0	41.	13.	13.	11.
21.0	42.	17.	10.	12.
22.1	52.	16.	14.	16.
23.2	53.	19.	16.	16.
24.3	55.	22.	18.	17.
25.1	56.	21.	22.	15.
25.5	57.	21.	22.	15.
26.8	53.	21.	23.	12.
28.1	41.	15.	21.	20.
29.6	36.	16.	13.	15.
31.0	20.	9.	14.	11.
32.6	17.	8.	12.	8.
34.2	12.	9.	7.	7.
35.9	12.	6.	6.	7.
37.7	9.	5.	7.	8.

TABLE B 3(b)
Magnesium, Unfiltered Spectrum
Electron Counts with Error, X-Ray Counts

B, GAUSS	N1, COUNTS	ERROR	N2, COUNTS	ERROR	N3, COUNTS	ERROR	N4, COUNTS	ERROR	NX, X10000
3.5	32.	6.	17.	5.	6.	4.	12.	4.	14749.
4.0	53.	8.	11.	4.	8.	4.	12.	4.	14905.
4.5	55.	8.	9.	4.	15.	5.	12.	4.	14925.
5.0	53.	8.	11.	4.	36.	7.	20.	5.	14915.
5.3	48.	8.	22.	6.	12.	4.	17.	5.	14845.
5.6	70.	9.	15.	5.	4.	3.	13.	5.	14714.
5.8	76.	9.	31.	6.	5.	4.	8.	4.	14842.
6.2	114.	11.	36.	7.	14.	5.	18.	5.	14957.
6.5	79.	9.	4.	4.	27.	6.	18.	5.	14834.
6.8	109.	11.	32.	6.	11.	4.	20.	5.	14782.
7.2	127.	12.	36.	7.	21.	5.	10.	4.	14690.
7.6	138.	12.	53.	8.	32.	6.	22.	5.	14749.
7.9	140.	12.	59.	8.	27.	6.	24.	6.	14724.
8.4	186.	14.	54.	8.	19.	5.	21.	5.	13905.
8.8	216.	15.	65.	9.	21.	6.	31.	6.	14590.
9.3	247.	16.	94.	10.	29.	6.	24.	6.	14671.
9.8	341.	19.	84	10.	51.	8.	27.	6.	14699.
10.3	320.	18.	105.	11.	30.	6.	39.	7.	14629.
10.8	336.	19.	116.	11.	55.	8.	36.	7.	14205.
11.4	427.	21.	139.	12.	40.	7.	33.	6.	14689.
12.0	514.	23.	157.	13.	71.	9.	50.	8.	14774.
12.6	625.	25.	186.	14.	79.	9.	47.	7.	14581.
13.3	698.	27.	191.	14.	92.	10.	53.	8.	14567.
14.0	809.	29.	231.	16.	123.	11.	73.	9.	14610.
14.7	899.	30.	306.	18.	106.	11.	86.	10.	14565.
15.5	1070.	33.	316.	18.	112.	11.	73.	9.	14558.
16.3	1173.	35.	362.	19.	133.	12.	105.	11.	14643.
17.2	1271.	36.	427.	21.	199.	14.	116.	11.	14681.
18.1	1441.	38.	454.	22.	138.	12.	101.	11.	14094.
19.0	1701.	42.	531.	23.	207.	15.	121.	11.	14480.

TABLE B 3(b) continued

<u>B, GAUSS</u>	<u>N1, COUNTS</u>	<u>ERROR</u>	<u>N2, COUNTS</u>	<u>ERROR</u>	<u>N3, COUNTS</u>	<u>ERROR</u>	<u>N4, COUNTS</u>	<u>ERROR</u>	<u>NX, X10000</u>
20.0	1916.	44.	574.	24.	253.	16.	129.	12.	14500.
21.0	2069.	46.	648.	26.	246.	16.	136.	12.	14537.
22.1	1767.	43.	567.	24.	209.	15.	129.	12.	14558.
23.2	1532.	40.	529.	23.	212.	15.	130.	12.	14496.
24.3	1369.	38.	451.	22.	185.	14.	128.	12.	14406.
25.1	1352.	38.	435.	21.	162.	14.	131.	12.	14349.
25.5	1258.	36.	434.	21.	187.	14.	131.	12.	14664.
26.8	1346.	37.	449.	22.	182.	14.	157.	13.	14660.
28.1	1109.	34.	432.	21.	184.	14.	70.	9.	14608.
29.6	851.	30.	318.	18.	162.	13.	75.	9.	14583.
31.0	589.	25.	191.	14.	114.	11.	81.	10.	14593.
32.6	534.	23.	209.	15.	113.	11.	68.	9.	14585.
34.2	419.	21.	127.	12.	65.	8.	50.	8.	14595.
35.9	362.	19.	112.	11.	73.	9.	34.	6.	14526.
37.7	282.	17.	108.	11.	73.	9.	33.	6.	14667.

TABLE B 3(c)
Magnesium, Unfiltered Spectrum
Differential Yield, Detector Efficiency, Energy Integrated Yield

E, KEV	G1, /1000	E1, /1000	G2, /1000	E2, /1000	G3, /1000	E3, /1000	G4, /1000	E4, /1000	ED
.11	.0556	.0086	.0748	.0144	.0406	.0105	.1294	.0289	.9460
.14	.0686	.0087	.0360	.0081	.0403	.0101	.0964	.0221	.9626
.18	.0556	.0070	.0230	.0056	.0590	.0126	.0753	.0173	.9726
.22	.0432	.0054	.0227	.0051	.1140	.0174	.1011	.0194	.9785
.25	.0349	.0045	.0404	.0071	.0339	.0078	.0766	.0156	.9808
.28	.0459	.0052	.0249	.0051	.0102	.0031	.0529	.0115	.9823
.30	.0460	.0051	.0475	.0077	.0118	.0033	.0301	.0071	.9830
.34	.0599	.0054	.0479	.0071	.0286	.0062	.0587	.0113	.9838
.37	.0381	.0041	.0049	.0013	.0506	.0088	.0538	.0106	.9840
.41	.0482	.0044	.0358	.0055	.0189	.0046	.0548	.0104	.9839
.46	.0504	.0043	.0362	.0055	.0324	.0062	.0246	.0058	.9834
.51	.0490	.0040	.0476	.0060	.0442	.0072	.0485	.0089	.9825
.55	.0461	.0038	.0492	.0060	.0346	.0060	.0491	.0085	.9818
.62	.0575	.0041	.0422	.0053	.0228	.0044	.0403	.0074	.9802
.68	.0580	.0038	.0442	.0051	.0220	.0039	.0517	.0082	.9788
.76	.0592	.0037	.0570	.0056	.0270	.0044	.0357	.0062	.9769
.85	.0737	.0039	.0459	.0048	.0428	.0056	.0362	.0061	.9749
.93	.0630	.0034	.0523	.0049	.0230	.0037	.0477	.0070	.9727
1.03	.0621	.0033	.0543	.0049	.0396	.0050	.0413	.0062	.9705
1.14	.0687	.0033	.0566	.0047	.0250	.0036	.0330	.0051	.9678
1.27	.0745	.0032	.0576	.0045	.0400	.0045	.0449	.0059	.9650
1.40	.0835	.0033	.0629	.0045	.0410	.0044	.0389	.0053	.9622
1.56	.0840	.0031	.0582	.0041	.0431	.0043	.0396	.0052	.9589
1.72	.0880	.0031	.0636	.0041	.0520	.0046	.0493	.0055	.9555
1.90	.0893	.0029	.0769	.0043	.0409	.0039	.0530	.0055	.9522
2.11	.0960	.0029	.0718	.0040	.0391	.0036	.0407	.0045	.9483
2.34	.0950	.0027	.0742	.0038	.0419	.0035	.0528	.0049	.9444
2.60	.0927	.0026	.0788	.0038	.0565	.0039	.0525	.0047	.9400

TABLE B 3(c) continued

<u>E,KEV</u>	<u>G1,/1000</u>	<u>E1,/1000</u>	<u>G2,/1000</u>	<u>E2,/1000</u>	<u>G3,/1000</u>	<u>E3,/1000</u>	<u>G4,/1000</u>	<u>E4,/1000</u>	<u>ED</u>
2.88	.0994	.0026	.0792	.0037	.0370	.0030	.0432	.0041	.9356
3.18	.1041	.0025	.0823	.0035	.0493	.0033	.0460	.0040	.9312
3.52	.1063	.0024	.0806	.0033	.0546	.0033	.0444	.0038	.9262
3.88	.1044	.0023	.0828	.0032	.0483	.0030	.0426	.0035	.9212
4.30	.0809	.0019	.0657	.0027	.0372	.0025	.0367	.0030	.9157
4.74	.0644	.0016	.0563	.0024	.0346	.0023	.0339	.0028	.9101
5.20	.0531	.0014	.0443	.0020	.0279	.0020	.0308	.0026	.9045
5.54	.0496	.0013	.0404	.0019	.0231	.0017	.0298	.0025	.9004
5.72	.0439	.0012	.0383	.0018	.0254	.0018	.0283	.0023	.8983
6.32	.0428	.0011	.0362	.0017	.0225	.0016	.0310	.0024	.8915
6.95	.0325	.0010	.0320	.0015	.0210	.0015	.0127	.0013	.8846
7.71	.0227	.0008	.0215	.0012	.0168	.0013	.0124	.0013	.8766
8.46	.0145	.0006	.0119	.0008	.0109	.0010	.0124	.0013	.8689
9.35	.0120	.0005	.0119	.0008	.0099	.0009	.0095	.0011	.8600
10.29	.0087	.0004	.0066	.0006	.0052	.0006	.0064	.0008	.8510
11.34	.0069	.0004	.0054	.0005	.0054	.0006	.0040	.0006	.8412
12.51	.0049	.0003	.0047	.0004	.0049	.0006	.0036	.0006	.8306

TOTAL G1	ERROR	TOTAL G2	ERROR	TOTAL G3	ERROR	TOTAL G4	ERROR
.5632	.0249	.4596	.0323	.3027	.0368	.3172	.0600

DATE	DESCRIPTION	AMOUNT	CHECK	DEBIT	CREDIT	BALANCE
12/31/2010	Opening Balance	100.00				100.00
1/1/2011	Deposit	50.00			50.00	150.00
1/15/2011	Withdrawal	25.00		25.00		125.00
2/1/2011	Deposit	75.00			75.00	200.00
2/15/2011	Withdrawal	30.00		30.00		170.00
3/1/2011	Deposit	60.00			60.00	230.00
3/15/2011	Withdrawal	40.00		40.00		190.00
4/1/2011	Deposit	80.00			80.00	270.00
4/15/2011	Withdrawal	50.00		50.00		220.00
5/1/2011	Deposit	90.00			90.00	310.00
5/15/2011	Withdrawal	60.00		60.00		250.00
6/1/2011	Deposit	100.00			100.00	350.00
6/15/2011	Withdrawal	70.00		70.00		280.00
7/1/2011	Deposit	110.00			110.00	390.00
7/15/2011	Withdrawal	80.00		80.00		310.00
8/1/2011	Deposit	120.00			120.00	430.00
8/15/2011	Withdrawal	90.00		90.00		340.00
9/1/2011	Deposit	130.00			130.00	470.00
9/15/2011	Withdrawal	100.00		100.00		370.00
10/1/2011	Deposit	140.00			140.00	510.00
10/15/2011	Withdrawal	110.00		110.00		400.00
11/1/2011	Deposit	150.00			150.00	550.00
11/15/2011	Withdrawal	120.00		120.00		430.00
12/1/2011	Deposit	160.00			160.00	590.00
12/15/2011	Withdrawal	130.00		130.00		460.00
12/31/2011	Closing Balance					460.00

TABLE B 4(a)
Aluminum, Unfiltered Spectrum
Corrected Background

<u>B, GAUSS</u>	<u>BKG1</u>	<u>BKG2</u>	<u>BKG3</u>	<u>BKG4</u>
3.5	11.	10.	9.	8.
4.0	10.	10.	8.	8.
4.5	8.	9.	7.	7.
5.0	10.	10.	7.	7.
5.3	12.	11.	7.	7.
6.2	8.	9.	7.	9.
7.2	13.	9.	7.	8.
8.4	13.	11.	9.	5.
9.8	15.	10.	8.	8.
10.8	18.	9.	9.	9.
12.0	16.	9.	9.	8.
13.3	17.	12.	8.	6.
14.7	21.	9.	7.	8.
16.3	29.	12.	8.	10.
18.1	27.	13.	13.	12.
19.0	35.	13.	13.	12.
20.0	44.	14.	13.	12.
21.0	45.	18.	11.	12.
22.1	54.	17.	15.	17.
23.2	56.	20.	16.	17.
24.3	60.	24.	20.	18.
25.1	61.	23.	24.	17.
25.5	60.	22.	24.	16.
26.8	55.	21.	24.	12.
28.1	43.	16.	22.	21.
29.6	38.	16.	14.	15.
31.0	21.	9.	15.	12.
32.6	18.	9.	13.	8.
34.2	13.	10.	8.	8.
35.9	14.	7.	7.	8.
37.7	10.	6.	7.	8.
39.6	10.	7.	8.	7.
41.6	7.	5.	7.	8.
43.7	6.	4.	6.	8.
45.8	6.	4.	4.	7.
48.1	5.	4.	5.	6.
50.5	5.	5.	5.	6.
53.1	4.	5.	4.	4.
55.7	2.	5.	3.	2.
58.5	3.	3.	3.	0.

TABLE B 4 (b)
Aluminum, Unfiltered Spectrum
Electron Counts with Error, X-Ray Counts

<u>B, GAUSS</u>	<u>N1, COUNTS</u>	<u>ERROR</u>	<u>N2, COUNTS</u>	<u>ERROR</u>	<u>N3, COUNTS</u>	<u>ERROR</u>	<u>N4, COUNTS</u>	<u>ERROR</u>	<u>NX, X10000</u>
3.5	40.	7.	17.	5.	16.	5.	9.	4.	15250.
4.0	49.	8.	8.	4.	16.	5.	5.	4.	15311.
4.5	65.	9.	20.	5.	15.	5.	9.	4.	15362.
5.0	69.	9.	11.	5.	26.	6.	16.	5.	15454.
5.3	85.	10.	4.	4.	25.	6.	7.	4.	15576.
6.2	118.	11.	37.	7.	34.	6.	3.	3.	15617.
7.2	137.	12.	47.	7.	31.	6.	5.	4.	15648.
8.4	160.	13.	32.	7.	46.	7.	1.	2.	15714.
9.8	247.	16.	64.	9.	38.	7.	15.	5.	15662.
10.8	333.	19.	96.	10.	52.	8.	6.	4.	15670.
12.0	429.	21.	142.	12.	69.	9.	12.	4.	15722.
13.3	614.	25.	182.	14.	88.	10.	24.	5.	15266.
14.7	808.	29.	261.	16.	121.	11.	42.	7.	15599.
16.3	1104.	34.	357.	19.	204.	15.	55.	8.	15689.
18.1	1550.	40.	485.	22.	219.	15.	58.	8.	15661.
19.0	1771.	42.	549.	24.	290.	17.	64.	9.	15419.
20.0	2130.	47.	693.	27.	327.	18.	76.	9.	15399.
21.0	2458.	50.	647.	26.	378.	20.	107.	11.	15344.
22.1	2736.	53.	842.	29.	428.	21.	82.	10.	15200.
23.2	3034.	56.	942.	31.	429.	21.	121.	12.	15414.
24.3	3181.	57.	1004.	32.	532.	23.	116.	12.	15548.
25.1	3253.	58.	1057.	33.	528.	23.	163.	13.	15719.
25.5	3170.	57.	1021.	32.	482.	22.	136.	12.	15491.
26.8	2630.	52.	852.	30.	485.	23.	129.	12.	15183.
28.1	2303.	48.	752.	28.	409.	21.	132.	12.	15365.
29.6	1561.	40.	572.	24.	357.	19.	109.	11.	15296.
31.0	1168.	34.	407.	20.	217.	15.	97.	10.	15136.
32.6	1044.	33.	376.	20.	207.	15.	79.	9.	15947.
34.2	836.	29.	213.	15.	131.	12.	57.	8.	15927.

TABLE B 4(b) continued

<u>B, GAUSS</u>	<u>N1, COUNTS</u>	<u>ERROR</u>	<u>N2, COUNTS</u>	<u>ERROR</u>	<u>N3, COUNTS</u>	<u>ERROR</u>	<u>N4, COUNTS</u>	<u>ERROR</u>	<u>NX, X10000</u>
35.9	667.	26.	236.	16.	129.	12.	38.	7.	15978.
37.7	562.	24.	205.	15.	116.	11.	40.	7.	15960.
39.6	438.	21.	151.	13.	93.	10.	33.	6.	15815.
41.6	358.	19.	113.	11.	65.	8.	18.	5.	15882.
43.7	292.	17.	97.	10.	55.	8.	16.	5.	15864.
45.8	213.	15.	70.	9.	49.	7.	21.	5.	15744.
48.1	138.	12.	45.	7.	40.	7.	6.	3.	15722.
50.5	81.	9.	43.	7.	28.	6.	43.	7.	15631.
53.1	50.	7.	25.	5.	3.	3.	20.	5.	15578.
55.7	35.	6.	5.	3.	10.	4.	15.	4.	15571.
58.5	18.	5.	1.	2.	9.	3.	1.	1.	15496.

TABLE B 4(c)
Aluminum, Unfiltered Spectrum
Differential Yield, Detector Efficiency, Energy Integrated Yield

E, KEV	G1, /1000	E1, /1000	G2, /1000	E2, /1000	G3, /1000	E3, /1000	G4, /1000	E4, /1000	ED
.11	.0672	.0094	.0723	.0139	.1046	.0209	.0939	.0228	.9046
.14	.0617	.0080	.0255	.0060	.0784	.0160	.0391	.0108	.9626
.18	.0638	.0075	.0497	.0092	.0573	.0122	.0548	.0137	.9726
.22	.0542	.0061	.0219	.0048	.0795	.0138	.0780	.0163	.9785
.25	.0588	.0060	.0070	.0018	.0673	.0119	.0301	.0080	.9808
.34	.0594	.0053	.0471	.0069	.0665	.0104	.0094	.0027	.9838
.46	.0510	.0042	.0443	.0059	.0449	.0073	.0116	.0032	.9834
.62	.0438	.0033	.0221	.0034	.0489	.0066	.0017	.0007	.9802
.85	.0501	.0031	.0328	.0038	.0300	.0044	.0189	.0039	.9749
1.03	.0558	.0030	.0407	.0040	.0339	.0043	.0062	.0016	.9705
1.27	.0584	.0028	.0489	.0040	.0365	.0041	.0101	.0023	.9650
1.56	.0705	.0028	.0529	.0038	.0393	.0040	.0171	.0031	.9589
1.90	.0749	.0026	.0612	.0037	.0436	.0039	.0242	.0034	.9522
2.34	.0835	.0025	.0683	.0036	.0600	.0041	.0258	.0032	.9444
2.88	.0962	.0024	.0762	.0034	.0529	.0035	.0223	.0027	.9356
3.18	.1018	.0024	.0799	.0034	.0648	.0037	.0228	.0026	.9312
3.52	.1113	.0024	.0916	.0034	.0664	.0036	.0246	.0026	.9262
3.88	.1176	.0023	.0783	.0030	.0703	.0036	.0318	.0029	.9212
4.30	.1200	.0023	.0935	.0032	.0730	.0035	.0223	.0022	.9157
4.74	.1199	.0022	.0942	.0030	.0659	.0031	.0297	.0025	.9101
5.20	.1143	.0020	.0913	.0028	.0744	.0032	.0259	.0022	.9045
5.54	.1089	.0019	.0896	.0027	.0688	.0029	.0339	.0025	.9004
5.72	.1046	.0018	.0853	.0026	.0619	.0028	.0279	.0023	.8983
6.32	.0808	.0016	.0663	.0022	.0580	.0026	.0246	.0021	.8915
6.95	.0642	.0013	.0530	.0019	.0443	.0021	.0228	.0018	.8846
7.71	.0398	.0010	.0369	.0015	.0354	.0018	.0172	.0015	.8766
8.46	.0277	.0008	.0244	.0012	.0200	.0013	.0143	.0014	.8689
9.35	.0215	.0007	.0196	.0010	.0166	.0011	.0101	.0011	.8600
10.29	.0158	.0005	.0102	.0007	.0096	.0008	.0067	.0008	.8510

TABLE B 4(c) continued

<u>E, KEV</u>	<u>G1,/1000</u>	<u>E1,/1000</u>	<u>G2,/1000</u>	<u>E2,/1000</u>	<u>G3,/1000</u>	<u>E3,/1000</u>	<u>G4,/1000</u>	<u>E4,/1000</u>	<u>ED</u>
11.34	.0116	.0004	.0104	.0007	.0087	.0007	.0041	.0006	.8412
12.51	.0090	.0004	.0083	.0006	.0072	.0006	.0040	.0006	.8306
13.80	.0065	.0003	.0057	.0005	.0054	.0005	.0030	.0005	.8192
15.23	.0049	.0003	.0039	.0004	.0034	.0004	.0015	.0003	.8069
16.81	.0037	.0002	.0031	.0003	.0027	.0003	.0012	.0003	.7937
18.46	.0025	.0002	.0021	.0002	.0022	.0003	.0015	.0003	.7803
20.36	.0015	.0001	.0012	.0002	.0017	.0003	.0004	.0001	.7652
22.44	.0008	.0001	.0011	.0002	.0011	.0002	.0027	.0004	.7491
24.81	.0005	.0001	.0006	.0001	.0001	.0000	.0012	.0002	.7314
27.30	.0003	.0001	.0001	.0000	.0003	.0001	.0008	.0002	.7133
30.12	.0001	.0000	.0000	.0000	.0003	.0001	.0001	.0001	.6934

TOTAL G1	ERROR	TOTAL G2	ERROR	TOTAL G3	ERROR	TOTAL G4	ERROR
.7810	.0209	.6231	.0250	.5256	.0400	.2427	.0360

TABLE B 5(a)
Copper, Unfiltered Spectrum
Corrected Background

<u>B, GAUSS</u>	<u>BKG1</u>	<u>BKG2</u>	<u>BKG3</u>	<u>BKG4</u>
3.5	20.	19.	18.	16.
4.0	18.	18.	15.	14.
4.5	15.	16.	13.	13.
5.0	18.	18.	13.	13.
5.6	17.	17.	14.	16.
6.5	17.	21.	11.	16.
7.6	22.	17.	12.	16.
8.8	27.	22.	20.	19.
9.8	29.	19.	15.	15.
10.8	34.	18.	17.	18.
12.0	30.	17.	17.	15.
13.3	33.	23.	16.	12.
14.7	41.	17.	14.	15.
16.3	54.	22.	15.	19.
18.1	49.	24.	24.	23.
19.0	64.	25.	24.	22.
20.0	80.	26.	25.	21.
21.0	85.	34.	21.	23.
22.1	106.	32.	29.	32.
23.2	109.	39.	32.	33.
24.3	117.	46.	39.	36.
25.1	113.	42.	44.	31.
25.5	113.	42.	44.	31.
26.8	109.	42.	48.	24.
28.1	87.	32.	44.	43.
29.6	75.	32.	27.	30.
31.0	41.	19.	29.	23.
32.6	34.	17.	24.	16.
34.2	25.	19.	15.	15.
35.9	26.	14.	14.	15.
37.7	18.	11.	14.	16.
39.6	19.	14.	15.	13.
41.6	13.	9.	14.	16.
43.7	12.	8.	11.	15.
45.8	11.	8.	8.	13.
48.1	11.	9.	9.	13.
50.5	10.	9.	10.	11.
53.1	7.	9.	8.	8.
55.7	4.	10.	7.	4.
58.5	5.	7.	6.	7.

TABLE B 5 (b)
Copper, Unfiltered Spectrum
Electron Counts with Error, X-Ray Counts

<u>B, GAUSS</u>	<u>N1, COUNTS</u>	<u>ERROR</u>	<u>N2, COUNTS</u>	<u>ERROR</u>	<u>N3, COUNTS</u>	<u>ERROR</u>	<u>N4, COUNTS</u>	<u>ERROR</u>	<u>NX, X10000</u>
3.5	242.	16.	97.	11.	81.	10.	60.	9.	28903.
4.0	262.	17.	111.	11.	135.	12.	52.	8.	28865.
4.5	269.	17.	112.	11.	130.	12.	57.	8.	28854.
5.0	266.	17.	106.	11.	131.	12.	45.	8.	28547.
5.6	340.	19.	123.	12.	124.	12.	39.	7.	28811.
6.5	377.	20.	165.	14.	121.	11.	51.	8.	29074.
7.6	537.	24.	212.	15.	178.	14.	52.	8.	29117.
8.8	742.	28.	274.	17.	185.	14.	50.	8.	29119.
9.8	1054.	33.	355.	19.	204.	15.	89.	10.	29274.
10.8	1413.	38.	488.	22.	270.	17.	93.	11.	29907.
12.0	2014.	45.	712.	27.	373.	20.	109.	11.	29755.
13.3	2712.	52.	876.	30.	508.	23.	174.	14.	29783.
14.7	3910.	63.	1329.	37.	665.	26.	194.	14.	29718.
16.3	5596.	75.	1768.	42.	902.	30.	269.	17.	29586.
18.1	7836.	89.	2499.	50.	1288.	36.	337.	19.	28824.
19.0	9140.	96.	2854.	54.	1466.	39.	412.	21.	28435.
20.0	10954.	105.	3446.	59.	1649.	41.	493.	23.	28476.
21.0	13582.	117.	4218.	65.	2030.	45.	592.	25.	29135.
22.1	16791.	130.	5151.	72.	2474.	50.	657.	26.	29722.
23.2	19127.	139.	5945.	77.	2811.	53.	792.	29.	30113.
24.3	21300.	146.	6530.	81.	3015.	55.	774.	28.	30284.
25.1	19265.	139.	5945.	77.	2774.	53.	687.	27.	29131.
25.5	14872.	136.	5584.	75.	2467.	50.	663.	26.	29166.
26.8	13664.	117.	4082.	64.	2075.	46.	609.	25.	29936.
28.1	10914.	105.	3337.	58.	1769.	43.	463.	22.	30774.
29.6	6451.	81.	2088.	46.	1137.	34.	392.	21.	30026.
31.0	5033.	71.	1597.	40.	904.	31.	298.	18.	29700.
32.6	4561.	68.	1458.	38.	795.	29.	282.	17.	30096.
34.2	4354.	66.	1366.	37.	745.	28.	227.	16.	30760.

TABLE B 5(b) continued

<u>B, GAUSS</u>	<u>N1, COUNTS</u>	<u>ERROR</u>	<u>N2, COUNTS</u>	<u>ERROR</u>	<u>N3, COUNTS</u>	<u>ERROR</u>	<u>N4, COUNTS</u>	<u>ERROR</u>	<u>NX, X10000</u>
35.9	3959.	63.	1201.	35.	662.	26.	172.	14.	30474.
37.7	3355.	58.	1061.	33.	618.	25.	190.	14.	30225.
39.6	2868.	54.	964.	31.	555.	24.	197.	14.	30103.
41.6	2447.	50.	847.	29.	467.	22.	170.	14.	30079.
43.7	2007.	45.	757.	28.	366.	29.	135.	12.	29871.
45.8	1533.	39.	521.	23.	298.	17.	98.	11.	29654.
48.1	1266.	36.	426.	21.	303.	18.	99.	11.	31498.
50.5	895.	30.	267.	17.	227.	15.	65.	9.	30301.
53.1	536.	23.	203.	15.	138.	12.	56.	8.	30572.
55.7	321.	18.	105.	11.	91.	10.	44.	7.	30483.
58.5	110.	11.	50.	8.	70.	9.	51.	8.	30192.

TABLE B 5 (c)
Copper, Unfiltered Spectrum
Differential Yield, Detector Efficiency, Energy Integrated Yield

E, KEV	G1,/1000	E1,/1000	G2,/1000	E2,/1000	G3,/1000	E3,/1000	G4,/1000	E4,/1000	ED
.11	.2146	.0133	.2177	.0202	.2794	.0281	.3303	.0379	.9460
.14	.1751	.0105	.1877	.0165	.3509	.0286	.2157	.0265	.6926
.18	.1406	.0083	.1482	.0131	.2643	.0221	.1849	.0221	.9726
.22	.1132	.0067	.1141	.0102	.2168	.0181	.1188	.0156	.9785
.28	.1138	.0060	.1042	.0088	.1614	.0137	.0810	.0109	.9823
.37	.0927	.0047	.1026	.0075	.1157	.0101	.0778	.0095	.9840
.51	.0966	.0041	.0965	.0064	.1245	.0090	.0580	.0070	.9825
.68	.0999	.0036	.0934	.0054	.0969	.0068	.0418	.0050	.9788
.85	.1143	.0035	.0974	.0050	.0861	.0058	.0599	.0059	.9749
1.03	.1241	.0033	.1085	.0048	.0922	.0054	.0507	.0048	.9705
1.27	.1448	.0032	.1296	.0048	.1043	.0053	.0487	.0044	.9650
1.56	.1597	.0030	.1305	.0044	.1163	.0051	.0636	.0047	.9589
1.90	.1903	.0030	.1637	.0045	.1259	.0048	.0586	.0041	.9522
2.34	.2244	.0030	.1794	.0042	.1407	.0046	.0669	.0039	.9444
2.88	.2642	.0030	.2132	.0042	.1689	.0047	.0705	.0037	.9356
3.18	.2849	.0030	.2251	.0042	.1777	.0046	.0797	.0038	.9312
3.52	.3095	.0029	.2464	.0042	.1812	.0044	.0864	.0038	.9262
3.88	.3421	.0029	.2689	.0041	.1989	.0044	.0925	.0037	.9212
4.30	.3768	.0029	.2925	.0041	.2159	.0043	.0915	.0035	.9157
4.74	.3869	.0028	.3043	.0039	.2212	.0041	.0994	.0035	.9101
5.20	.3931	.0027	.3050	.0038	.2164	.0039	.0887	.0031	.9045
5.54	.3481	.0025	.2719	.0035	.1950	.0037	.0770	.0029	.9004
5.72	.3238	.0024	.2477	.0033	.1682	.0034	.0721	.0027	.8983
6.32	.2130	.0018	.1611	.0025	.1258	.0027	.0589	.0023	.8915
6.95	.1518	.0014	.1175	.0020	.0957	.0022	.0400	.0018	.8846
7.71	.0837	.0010	.0686	.0015	.0574	.0017	.0316	.0015	.8766
8.46	.0608	.0009	.0488	.0012	.0425	.0014	.0223	.0012	.8689
9.35	.0497	.0007	.0402	.0010	.0337	.0012	.0191	.0011	.8600
10.29	.0427	.0006	.0339	.0009	.0284	.0010	.0138	.0009	.8510

TABLE B 5(c) continued

<u>E, KEV</u>	<u>G1,/1000</u>	<u>E1,/1000</u>	<u>G2,/1000</u>	<u>E2,/1000</u>	<u>G3,/1000</u>	<u>E3,/1000</u>	<u>G4,/1000</u>	<u>E4,/1000</u>	<u>ED</u>
11.34	.0360	.0006	.0276	.0008	.0234	.0009	.0097	.0007	.8412
12.51	.0283	.0005	.0226	.0007	.0203	.0008	.0099	.0407	.0007
13.80	.0223	.0004	.0290	.0006	.0168	.0007	.0095	.0007	.8192
15.23	.0176	.0004	.0154	.0005	.0130	.0006	.0076	.0006	.8069
16.81	.0134	.0003	.0138	.0005	.0095	.0005	.0056	.0005	.7937
18.46	.0095	.0002	.0082	.0004	.0072	.0004	.0038	.0004	.7803
20.36	.0069	.0002	.0059	.0003	.0064	.0004	.0033	.0003	.7652
22.44	.0047	.0002	.0035	.0002	.0046	.0003	.0021	.0002	.7491
24.81	.0026	.0001	.0025	.0002	.0026	.0002	.0017	.0002	.7314
27.30	.0015	.0001	.0012	.0001	.0016	.0002	.0012	.0002	.7133
30.12	.0005	.0000	.0005	.0001	.0012	.0001	.0013	.0002	.6934
TOTAL G1	ERROR	TOTAL G2	ERROR	TOTAL G3	ERROR	TOTAL G4	ERROR		
2.1879	.0251	1.7596	.0381	1.4182	.0564	.6774	.0584		

Line	Account	Amount	Balance	Debit	Credit	Balance
1	1000000	1000000				1000000
2	1000000	1000000				1000000
3	1000000	1000000				1000000
4	1000000	1000000				1000000
5	1000000	1000000				1000000
6	1000000	1000000				1000000
7	1000000	1000000				1000000
8	1000000	1000000				1000000
9	1000000	1000000				1000000
10	1000000	1000000				1000000
11	1000000	1000000				1000000
12	1000000	1000000				1000000
13	1000000	1000000				1000000
14	1000000	1000000				1000000
15	1000000	1000000				1000000
16	1000000	1000000				1000000
17	1000000	1000000				1000000
18	1000000	1000000				1000000
19	1000000	1000000				1000000
20	1000000	1000000				1000000
21	1000000	1000000				1000000
22	1000000	1000000				1000000
23	1000000	1000000				1000000
24	1000000	1000000				1000000
25	1000000	1000000				1000000
26	1000000	1000000				1000000
27	1000000	1000000				1000000
28	1000000	1000000				1000000
29	1000000	1000000				1000000
30	1000000	1000000				1000000
31	1000000	1000000				1000000
32	1000000	1000000				1000000
33	1000000	1000000				1000000
34	1000000	1000000				1000000
35	1000000	1000000				1000000
36	1000000	1000000				1000000
37	1000000	1000000				1000000
38	1000000	1000000				1000000
39	1000000	1000000				1000000
40	1000000	1000000				1000000
41	1000000	1000000				1000000
42	1000000	1000000				1000000
43	1000000	1000000				1000000
44	1000000	1000000				1000000
45	1000000	1000000				1000000
46	1000000	1000000				1000000
47	1000000	1000000				1000000
48	1000000	1000000				1000000
49	1000000	1000000				1000000
50	1000000	1000000				1000000
51	1000000	1000000				1000000
52	1000000	1000000				1000000
53	1000000	1000000				1000000
54	1000000	1000000				1000000
55	1000000	1000000				1000000
56	1000000	1000000				1000000
57	1000000	1000000				1000000
58	1000000	1000000				1000000
59	1000000	1000000				1000000
60	1000000	1000000				1000000
61	1000000	1000000				1000000
62	1000000	1000000				1000000
63	1000000	1000000				1000000
64	1000000	1000000				1000000
65	1000000	1000000				1000000
66	1000000	1000000				1000000
67	1000000	1000000				1000000
68	1000000	1000000				1000000
69	1000000	1000000				1000000
70	1000000	1000000				1000000
71	1000000	1000000				1000000
72	1000000	1000000				1000000
73	1000000	1000000				1000000
74	1000000	1000000				1000000
75	1000000	1000000				1000000
76	1000000	1000000				1000000
77	1000000	1000000				1000000
78	1000000	1000000				1000000
79	1000000	1000000				1000000
80	1000000	1000000				1000000
81	1000000	1000000				1000000
82	1000000	1000000				1000000
83	1000000	1000000				1000000
84	1000000	1000000				1000000
85	1000000	1000000				1000000
86	1000000	1000000				1000000
87	1000000	1000000				1000000
88	1000000	1000000				1000000
89	1000000	1000000				1000000
90	1000000	1000000				1000000
91	1000000	1000000				1000000
92	1000000	1000000				1000000
93	1000000	1000000				1000000
94	1000000	1000000				1000000
95	1000000	1000000				1000000
96	1000000	1000000				1000000
97	1000000	1000000				1000000
98	1000000	1000000				1000000
99	1000000	1000000				1000000
100	1000000	1000000				1000000

TABLE B 6(a)
Tantalum, Unfiltered Spectrum
Corrected Background

<u>B, GAUSS</u>	<u>BKG1</u>	<u>BKG2</u>	<u>BKG3</u>	<u>BKG4</u>
3.5	15.	14.	12.	11.
4.0	13.	13.	11.	10.
4.5	11.	12.	9.	9.
5.0	13.	13.	9.	9.
5.3	15.	14.	9.	10.
6.2	10.	12.	9.	12.
7.2	17.	12.	9.	11.
8.4	16.	14.	11.	13.
9.8	20.	13.	11.	11.
10.8	23.	12.	11.	12.
12.0	21.	12.	12.	10.
13.3	22.	16.	11.	8.
14.7	27.	12.	9.	10.
16.3	36.	15.	10.	13.
18.1	34.	17.	17.	16.
19.0	46.	18.	17.	16.
20.0	57.	18.	18.	15.
21.0	59.	24.	15.	16.
22.1	71.	22.	20.	22.
23.2	68.	24.	20.	21.
24.3	72.	28.	24.	22.
25.5.	79.	30.	31.	22.
26.8	76.	29.	33.	17.
28.1	60.	22.	30.	29.
29.6	53.	23.	19.	21.
31.0	29.	13.	21.	16.
32.6	24.	11.	17.	11.
34.2	17.	13.	10.	10.
35.9	18.	9.	9.	10.
37.7	13.	8.	9.	11.
39.6	14.	10.	10.	9.
41.6	9.	6.	10.	11.
43.7	8.	6.	8.	10.
45.8	8.	5.	5.	9.
48.1	7.	6.	6.	8.
50.5	7.	6.	7.	8.
53.1	5.	6.	6.	5.
55.7	3.	7.	4.	3.
58.5	3.	5.	4.	5.
61.4	4.	3.	4.	6.

TABLE 2 (a)
 Relative Wetland Species
 Counting Methods

Wetland	Wetland	Wetland	Wetland	Wetland
1.1	1.1	1.1	1.1	1.1
1.2	1.2	1.2	1.2	1.2
1.3	1.3	1.3	1.3	1.3
1.4	1.4	1.4	1.4	1.4
1.5	1.5	1.5	1.5	1.5
1.6	1.6	1.6	1.6	1.6
1.7	1.7	1.7	1.7	1.7
1.8	1.8	1.8	1.8	1.8
1.9	1.9	1.9	1.9	1.9
1.10	1.10	1.10	1.10	1.10
1.11	1.11	1.11	1.11	1.11
1.12	1.12	1.12	1.12	1.12
1.13	1.13	1.13	1.13	1.13
1.14	1.14	1.14	1.14	1.14
1.15	1.15	1.15	1.15	1.15
1.16	1.16	1.16	1.16	1.16
1.17	1.17	1.17	1.17	1.17
1.18	1.18	1.18	1.18	1.18
1.19	1.19	1.19	1.19	1.19
1.20	1.20	1.20	1.20	1.20
1.21	1.21	1.21	1.21	1.21
1.22	1.22	1.22	1.22	1.22
1.23	1.23	1.23	1.23	1.23
1.24	1.24	1.24	1.24	1.24
1.25	1.25	1.25	1.25	1.25
1.26	1.26	1.26	1.26	1.26
1.27	1.27	1.27	1.27	1.27
1.28	1.28	1.28	1.28	1.28
1.29	1.29	1.29	1.29	1.29
1.30	1.30	1.30	1.30	1.30
1.31	1.31	1.31	1.31	1.31
1.32	1.32	1.32	1.32	1.32
1.33	1.33	1.33	1.33	1.33
1.34	1.34	1.34	1.34	1.34
1.35	1.35	1.35	1.35	1.35
1.36	1.36	1.36	1.36	1.36
1.37	1.37	1.37	1.37	1.37
1.38	1.38	1.38	1.38	1.38
1.39	1.39	1.39	1.39	1.39
1.40	1.40	1.40	1.40	1.40
1.41	1.41	1.41	1.41	1.41
1.42	1.42	1.42	1.42	1.42
1.43	1.43	1.43	1.43	1.43
1.44	1.44	1.44	1.44	1.44
1.45	1.45	1.45	1.45	1.45
1.46	1.46	1.46	1.46	1.46
1.47	1.47	1.47	1.47	1.47
1.48	1.48	1.48	1.48	1.48
1.49	1.49	1.49	1.49	1.49
1.50	1.50	1.50	1.50	1.50
1.51	1.51	1.51	1.51	1.51
1.52	1.52	1.52	1.52	1.52
1.53	1.53	1.53	1.53	1.53
1.54	1.54	1.54	1.54	1.54
1.55	1.55	1.55	1.55	1.55
1.56	1.56	1.56	1.56	1.56
1.57	1.57	1.57	1.57	1.57
1.58	1.58	1.58	1.58	1.58
1.59	1.59	1.59	1.59	1.59
1.60	1.60	1.60	1.60	1.60
1.61	1.61	1.61	1.61	1.61
1.62	1.62	1.62	1.62	1.62
1.63	1.63	1.63	1.63	1.63
1.64	1.64	1.64	1.64	1.64
1.65	1.65	1.65	1.65	1.65
1.66	1.66	1.66	1.66	1.66
1.67	1.67	1.67	1.67	1.67
1.68	1.68	1.68	1.68	1.68
1.69	1.69	1.69	1.69	1.69
1.70	1.70	1.70	1.70	1.70
1.71	1.71	1.71	1.71	1.71
1.72	1.72	1.72	1.72	1.72
1.73	1.73	1.73	1.73	1.73
1.74	1.74	1.74	1.74	1.74
1.75	1.75	1.75	1.75	1.75
1.76	1.76	1.76	1.76	1.76
1.77	1.77	1.77	1.77	1.77
1.78	1.78	1.78	1.78	1.78
1.79	1.79	1.79	1.79	1.79
1.80	1.80	1.80	1.80	1.80
1.81	1.81	1.81	1.81	1.81
1.82	1.82	1.82	1.82	1.82
1.83	1.83	1.83	1.83	1.83
1.84	1.84	1.84	1.84	1.84
1.85	1.85	1.85	1.85	1.85
1.86	1.86	1.86	1.86	1.86
1.87	1.87	1.87	1.87	1.87
1.88	1.88	1.88	1.88	1.88
1.89	1.89	1.89	1.89	1.89
1.90	1.90	1.90	1.90	1.90
1.91	1.91	1.91	1.91	1.91
1.92	1.92	1.92	1.92	1.92
1.93	1.93	1.93	1.93	1.93
1.94	1.94	1.94	1.94	1.94
1.95	1.95	1.95	1.95	1.95
1.96	1.96	1.96	1.96	1.96
1.97	1.97	1.97	1.97	1.97
1.98	1.98	1.98	1.98	1.98
1.99	1.99	1.99	1.99	1.99
2.00	2.00	2.00	2.00	2.00

TABLE B 6 (b)
Tantalum, Unfiltered Spectrum
Electron Counts with Error, X-Ray Counts

<u>B, GAUSS</u>	<u>N1, COUNTS</u>	<u>ERROR</u>	<u>N2, COUNTS</u>	<u>ERROR</u>	<u>N3, COUNTS</u>	<u>ERROR</u>	<u>N4, COUNTS</u>	<u>ERROR</u>	<u>NX, X1000</u>
3.5	400.	20.	190.	14.	160.	13.	47.	8.	20556.
4.0	560.	24.	216.	15.	183.	14.	36.	7.	20374.
4.5	752.	28.	306.	18.	237.	16.	76.	9.	20262.
5.0	932.	31.	367.	19.	250.	16.	75.	9.	20276.
5.3	765.	28.	359.	19.	232.	16.	69.	9.	20273.
6.2	1181.	35.	454.	22.	285.	17.	77.	9.	20289.
7.2	1622.	40.	612.	25.	310.	18.	120.	11.	20378.
8.4	2170.	47.	779.	28.	375.	20.	86.	10.	20428.
9.8	3364.	58.	1129.	34.	535.	23.	134.	12.	20441.
10.8	4270.	66.	1398.	38.	625.	25.	176.	14.	20558.
12.0	5104.	72.	1599.	40.	790.	28.	220.	15.	20450.
13.3	5806.	76.	1973.	45.	916.	30.	304.	18.	20358.
14.7	7255.	85.	2372.	49.	1157.	34.	341.	19.	19939.
16.3	10014.	100.	3260.	57.	1586.	40.	423.	21.	19943.
18.1	14138.	119.	4533.	67.	2072.	46.	603.	25.	20003.
19.0	17184.	131.	5391.	74.	2673.	52.	701.	27.	20203.
20.0	20350.	143.	6529.	81.	3128.	56.	863.	30.	20287.
21.0	24590.	157.	7588.	87.	3688.	61.	1006.	32.	20240.
22.1	29087.	171.	8931.	95.	4326.	66.	1147.	34.	19998.
23.2	30915.	176.	9464.	97.	4488.	67.	1180.	35.	18853.
24.3	34545.	186.	10755.	104.	5105.	72.	1420.	38.	18780.
25.5	40969.	203.	12679.	113.	5999.	78.	1680.	41.	20504.
26.8	37834.	195.	11712.	108.	5873.	77.	1646.	41.	20938.
28.1	35215.	188.	10941.	105.	5407.	74.	1478.	39.	21138.
29.6	26308.	162.	8254.	91.	4369.	66.	1298.	36.	21199.
31.0	17872.	134.	5501.	74.	2791.	53.	826.	29.	20991.
32.6	12193.	111.	3884.	62.	2169.	47.	664.	26.	20639.
34.2	10050.	100.	3140.	56.	1500.	39.	479.	22.	20787.
35.9	8567.	93.	2729.	52.	1457.	38.	404.	20.	21035.

TABLE B 6(b) continued

<u>B, GAUSS</u>	<u>N1, COUNTS</u>	<u>ERROR</u>	<u>N2, COUNTS</u>	<u>ERROR</u>	<u>N3, COUNTS</u>	<u>ERROR</u>	<u>N4, COUNTS</u>	<u>ERROR</u>	<u>NX, X1000</u>
37.7	7875.	89.	2422.	49.	1248.	35.	346.	19.	21037.
39.6	6954.	83.	2095.	46.	1087.	33.	332.	18.	21066.
41.6	5944.	77.	1813.	43.	967.	31.	273.	17.	21036.
43.7	4987.	71.	1552.	39.	801.	28.	258.	16.	20940.
45.8	3906.	63.	1255.	35.	615.	25.	179.	14.	20837.
48.1	2973.	55.	941.	31.	518.	23.	155.	13.	20858.
50.5	2103.	46.	660.	26.	383.	20.	125.	12.	20720.
53.1	1381.	37.	457.	22.	221.	15.	96.	10.	20509.
55.7	836.	29.	226.	15.	159.	13.	68.	8.	20529.
58.5	464.	22.	144.	12.	81.	9.	37.	6.	20742.
61.4	191.	14.	74.	9.	52.	7.	29.	6.	20892.

TABLE B 6(c)
Tantalum, Unfiltered Spectrum
Differential Yield, Detector Efficiency, Energy Integrated Yield

E, KEV	G1,/1000	E1,/1000	G2,/1000	E2,/1000	G3,/1000	E3,/1000	G4,/1000	E4,/1000	ED
.11	.4988	.0245	.5996	.0420	.7761	.0592	.3638	.0478	.9460
.14	.5302	.0221	.5175	.0342	.6739	.0484	.2115	.0312	.9626
.18	.5598	.0203	.5765	.0323	.6862	.0438	.3511	.0381	.9726
.22	.5582	.0182	.5563	.0285	.5824	.0362	.2788	.0304	.9785
.25	.4069	.0146	.4833	.0250	.4800	.0309	.2278	.0256	.9808
.34	.4573	.0133	.4449	.0206	.4292	.0250	.1850	.0196	.9838
.46	.4640	.0115	.4430	.0177	.3449	.0193	.2130	.0186	.9834
.62	.4565	.0098	.4147	.0147	.3068	.0156	.1123	.0113	.9802
.85	.5225	.0090	.4438	.0131	.3232	.0138	.1292	.0107	.9749
1.03	.5455	.0083	.4520	.0120	.3106	.0123	.1395	.0102	.9705
1.27	.5341	.0075	.4235	.0106	.3215	.0114	.1429	.0094	.9650
1.56	.5002	.0066	.4301	.0096	.3069	.0101	.1625	.0092	.9589
1.90	.5262	.0062	.4354	.0089	.3264	.0096	.1535	.0082	.9522
2.34	.5957	.0059	.4908	.0086	.3670	.0092	.1562	.0075	.9444
2.88	.6868	.0058	.5573	.0083	.3915	.0086	.1818	.0073	.9356
3.18	.7539	.0057	.5986	.0081	.4561	.0088	.1909	.0071	.9312
3.52	.8069	.0056	.6552	.0081	.4824	.0086	.2124	.0072	.9262
3.88	.8916	.0057	.6963	.0080	.5201	.0085	.2264	.0071	.9212
4.30	.9700	.0057	.7537	.0080	.5611	.0085	.2374	.0069	.9157
4.74	.9988	.0057	.7738	.0079	.5640	.0084	.2366	.0068	.9101
5.20	1.0281	.0055	.8101	.0078	.5909	.0083	.2623	.0069	.9045
5.72	1.0216	.0050	.8002	.0071	.5819	.0075	.2600	.0063	.8983
6.32	.8433	.0043	.6607	.0061	.5092	.0066	.2277	.0056	.8915
6.95	.7132	.0038	.5608	.0054	.4259	.0058	.1858	.0048	.8846
7.71	.4835	.0030	.3839	.0042	.3123	.0047	.1481	.0041	.8766
8.46	.3053	.0023	.2378	.0032	.1855	.0035	.0876	.0030	.8689
9.35	.1937	.0018	.1562	.0025	.1340	.0029	.0655	.0025	.8600
10.29	.1457	.0015	.1152	.0021	.0846	.0022	.0431	.0019	.8510

TABLE B 6(c) continued

E, KEV	G1,/1000	E1,/1000	G2,/1000	E2,/1000	G3,/1000	E3,/1000	G4,/1000	E4,/1000	ED
11.34	.1128	.0012	.0909	.0017	.0746	.0019	.0330	.0016	.8412
12.51	.0953	.0011	.0742	.0015	.0588	.0017	.0260	.0014	.8306
13.80	.0773	.0009	.0590	.0013	.0470	.0014	.0229	.0012	.8192
15.23	.0610	.0008	.0471	.0011	.0386	.0012	.0174	.0010	.8069
16.81	.0474	.0007	.0374	.0009	.0296	.0010	.0152	.0009	.7937
18.46	.0346	.0006	.0282	.0008	.0212	.0009	.0098	.0007	.7803
20.36	.0244	.0004	.0195	.0006	.0165	.0007	.0079	.0006	.7652
22.44	.0161	.0004	.0128	.0005	.0114	.0006	.0059	.0005	.7491
24.81	.0099	.0003	.0083	.0004	.0062	.0004	.0043	.0004	.7314
27.30	.0056	.0002	.0038	.0003	.0041	.0003	.0028	.0003	.7133
30.12	.0029	.0001	.0023	.0002	.0020	.0002	.0014	.0002	.6934
33.18	.0011	.0001	.0011	.0001	.0012	.0002	.0010	.0002	.6724
TOTAL G1	ERROR	TOTAL G2	ERROR	TOTAL G3	ERROR	TOTAL G4	ERROR		
7.0788	.0555	5.6753	.0876	4.3374	.1128	1.9623	.0903		

TABLE B 7(a)
Lead, Unfiltered Spectrum
Corrected Background

<u>B, GAUSS</u>	<u>BKG1</u>	<u>BKG2</u>	<u>BKG3</u>	<u>BKG4</u>
3.5	17.	17.	15.	13.
4.0	15.	15.	13.	12.
4.5	13.	14.	12.	12.
5.0	16.	16.	11.	12.
5.8	11.	13.	14.	17.
6.8	18.	16.	10.	14.
7.9	17.	15.	10.	15.
8.8	24.	19.	17.	16.
9.8	25.	16.	13.	13.
10.8	28.	14.	14.	14.
12.0	26.	15.	15.	13.
13.3	28.	20.	14.	10.
14.7	35.	15.	12.	13.
16.3	47.	19.	13.	16.
18.1	44.	21.	21.	20.
19.0	57.	22.	21.	19.
20.0	69.	22.	21.	18.
21.0	72.	29.	18.	20.
22.1	90.	27.	25.	27.
23.2	94.	33.	28.	28.
24.3	98.	39.	32.	30.
25.1	95.	35.	37.	26.
25.5	96.	36.	38.	26.
26.8	91.	35.	40.	20.
28.1	71.	26.	36.	35.
29.6	62.	27.	22.	25.
31.0	34.	15.	24.	19.
32.6	28.	14.	20.	13.
34.2	20.	16.	12.	12.
35.9	22.	11.	11.	12.
37.7	15.	9.	11.	13.
39.6	16.	11.	12.	10.
41.6	11.	7.	11.	13.
43.7	10.	7.	9.	12.
45.8	9.	6.	6.	11.
48.1	8.	7.	7.	10.
50.5	8.	7.	8.	9.
53.1	6.	8.	7.	6.
55.7	4.	8.	6.	4.
58.5	4.	6.	5.	6.
61.4	5.	4.	5.	8.

TABLE B 7 (b)
Lead, Unfiltered Spectrum
Electron Counts with Error, X-ray Counts

B, GAUSS	N1, COUNTS	ERROR	N2, COUNTS	ERROR	N3, COUNTS	ERROR	N4, COUNTS	ERROR	NX, X10000
3.5	820.	29.	357.	19.	312.	18.	77.	9.	24589.
4.0	980.	32.	432.	21.	333.	19.	86.	10.	24661.
4.5	1203.	35.	509.	23.	372.	20.	104.	11.	24991.
5.0	1717.	42.	682.	26.	471.	22.	166.	13.	25492.
5.8	1745.	42.	732.	27.	448.	21.	112.	11.	25685.
6.8	2406.	49.	873.	30.	579.	24.	161.	13.	25530.
7.9	3331.	58.	1227.	35.	691.	26.	175.	14.	25244.
8.8	4621.	68.	1681.	41.	781.	28.	239.	16.	25307.
9.8	6416.	80.	2172.	47.	1121.	34.	359.	19.	25450.
10.8	8003.	90.	2582.	51.	1259.	36.	377.	20.	24513.
12.0	11396.	107.	3737.	61.	1897.	44.	562.	24.	25657.
13.3	14652.	121.	5011.	71.	2382.	49.	688.	26.	25843.
14.7	16317.	128.	5488.	74.	2696.	52.	760.	28.	25675.
16.3	17656.	133.	6047.	78.	3022.	55.	880.	30.	25835.
18.1	22243.	149.	7484.	87.	3775.	62.	1165.	34.	25747.
19.0	23289.	153.	8015.	90.	3877.	62.	1133.	34.	24985.
20.0	25534.	160.	8518.	92.	4203.	65.	1294.	36.	24406.
21.0	30591.	175.	10195.	101.	5055.	71.	1442.	38.	24820.
22.1	35763.	189.	11950.	109.	6221.	79.	1753.	42.	25196.
23.2	41630.	204.	13917.	118.	7074.	84.	2068.	46.	25810.
24.3	43108.	208.	14394.	120.	7462.	87.	2124.	46.	25431.
25.1	41283.	203.	13461.	116.	7021.	84.	2143.	47.	24408.
25.5	41021.	203.	13540.	117.	7111.	85.	2141.	47.	24881.
26.8	40840.	202.	13183.	115.	7032.	84.	2133.	46.	25012.
28.1	39140.	198.	12871.	114.	6777.	83.	2083.	46.	25055.
29.6	30859.	176.	10142.	101.	5639.	75.	1756.	42.	24864.
31.0	26868.	164.	8660.	93.	4654.	68.	1460.	38.	24564.
32.6	20940.	145.	6819.	83.	3861.	62.	1149.	34.	24484.
34.2	15004.	123.	4754.	69.	2712.	52.	908.	30.	24769.

TABLE B 7(b) continued

<u>B, GAUSS</u>	<u>N1, COUNTS</u>	<u>ERROR</u>	<u>N2, COUNTS</u>	<u>ERROR</u>	<u>N3, COUNTS</u>	<u>ERROR</u>	<u>N4, COUNTS</u>	<u>ERROR</u>	<u>NX, X10000</u>
35.9	13673.	117.	4532.	67.	2491.	50.	759.	28.	25646.
37.7	10067.	100.	3262.	57.	1831.	43.	584.	24.	25151.
39.6	8782.	94.	2887.	54.	1554.	40.	495.	22.	25195.
41.6	6827.	83.	2305.	48.	1219.	35.	443.	21.	24829.
43.7	5746.	76.	1805.	43.	1002.	32.	359.	19.	24178.
45.8	4396.	66.	1432.	38.	874.	30.	262.	17.	23817.
48.1	3400.	58.	1120.	34.	658.	26.	216.	15.	23920.
50.5	2637.	51.	918.	30.	530.	23.	201.	14.	25427.
53.1	1708.	41.	582.	24.	339.	19.	99.	10.	25479.
55.7	1118.	33.	350.	19.	239.	16.	97.	10.	25586.
58.5	634.	25.	210.	15.	126.	11.	50.	7.	25559.
61.4	301.	17.	127.	11.	85.	9.	27.	6.	25618.

TABLE B 7 (c)
Lead, Unfiltered Spectrum
Differential Yield, Detector Efficiency, Energy Integrated Yield

E, KEV	G1,/1000	E1,/1000	G2,/1000	E2,/1000	G3,/1000	E3,/1000	G4,/1000	E4,/1000	ED
.11	.8548	.0295	.9419	.0487	1.2651	.0700	.4982	.0525	.9460
.14	.7665	.0243	.8551	.0404	1.0130	.0545	.4175	.0422	.9626
.18	.7261	.0208	.7775	.0340	.8733	.0446	.3896	.0362	.9726
.22	.8180	.0196	.8222	.0311	.8727	.0398	.4908	.0368	.9785
.30	.6104	.0146	.6480	.0237	.6095	.0284	.2431	.0214	.9830
.41	.6155	.0125	.5652	.0190	.5761	.0237	.2556	.0193	.9839
.55	.6400	.0111	.5966	.0169	.5164	.0195	.2087	.0151	.9818
.68	.7160	.0105	.6592	.0160	.4707	.0167	.2298	.0144	.9788
.85	.8004	.0100	.6858	.0147	.5439	.0162	.2780	.0144	.9749
1.03	.8575	.0096	.7001	.0137	.5247	.0147	.2507	.0127	.9705
1.27	.9505	.0089	.7888	.0129	.6154	.0141	.2909	.0121	.9650
1.56	.9943	.0082	.8606	.0121	.6287	.0128	.2898	.0110	.9589
1.90	.9191	.0072	.7823	.0105	.5907	.0114	.2657	.0096	.9522
2.34	.8108	.0061	.7028	.0090	.5398	.0098	.2508	.0084	.9444
2.88	.8395	.0056	.7149	.0083	.5542	.0090	.2729	.0079	.9356
3.18	.8262	.0054	.7196	.0080	.5349	.0086	.2494	.0073	.9312
3.52	.8416	.0053	.7106	.0077	.5388	.0083	.2647	.0073	.9262
3.88	.9045	.0052	.7629	.0075	.5813	.0082	.2646	.0069	.9212
4.30	.9466	.0050	.8005	.0073	.6404	.0081	.2880	.0068	.9157
4.74	.9825	.0048	.8312	.0070	.6493	.0077	.3029	.0066	.9101
5.20	.9474	.0046	.8006	.0067	.6379	.0074	.2897	.0062	.9045
5.54	.8904	.0044	.7347	.0063	.5890	.0070	.2869	.0062	.9004
5.72	.8430	.0042	.7042	.0060	.5684	.0067	.2731	.0059	.8983
6.32	.7620	.0038	.6225	.0054	.5103	.0061	.2470	.0053	.8915
6.95	.6687	.0034	.5565	.0049	.4504	.0055	.2209	.0048	.8846
7.71	.4836	.0028	.4022	.0040	.3437	.0046	.1708	.0040	.8766
8.46	.3922	.0024	.3200	.0034	.2643	.0039	.1323	.0034	.8689
9.35	.2804	.0019	.2311	.0028	.2011	.0032	.0955	.0023	.8600

TABLE B 7(c) continued

E, KEV	G1,/1000	E1,/1000	G2,/1000	E2,/1000	G3,/1000	E3,/1000	G4,/1000	E4,/1000	ED
10.29	.1826	.0015	.1464	.0021	.1284	.0025	.0686	.0023	.8510
11.34	.1477	.0013	.1239	.0018	.1046	.0021	.0509	.0018	.8412
12.51	.1019	.0010	.0836	.0015	.0721	.0017	.0367	.0015	.8306
13.80	.0817	.0009	.0679	.0013	.0562	.0014	.0286	.0013	.8192
15.23	.0593	.0007	.0507	.0011	.0412	.0012	.0239	.0011	.8069
16.81	.0473	.0006	.0376	.0009	.0321	.0010	.0183	.0010	.7937
18.46	.0341	.0005	.0281	.0007	.0264	.0009	.0126	.0008	.7803
20.36	.0243	.0004	.0203	.0006	.0183	.0007	.0096	.0006	.7652
22.44	.0165	.0003	.0145	.0005	.0129	.0006	.0078	.0005	.7491
24.81	.0099	.0002	.0085	.0004	.0076	.0004	.0036	.0003	.7314
27.30	.0060	.0002	.0048	.0003	.0050	.0003	.0032	.0003	.7133
30.12	.0032	.0001	.0027	.0002	.0025	.0002	.0016	.0002	.6934
33.18	.0014	.0001	.0015	.0001	.0016	.0002	.0008	.0001	.6724

TOTAL G1	ERROR	TOTAL G2	ERROR	TOTAL G3	ERROR	TOTAL G4	ERROR
7.9641	.0598	6.7443	.0953	5.4556	.1233	2.6154	.0989

TABLE B 8(a)
Cover Glass, Unfiltered Spectrum
Corrected Background

<u>B,GAUSS</u>	<u>BKG1</u>	<u>BKG2</u>	<u>BKG3</u>	<u>BKG4</u>
3.5	19.	0.	8.	8.
4.5	14.	15.	12.	12.
5.3	20.	17.	12.	13.
5.8	11.	13.	14.	16.
6.5	15.	19.	10.	14.
7.2	21.	15.	11.	14.
7.9	18.	16.	11.	16.
8.8	25.	20.	18.	17.
9.8	25.	17.	14.	14.
10.8	29.	15.	14.	15.
12.0	26.	15.	15.	13.
13.3	28.	19.	14.	10.
14.7	36.	15.	12.	13.
16.3	47.	19.	13.	16.
18.1	44.	21.	21.	20.
20.0	73.	23.	22.	19.
21.0	74.	30.	18.	20.
22.1	91.	28.	25.	28.
23.2	92.	33.	27.	28.
24.0	92.	40.	28.	27.
24.5	99.	39.	33.	30.
25.0	108.	39.	38.	34.
25.5	102.	38.	40.	28.
26.0	101.	38.	39.	27.
26.8	95.	37.	42.	21.
28.1	74.	28.	37.	36.
29.0	69.	28.	30.	31.
29.6	65.	28.	23.	26.
31.0	36.	16.	26.	20.
34.2	21.	17.	13.	13.
37.7	16.	10.	12.	14.
41.6	11.	7.	12.	14.
45.8	10.	7.	7.	12.
50.5	9.	8.	9.	10.

TABLE 2 (Cont.)
 Growth Rates, Gallinules, and
 Coots, and Ducklings

Age	Weight	Length	Wing	Height
10	20.5	8	10	10
11	22.8	10	11	12
12	24.6	11	12	13
13	26.1	12	13	14
14	26.8	13	14	15
15	28.0	14	15	16
16	29.6	15	16	17
17	31.0	16	17	18
18	32.3	17	18	19
19	34.0	18	19	20
20	34.5	19	20	21
21	35.0	20	21	22
22	35.5	21	22	23
23	36.8	22	23	24
24	38.1	23	24	25
25	38.5	24	25	26
26	39.6	25	26	27
27	40.8	26	27	28
28	41.6	27	28	29
29	42.8	28	29	30
30	43.8	29	30	31
31	44.6	30	31	32
32	46.1	31	32	33
33	47.3	32	33	34
34	48.0	33	34	35
35	49.6	34	35	36
36	50.8	35	36	37
37	52.3	36	37	38
38	53.0	37	38	39
39	54.0	38	39	40
40	55.0	39	40	41
41	56.1	40	41	42
42	57.3	41	42	43
43	58.0	42	43	44
44	59.6	43	44	45
45	60.8	44	45	46
46	62.3	45	46	47
47	63.0	46	47	48
48	64.6	47	48	49
49	65.8	48	49	50
50	67.3	49	50	51
51	68.0	50	51	52
52	69.6	51	52	53
53	70.8	52	53	54
54	72.3	53	54	55
55	73.0	54	55	56
56	74.6	55	56	57
57	75.8	56	57	58
58	77.3	57	58	59
59	78.0	58	59	60
60	79.6	59	60	61
61	80.8	60	61	62
62	82.3	61	62	63
63	83.0	62	63	64
64	84.6	63	64	65
65	85.8	64	65	66
66	87.3	65	66	67
67	88.0	66	67	68
68	89.6	67	68	69
69	90.8	68	69	70
70	92.3	69	70	71
71	93.0	70	71	72
72	94.6	71	72	73
73	95.8	72	73	74
74	97.3	73	74	75
75	98.0	74	75	76
76	99.6	75	76	77
77	100.8	76	77	78
78	102.3	77	78	79
79	103.0	78	79	80
80	104.6	79	80	81
81	105.8	80	81	82
82	107.3	81	82	83
83	108.0	82	83	84
84	109.6	83	84	85
85	110.8	84	85	86
86	112.3	85	86	87
87	113.0	86	87	88
88	114.6	87	88	89
89	115.8	88	89	90
90	117.3	89	90	91
91	118.0	90	91	92
92	119.6	91	92	93
93	120.8	92	93	94
94	122.3	93	94	95
95	123.0	94	95	96
96	124.6	95	96	97
97	125.8	96	97	98
98	127.3	97	98	99
99	128.0	98	99	100

TABLE B 8(b)
Cover Glass, Unfiltered Spectrum
Electron Counts with Error, X-ray Counts

<u>B, GAUSS</u>	<u>N1, COUNTS</u>	<u>ERROR</u>	<u>N2, COUNTS</u>	<u>ERROR</u>	<u>N3, COUNTS</u>	<u>ERROR</u>	<u>N4, COUNTS</u>	<u>ERROR</u>	<u>NX, X10000</u>
3.5	45.	8.	1.	1.	1.	3.	1.	3.	26440.
4.5	65.	9.	16.	6.	16.	5.	16.	5.	26496.
5.3	75.	10.	1.	4.	13.	5.	9.	5.	26371.
5.8	124.	12.	12.	5.	27.	6.	1.	4.	26444.
6.5	171.	14.	26.	7.	47.	8.	14.	5.	26319.
7.2	189.	14.	46.	8.	34.	7.	33.	7.	26122.
7.9	246.	16.	51.	8.	54.	8.	27.	7.	26204.
8.8	232.	16.	58.	9.	29.	7.	13.	5.	26192.
9.8	376.	20.	109.	11.	80.	10.	47.	8.	26031.
10.8	381.	20.	118.	12.	82.	10.	40.	7.	25528.
12.0	567.	24.	142.	13.	94.	10.	56.	8.	25381.
13.3	890.	30.	202.	15.	133.	12.	70.	9.	25221.
14.7	1211.	35.	303.	18.	221.	15.	102.	11.	25837.
16.3	1555.	40.	400.	20.	259.	16.	136.	12.	25701.
18.1	2116.	46.	506.	23.	336.	19.	152.	13.	25617.
20.0	2500.	51.	632.	26.	463.	22.	254.	17.	25697.
21.0	2842.	54.	616.	25.	492.	23.	258.	17.	25363.
22.1	2927.	55.	715.	27.	580.	25.	266.	17.	25360.
23.2	3217.	58.	807.	29.	664.	26.	302.	18.	25390.
24.0	3551.	60.	942.	31.	693.	27.	316.	19.	25814.
24.5	3482.	60.	822.	29.	689.	27.	324.	19.	25798.
25.0	3342.	59.	890.	30.	728.	28.	371.	20.	26346.
25.5	3241.	58.	838.	30.	731.	28.	384.	20.	26460.
26.0	3296.	58.	854.	30.	702.	27.	400.	21.	25945.

TABLE B 8(b) continued

<u>B, GAUSS</u>	<u>N1, COUNTS</u>	<u>ERROR</u>	<u>N2, COUNTS</u>	<u>ERROR</u>	<u>N3, COUNTS</u>	<u>ERROR</u>	<u>N4, COUNTS</u>	<u>ERROR</u>	<u>NX, X10000</u>
26.8	3097.	56.	929.	31.	766.	28.	402.	21.	26241.
28.1	2221.	48.	600.	25.	528.	24.	313.	19.	26110.
29.9	1750.	43.	497.	23.	489.	23.	287.	18.	25927.
29.6	1483.	39.	431.	21.	436.	21.	269.	17.	26066.
31.0	1132.	34.	331.	19.	291.	18.	177.	14.	26077.
34.2	913.	31.	254.	16.	240.	16.	130.	12.	26339.
37.7	682.	26.	184.	14.	175.	14.	46.	9.	26371.
41.6	433.	21.	139.	12.	119.	11.	53.	8.	26254.
45.8	254.	16.	72.	9.	88.	10.	34.	7.	26213.
50.5	110.	11.	32.	6.	42.	7.	4.	4.	26156.

TABLE B 8 (c)
Cover Glass, Unfiltered Spectrum
Differential Yield, Detector Efficiency, Energy Integrated Yield

E, KEV	G1, /1000	E1, /1000	G2, /1000	E2, /1000	G3, /1000	E3, /1000	G4, /1000	E4, /10000	ED
.11	.0436	.0055	.0025	.0025	.0038	.0013	.0060	.0020	.9460
.18	.0370	.0042	.0231	.0041	.0354	.0067	.0565	.0107	.9726
.25	.0307	.0031	.0010	.0002	.0207	.0041	.0228	.0049	.9808
.30	.0421	.0036	.0103	.0021	.0357	.0056	.0021	.0005	.9830
.37	.0464	.0034	.0179	.0027	.0496	.0066	.0236	.0045	.9840
.46	.0422	.0029	.0260	.0033	.0295	.0044	.0457	.0067	.9834
.55	.0455	.0028	.0239	.0029	.0389	.0048	.0310	.0047	.9818
.68	.0347	.0022	.0220	.0025	.0169	.0025	.0121	.0022	.9788
.85	.0459	.0023	.0336	.0030	.0380	.0039	.0356	.0046	.9749
1.03	.0392	.0019	.0307	.0027	.0328	.0033	.0255	.0034	.9705
1.27	.0478	.0020	.0303	.0024	.0308	.0030	.0293	.0035	.9650
1.56	.0619	.0020	.0355	.0024	.0360	.0030	.0302	.0034	.9589
1.90	.0678	.0019	.0429	.0024	.0481	.0032	.0354	.0033	.9522
2.34	.0718	.0018	.0467	.0023	.0465	.0028	.0390	.0032	.9444
2.88	.0803	.0017	.0486	.0021	.0496	.0026	.0358	.0027	.9356
3.52	.0783	.0015	.0501	.0020	.0564	.0026	.0493	.0030	.9262
3.88	.0822	.0015	.0451	.0018	.0554	.0025	.0463	.0028	.9212
4.30	.0770	.0014	.0476	.0017	.0593	.0024	.0434	.0025	.9157
4.74	.0772	.0013	.0490	.0017	.0620	.0024	.0450	.0025	.9101
5.07	.0787	.0013	.0528	.0017	.0597	.0022	.0435	.0023	.9061
5.28	.0743	.0012	.0444	.0015	.0572	.0021	.0429	.0023	.9035
5.50	.0673	.0011	.0453	.0015	.0570	.0021	.0463	.0023	.9009
5.72	.0626	.0011	.0410	.0014	.0549	.0020	.0461	.0023	.8983
5.95	.0627	.0011	.0411	.0014	.0519	.0019	.0472	.0023	.8957
6.32	.0551	.0010	.0419	.0013	.0530	.0019	.0444	.0022	.8915
6.95	.0364	.0008	.0249	.0010	.0337	.0014	.0318	.0017	.8846
7.40	.0273	.0006	.0196	.0009	.0297	.0013	.0278	.0016	.8798
7.71	.0222	.0006	.0163	.0008	.0253	.0012	.0250	.0015	.8766

К. КЭД	01/1000	02/1000	03/1000	04/1000	05/1000	06/1000	07/1000
1.31	0.15	0.000	0.193	0.008	0.323	0.078	0.000
1.32	0.17	0.000	0.198	0.008	0.381	0.078	0.000
1.33	0.19	0.008	0.348	0.010	0.331	0.078	0.000
1.34	0.21	0.010	0.413	0.013	0.298	0.078	0.000
1.35	0.23	0.017	0.471	0.014	0.218	0.078	0.000
1.36	0.25	0.011	0.470	0.014	0.248	0.078	0.000
1.37	0.27	0.011	0.423	0.012	0.230	0.078	0.000
1.38	0.29	0.013	0.444	0.012	0.213	0.078	0.000
1.39	0.31	0.013	0.288	0.013	0.281	0.078	0.000
1.40	0.33	0.013	0.480	0.013	0.280	0.078	0.000
1.41	0.35	0.014	0.416	0.013	0.283	0.078	0.000
1.42	0.37	0.012	0.421	0.018	0.224	0.078	0.000
1.43	0.39	0.012	0.201	0.030	0.284	0.078	0.000
1.44	0.41	0.013	0.482	0.051	0.486	0.078	0.000
1.45	0.43	0.018	0.481	0.053	0.482	0.078	0.000
1.46	0.45	0.019	0.438	0.054	0.481	0.078	0.000
1.47	0.47	0.020	0.329	0.054	0.380	0.078	0.000
1.48	0.49	0.020	0.363	0.054	0.308	0.078	0.000
1.49	0.51	0.020	0.321	0.053	0.376	0.078	0.000
1.50	0.53	0.023	0.336	0.050	0.380	0.078	0.000
1.51	0.55	0.023	0.350	0.052	0.389	0.078	0.000
1.52	0.57	0.025	0.356	0.053	0.363	0.078	0.000
1.53	0.59	0.025	0.359	0.053	0.382	0.078	0.000
1.54	0.61	0.024	0.310	0.053	0.446	0.078	0.000
1.55	0.63	0.026	0.193	0.053	0.321	0.078	0.000
1.56	0.65	0.031	0.070	0.053	0.303	0.078	0.000
1.57	0.67	0.045	0.037	0.047	0.324	0.078	0.000
1.58	0.69	0.022	0.059	0.052	0.338	0.078	0.000

ВЫВЕДЕНИЕ ИЗВЕЩАНИЯ: ВВЕДЕНИЕ

Содержание: ВВЕДЕНИЕ

ВВЕДЕНИЕ

TABLE B 8(c) continued

<u>E, KEV</u>	<u>G1,/1000</u>	<u>E1,/1000</u>	<u>G2,/1000</u>	<u>E2,/1000</u>	<u>G3,/1000</u>	<u>E3,/1000</u>	<u>G4,/1000</u>	<u>E4,/10000</u>	<u>ED</u>
8.46	.0156	.0005	.0115	.0006	.0156	.0009	.0151	.0011	.8689
10.29	.0104	.0003	.0074	.0004	.0107	.0007	.0092	.0008	.8510
12.51	.0066	.0002	.0045	.0003	.0066	.0005	.0037	.0004	.8306
15.23	.0036	.0002	.0029	.0002	.0038	.0003	.0027	.0003	.8069
18.46	.0018	.0001	.0013	.0001	.0024	.0002	.0015	.0002	.7803
22.44	.0007	.0001	.0005	.0001	.0010	.0001	.0002	.0000	.7491
TOTAL G1	ERROR	TOTAL G2	ERROR	TOTAL G3	ERROR	TOTAL G4	ERROR		
.5479	.0122	.3548	.0115	.4408	.0176	.3584	.0197		

TABLE B 9(a)
Silica Cloth, Unfiltered Spectrum
Corrected Background

<u>B, GAUSS</u>	<u>BKG1</u>	<u>BKG2</u>	<u>BKG3</u>	<u>BKG4</u>
4.5	15.	16.	13.	9.
5.3	22.	20.	13.	14.
5.8	12.	14.	15.	10.
6.5	16.	20.	11.	15.
7.2	23.	16.	12.	11.
7.9	19.	17.	11.	17.
8.8	26.	21.	19.	18.
9.8	28.	18.	15.	15.
10.8	32.	17.	16.	17.
12.0	29.	16.	16.	14.
13.3	31.	22.	15.	11.
14.7	40.	17.	14.	15.
16.3	52.	21.	15.	18.
18.1	49.	24.	24.	23.
20.0	81.	26.	25.	21.
21.0	83.	33.	21.	23.
22.1	102.	31.	28.	31.
22.5	102.	30.	29.	31.
23.0	104.	30.	30.	32.
23.5	103.	37.	30.	31.
24.0	103.	44.	31.	30.
24.5	111.	44.	37.	34.
25.0	119.	43.	42.	38.
25.5	111.	42.	44.	30.
26.8	105.	41.	46.	24.
28.1	82.	31.	41.	40.
31.0	40.	18.	28.	22.
34.2	23.	18.	14.	14.
37.7	16.	10.	12.	14.
41.6	11.	8.	12.	14.
45.8	10.	7.	7.	12.

TABLE 2 (cont.)
 51100 Class, (continued)
 Continued

51100	51101	51102	51103	51104
4.5	18	18	18	18
5.2	20	20	20	20
5.9	22	22	22	22
6.6	24	24	24	24
7.3	26	26	26	26
8.0	28	28	28	28
8.7	30	30	30	30
9.4	32	32	32	32
10.1	34	34	34	34
10.8	36	36	36	36
11.5	38	38	38	38
12.2	40	40	40	40
12.9	42	42	42	42
13.6	44	44	44	44
14.3	46	46	46	46
15.0	48	48	48	48
15.7	50	50	50	50
16.4	52	52	52	52
17.1	54	54	54	54
17.8	56	56	56	56
18.5	58	58	58	58
19.2	60	60	60	60
19.9	62	62	62	62
20.6	64	64	64	64
21.3	66	66	66	66
22.0	68	68	68	68
22.7	70	70	70	70
23.4	72	72	72	72
24.1	74	74	74	74
24.8	76	76	76	76
25.5	78	78	78	78
26.2	80	80	80	80
26.9	82	82	82	82
27.6	84	84	84	84
28.3	86	86	86	86
29.0	88	88	88	88
29.7	90	90	90	90
30.4	92	92	92	92
31.1	94	94	94	94
31.8	96	96	96	96
32.5	98	98	98	98
33.2	100	100	100	100

TABLE B 9(b)
Silica Cloth, Unfiltered Spectrum
Electron Counts with Error, X-ray Counts

B, GAUSS	N1, COUNTS	ERROR	N2, COUNTS	ERROR	N3, COUNTS	ERROR	N4, COUNTS	ERROR	NX, X10000
4.5	86.	10.	23	6.	9.	5.	1.	3.	28968.
5.3	61.	9.	12.	6.	5.	4.	14.	5.	29016.
5.8	125.	12.	41.	7.	14.	5.	1.	3.	29146.
6.5	157.	13.	36.	7.	45.	7.	6.	5.	28408.
7.2	192.	15.	58.	9.	23.	6.	1.	3.	28354.
7.9	270.	17.	74.	10.	52.	8.	2.	4.	27981.
8.8	347.	19.	100.	11.	27.	7.	10.	5.	27888.
9.8	461.	22.	164.	13.	61.	9.	37.	7.	28274.
10.8	451.	22.	141.	13.	66.	9.	53.	8.	28217.
12.0	493.	23.	146.	13.	66.	9.	30.	7.	28229.
13.3	603.	25.	189.	15.	106.	11.	72.	9.	28168.
14.7	844.	30.	258.	17.	158.	13.	69.	9.	28780.
16.3	1109.	34.	367.	20.	200.	15.	85.	10.	28621.
18.1	1568.	40.	476.	22.	215.	15.	120.	12.	28523.
20.0	1956.	45.	598.	25.	311.	18.	135.	12.	28514.
21.0	2012.	46.	721.	27.	366.	20.	172.	14.	28582.
22.1	2149.	47.	748.	28.	388.	20.	189.	15.	28500.
22.5	2261.	49.	720.	27.	351.	19.	202.	15.	28305.
23.0	2335.	49.	814.	29.	421.	21.	157.	14.	28286.
23.5	2313.	49.	864.	30.	434.	22.	182.	15.	28296.
24.0	2178.	48.	810.	29.	443.	22.	213.	16.	28720.
24.5	2351.	50.	811.	29.	448.	22.	248.	17.	28847.
25.0	2296.	49.	802.	29.	442.	22.	240.	17.	28932.
25.5	2145.	47.	811.	29.	443.	22.	231.	16.	28732.
26.8	1570.	41.	644.	26.	342.	20.	222.	16.	28855.
28.1	1372.	38.	573.	25.	348.	20.	160.	14.	28950.
31.0	690.	27.	274.	17.	141.	13.	94.	11.	28718.

TABLE B 9(b) continued

<u>B, GAUSS</u>	<u>N1, COUNTS</u>	<u>ERROR</u>	<u>N2, COUNTS</u>	<u>ERROR</u>	<u>N3, COUNTS</u>	<u>ERROR</u>	<u>N4, COUNTS</u>	<u>ERROR</u>	<u>NX, X10000</u>
34.2	450.	22.	149.	13.	98.	11.	52.	8.	28556.
37.7	303.	18.	108.	11.	83.	10.	22.	6.	26906.
41.6	191.	14.	69.	9.	35.	7.	16.	5.	26949.
45.8	104.	11.	46.	7.	33.	6.	3.	4.	26697.

TABLE B 9(c)
Silica Cloth, Unfiltered Spectrum
Differential Yield, Detector Efficiency, Energy Integrated Yield

<u>E, KEV</u>	<u>G1,/1000</u>	<u>E1,/1000</u>	<u>G2,/1000</u>	<u>E2,/1000</u>	<u>G3,/1000</u>	<u>E3,/1000</u>	<u>G4,/1000</u>	<u>E4,/1000</u>	<u>ED</u>
.18	.0448	.0045	.0303	.0049	.0182	.0039	.0032	.0010	.9726
.25	.0227	.0025	.0113	.0020	.0072	.0017	.0323	.0061	.9808
.30	.0385	.0033	.0320	.0043	.0168	.0031	.0019	.0006	.9830
.37	.0395	.0030	.0229	.0031	.0440	.0059	.0094	.0020	.9840
.46	.0395	.0027	.0302	.0035	.0184	.0031	.0013	.0004	.9834
.55	.0468	.0028	.0325	.0034	.0351	.0044	.0022	.0005	.9818
.68	.0488	.0025	.0356	.0032	.0148	.0022	.0087	.0016	.9788
.85	.0518	.0023	.0466	.0035	.0266	.0031	.0258	.0036	.9749
1.03	.0420	.0019	.0332	.0026	.0239	.0026	.0306	.0037	.9705
1.27	.0374	.0016	.0280	.0022	.0195	.0021	.0141	.0021	.9650
1.56	.0375	.0015	.0298	.0021	.0257	.0023	.0278	.0031	.9589
1.90	.0424	.0014	.0328	.0020	.0309	.0024	.0215	.0023	.9522
2.34	.0460	.0013	.0385	.0020	.0322	.0022	.0219	.0022	.9444
2.88	.0534	.0013	.0410	.0018	.0285	.0018	.0254	.0021	.9356
3.52	.0552	.0012	.0427	.0017	.0341	.0019	.0236	.0019	.9262
3.88	.0517	.0011	.0469	.0017	.0366	.0019	.0274	.0020	.9212
4.30	.0503	.0011	.0443	.0016	.0353	.0017	.0274	.0019	.9157
4.46	.0515	.0011	.0415	.0015	.0311	.0016	.0286	.0019	.9137
4.66	.0511	.0010	.0451	.0016	.0358	.0017	.0213	.0016	.9112
4.86	.0486	.0010	.0460	.0015	.0355	.0016	.0237	.0016	.9086
5.07	.0434	.0009	.0408	.0014	.0343	.0016	.0263	.0017	.9061
5.28	.0449	.0009	.0392	.0013	.0333	.0015	.0294	.0017	.9035
5.50	.0421	.0009	.0372	.0013	.0315	.0014	.0273	.0016	.9009
5.72	.0382	.0008	.0365	.0013	.0307	.0014	.0255	.0016	.8983
6.32	.0254	.0006	.0264	.0010	.0215	.0011	.0223	.0014	.8915
6.95	.0203	.0005	.0214	.0009	.0200	.0010	.0147	.0010	.8846

TABLE B 9(c) continued

<u>E, KEV</u>	<u>G1,/1000</u>	<u>E1,/1000</u>	<u>G2,/1000</u>	<u>E2,/1000</u>	<u>G3,/1000</u>	<u>E3,/1000</u>	<u>G4,/1000</u>	<u>E4,/1000</u>	<u>ED</u>
8.46	.0086	.0003	.0087	.0005	.0068	.0005	.0073	.0007	.8689
10.29	.0047	.0002	.0040	.0003	.0040	.0004	.0034	.0004	.8510
12.51	.0029	.0002	.0026	.0002	.0031	.0003	.0013	.0002	.8306
15.23	.0015	.0001	.0014	.0002	.0011	.0002	.0008	.0001	.8069
18.46	.0007	.0001	.0008	.0001	.0009	.0001	.0001	.0000	.7803
TOTAL G1	ERROR	TOTAL G2	ERROR	TOTAL G3	ERROR	TOTAL G4	ERROR		
.3442	.0099	.2970	.0124	.2429	.0129	.1894	.0116		

TABLE B 10 (a)
Thermal Control Paint, Unfiltered Spectrum
Corrected Background

<u>B,GAUSS</u>	<u>BKG1</u>	<u>BKG2</u>	<u>BKG3</u>	<u>BKG4</u>
3.5	14.	2.	5.	10.
4.0	12.	0.	4.	10.
4.5	11.	11.	9.	9.
5.0	13.	10.	9.	9.
5.3	15.	9.	9.	4.
6.2	10.	12.	10.	6.
7.2	16.	11.	8.	1.
8.4	16.	13.	11.	12.
9.3	19.	14.	6.	3.
10.3	21.	12.	11.	11.
11.4	21.	11.	11.	10.
12.6	21.	13.	11.	9.
14.0	25.	13.	10.	9.
15.5	31.	13.	10.	11.
17.2	37.	16.	14.	15.
18.1	36.	17.	17.	17.
19.0	47.	18.	18.	16.
20.0	59.	19.	18.	16.
21.0	60.	24.	15.	16.
22.1	75.	23.	20.	23.
23.2	80.	28.	24.	24.
24.3	85.	34.	28.	26.
25.5	81.	30.	32.	22.
26.8	76.	29.	33.	17.
28.1	59.	22.	30.	29.
29.6	50.	22.	18.	20.
31.0	28.	12.	20.	15.
32.6	24.	12.	17.	11.
34.2	17.	13.	10.	10.
35.9	17.	9.	9.	10.
37.7	12.	7.	9.	10.
39.6	13.	9.	10.	8.
41.6	9.	6.	9.	5.
43.7	8.	6.	8.	6.
45.8	7.	5.	5.	8.
48.1	7.	6.	5.	4.
50.5	6.	6.	6.	0.
53.1	5.	6.	5.	5.
55.7	3.	0.	0.	3.
58.5	3.	3.	4.	0.
61.4	4.	3.	3.	0.
64.5	0.	0.	0.	0.

TABLE 3.10 (a)
Thermal Conductivity, k , of Various Solids
in Various Units

k , Btu/hr-ft-F	k , W/m-K	k , cal/cm-sec-°C	k , Btu/hr-in-F	k , W/m-K
0.0	0.0	0.0	0.0	0.0
0.1	0.1	0.1	0.1	0.1
0.2	0.2	0.2	0.2	0.2
0.3	0.3	0.3	0.3	0.3
0.4	0.4	0.4	0.4	0.4
0.5	0.5	0.5	0.5	0.5
0.6	0.6	0.6	0.6	0.6
0.7	0.7	0.7	0.7	0.7
0.8	0.8	0.8	0.8	0.8
0.9	0.9	0.9	0.9	0.9
1.0	1.0	1.0	1.0	1.0
1.1	1.1	1.1	1.1	1.1
1.2	1.2	1.2	1.2	1.2
1.3	1.3	1.3	1.3	1.3
1.4	1.4	1.4	1.4	1.4
1.5	1.5	1.5	1.5	1.5
1.6	1.6	1.6	1.6	1.6
1.7	1.7	1.7	1.7	1.7
1.8	1.8	1.8	1.8	1.8
1.9	1.9	1.9	1.9	1.9
2.0	2.0	2.0	2.0	2.0
2.1	2.1	2.1	2.1	2.1
2.2	2.2	2.2	2.2	2.2
2.3	2.3	2.3	2.3	2.3
2.4	2.4	2.4	2.4	2.4
2.5	2.5	2.5	2.5	2.5
2.6	2.6	2.6	2.6	2.6
2.7	2.7	2.7	2.7	2.7
2.8	2.8	2.8	2.8	2.8
2.9	2.9	2.9	2.9	2.9
3.0	3.0	3.0	3.0	3.0
3.1	3.1	3.1	3.1	3.1
3.2	3.2	3.2	3.2	3.2
3.3	3.3	3.3	3.3	3.3
3.4	3.4	3.4	3.4	3.4
3.5	3.5	3.5	3.5	3.5
3.6	3.6	3.6	3.6	3.6
3.7	3.7	3.7	3.7	3.7
3.8	3.8	3.8	3.8	3.8
3.9	3.9	3.9	3.9	3.9
4.0	4.0	4.0	4.0	4.0
4.1	4.1	4.1	4.1	4.1
4.2	4.2	4.2	4.2	4.2
4.3	4.3	4.3	4.3	4.3
4.4	4.4	4.4	4.4	4.4
4.5	4.5	4.5	4.5	4.5
4.6	4.6	4.6	4.6	4.6
4.7	4.7	4.7	4.7	4.7
4.8	4.8	4.8	4.8	4.8
4.9	4.9	4.9	4.9	4.9
5.0	5.0	5.0	5.0	5.0

TABLE B 10(b)
Thermal Control Pain, Unfiltered Spectrum
Electron Counts with Error, X-Ray Counts

<u>B, GAUSS</u>	<u>N1, COUNTS</u>	<u>ERROR</u>	<u>N2, COUNTS</u>	<u>ERROR</u>	<u>N3, COUNTS</u>	<u>ERROR</u>	<u>N4, COUNTS</u>	<u>ERROR</u>	<u>NX, X1000</u>
3.5	16.	5.	1.	2.	1.	2.	13.	5.	19480.
4.0	17.	5.	1.	1.	1.	2.	8.	4.	19717.
4.5	30.	6.	1.	3.	7.	4.	17.	5.	19735.
5.0	19.	6.	1.	3.	12.	5.	17.	5.	19701.
5.3	15.	5.	1.	3.	12.	5.	1.	2.	19647.
6.2	46.	7.	5.	4.	17.	5.	1.	3.	20756.
7.2	37.	7.	9.	4.	14.	5.	1.	1.	19794.
8.4	51.	8.	14.	5.	17.	5.	4.	4.	19738.
9.3	86.	10.	15.	5.	1.	3.	1.	2.	19509.
10.3	113.	12.	38.	7.	33.	7.	1.	3.	19729.
11.4	128.	12.	20.	6.	22.	6.	1.	3.	19090.
12.6	223	16.	76.	9.	37.	7.	26.	6.	19570.
14.0	180.	14.	93.	10.	47.	8.	26.	6.	19939.
15.5	323.	19.	115.	11.	65.	9.	25.	6.	19621.
17.2	526.	24.	126.	13.	81.	10.	8.	5.	20887.
18.1	626.	26.	181.	14.	73.	9.	13.	5.	20860.
19.0	32.	9.	189.	14.	95.	11.	44.	8.	20769.
20.0	594.	26.	251.	16.	94.	11.	20.	6.	20709.
21.0	702.	28.	278.	17.	136.	12.	34.	7.	20669.
22.1	802.	30.	288.	18.	157.	13.	43.	8.	20893.
23.2	1036.	33.	354.	20.	209.	15.	57.	9.	21978.
24.3	1096.	34.	359.	20.	198.	15.	114.	12.	22150.
25.5.	801.	30.	301.	18.	141.	13.	48.	8.	20839.
26.8	680.	27.	289.	18.	141.	13.	56.	9.	20882.
28.1	644.	27.	261.	17.	123.	12.	12.	6.	20852.
29.6	348.	20.	168.	14.	108.	11.	18.	6.	20174.
31.0	300.	18.	130.	12.	61.	9.	28.	7.	19998.
32.6	256.	17.	116.	11.	62.	9.	21.	6.	20854.
34.2	205.	15.	37.	7.	44.	7.	16.	5.	20353.

TABLE B 10(b) continued

B, GAUSS	N1, COUNTS	ERROR	N2, COUNTS	ERROR	N3, COUNTS	ERROR	N4, COUNTS	ERROR	NX, X10000
35.9	151.	13.	41.	7.	31.	6.	20.	5.	20353.
37.7	144.	12.	53.	8.	25.	6.	11.	5.	19849.
39.6	94.	10.	37.	7.	13.	5.	1.	3.	19867.
41.6	73.	9.	32.	6.	6.	4.	1.	2.	20078.
43.7	90.	10.	34.	6.	8.	4.	1.	3.	20699.
45.8	46.	7.	27.	6.	11.	4.	1.	3.	20081.
48.1	23.	5.	3.	3.	1.	2.	1.	2.	20230.
50.5	22.	5.	17.	5.	2.	3.	1.	1.	19584.
53.1	12.	4.	2.	3.	3.	3.	4.	3.	20062.
55.7	12.	4.	1.	1.	1.	1.	6.	3.	20140.
58.5	2.	2.	1.	2.	5.	3.	1.	1.	20509.
61.4	2.	2.	2.	2.	2.	2.	1.	1.	20554.
64.5	1.	1.	1.	1.	1.	1.	1.	1.	20602.

TABLE B 10(c)
Thermal Control Paint, Unfiltered Spectrum
Differential Yield, Detector Efficiency, Energy Integrated Yield

E, KEV	G1,/1000	E1,/1000	G2,/1000	E2,/1000	G3,/1000	E3,/1000	G4,/1000	E4,/1000	ED
.11	.0211	.0038	.0033	.0019	.0051	.0021	.1062	.0221	.9460
.14	.0166	.0031	.0025	.0025	.0038	.0017	.0486	.0114	.9626
.18	.0229	.0036	.0019	.0006	.0208	.0052	.0806	.0158	.9726
.22	.0117	.0021	.0016	.0005	.0288	.0063	.0650	.0128	.9785
.25	.0082	.0015	.0014	.0004	.0256	.0056	.0034	.0015	.9808
.34	.0174	.0023	.0048	.0012	.0250	.0048	.0023	.0009	.9838
.46	.0109	.0015	.0067	.0015	.0160	.0034	.0018	.0013	.9834
.62	.0111	.0014	.0077	.0015	.0144	.0027	.0054	.0014	.9802
.76	.0155	.0015	.0068	.0013	.0007	.0003	.0011	.0006	.9769
.93	.0165	.0014	.0140	.0020	.0187	.0028	.0009	.0003	.9727
1.14	.0159	.0013	.0063	.0011	.0106	.0018	.0008	.0002	.9678
1.40	.0222	.0014	.0191	.0020	.0143	.0021	.0161	.0027	.9622
1.72	.0143	.0010	.0188	.0018	.0146	.0019	.0129	.0022	.9555
2.11	.0215	.0011	.0194	.0017	.0168	.0019	.0103	.0017	.9483
2.60	.0270	.0011	.0211	.0016	.0162	.0017	.0025	.0005	.9400
2.88	.0292	.0011	.0213	.0015	.0132	.0014	.0038	.0007	.9356
3.18	.0014	.0002	.0204	.0014	.0158	.0015	.0117	.0015	.9312
3.52	.0231	.0009	.0247	.0015	.0142	.0013	.0048	.0008	.9262
3.88	.0249	.0009	.0250	.0014	.0188	.0015	.0075	.0011	.9212
4.30	.0256	.0009	.0233	.0013	.0195	.0015	.0085	.0010	.9157
4.74	.0287	.0009	.0248	.0013	.0225	.0015	.0098	.0011	.9101
5.20	.0277	.0008	.0229	.0012	.0194	.0013	.0179	.0015	.9045
5.72	.0197	.0007	.0187	.0010	.0135	.0010	.0073	.0009	.8983
6.32	.0152	.0006	.0163	.0009	.0123	.0009	.0078	.0009	.8915
6.95	.0132	.0005	.0136	.0008	.0098	.0008	.0015	.0002	.8846
7.71	.0067	.0003	.0082	.0006	.0081	.0007	.0022	.0003	.8766
8.46	.0054	.0003	.0059	.0005	.0043	.0005	.0031	.0005	.8689
9.35	.0040	.0002	.0046	.0004	.0038	.0004	.0020	.0004	.8600
10.29	.0030	.0002	.0014	.0002	.0025	.0003	.0015	.0003	.8510
11.34	.0021	.0002	.0015	.0002	.0017	.0003	.0017	.0003	.8412

TABLE B 10(c) continued

E, KEV	G1,/1000	E1,/1000	G2,/1000	E2,/1000	G3,/1000	E3,/1000	G4,/1000	E4,/1000	ED
12.51	.0018	.0001	.0017	.0002	.0012	.0002	.0009	.0002	.8306
13.80	.0011	.0001	.0011	.0002	.0006	.0001	.0001	.0000	.8192
15.23	.0008	.0001	.0009	.0001	.0003	.0001	.0001	.0000	.8069
16.81	.0009	.0001	.0008	.0001	.0003	.0001	.0001	.0000	.7937
18.46	.0004	.0001	.0006	.0001	.0004	.0001	.0001	.0000	.7803
20.36	.0002	.0000	.0001	.0000	.0000	.0000	.0001	.0000	.7652
22.44	.0002	.0000	.0003	.0001	.0001	.0000	.0001	.0001	.7491
24.81	.0001	.0000	.0000	.0000	.0001	.0000	.0002	.0001	.7314
27.30	.0001	.0000	.0000	.0000	.0000	.0000	.0003	.0001	.7133
30.12	.0000	.0000	.0000	.0000	.0001	.0000	.0000	.0000	.6934
33.18	.0000	.0000	.0000	.0000	.0000	.0000	.0000	.0000	.6724
36.61	.0000	.0000	.0000	.0000	.0000	.0000	.0000	.0000	.6497

TOTAL G1	ERROR	TOTAL G2	ERROR	TOTAL G3	ERROR	TOTAL G4	ERROR
.1690	.0084	.1573	.0073	.1332	.0138	.0745	.0327

TABLE B 11(a)
Kevlar, Unfiltered Spectrum
Corrected Background

<u>B, GAUSS</u>	<u>BKG1</u>	<u>BKG2</u>	<u>BKG3</u>	<u>BKG4</u>
3.5	4.	1.	0.	11.
4.5	14.	10.	7.	6.
5.3	19.	11.	1.	12.
5.8	11.	12.	8.	3.
6.5	14.	12.	10.	8.
7.2	21.	14.	0.	14.
7.9	17.	15.	8.	6.
8.8	23.	7.	3.	0.
9.8	24.	16.	13.	9.
10.8	29.	15.	14.	11.
12.0	25.	15.	15.	13.
13.3	28.	19.	14.	10.
14.7	34.	14.	12.	13.
16.3	45.	18.	13.	16.
18.1	42.	20.	20.	20.
20.0	69.	22.	21.	19.
21.0	71.	29.	18.	19.
22.1	87.	27.	24.	27.
22.5	88.	26.	25.	27.
23.0	93.	27.	27.	28.
23.5	92.	33.	27.	28.
24.0	90.	39.	28.	27.
24.5	97.	38.	32.	30.
25.0	104.	37.	36.	33.
25.5	98.	37.	39.	27.
26.8	92.	35.	40.	21.
28.1	70.	26.	35.	35.
31.0	35.	16.	23.	19.
34.2	20.	16.	12.	12.
37.7	15.	9.	11.	4.
41.6	11.	7.	4.	0.
45.8	9.	7.	6.	0.
50.5	3.	7.	0.	6.
55.7	4.	0.	0.	0.

TABLE 1
 PHYSICAL PROPERTIES
 OF THE POLYMER

Sample	Weight	Volume	Density	Specific Gravity
1	1.0	1.0	1.0	1.0
2	1.0	1.0	1.0	1.0
3	1.0	1.0	1.0	1.0
4	1.0	1.0	1.0	1.0
5	1.0	1.0	1.0	1.0
6	1.0	1.0	1.0	1.0
7	1.0	1.0	1.0	1.0
8	1.0	1.0	1.0	1.0
9	1.0	1.0	1.0	1.0
10	1.0	1.0	1.0	1.0
11	1.0	1.0	1.0	1.0
12	1.0	1.0	1.0	1.0
13	1.0	1.0	1.0	1.0
14	1.0	1.0	1.0	1.0
15	1.0	1.0	1.0	1.0
16	1.0	1.0	1.0	1.0
17	1.0	1.0	1.0	1.0
18	1.0	1.0	1.0	1.0
19	1.0	1.0	1.0	1.0
20	1.0	1.0	1.0	1.0
21	1.0	1.0	1.0	1.0
22	1.0	1.0	1.0	1.0
23	1.0	1.0	1.0	1.0
24	1.0	1.0	1.0	1.0
25	1.0	1.0	1.0	1.0
26	1.0	1.0	1.0	1.0
27	1.0	1.0	1.0	1.0
28	1.0	1.0	1.0	1.0
29	1.0	1.0	1.0	1.0
30	1.0	1.0	1.0	1.0
31	1.0	1.0	1.0	1.0
32	1.0	1.0	1.0	1.0
33	1.0	1.0	1.0	1.0
34	1.0	1.0	1.0	1.0
35	1.0	1.0	1.0	1.0
36	1.0	1.0	1.0	1.0
37	1.0	1.0	1.0	1.0
38	1.0	1.0	1.0	1.0
39	1.0	1.0	1.0	1.0
40	1.0	1.0	1.0	1.0
41	1.0	1.0	1.0	1.0
42	1.0	1.0	1.0	1.0
43	1.0	1.0	1.0	1.0
44	1.0	1.0	1.0	1.0
45	1.0	1.0	1.0	1.0
46	1.0	1.0	1.0	1.0
47	1.0	1.0	1.0	1.0
48	1.0	1.0	1.0	1.0
49	1.0	1.0	1.0	1.0
50	1.0	1.0	1.0	1.0
51	1.0	1.0	1.0	1.0
52	1.0	1.0	1.0	1.0
53	1.0	1.0	1.0	1.0
54	1.0	1.0	1.0	1.0
55	1.0	1.0	1.0	1.0
56	1.0	1.0	1.0	1.0
57	1.0	1.0	1.0	1.0
58	1.0	1.0	1.0	1.0
59	1.0	1.0	1.0	1.0
60	1.0	1.0	1.0	1.0
61	1.0	1.0	1.0	1.0
62	1.0	1.0	1.0	1.0
63	1.0	1.0	1.0	1.0
64	1.0	1.0	1.0	1.0
65	1.0	1.0	1.0	1.0
66	1.0	1.0	1.0	1.0
67	1.0	1.0	1.0	1.0
68	1.0	1.0	1.0	1.0
69	1.0	1.0	1.0	1.0
70	1.0	1.0	1.0	1.0
71	1.0	1.0	1.0	1.0
72	1.0	1.0	1.0	1.0
73	1.0	1.0	1.0	1.0
74	1.0	1.0	1.0	1.0
75	1.0	1.0	1.0	1.0
76	1.0	1.0	1.0	1.0
77	1.0	1.0	1.0	1.0
78	1.0	1.0	1.0	1.0
79	1.0	1.0	1.0	1.0
80	1.0	1.0	1.0	1.0
81	1.0	1.0	1.0	1.0
82	1.0	1.0	1.0	1.0
83	1.0	1.0	1.0	1.0
84	1.0	1.0	1.0	1.0
85	1.0	1.0	1.0	1.0
86	1.0	1.0	1.0	1.0
87	1.0	1.0	1.0	1.0
88	1.0	1.0	1.0	1.0
89	1.0	1.0	1.0	1.0
90	1.0	1.0	1.0	1.0
91	1.0	1.0	1.0	1.0
92	1.0	1.0	1.0	1.0
93	1.0	1.0	1.0	1.0
94	1.0	1.0	1.0	1.0
95	1.0	1.0	1.0	1.0
96	1.0	1.0	1.0	1.0
97	1.0	1.0	1.0	1.0
98	1.0	1.0	1.0	1.0
99	1.0	1.0	1.0	1.0
100	1.0	1.0	1.0	1.0

TABLE B 11 (b)
Kevlar, Unfiltered Spectrum
Electron Counts with Error, X-Ray Counts

B, GAUSS	N1, COUNTS	ERROR	N2, COUNTS	ERROR	N3, COUNTS	ERROR	N4, COUNTS	ERROR	NX, X1000
3.5	1.	2.	1.	1.	1.	1.	1.	3.	25478.
4.5	25.	6.	1.	3.	3.	3.	1.	3.	25603.
5.3	22.	6.	1.	3.	3.	1.	4.	4.	25481.
5.8	46.	8.	17.	5.	5.	3.	1.	2.	25377.
6.5	45.	8.	1.	4.	4.	3.	1.	3.	25348.
7.2	57.	9.	14.	5.	5.	1.	3.	4.	25219.
7.9	62.	9.	7.	5.	5.	3.	1.	3.	25011.
8.8	58.	9.	1.	3.	3.	2.	1.	1.	24845.
9.8	97.	11.	24.	6.	3.	4.	1.	3.	24647.
10.8	137.	13.	48.	8.	9.	5.	1.	3.	25105.
12.0	257.	17.	81.	10.	18.	6.	25.	6.	25064.
13.3	237.	16.	66.	9.	13.	5.	16.	5.	25050.
14.7	302.	18.	102.	11.	48.	8.	25.	6.	25051.
16.3	365.	20.	119.	12.	40.	7.	16.	6.	24783.
18.1	499.	23.	113.	12.	63.	9.	1.	5.	24539.
20.0	515.	24.	162.	14.	70.	10.	29.	7.	24571.
21.0	585.	26.	179.	14.	95.	11.	41.	8.	24457.
22.1	620.	27.	200.	15.	85.	10.	57.	9.	24336.
22.5	595.	26.	203.	15.	90.	11.	39.	8.	24369.
23.0	626.	27.	206.	15.	84.	11.	50.	9.	24380.
23.5	606.	26.	200.	15.	110.	12.	39.	8.	25288.
24.0	620.	27.	174.	15.	71.	10.	34.	8.	25200.
24.5	590.	26.	176.	15.	81.	11.	67.	10.	25131.
25.0	513.	25.	179.	15.	69.	10.	45.	9.	25226.
25.5	502.	24.	152.	14.	73.	11.	64.	10.	25345.
26.8	422.	23.	172.	14.	50.	9.	63.	9.	25214.
28.1	255.	18.	155.	13.	39.	9.	18.	7.	24782.
31.0	102.	12.	68.	9.	1.	5.	25.	7.	24925.

TABLE B 11(b) continued

<u>B, GAUSS</u>	<u>N1, COUNTS</u>	<u>ERROR</u>	<u>N2, COUNTS</u>	<u>ERROR</u>	<u>N3, COUNTS</u>	<u>ERROR</u>	<u>N4, COUNTS</u>	<u>ERROR</u>	<u>NX, X1000</u>
34.2	68.	9.	16.	6.	18.	5.	11.	5.	24839.
37.7	45.	8.	11.	4.	3.	4.	1.	2.	24894.
41.6	28.	6.	18.	5.	1.	2.	1.	1.	25515.
45.8	5.	4.	2.	3.	1.	3.	1.	1.	25338.
50.5	1.	2.	2.	3.	1.	1.	1.	3.	25425.
55.7	8.	3.	1.	1.	1.	1.	1.	1.	25515.

TABLE B 11(c)
Kevlar, Unfiltered Spectrum
Differential Yield, Detector Efficiency, Energy Integrated Yield

E, KEV	G1,/1000	E1,/1000	G2,/1000	E2,/1000	G3,/1000	E3,/1000	G4,/1000	E4,/1000	ED
.11	.0010	.0004	.0025	.0018	.0039	.0039	.0062	.0018	.9460
.18	.0147	.0024	.0015	.0004	.0023	.0008	.0037	.0014	.9726
.25	.0093	.0015	.0011	.0003	.0016	.0012	.0105	.0026	.9808
.30	.0163	.0022	.0152	.0028	.0014	.0005	.0022	.0011	.9830
.37	.0127	.0017	.0007	.0002	.0022	.0006	.0017	.0006	.9840
.46	.0132	.0015	.0082	.0015	.0009	.0009	.0043	.0010	.9834
.55	.0120	.0014	.0034	.0007	.0008	.0003	.0012	.0005	.9818
.68	.0092	.0010	.0004	.0001	.0006	.0003	.0010	.0010	.9788
.85	.0125	.0011	.0078	.0012	.0015	.0004	.0008	.0003	.9749
1.03	.0143	.0011	.0127	.0016	.0037	.0008	.0006	.0002	.9705
1.27	.0219	.0013	.0175	.0018	.0060	.0010	.0132	.0021	.9650
1.56	.0166	.0010	.0117	.0013	.0035	.0007	.0070	.0014	.9589
1.90	.0174	.0010	.0149	.0014	.0108	.0014	.0090	.0015	.9522
2.34	.0175	.0009	.0144	.0012	.0074	.0010	.0048	.0008	.9444
2.88	.0198	.0008	.0113	.0010	.0097	.0011	.0002	.0001	.9356
3.52	.0169	.0007	.0134	.0010	.0089	.0009	.0059	.0009	.9262
3.88	.0176	.0007	.0136	.0009	.0111	.0010	.0076	.0010	.9212
4.30	.0170	.0006	.0139	.0009	.0091	.0009	.0097	.0011	.9157
4.46	.0157	.0006	.0136	.0009	.0093	.0009	.0064	.0008	.9137
4.66	.0153	.0006	.0127	.0008	.0080	.0008	.0076	.0009	.9112
4.86	.0143	.0005	.0119	.0008	.0101	.0009	.0057	.0007	.9086
5.07	.0141	.0005	.0100	.0007	.0063	.0006	.0048	.0006	.9061
5.28	.0129	.0005	.0098	.0007	.0069	.0006	.0091	.0009	.9035
5.50	.0108	.0004	.0095	.0006	.0056	.0006	.0059	.0007	.9009
5.72	.0101	.0004	.0078	.0006	.0057	.0005	.0080	.0008	.8983
6.32	.0078	.0003	.0081	.0006	.0036	.0004	.0072	.0008	.8915
6.95	.0044	.0002	.0068	.0005	.0026	.0003	.0019	.0003	.8846
8.46	.0015	.0001	.0025	.0003	.0001	.0000	.0022	.0003	.8689

TABLE B 11(c) continued

<u>E, KEV</u>	<u>G1,/1000</u>	<u>E1,/1000</u>	<u>G2,/1000</u>	<u>E2,/1000</u>	<u>G3,/1000</u>	<u>E3,/1000</u>	<u>G4,/1000</u>	<u>E4,/1000</u>	<u>ED</u>
10.29	.0008	.0001	.0005	.0001	.0008	.0002	.0008	.0002	.8510
12.51	.0005	.0001	.0003	.0001	.0001	.0000	.0001	.0000	.8306
15.23	.0002	.0000	.0004	.0001	.0000	.0000	.0001	.0001	.8069
18.46	.0000	.0000	.0000	.0000	.0000	.0000	.0000	.0000	.7803
22.44	.0000	.0000	.0000	.0000	.0000	.0000	.0000	.0000	.7491
27.30	.0000	.0000	.0000	.0000	.0000	.0000	.0000	.0000	.7133

<u>TOTAL G1</u>	<u>ERROR</u>	<u>TOTAL G2</u>	<u>ERROR</u>	<u>TOTAL G3</u>	<u>ERROR</u>	<u>TOTAL G4</u>	<u>ERROR</u>
.1078	.0056	.0868	.0059	.0488	.0056	.0467	.0058

TABLE B 12(a)
Mylar, Unfiltered Spectrum
Corrected Background

<u>B, GAUSS</u>	<u>BKG1</u>	<u>BKG2</u>	<u>BKG3</u>	<u>BKG4</u>
3.5	28.	27.	24.	21.
4.0	25.	25.	21.	20.
4.5	21.	22.	18.	18.
5.0	25.	25.	18.	19.
5.3	30.	27.	17.	19.
6.2	20.	24.	18.	24.
7.2	31.	22.	16.	20.
7.9	26.	23.	16.	23.
8.8	36.	29.	26.	24.
9.8	37.	24.	20.	20.
10.8	44.	23.	21.	23.
12.0	39.	22.	22.	20.
13.3	42.	30.	21.	16.
14.7	55.	23.	19.	20.
16.3	71.	29.	20.	25.
18.1	64.	31.	31.	30.
19.0	87.	33.	33.	30.
20.0	109.	35.	34.	29.
21.0	114.	46.	28.	31.
22.1	140.	43.	38.	43.
23.2	141.	51.	42.	43.
24.3	158.	62.	52.	48.
25.5	147.	55.	58.	40.
26.8	135.	52.	59.	30.
28.1	105.	39.	53.	52.
29.6	95.	41.	34.	38.
31.0	54.	24.	38.	30.
32.6	45.	22.	32.	20.
34.2	32.	24.	19.	19.
35.9	34.	18.	18.	19.
37.7	24.	15.	18.	21.
39.6	26.	18.	20.	17.
41.6	17.	12.	19.	22.
43.7	16.	11.	15.	20.
45.8	15.	11.	11.	18.
48.1	14.	11.	12.	16.
50.5	13.	12.	13.	15.
53.1	10.	13.	11.	10.
55.7	6.	14.	9.	6.
58.5	7.	10.	8.	9.
61.4	8.	6.	8.	12.
64.5	5.	8.	8.	3.
67.7	3.	9.	9.	9.
71.1	2.	8.	7.	12.
74.7	1.	7.	6.	15.

TABLE 1
 PHYSICAL PROPERTIES OF
 POLYMER 1

TEMPERATURE, °C.	DENSITY, g./cc.	REFRACTIVE INDEX, n_D^{20}	WATER ABSORPTION, %	INHERENT VISCOSITY, dl./g.
-78	1.18	1.47	0	0
-70	1.18	1.47	0	0
-60	1.18	1.47	0	0
-50	1.18	1.47	0	0
-40	1.18	1.47	0	0
-30	1.18	1.47	0	0
-20	1.18	1.47	0	0
-10	1.18	1.47	0	0
0	1.18	1.47	0	0
10	1.18	1.47	0	0
20	1.18	1.47	0	0
30	1.18	1.47	0	0
40	1.18	1.47	0	0
50	1.18	1.47	0	0
60	1.18	1.47	0	0
70	1.18	1.47	0	0
80	1.18	1.47	0	0
90	1.18	1.47	0	0
100	1.18	1.47	0	0
110	1.18	1.47	0	0
120	1.18	1.47	0	0
130	1.18	1.47	0	0
140	1.18	1.47	0	0
150	1.18	1.47	0	0
160	1.18	1.47	0	0
170	1.18	1.47	0	0
180	1.18	1.47	0	0
190	1.18	1.47	0	0
200	1.18	1.47	0	0
210	1.18	1.47	0	0
220	1.18	1.47	0	0
230	1.18	1.47	0	0
240	1.18	1.47	0	0
250	1.18	1.47	0	0
260	1.18	1.47	0	0
270	1.18	1.47	0	0
280	1.18	1.47	0	0
290	1.18	1.47	0	0
300	1.18	1.47	0	0
310	1.18	1.47	0	0
320	1.18	1.47	0	0
330	1.18	1.47	0	0
340	1.18	1.47	0	0
350	1.18	1.47	0	0
360	1.18	1.47	0	0
370	1.18	1.47	0	0
380	1.18	1.47	0	0
390	1.18	1.47	0	0
400	1.18	1.47	0	0
410	1.18	1.47	0	0
420	1.18	1.47	0	0
430	1.18	1.47	0	0
440	1.18	1.47	0	0
450	1.18	1.47	0	0
460	1.18	1.47	0	0
470	1.18	1.47	0	0
480	1.18	1.47	0	0
490	1.18	1.47	0	0
500	1.18	1.47	0	0
510	1.18	1.47	0	0
520	1.18	1.47	0	0
530	1.18	1.47	0	0
540	1.18	1.47	0	0
550	1.18	1.47	0	0
560	1.18	1.47	0	0
570	1.18	1.47	0	0
580	1.18	1.47	0	0
590	1.18	1.47	0	0
600	1.18	1.47	0	0
610	1.18	1.47	0	0
620	1.18	1.47	0	0
630	1.18	1.47	0	0
640	1.18	1.47	0	0
650	1.18	1.47	0	0
660	1.18	1.47	0	0
670	1.18	1.47	0	0
680	1.18	1.47	0	0
690	1.18	1.47	0	0
700	1.18	1.47	0	0
710	1.18	1.47	0	0
720	1.18	1.47	0	0
730	1.18	1.47	0	0
740	1.18	1.47	0	0
750	1.18	1.47	0	0
760	1.18	1.47	0	0
770	1.18	1.47	0	0
780	1.18	1.47	0	0
790	1.18	1.47	0	0
800	1.18	1.47	0	0
810	1.18	1.47	0	0
820	1.18	1.47	0	0
830	1.18	1.47	0	0
840	1.18	1.47	0	0
850	1.18	1.47	0	0
860	1.18	1.47	0	0
870	1.18	1.47	0	0
880	1.18	1.47	0	0
890	1.18	1.47	0	0
900	1.18	1.47	0	0
910	1.18	1.47	0	0
920	1.18	1.47	0	0
930	1.18	1.47	0	0
940	1.18	1.47	0	0
950	1.18	1.47	0	0
960	1.18	1.47	0	0
970	1.18	1.47	0	0
980	1.18	1.47	0	0
990	1.18	1.47	0	0
1000	1.18	1.47	0	0

TABLE B 12(b)
Mylar, Unfiltered Spectrum
Electron Counts with Error, X-Ray Counts

B, GAUSS	N1, COUNTS	ERROR	N2, COUNTS	ERROR	N3, COUNTS	ERROR	N4, COUNTS	ERROR	NX, X10000
3.5	94.	11.	36.	8.	37.	8.	23.	7.	39906.
4.0	77.	10.	30.	7.	51.	8.	45.	8.	39921.
4.5	49.	8.	54.	9.	48.	8.	30.	7.	39565.
5.0	88.	11.	38.	8.	38.	7.	45.	8.	39674.
5.3	70.	10.	28.	7.	33.	7.	38.	8.	39707.
6.2	74.	10.	28.	7.	48.	8.	19.	7.	39616.
7.2	57.	9.	44.	8.	43.	8.	31.	7.	38161.
7.9	97.	11.	41.	8.	49.	8.	34.	8.	38045.
8.8	84.	11.	53.	9.	47.	9.	23.	7.	38035.
9.8	132.	13.	32.	7.	56.	9.	39.	8.	38092.
10.8	117.	13.	65.	9.	61.	9.	40.	8.	38221.
12.0	236.	17.	98.	11.	91.	11.	39.	8.	38375.
13.3	238.	17.	79.	10.	78.	10.	52.	8.	38634.
14.7	358.	20.	119.	12.	116.	12.	58.	9.	40000.
16.3	379.	21.	132.	13.	123.	12.	58.	9.	38753.
18.1	476.	23.	126.	13.	122.	12.	81.	11.	37639.
19.0	507.	24.	182.	15.	147.	13.	58.	9.	38348.
20.0	588.	26.	204.	15.	212.	16.	59.	9.	38658.
21.0	725.	29.	213.	16.	186.	15.	80.	11.	39097.
22.1	810.	31.	278.	18.	216.	16.	79.	11.	39326.
23.2	804.	31.	279.	18.	235.	17.	55.	10.	39038.
24.3	911.	33.	304.	19.	248.	17.	90.	12.	40938.
25.5	780.	30.	256.	18.	183.	16.	133.	13.	38008.
26.8	676.	28.	257.	18.	218.	17.	104.	12.	37076.
28.1	566.	26.	259.	17.	210.	16.	111.	13.	37076.
29.6	370.	22.	142.	14.	189.	15.	100.	12.	37918.
31.0	225.	17.	151.	13.	118.	12.	97.	11.	38710.
32.6	196.	16.	86.	10.	59.	10.	79.	10.	39008.

TABLE B 12(b) continued

<u>B, GAUSS</u>	<u>N1, COUNTS</u>	<u>ERROR</u>	<u>N2, COUNTS</u>	<u>ERROR</u>	<u>N3, COUNTS</u>	<u>ERROR</u>	<u>N4, COUNTS</u>	<u>ERROR</u>	<u>NX, X10000</u>
34.2	166.	14.	70.	10.	77.	10.	35.	7.	38779.
35.9	116.	12.	66.	9.	47.	8.	68.	9.	39523.
37.7	130.	12.	64.	9.	46.	8.	39.	8.	40452.
39.6	89.	11.	57.	9.	34.	7.	33.	7.	40449.
41.6	76.	10.	26.	6.	25.	7.	18.	6.	40544.
43.7	67.	9.	29.	6.	46.	8.	45.	8.	40570.
45.8	26.	6.	15.	5.	34.	7.	19.	6.	40496.
48.1	24.	6.	17.	5.	24.	6.	15.	6.	40328.
50.5	19.	6.	29.	6.	7.	4.	24.	6.	40537.
53.1	20.	5.	5.	4.	10.	5.	25.	6.	40435.
55.7	12.	4.	13.	5.	19.	5.	44.	7.	41235.
58.5	11.	4.	9.	4.	25.	6.	15.	5.	41258.
61.4	7.	4.	10.	4.	17.	5.	14.	5.	41193.
64.5	15.	4.	9.	4.	16.	5.	1.	2.	41056.
67.7	18.	5.	14.	5.	22.	6.	33.	6.	40775.
71.1	19.	5.	21.	5.	24.	6.	32.	7.	40770.
74.7	21.	5.	36.	7.	38.	7.	74.	9.	40581.

TABLE B 12(c)
Mylar, Unfiltered Spectrum
Differential Yield, Detector Efficiency, Energy Integrated Yield

E, KEV	G1,/1000	E1,/1000	G2,/1000	E2,/1000	G3,/1000	E3,/1000	G4,/1000	E4,/1000	ED
.11	.0604	.0055	.0585	.0074	.0924	.0118	.0917	.0138	.9460
.14	.0372	.0037	.0367	.0049	.0958	.0113	.1349	.0167	.9626
.18	.0187	.0022	.0521	.0060	.0712	.0088	.0710	.0102	.9726
.22	.0269	.0025	.0294	.0037	.0452	.0060	.0855	.0107	.9785
.25	.0190	.0019	.0192	.0026	.0239	.0049	.0640	.0085	.9808
.34	.0147	.0015	.0141	.0019	.0370	.0046	.0234	.0036	.9838
.46	.0087	.0009	.0170	.0021	.0255	.0033	.0294	.0041	.9834
.55	.0124	.0011	.0132	.0017	.0243	.0030	.0269	.0036	.9818
.68	.0087	.0008	.0138	.0015	.0188	.0022	.0147	.0021	.9788
.85	.0110	.0008	.0068	.0009	.0182	.0021	.0202	.0026	.9749
1.03	.0080	.0006	.0113	.0012	.0163	.0018	.0171	.0021	.9705
1.27	.0132	.0008	.0138	.0013	.0197	.0019	.0135	.0018	.9650
1.56	.0108	.0006	.0091	.0009	.0138	.0014	.0146	.0018	.9589
1.90	.0129	.0006	.0109	.0009	.0163	.0014	.0130	.0015	.9522
2.34	.0116	.0005	.0102	.0008	.0146	.0012	.0110	.0012	.9444
2.88	.0123	.0005	.0082	.0007	.0123	.0010	.0130	.0012	.9356
3.18	.0117	.0005	.0106	.0007	.0132	.0010	.0083	.0009	.9312
3.52	.0122	.0005	.0107	.0007	.0172	.0011	.0076	.0008	.9262
3.88	.0136	.0005	.0101	.0006	.0136	.0009	.0093	.0009	.9212
4.30	.0137	.0004	.0119	.0007	.0142	.0009	.0083	.0008	.9157
4.74	.0125	.0004	.0110	.0006	.0143	.0009	.0053	.0005	.9101
5.20	.0124	.0004	.0105	.0005	.0132	.0008	.0076	.0006	.9045
5.72	.0105	.0003	.0087	.0005	.0096	.0006	.0111	.0008	.8983
6.32	.0085	.0003	.0082	.0005	.0107	.0006	.0081	.0007	.8915
6.95	.0065	.0003	.0076	.0004	.0094	.0006	.0080	.0006	.8846
7.71	.0038	.0002	.0037	.0003	.0076	.0005	.0064	.0005	.8766
8.46	.0021	.0001	.0035	.0003	.0043	.0003	.0056	.0005	.8689
9.35	.0016	.0001	.0018	.0002	.0019	.0002	.0041	.0004	.8600

TABLE B 12 (c) continued

E, KEV	G1,/1000	E1,/1000	G2,/1000	E2,/1000	G3,/1000	E3,/1000	G4,/1000	E4,/1000	ED
10.29	.0013	.0001	.0014	.0001	.0023	.0002	.0017	.0002	.8510
11.34	.0008	.0001	.0012	.0001	.0013	.0002	.0030	.0003	.8412
12.51	.0008	.0001	.0010	.0001	.0011	.0001	.0015	.0002	.8306
13.80	.0005	.0000	.0008	.0001	.0008	.0001	.0012	.0002	.8192
15.23	.0004	.0000	.0004	.0001	.0005	.0001	.0006	.0001	.8069
16.81	.0003	.0000	.0004	.0001	.0009	.0001	.0014	.0002	.7937
18.46	.0001	.0000	.0002	.0000	.0006	.0001	.0005	.0001	.7803
20.36	.0001	.0000	.0002	.0000	.0004	.0001	.0004	.0001	.7652
22.44	.0001	.0000	.0003	.0000	.0001	.0000	.0006	.0001	.7491
24.81	.0001	.0000	.0000	.0000	.0001	.0000	.0006	.0001	.7314
27.30	.0000	.0000	.0001	.0000	.0002	.0000	.0009	.0001	.7133
30.12	.0000	.0000	.0001	.0000	.0003	.0001	.0003	.0001	.6934
33.18	.0000	.0000	.0001	.0000	.0002	.0000	.0003	.0000	.6724
36.63	.0000	.0000	.0001	.0000	.0002	.0000	.0000	.0000	.6497
40.33	.0000	.0000	.0001	.0000	.0002	.0000	.0005	.0001	.6259
44.49	.0000	.0000	.0001	.0000	.0002	.0000	.0005	.0001	.6003
49.10	.0001	.0000	.0002	.0000	.0004	.0001	.0011	.0001	.5730
TOTAL G1		TOTAL G2	ERROR	TOTAL G3	ERROR	TOTAL G4	ERROR		
.0961		.0950	.0126	.1386	.0218	.1334	.0290		

TABLE B 13 (a)
Nonconducting Epoxy, Unfiltered Spectrum
Corrected Background

<u>B, GAUSS</u>	<u>BKG1</u>	<u>BKG2</u>	<u>BKG3</u>	<u>BKG4</u>
3.5	19.	0.	0.	5.
4.5	14.	15.	0.	12.
5.3	20.	18.	12.	13.
5.8	11.	13.	3.	0.
6.5	15.	15.	10.	3.
7.2	21.	15.	4.	0.
8.8	24.	19.	7.	12.
9.8	26.	17.	7.	14.
10.8	30.	15.	11.	7.
12.0	27.	15.	15.	13.
13.3	29.	20.	14.	10.
14.7	36.	15.	12.	13.
16.3	47.	19.	13.	16.
18.1	44.	21.	21.	21.
20.0	73.	23.	22.	19.
21.0	76.	31.	19.	21.
22.1	93.	29.	26.	29.
23.2	95.	34.	28.	29.
24.0	93.	40.	29.	28.
24.5	100.	39.	33.	31.
25.0	107.	38.	34.	34.
25.5	100.	37.	39.	27.
26.0	98.	37.	38.	27.
26.8	92.	36.	39.	21.
28.1	72.	27.	36.	36.
31.0	35.	16.	3.	20.
34.2	21.	14.	10.	13.
37.7	16.	10.	8.	5.
41.6	11.	8.	0.	0.
45.8	10.	7.	6.	0.
50.5	0.	0.	0.	5.

TABLE 2.13 (a)
 Hydrographic Survey, Baltimore Sound
 Tidal Current Data

Station	1951	1952	1953	1954
1.2	19	19	19	19
1.3	19	19	19	19
1.4	19	19	19	19
1.5	19	19	19	19
1.6	19	19	19	19
1.7	19	19	19	19
1.8	19	19	19	19
1.9	19	19	19	19
2.0	19	19	19	19
2.1	19	19	19	19
2.2	19	19	19	19
2.3	19	19	19	19
2.4	19	19	19	19
2.5	19	19	19	19
2.6	19	19	19	19
2.7	19	19	19	19
2.8	19	19	19	19
2.9	19	19	19	19
3.0	19	19	19	19
3.1	19	19	19	19
3.2	19	19	19	19
3.3	19	19	19	19
3.4	19	19	19	19
3.5	19	19	19	19
3.6	19	19	19	19
3.7	19	19	19	19
3.8	19	19	19	19
3.9	19	19	19	19
4.0	19	19	19	19
4.1	19	19	19	19
4.2	19	19	19	19
4.3	19	19	19	19
4.4	19	19	19	19
4.5	19	19	19	19
4.6	19	19	19	19
4.7	19	19	19	19
4.8	19	19	19	19
4.9	19	19	19	19
5.0	19	19	19	19

TABLE B 13(b)
Nonconducting Epoxy, Unfiltered Spectrum
Electron Counts with Error, X-Ray Counts

<u>B,GAUSS</u>	<u>N1,COUNTS</u>	<u>ERROR</u>	<u>N2,COUNTS</u>	<u>ERROR</u>	<u>N3,COUNTS</u>	<u>ERROR</u>	<u>N4,COUNTS</u>	<u>ERROR</u>	<u>NX,X10000</u>
3.5	3.	5.	1.	1.	1.	1.	1.	2.	26493.
4.5	40.	7.	12.	5.	1.	1.	4.	4.	26356.
5.3	15.	6.	1.	4.	2.	4.	10.	5.	26442.
5.8	61.	8.	12.	5.	1.	2.	1.	1.	26456.
6.5	35.	7.	1.	4.	4.	4.	1.	2.	26290.
7.2	28.	7.	5.	4.	1.	2.	1.	1.	26082.
8.8	21.	7.	11.	5.	1.	3.	1.	4.	25938.
9.8	64.	9.	35.	7.	1.	3.	7.	5.	26379.
10.8	84.	11.	22.	6.	1.	3.	1.	3.	26202.
12.0	208.	15.	53.	8.	7.	5.	27.	6.	26077.
13.3	164.	14.	31.	7.	18.	6.	22.	6.	26050.
14.7	249.	17.	93.	10.	32.	7.	23.	6.	26044.
16.3	245.	17.	80.	10.	50.	8.	26.	6.	25855.
18.1	330.	19.	79.	10.	29.	7.	20.	6.	25785.
20.0	340.	20.	135.	13.	44.	8.	44.	8.	25750.
21.0	369.	21.	118.	12.	63.	9.	29.	7.	26073.
22.1	366.	21.	131.	13.	45.	8.	8.	6.	26170.
23.2	412.	23.	135.	13.	55.	9.	40.	8.	26235.
24.0	402.	22.	90.	11.	39.	8.	28.	7.	26082.
24.5	309.	20.	104.	12.	29.	8.	24.	7.	25917.
25.0	340.	21.	99.	12.	1.	6.	31.	8.	25893.
25.5	324.	21.	85.	11.	2.	7.	40.	8.	25310.
26.0	305.	20.	72.	10.	12.	7.	31.	8.	25310.
26.8	210.	17.	100.	12.	1.	6.	83.	10.	25352.
28.1	103.	13.	96.	11.	7.	7.	9.	7.	25494.
31.0	68.	10.	24.	6.	1.	2.	7.	5.	25413.
34.2	48.	8.	1.	4.	1.	3.	2.	4.	26385.
37.7	26.	6.	13.	5.	1.	3.	1.	2.	26687.
41.6	11.	5.	13.	5.	1.	1.	1.	1.	26616.

TABLE B 13(b) continued

<u>B, GAUSS</u>	<u>N1, COUNTS</u>	<u>ERROR</u>	<u>N2, COUNTS</u>	<u>ERROR</u>	<u>N3, COUNTS</u>	<u>ERROR</u>	<u>N4, COUNTS</u>	<u>ERROR</u>	<u>NX, X10000</u>
45.8	7.	4.	2.	3.	1.	2.	1.	1.	26845.
50.5	1.	1.	1.	1.	1.	1.	1.	2.	26777.

TABLE B 13(E)
Nonconducting Epoxy, Unfiltered Spectrum
Differential Yield, Detector Efficiency, Energy Integrated Yield

E, KEV	G1,/1000	E1,/1000	G2,/1000	E2,/1000	G3,/1000	E3,/1000	G4,/1000	E4,/1000	ED
.11	.0029	.0006	.0024	.0024	.0038	.0038	.0060	.0025	.9460
.18	.0229	.0031	.0174	.0033	.0022	.0022	.0142	.0036	.9726
.25	.0061	.0010	.0010	.0002	.0032	.0008	.0253	.0053	.9808
.30	.0207	.0024	.0103	.0021	.0013	.0007	.0021	.0021	.9830
.37	.0095	.0013	.0007	.0002	.0042	.0011	.0017	.0008	.9840
.46	.0063	.0009	.0028	.0006	.0009	.0004	.0014	.0014	.9834
.68	.0032	.0005	.0042	.0008	.0006	.0002	.0009	.0003	.9788
.85	.0077	.0008	.0107	.0015	.0005	.0002	.0052	.0011	.9749
1.03	.0084	.0008	.0056	.0009	.0004	.0001	.0006	.0002	.9705
1.27	.0171	.0011	.0110	.0013	.0022	.0005	.0138	.0022	.9650
1.56	.0110	.0008	.0053	.0007	.0047	.0008	.0092	.0016	.9589
1.90	.0138	.0008	.0131	.0013	.0069	.0010	.0079	.0013	.9522
2.34	.0112	.0007	.0093	.0009	.0099	.0011	.0074	.0011	.9444
2.88	.0124	.0006	.0075	.0008	.0043	.0006	.0047	.0007	.9356
3.52	.0106	.0005	.0107	.0008	.0053	.0007	.0085	.0011	.9262
3.88	.0104	.0005	.0084	.0007	.0069	.0008	.0051	.0007	.9212
4.30	.0093	.0004	.0084	.0007	.0045	.0005	.0013	.0002	.9157
4.74	.0096	.0004	.0079	.0006	.0050	.0005	.0058	.0007	.9101
5.07	.0088	.0004	.0050	.0004	.0033	.0004	.0038	.0005	.9061
5.28	.0066	.0003	.0056	.0005	.0024	.0003	.0032	.0004	.9035
5.50	.0070	.0003	.0051	.0004	.0001	.0000	.0039	.0005	.9009
5.72	.0064	.0003	.0043	.0004	.0002	.0000	.0049	.0006	.8983
5.95	.0059	.0003	.0036	.0003	.0009	.0001	.0038	.0005	.8957
6.32	.0039	.0002	.0047	.0004	.0001	.0000	.0095	.0009	.8915
6.95	.0017	.0001	.0041	.0004	.0005	.0001	.0009	.0001	.8846
10.29	.0005	.0001	.0000	.0000	.0000	.0000	.0001	.0000	.8510
12.51	.0002	.0000	.0003	.0001	.0000	.0000	.0001	.0000	.8306
15.23	.0001	.0000	.0003	.0001	.0000	.0000	.0001	.0001	.8069

TABLE B 13(c) continued

<u>E, KEV</u>	<u>G1,/1000</u>	<u>E1,/1000</u>	<u>G2,/1000</u>	<u>E2,/1000</u>	<u>G3,/1000</u>	<u>E3,/1000</u>	<u>G4,/1000</u>	<u>E4,/1000</u>	<u>ED</u>
18.46	.0000	.0000	.0000	.0000	.0000	.0000	.0000	.0000	.7803
22.44	.0000	.0000	.0000	.0000	.0000	.0000	.0000	.0000	.7491
TOTAL G1	ERROR	TOTAL G2	ERROR	TOTAL G3	ERROR	TOTAL G4	ERROR		
.0682	.0051	.0559	.0058	.0249	.0052	.0418	.0084		

DEPARTMENT OF THE ARMY

DATE	0001, 01	0001, 02	0001, 03	0001, 04	0001, 05	0001, 06	0001, 07	0001, 08	0001, 09	0001, 10	0001, 11	0001, 12	TOTAL
1951	0000	0000	0000	0000	0000	0000	0000	0000	0000	0000	0000	0000	00.00
1952	0000	0000	0000	0000	0000	0000	0000	0000	0000	0000	0000	0000	00.00

NAME	01	02	03	04	05	06	07	08	09	10	11	12	TOTAL
JOHN J. JAMES	0000	0000	0000	0000	0000	0000	0000	0000	0000	0000	0000	0000	00.00
JOHN J. JAMES	0000	0000	0000	0000	0000	0000	0000	0000	0000	0000	0000	0000	00.00

TABLE B 14(a)
Conducting Epoxy, Unfiltered Spectrum
Corrected Background

<u>B, GAUSS</u>	<u>BKG1</u>	<u>BKG2</u>	<u>BKG3</u>	<u>BKG4</u>
3.5	21.	20.	11.	16.
4.5	15.	16.	13.	13.
5.3	22.	12.	13.	14.
5.8	12.	14.	3.	19.
6.5	17.	10.	11.	16.
7.2	24.	17.	8.	16.
7.9	19.	17.	10.	17.
8.8	27.	9.	9.	18.
9.8	28.	18.	15.	15.
10.8	33.	17.	16.	17.
12.0	29.	17.	17.	15.
13.3	31.	22.	16.	11.
14.7	39.	16.	13.	14.
16.3	52.	21.	15.	18.
18.1	49.	24.	24.	23.
19.0	64.	25.	24.	22.
20.0	80.	26.	24.	21.
21.0	82.	33.	20.	22.
22.1	100.	30.	27.	30.
23.2	101.	36.	30.	30.
24.3	107.	42.	35.	33.
25.5	107.	40.	42.	29.
26.8	99.	39.	44.	22.
28.1	78.	29.	39.	39.
31.0	38.	17.	27.	21.
34.2	22.	17.	13.	13.
37.7	16.	10.	11.	14.

1940 1940 1940

1940	1940	1940	1940
1.4	1.4	1.4	1.4
2.4	2.4	2.4	2.4
3.4	3.4	3.4	3.4
4.4	4.4	4.4	4.4
5.4	5.4	5.4	5.4
6.4	6.4	6.4	6.4
7.4	7.4	7.4	7.4
8.4	8.4	8.4	8.4
9.4	9.4	9.4	9.4
10.4	10.4	10.4	10.4
11.4	11.4	11.4	11.4
12.4	12.4	12.4	12.4
13.4	13.4	13.4	13.4
14.4	14.4	14.4	14.4
15.4	15.4	15.4	15.4
16.4	16.4	16.4	16.4
17.4	17.4	17.4	17.4
18.4	18.4	18.4	18.4
19.4	19.4	19.4	19.4
20.4	20.4	20.4	20.4
21.4	21.4	21.4	21.4
22.4	22.4	22.4	22.4
23.4	23.4	23.4	23.4
24.4	24.4	24.4	24.4
25.4	25.4	25.4	25.4
26.4	26.4	26.4	26.4
27.4	27.4	27.4	27.4
28.4	28.4	28.4	28.4
29.4	29.4	29.4	29.4
30.4	30.4	30.4	30.4
31.4	31.4	31.4	31.4
32.4	32.4	32.4	32.4
33.4	33.4	33.4	33.4
34.4	34.4	34.4	34.4
35.4	35.4	35.4	35.4
36.4	36.4	36.4	36.4
37.4	37.4	37.4	37.4
38.4	38.4	38.4	38.4
39.4	39.4	39.4	39.4
40.4	40.4	40.4	40.4
41.4	41.4	41.4	41.4
42.4	42.4	42.4	42.4
43.4	43.4	43.4	43.4
44.4	44.4	44.4	44.4
45.4	45.4	45.4	45.4
46.4	46.4	46.4	46.4
47.4	47.4	47.4	47.4
48.4	48.4	48.4	48.4
49.4	49.4	49.4	49.4
50.4	50.4	50.4	50.4

TABLE B 14(b)
Conducting Epoxy, Unfiltered Spectrum
Electron Counts with Error, X-Ray Counts

B, GAUSS	N1, COUNTS	ERROR	N2, COUNTS	ERROR	N3, COUNTS	ERROR	N4, COUNTS	ERROR	NX, X10000
3.5	23.	7.	1.	5.	1.	3.	12.	5.	29057.
4.5	15.	5.	5.	5.	12.	5.	21.	6.	28768.
5.3	4.	5.	1.	4.	10.	5.	25.	6.	29076.
5.8	38.	7.	13.	5.	1.	2.	8.	5.	29184.
6.5	20.	6.	1.	3.	11.	5.	9.	5.	29028.
7.2	3.	5.	6.	5.	1.	3.	6.	5.	28914.
7.9	28.	7.	5.	5.	1.	3.	27.	7.	28923.
8.8	10.	6.	1.	3.	1.	3.	12.	5.	28896.
9.8	66.	10.	1.	4.	4.	4.	25.	6.	28854.
10.8	72.	10.	41.	8.	10.	5.	26.	7.	28758.
12.0	107.	12.	18.	6.	16.	6.	30.	7.	28542.
13.3	169.	14.	55.	9.	17.	6.	52.	8.	28525.
14.7	210.	16.	78.	10.	49.	8.	54.	8.	28454.
16.3	244.	17.	74.	10.	55.	8.	49.	8.	28465.
18.1	383.	21.	154.	13.	45.	8.	45.	8.	28527.
19.0	342.	20.	105.	11.	53.	9.	53.	9.	28406.
20.0	379.	21.	119.	12.	67.	10.	80.	10.	28229.
21.0	342.	21.	135.	13.	115.	12.	59.	9.	28090.
22.1	343.	21.	138.	13.	122.	12.	75.	10.	27908.
23.2	386.	22.	127.	13.	98.	11.	72.	10.	27776.
24.3	318.	21.	125.	13.	81.	11.	65.	10.	27710.
25.5	239.	19.	112.	12.	38.	9.	92.	11.	27605.
26.8	220.	18.	110.	12.	59.	10.	107.	11.	27364.
28.1	185.	16.	113.	12.	21.	8.	44.	9.	27638.
31.0	92.	11.	78.	10.	25.	7.	34.	7.	27566.
34.2	56.	9.	3.	4.	12.	5.	15.	5.	27589.
37.7	29.	7.	6.	4.	1.	3.	14.	5.	27420.

TABLE B 14(c)
Conducting Epoxy, Unfiltered Spectrum
Differential Yield, Detector Efficiency, Energy Integrated Yield

E, KEV	G1,/1000	E1,/1000	G2,/1000	E2,/1000	G3,/1000	E3,/1000	G4,/1000	E4,/1000	ED
.11	.0203	.0031	.0022	.0005	.0034	.0010	.0657	.0124	.9460
.18	.0079	.0014	.0066	.0014	.0245	.0049	.0683	.0117	.9726
.25	.0015	.0003	.0009	.0003	.0144	.0030	.0575	.0092	.9808
.30	.0117	.0017	.0101	.0019	.0012	.0006	.0153	.0029	.9830
.37	.0049	.0008	.0006	.0002	.0105	.0022	.0138	.0028	.9840
.46	.0006	.0001	.0031	.0006	.0008	.0003	.0075	.0016	.9834
.55	.0047	.0007	.0021	.0005	.0007	.0002	.0281	.0042	.9818
.68	.0014	.0002	.0003	.0001	.0005	.0002	.0101	.0018	.9788
.85	.0073	.0007	.0003	.0001	.0017	.0004	.0171	.0027	.9749
1.03	.0066	.0006	.0095	.0012	.0036	.0007	.0147	.0022	.9705
1.27	.0080	.0007	.0034	.0006	.0047	.0008	.0140	.0021	.9650
1.56	.0104	.0007	.0086	.0010	.0041	.0007	.0198	.0025	.9589
1.90	.0107	.0007	.0100	.0010	.0097	.0012	.0170	.0021	.9522
2.34	.0102	.0006	.0078	.0008	.0089	.0011	.0127	.0015	.9444
2.88	.0130	.0006	.0133	.0010	.0060	.0007	.0095	.0012	.9356
3.18	.0107	.0005	.0083	.0007	.0064	.0007	.0103	.0012	.9312
3.52	.0108	.0005	.0086	.0007	.0074	.0008	.0141	.0014	.9262
3.88	.0089	.0004	.0089	.0007	.0117	.0010	.0096	.0011	.9212
4.30	.0082	.0004	.0083	.0006	.0113	.0009	.0111	.0011	.9157
4.74	.0085	.0004	.0070	.0006	.0084	.0007	.0098	.0010	.9101
5.20	.0064	.0003	.0064	.0005	.0064	.0006	.0081	.0008	.9045
5.72	.0044	.0002	.0053	.0004	.0027	.0003	.0106	.0010	.8983
6.32	.0038	.0002	.0047	.0004	.0039	.0004	.0113	.0010	.8915
6.95	.0029	.0002	.0044	.0004	.0013	.0002	.0042	.0005	.8846
8.46	.0012	.0001	.0026	.0003	.0013	.0002	.0027	.0004	.8689
10.29	.0006	.0001	.0001	.0000	.0005	.0001	.0010	.0002	.8510

TABLE B 14(ε) continued

<u>E,KEV</u>	<u>G1,/1000</u>	<u>E1,/1000</u>	<u>G2,/1000</u>	<u>E2,/1000</u>	<u>G3,/1000</u>	<u>E3,/1000</u>	<u>G4,/1000</u>	<u>E4,/1000</u>	<u>ED</u>
12.51	.0003	.0000	.0001	.0000	.0000	.0000	.0008	.0002	.8306
TOTAL G1	ERROR	TOTAL G2	ERROR	TOTAL G3	ERROR	TOTAL G4	ERROR		
.0585	.0045	.0551	.0039	.0475	.0070	.1009	.0214		

REFERENCES

REFERENCES

LIST OF REFERENCES

1. Schaefer, R.R., "Simple Model of Soft X-ray Photoemission," Journal of Applied Physics, Vol 44, No 1, pp 152-156, January 1973.
2. Ganeev, A.S. and Izrailev, I.M., "Photoelectric Yield for Soft X Rays," Soviet Physics - Technical Physics, Vol 31, No 3, pp 270-274, September 1961.
3. Izrailev, I.M., "Photoelectric Yield for Soft X rays," Soviet Physics - Technical Physics, Vol 7, No 11, pp 1020-1022, May 1963.
4. Shchemelev, V.N. and Rumsh, M.A., "Investigation of an Elementary Event of X-ray Photoeffect by Analyzing the Pulse-Height Distribution at the Output of a Secondary Electron Multiplier," Soviet Physics - Solid State, Vol 4, No 10, pp 2048-2052, April 1963.
5. Rumsh, M.A. and Shchemelev, V.N., "Role of Secondary Emission Phenomena in the X-ray Photoeffect in Metallic Cathodes," Soviet Physics - Solid State, Vol 5, No 1, pp 46-50, July 1963.
6. Denisov, E.P., Shchemelev, V.N., Mezhevich, A.N., and Rumsh, M.A., "Analysis of the Energy Structure of X-ray Photoemission from a Massive Cathode," Soviet Physics - Solid State, Vol 6, No 9, pp 2047-2050, March 1965.
7. Eliseenko, L.G., Shchemelev, V.N. and Rumsh, M.A., "A Study of the Spatial and Energy Distribution of X-ray Photoemission from Thick Cathodes," JETP, Vol 25, No 2, pp 211-216, August 1967.
8. Bradford, J.N., "Absolute Yields of X-ray Induced Photoemission from Metals," IEEE Trans. on Nuclear Science, Vols NS-19, pp 167-171, December 1972.
9. Bradford, J.N., "X-ray Induced Electron Emission II," IEEE Trans. on Nuclear Science, Vol NS-20, pp 105-110, December 1973.
10. Dolan, K.W., "X-ray Induced Electron Emission from Metals," Journal of Applied Physics, Vol 46, pp 2456-2463, June 1975.

LIST OF REFERENCES

1. Gerasimov, S.R., "X-ray Photoelectron Spectroscopy," Journal of Applied Physics, No. 1, pp. 152-155, January 1965.
2. Gerasimov, S.R. and Kiselev, V.N., "X-ray Photoelectron Spectroscopy," Journal of Applied Physics, No. 1, pp. 152-155, January 1965.
3. Kiselev, V.N., "X-ray Photoelectron Spectroscopy," Journal of Applied Physics, No. 1, pp. 152-155, January 1965.
4. Gerasimov, S.R. and Kiselev, V.N., "X-ray Photoelectron Spectroscopy," Journal of Applied Physics, No. 1, pp. 152-155, January 1965.
5. Gerasimov, S.R. and Kiselev, V.N., "X-ray Photoelectron Spectroscopy," Journal of Applied Physics, No. 1, pp. 152-155, January 1965.
6. Gerasimov, S.R. and Kiselev, V.N., "X-ray Photoelectron Spectroscopy," Journal of Applied Physics, No. 1, pp. 152-155, January 1965.
7. Gerasimov, S.R. and Kiselev, V.N., "X-ray Photoelectron Spectroscopy," Journal of Applied Physics, No. 1, pp. 152-155, January 1965.
8. Gerasimov, S.R. and Kiselev, V.N., "X-ray Photoelectron Spectroscopy," Journal of Applied Physics, No. 1, pp. 152-155, January 1965.
9. Gerasimov, S.R. and Kiselev, V.N., "X-ray Photoelectron Spectroscopy," Journal of Applied Physics, No. 1, pp. 152-155, January 1965.
10. Gerasimov, S.R. and Kiselev, V.N., "X-ray Photoelectron Spectroscopy," Journal of Applied Physics, No. 1, pp. 152-155, January 1965.

11. ETRAN: Monte Carlo Code System for Electron and Photon Transport through Extended Media, NBS Reports 9836 and 9837.
12. Colbert, H.M., SANDYL: A Computer Program for Calculating Combined Photon-Electron Transport in Complex Systems, Sandia Laboratories, SLL-74-0012, 1974.
13. Delin, T.A. and MacCallum, C.J., QUICKE 2: A One-Dimensional Code for Calculating Bulk and Vacuum Emitted Photo-Compton Currents, Sandia Laboratories, SLL-74-0218, April 1974.
14. Chadsey, W.L., "A Monte Carlo Photo-Current/Photo-Emission Computer Program," National Symposium on Natural and Man-Made Radiation in Space, Las Vegas, NV, March 1971.
15. Inada, T., Kawashima, K., Hoshino, K. and Matsuzawa, H., "Energy Spectra of Electrons Emerging from Lead Exposed to 320 kVp White X-rays," Japanese Journal of Applied Physics, Vol 2, No 2, pp 99-105, February 1963.
16. Matsuzawa, H., Hoshino, K., Inada, T. and Kawashima, K., "Energy Distribution of Electrons Ejected from Bone and Lucite by 150-300 kVp X-rays," British Journal of Radiology, Vol 38, pp 131-142, February 1965.
17. Ebert, P. and Lauzon, A., "Measurement of Gamma-Ray-Induced Secondary Electron Current from Various Elements," IEEE Trans. Nuclear Science, NS-13, pp 735-741, February 1966.
18. Bernstein, M.J., "Photoelectron Energy Spectra Generated by Low-Energy X Rays from Intense Plasmas," IEEE Trans. Nuclear Science, Vol NS-24, pp 2512-2515, December 1977.
19. Bernstein, M.J. and Smith, J.A., "Photoelectron Spectral Yields Generated by Monochromatic Soft X Radiation," IEEE Trans. Nuclear Science, Vol NS-25, pp 1577-1580, December 1978.
20. Siegbahn, K. (ed.) Alpha- Beta- and Gamma-Ray Spectroscopy (Vol 1), North-Holland Publishing Company, Amsterdam, 1965.
21. Storm, E., Israel, H.I. and Lier, D.W., Bremsstrahlung Emission Measurement from Thick

Tungsten Targets in the Energy Range 12 to 300 kV,
Los Alamos Scientific Laboratories, LA-4624, April
1971.

22. Barnett, C.F. and Ray, J.A., "Channel Electron Multipliers in Magnetic Fields," Review of Scientific Instruments, Vol 41, No 11, pg 1665, November 1970.
23. Hahn, Y.B. Hebner, R.E., Kastelein, D.R. and Kaare, J.N., "Channeltron Gain in Magnetic Fields," Review of Scientific Instruments, Vol 43, No 4, pp 695-696, April 1972.
24. Evans, R.D., The Atomic Nucleus, McGraw-Hill Book Company, New York, 1955.
25. Archuleta, R.J. and DeForest, S.E., "Efficiency of Channel Electron Multipliers for Electrons of 1-50 keV," Review of Scientific Instruments, Vol 42, No 1, pp 89-91, January 1971.
26. Bethe, H.A., Rose, M.E. and Smith, "Multiple Scattering of Electrons," Proceedings of American Philosophical Society, Vol 78, pp 573-585, 1938.

Thomson, E. J. and W. J. ...
 Los Angeles Scientific ...
 1971.

21. Barnett, C. F. and W. J. ...
 Multiplication in ...
 Scientific Publications, Vol. 11, No. 11, 1973.
 November 1973.

22. Hahn, Y. H., Hehnert, E. H., ...
 J. H., "Channel ...
 of Scientific Publications, Vol. 11, No. 11, 1973.
 695-696, April 1973.

23. Evans, R. D., The ...
 Company, New York, 1985.

24. Archibald, R. J. and ...
 Channel ...
 Rev., "Review of ...
 1, pp 89-91, January 1971.

25. Botter, E. A., ...
 Scientific ...
 Philosophical Society, Vol. 19, pp 573-582, 1973.

SECTION EIGHT
RECEIVED
(BOND)
(FORWASATF)
CANTON
CO.

